Conceptual System Design of a Solar Electric Propulsion Stage for Earth-Moon Cargo Transfer Missions

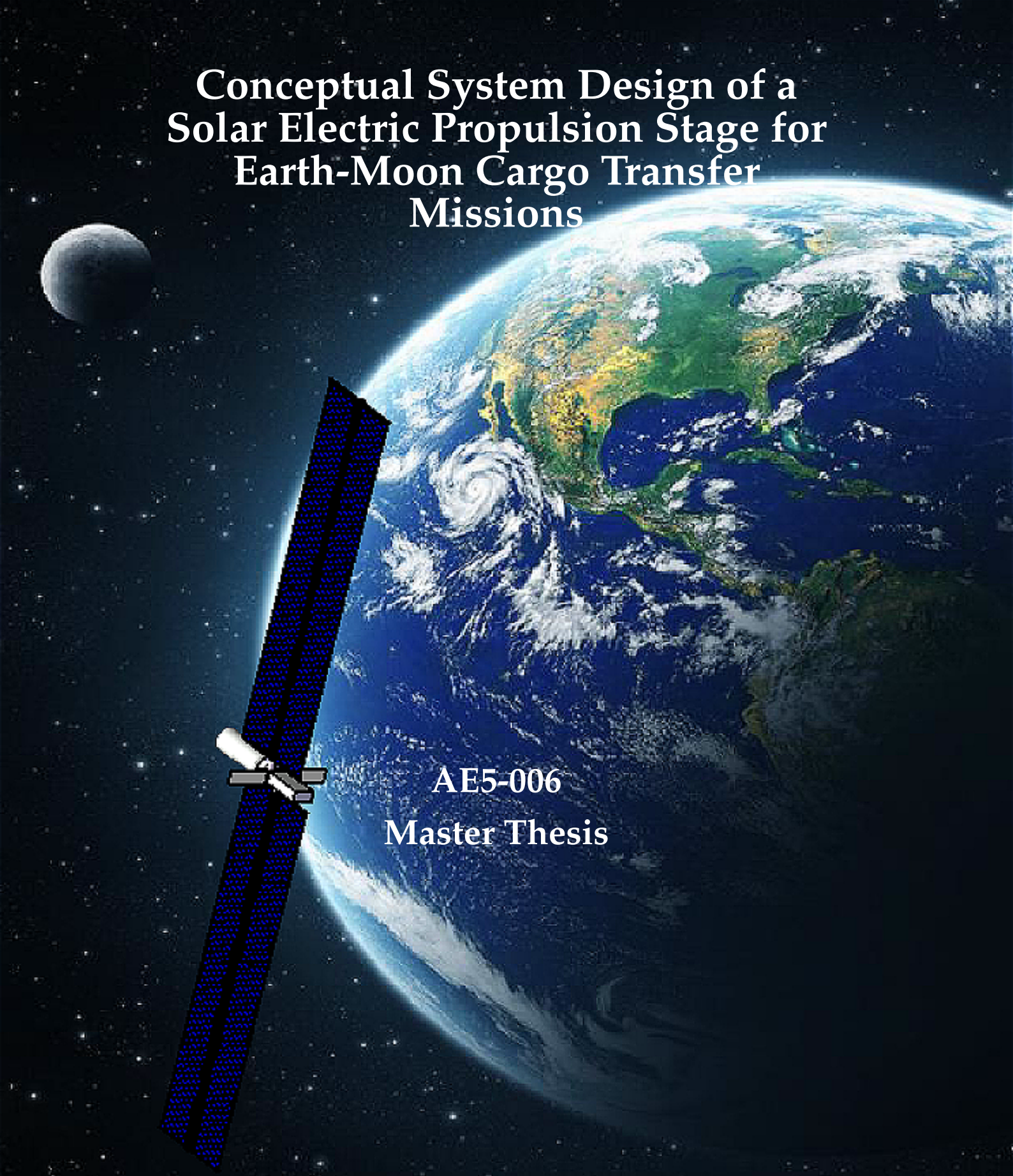

AE5-006
Master Thesis

C.R. Bos
1260693

Final Report
January 17, 2013

TU Delft Delft University of Technology

OHB

Challenge the future

Master Thesis

Conceptual System Design of a Solar Electric Propulsion Stage for Earth-Moon Cargo Transfer Missions

Remco (C.R.) Bos
1260693

Final Report
January 17, 2013

Company supervisor:
Dr. rer. nat. F. Gamgami
OHB System AG
Space System Study
Universitätsallee 27-29, 28359 Bremen

University supervisor:
Prof. dr. E.K.A. Gill
Delft University of Technology
Faculty of Aerospace Engineering
Kluyverweg 1, 2629 HS Delft

University mentor:
Ir. B.T.C. Zandbergen

Exam committee members:
Prof. dr. E.K.A. Gill
Ir. B.T.C. Zandbergen
Ir. R. Noomen

Abstract

There is a renewed interest, expressed by ISECG, to return to the Moon and establish a longer human presence on the lunar surface. Long term missions require supplies, which can be transported to the Moon by a new promising solution: the Solar Electric Propulsion (SEP) stage. The goal of this study is to create a conceptual system design (phase 0) of such a SEP stage for Earth-Moon cargo transfer missions. The design is driven by the propulsion and electric power system, which are the main focus of the study, although all other subsystems are also covered to obtain a holistic system design.

Designing a SEP stage is a multi-disciplinary task, in which the trajectory analysis, propulsion system and electric power system are tightly coupled. A mission analysis program is created for simulation of the spiral transfer, while flexible design tools are developed to create the conceptual design. The tools provide the possibility to quickly evaluate a different mission scenario, such that the most suitable scenario, in consultation with the customer, can be selected.

A conceptual design is created that meets the mission objectives and requirements. During the design phase it was identified that the concept of a solar electric propulsion stage, accommodates some critical issues and technological challenges. Especially the high power demand, leads to the usage of highly conceptual power conditioning techniques, which still have to be proven in space, possibly by a precursor mission. It was also found that the SEP stage, compared to a chemical rocket, is capable of transporting 32% more payload, while having the same initial mass. This number can even increase to 90% in case a different mission scenario, with a longer transfer duration, is selected.

Executive Summary

Abstract

There is a renewed interest, expressed by ISECG, to return to the Moon and establish a longer human presence on the lunar surface. Long term missions require supplies, which can be transported to the Moon by a new promising solution: the Solar Electric Propulsion (SEP) stage. The goal of this study is to create a conceptual system design (phase 0) of such a SEP stage for Earth-Moon cargo transfer missions. Designing a SEP stage is a multi-disciplinary task, in which the trajectory analysis, propulsion system and electric power system are tightly coupled. A mission analysis program is created for simulation of the spiral transfer, while flexible design tools are developed to create the conceptual design. The tools provide the possibility to quickly evaluate a different mission scenario, such that the most suitable scenario, in consultation with the customer, can be selected. During the design phase it was identified that the concept of a solar electric propulsion stage, accommodates some critical issues and technological challenges. Especially the high power demand, leads to the usage of highly conceptual power conditioning techniques, which still have to be proven in space, possibly by a precursor mission. It was also found that the SEP stage, compared to a chemical rocket, is capable of transporting 32% more payload, while having the same initial mass. This number can even increase to 90% in case a different mission scenario, with a longer transfer duration, is selected.

Introduction

The International Space Exploration Coordination Group (ISECG) expressed a renewed interest to return to the Moon and establish a longer human presence on the lunar surface. The mission is planned for 2028 and will provide the engineers with the essential experience to achieve the ultimate goal: a human mission to Mars. Long term human missions, like the one envisioned for the Moon, require supplies. These supplies will be provided by cargo freighters, of which a potential and promising solution is to transport the cargo by a Solar Electric Propulsion (SEP) stage.

The goal of this study is to create a conceptual system design of such a SEP stage for Earth-Moon cargo transfer missions. This transfer stage is powered by photovoltaic cells and uses primarily electric propulsion. These two subsystems, propulsion and electric power system, drive the system architecture and are the main focus of the study, although all other subsystems are also covered to obtain a holistic system design. The aim is the assessment of the

system's feasibility, which is common for concept studies (phase 0), and to evaluate the impact of different mission scenarios on the conceptual design. This is achieved by developing engineering software tools that design the major aspects of the stage.

The study is done on behalf of OHB System AG located in Bremen, Germany. Together with OHB, the mission objectives and top-level requirements are identified. To meet these requirements, a mission analysis is needed for determining the mission architecture and Δv budget. Then the SEP stage will be designed, followed by a baseline configuration and evaluation of the SEP's performance. Eventually, a conclusion and recommendations are provided.

Mission Objectives & Requirements

The mission objective is to transport cargo (unmanned), at minimum 17 ton, from Earth environment to a Low Lunar Orbit (LLO), within 200 days, by means of a Solar Electric Propulsion stage and return to the Earth environment for a follow-up mission. From this objective, the top-level Mission Requirements (MR) and System Requirements (SR) are deduced and are obtained in agreement with OHB:

MR.1 The transfer stage shall transport a payload of minimal 17 ton (TBC) from Earth environment to a LLO of 100×100 km within 200 days (TBD).

MR.2 The stage shall be reusable, meaning that the transfer stage shall return from LLO to the initial Earth orbit and perform at least two missions to LLO with the potential of extension to three missions.

MR.3 The transfer stage and cargo should be launched together (TBC) with one super heavy lift launch vehicle (TBD). The launcher has to be available in the next decade (i.e. SLS or Falcon Heavy).

SR.1 The transfer stage shall primarily be using electric propulsion.

SR.2 The transfer stage shall be powered by solar panels.

SR.3 The transfer stage shall provide thermal control and radiate all excess heat to space.

SR.4 The transfer stage's configuration should be such that the direct impingement of the thrusters' exhaust on the solar arrays is limited.

SR.5 The structure shall be rigid enough to withstand the launch loads and the frequencies that are imposed by the launcher.

Mission Analysis

The mission analysis plays a crucial role in the conceptual design study and poses a complex task. The low continuous thrust that is provided by the engines, results in a spiral transfer to the Moon. The initial acceleration is decisive for the spiral trajectory, resulting in a Δv and transfer time required. Also, the initial acceleration that can be achieved by the spacecraft, is depending on the propulsion and electric power system, illustrating the strong interdependency between the mission analysis and these two subsystems (see figure 0.1).

The significance of the trajectory, demands for a robust and simple tool, which analyses the trajectory for various initial accelerations and specific impulses. The tool, specifically designed for a transfer

from an Earth orbit to a lunar orbit, is based on the following assumptions:

- The Earth and Moon are considered to be point masses
- The Earth and Moon stay at the same distance from each other.
- The Lunar sphere of influence is a perfect sphere.
- The problem is a two-body problem, meaning that first the spacecraft spirals in the Earth system up to the lunar sphere of influence and then spirals within the Moon system. No third-body perturbations are considered.
- Other perturbations, like solar radiation pressure and atmospheric drag, are not considered.
- The Moon is present when the spacecraft arrives at lunar sphere of influence radius.
- The Moon and the SEP stage are situated in the same orbital plane, i.e. they have the same inclination and longitude of the ascending node.

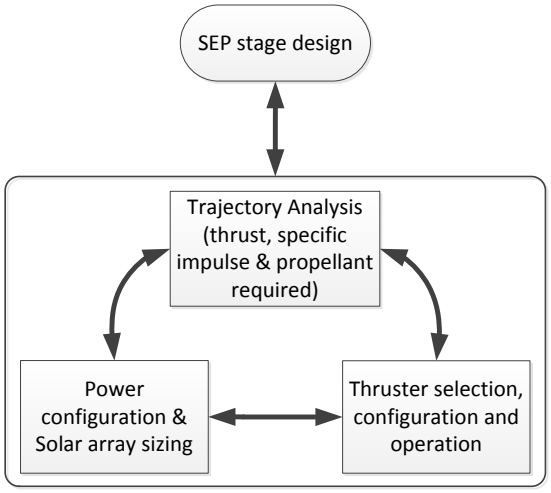

Figure 0.1.: The interdependencies in designing a SEP stage [22].

The transfer is calculated by using equations of motion, which are integrated by the Runge-Kutta-Fehlberg method. When the spacecraft reaches the lunar sphere of influence, in the so-called patch point, a coordinate transformation is made from the Earth reference frame to the Moon reference frame. During the transfer, no thrust is applied in the Earth's shadow due to power reasons. The resulting Δv and transfer time show a dependency on the eclipse and the selected patch point angle. The conditions that are achieved in the patch point, determine the perigee radius in the Moon's system, which might be highly favorable or unfavorable. Optimization of these conditions requires complex algorithms and long computation times, which is undesired for a phase 0 study. As a consequence, results of comparable initial accelerations, can have outcomes which are as large as $400\,\mathrm{m/s}$ apart (see figure 0.2). The overall tool is validated by using GMAT, which is a complex mission analysis tool from NASA, by running multiple simulation cases.

The launcher candidates are SLS and Falcon Heavy, which are capable of bringing $70\,\mathrm{ton}$ and $53\,\mathrm{ton}$, respectively, in a parking orbit of $200 \times 200\,\mathrm{km}$. However, at this altitude the atmospheric drag influences the orbit stability of the SEP stage. To obtain a stable long-term orbit with negligible atmospheric drag, the SEP stage requires a parking orbit of minimally $500 \times 500\,\mathrm{km}$. The SLS, which is a 1.5 stage rocket, is not capable of bringing a payload to this orbit or it will come at a very high cost. On the contrary, the Falcon Heavy, which is a 2.5 stage rocket and restartable, is able to bring a payload of $49.6\,\mathrm{ton}$ to the selected Low Earth Orbit (LEO) of $500 \times 500\,\mathrm{km}$.

A simplified mass model is created to obtain a preliminary mass estimate as func-

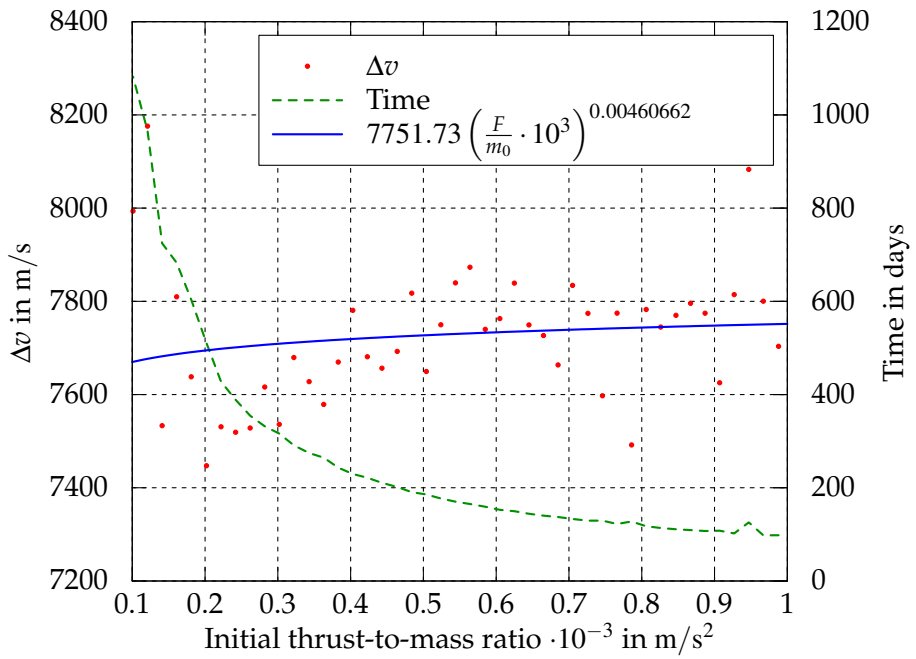

Figure 0.2.: The time and Δv as function of the initial acceleration for an I_{sp} of 2,000s.

tion of the specific impulse. The power system mass scales linearly with the thrust and specific impulse, while the propellant mass decreases exponentially with increasing specific impulse. This indicates that, for the proposed mission, there is an optimum specific impulse from the mass point of view (see figure 4.17). The required power at the optimum of $3,000\,\mathrm{s}$, is $690\,\mathrm{kW}$, which is 2.7 times more than the current state of the art. Therefore it is chosen to select a sub-optimum specific impulse of $2,000\,\mathrm{s}$ that corresponds to a much lower power demand of $460\,\mathrm{kW}$.

The transfer from LEO to LLO needs to be performed in $200\,\mathrm{days}$, which corresponds to an initial acceleration of $4.8 \cdot 10^{-4}\,\mathrm{m/s^2}$ (see figure 0.2). The Δv that is required, including a 10% margin, equals $8,498\,\mathrm{m/s}$. To return from LLO to LEO, a Δv of $8,134\,\mathrm{m/s}$ is needed.

Launching the payload and SEP stage together with a single Falcon Heavy launch, results, according to the preliminary mass model, in a payload mass of $14.7\,\mathrm{ton}$, while a payload of $17\,\mathrm{ton}$ is required. Also, during the design phase it was discovered that having a heavy payload on top of a SEP module, has severe consequences for the structural mass. Therefore, a dual launch scenario was selected, in which the payload requirement can be met and a significant structural mass saving is obtained. The resulting mission sequence (see figure 0.3) is thus, that the SEP stage and Payload Module are separately launched by a Falcon Heavy rocket. After docking in LEO, the transfer to LLO is performed, by using the propellant located in the Payload Module. Once the spacecraft arrives in LLO, the two undock and the Payload Module lands on the Moon, while the SEP stage returns to LEO and performs a second mission with another Payload Module. The SEP stage is designed to transport three Payload Modules in total.

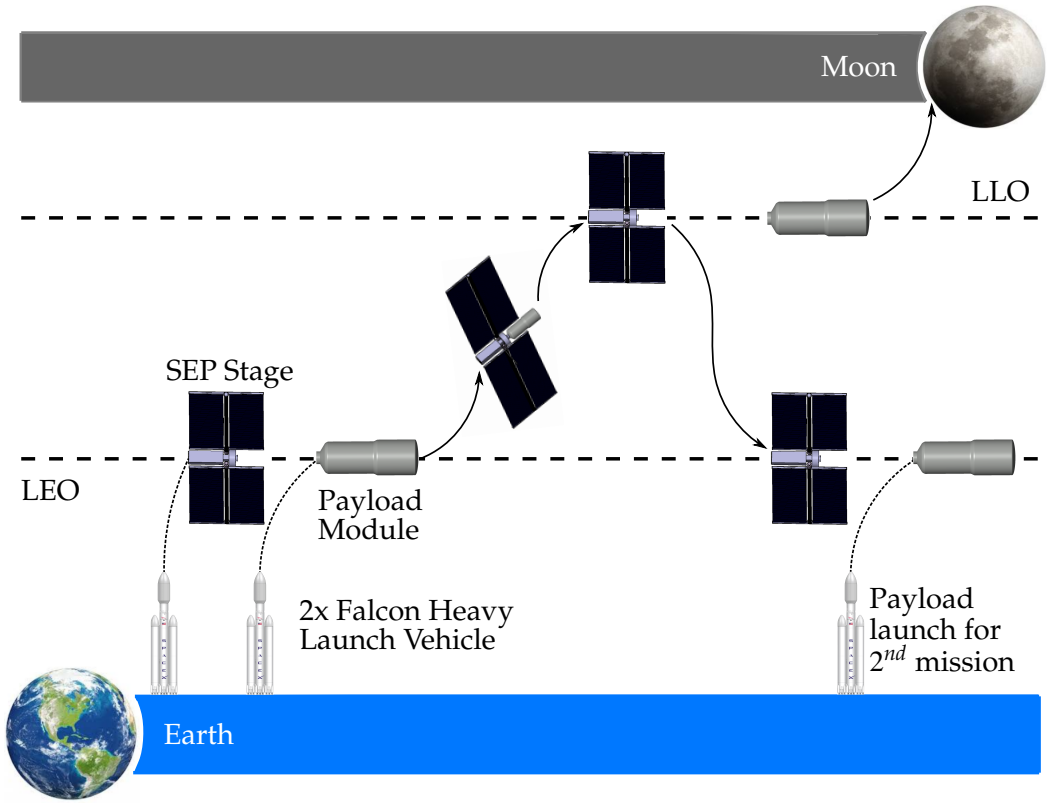

Figure 0.3.: The mission sequence of the SEP stage.

Stage Design

To obtain a feasible and holistic design, the subsystems are designed by using well-established methods and by applying a margin philosophy, on component and on system level. The SEP stage's system design is mainly driven by the mission requirements, especially the transfer time and payload mass requirement. During the design phase, iterations were needed to converge to the final design. The chosen methodology is, when having a fixed initial acceleration and a first preliminary mass estimate, to analyze the subsystems' mass and obtain a new initial mass. If the newly obtained initial mass is within 5% of the old initial mass, the design is converged and final. Three iterations are applied to meet this condition.

Propulsion System

The propulsion system enables the transfer from LEO to LLO and is required to operate at a specific impulse of $2,000\,\mathrm{s}$, which is mainly the domain of Hall thrusters and Magnetoplasmadynamic thrusters. However, the lifetime of a Magnetoplasmadynamic thruster is insufficient for this mission and therefore Hall thrusters, using Xenon as propellant, are selected. The Xenon is stored in composite overwrapped pressure vessels at a pressure of $12\,\mathrm{MPa}$ and a temperature in between $294 - 304\,\mathrm{K}$. The Xenon Feed System down-regulates the pressure by a single Propellant Management Assembly (PMA), while a Xenon Flow Controller (XFC) provides precise mass flow control at engine level (see figure 0.4).

An advantage of selecting a Hall thruster is, that a Direct Drive power processing Unit (DDU) can be used for the power conditioning. The working principle of

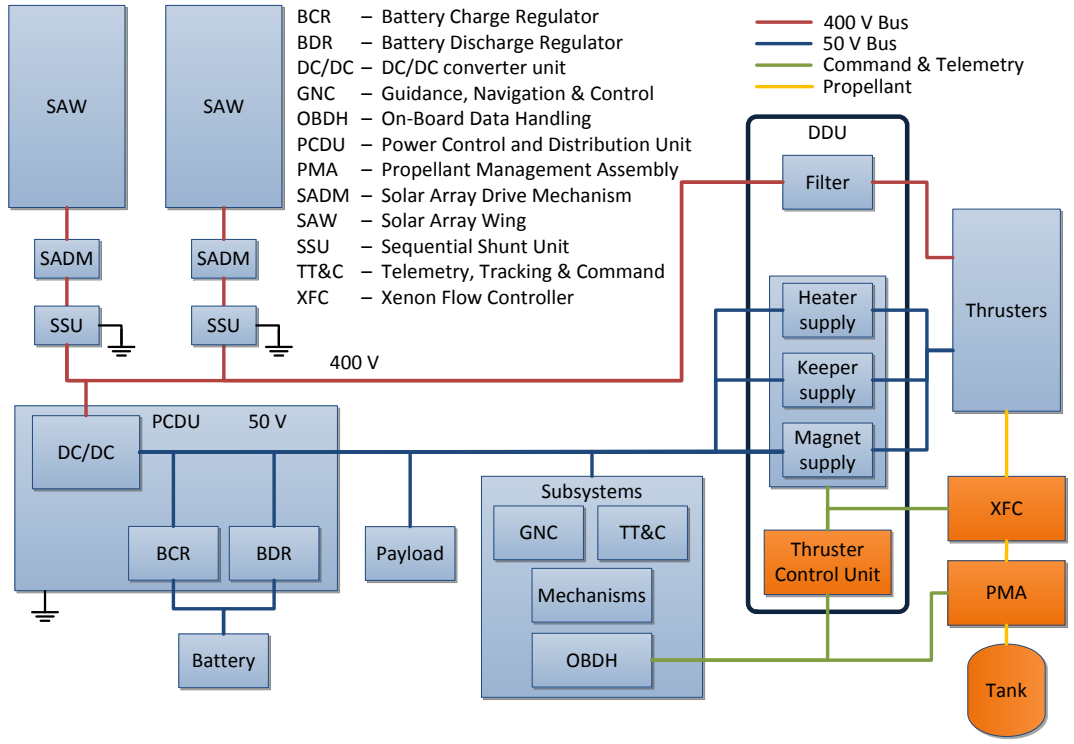

Figure 0.4.: Schematic of the electric power system.

a DDU is that the Power Processing Unit (PPU) of the Hall thruster is removed and the solar array is directly linked to the Hall thruster's anode. This approach increases the overall power efficiency, thereby reducing the waste heat and the Thermal Control System (TCS) mass. Also, elimination of the PPU results in a lower power demand and thus a significant mass saving, although operational stability becomes a point of concern.

As baseline thruster, the NASA-457M is selected, although an update, in which the magnetic shielding principle is applied, is required to meet the desired lifetime. In total fourteen thrusters are needed to provide the stage with 31.3 N of thrust. The mass of all the elements of a thruster string, including gimbals, DDU, cabling, tanks and the XFS, were estimated, by adopting and adjusting an existing model from JPL, at 2,815 kg.

Electric Power System

The Electric Power System (EPS) influences the performance and mission feasibility to a great extent and forms the most critical subsystem of the SEP stage. The power is generated by Solar Arrays (SA), which should be pointed perpendicular toward the Sun for maximum power production. The pointing can be accomplished by *1.)* a two-axis gimbal, *2.)* a one axis gimbal in combination with a roll-steering maneuver, and *3.)* a one axis gimbal and sizing the SA for off-pointing errors. The SEP stage is launched into the lunar plane, which is 5.1° inclined to the Sun vector. In this configuration, the power loss due to the off-pointing error is only 0.4%, which makes the third option the most logical choice. The one axis gimbal is incorporated in the Solar Array Drive Mechanism (SADM), which diverts the power coming from the solar ar-

rays, to the Sequential Shunt Units (SSU) and Hall thrusters. A small fraction of the power is converted, regulated and distributed by the Power Control and Distribution Unit (PCDU) to the subsystems and heater, keeper and magnet supply of the thrusters (see figure 0.4).

Regulation of the power operation point is provided by the SSU and by adjusting the Hall thrusters' mass flow and magnetic field strength. This method gives full control of the operation point and such the power system can operate at the maximum power point of the SA characteristic. The four SAs are flexible and consists out of 2040 m^2 Inverted Metamorphic four junction (IMM4J) solar cells, providing the stage with 608 kW of power at End-Of-Life (EOL) and under hot conditions, while operating at a voltage of 400 V. A single Solar Array Wing (SAW) contains two foldable SA blankets with a deployable truss in between, having a total width of 17.7 m and length of 63.3 m (see figure 0.5). The total mass of the flexible SAs and electronic equipment is calculated at $6,834$ kg.

Configuration, Structures & Mechanisms

All subsystems and components should be arranged into a suitable configuration. To avoid large structural stresses during launch and, consequently, a heavy structure, the center of mass should be located as close as possible to the launcher adapter. Therefore, the heavy components primarily drive the configuration, followed by the dimensions of certain components. For the SEP stage, the propellant tank, SAW assembly (i.e. SADM, canister and SA boom) and EPS are the driving components and placed as close as possible to the launcher adapter (see figure 0.5).

The primary load carrying structure, which is connected to the launcher adapter and sustains the launch loads, consists out of a primary cylinder and primary box (see figure 0.5), which are analyzed for their stiffness, strength and buckling by modeling them as a mass carrying cantilevered beam. The electric thrusters and DDUs are positioned on top of the primary box and enclosed by the secondary box, such that a significant mass saving is obtained for the secondary box structure. This structure also provides support to the SA booms and radiators during the launch, while in space it provides protection to the power and Xenon feed lines. Once the SEP stage is in orbit, the electric thrusters, radiators and SAWs deploy to their final configuration by using deployable trusses and mechanisms.

Thermal Control System

Thermal models are created for the SA and the spacecraft body. They are based upon simple heat balances, in which it is assumed that there is no interaction with other surfaces and the equilibrium temperature is reached. The model gives as result the cold and hot temperature of the SA and the minimal radiator area (73.6 m^2) which is required to radiate all excess heat to space.

Attitude and Orbit Control System

The Attitude and Orbit Control System (AOCS) controls the orientation and direction of the spacecraft by four gimbaled electric thrusters, which are located at the corners of the back plate and can tilt their thrust vector 12°. These thrusters provide

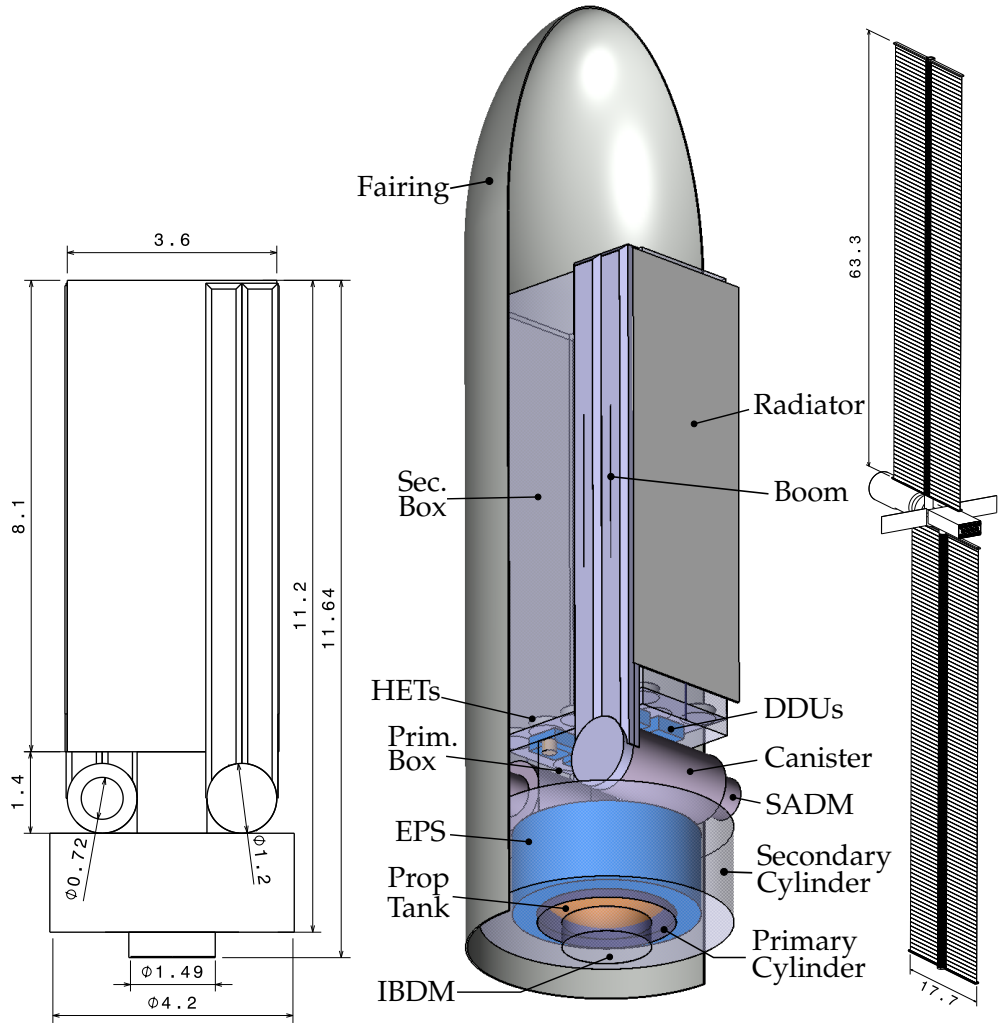

Figure 0.5.: The SEP stage in the folded configuration (left and middle) and in the deployed configuration with the Payload Module docked (right).

enough agility for the AOCS system to apply steering maneuvers and cancel out torques caused by the solar pressure force. Also, a set of sensors is identified, that are able to acquire the stage's position and attitude.

TELEMETRY, TRACKING & COMMAND AND ON-BOARD DATA HANDLING

The Telemetry, Tracking & Command (TT&C) and On-Board Data Handling (OBDH) subsystems do not drive the design. Therefore, a conventional design is made in which commercial off-the-shelf units are selected that fulfill similar tasks in other missions.

Performance Analysis

A SEP stage can have various component failures, without endangering the mission objectives. E.g., the impact of a single engine failure on the stage's performance is minimal and will lead to a longer transfer time of approximately one day. In case more engines fail, the impact on the transfer time will increase, although it is expected that sufficient propellant is available to fulfill the mission objective, except for the transfer time requirement. The failure of a SADM, leading to halved power output, will approximately double the transfer time, although it is expected

Mass budget	SEP stage	Payload Module	Total
$m_{structure}$ (kg)	2,308	-	2,308
$m_{propulsion}$ (kg)	2,815	1,818	4,632
m_{power} (kg)	6,834	-	6,834
$m_{thermal}$ (kg)	1,075	-	1,075
m_{AOCS} (kg)	81	-	81
m_{OBDH} (kg)	48	-	48
$m_{TT\&C}$ (kg)	36	-	36
$m_{harness}$ (kg)	1,320	-	1,320
$m_{subsystems}$ (ton) (20%)	17.4	2.2	19.6
$m_{payload}$ (ton)	-	17.0	17.0
m_{dry} (ton)	17.4	19.2	36.6
m_{prop} (ton)	8.2	23.2	31.5
m_0 (ton)	25.7	42.4	68.1

Table 0.1.: Resulting mass budget after the third iteration. Note that the payload module has to harbor the propellant to go from LEO to LLO.

that the other mission objectives can still be met.

The conceptual design meets all the top-level mission and system requirements, although a dual launch scenario was selected due to structural mass benefits and to meet the required payload mass. The complete spacecraft, with SEP stage and Payload Module docked, has a total mass of 68.1 ton (see table 0.1) and a payload mass fraction ($m_{payload}/m_0$) of 0.25. Another study performed at OHB showed that a chemical rocket can obtain a payload mass fraction of 0.19 [2], which means that the SEP stage is capable of transporting 32% more payload, while having the same initial mass.

A SEP stage is a new, unproven technology that has to overcome some critical issues and technological challenges. The high-voltage present on the SA causes potential differences, which can lead to electrostatic discharges. To reduce this risk and lower the spacecraft's potential, the thruster cathodes are operational at all times. Also, the operation of a DDU is a new development in which questions remain. Tests of JPL show promising results, although it is expected that a precursor mission is required to validate the operation of a high-voltage SA in combination with a DDU. A third critical issue is the deployment of the deployable trusses, which deploy the SA and thruster plate to its final position. However, there is substantial heritage of other missions (ISS, SRTM Space Shuttle and NuSTAR) and extensive ground testing can be performed for validation of the system. Another critical issue, for the current mission and configuration, is the size of the SADM and canister, which reach the outer limits of the fairing diameter. As a result,

Characteristic	Transfer time (days) 200		**400**		800	
$m_{payload}$ (kg)	17,000	10,000	**17,000**	10,000	17,000	10,000
P_{EOL} (kW)	608	486	**285**	212	189	129
$m_{SEP,dry}$ (ton)	17.4	15.1	**10.1**	8.3	7.3	6.0
m_{prop} (ton)	31.5	26.1	**18.6**	14.2	11.0	7.7
m_0 (ton)	68.1	52.8	**46.9**	33.4	35.9	24.1
$m_{payload}/m_0$	0.250	0.189	**0.362**	0.299	0.473	0.414

Table 0.2.: SEP stage characteristics when lowering the transfer time requirement and/or payload mass.

the cylindrical section is connected to the thrusters through a relatively small rectangular box. These issues show that the current mission scenario reaches the limit of the technological possibilities, therefore the impact of less demanding missions, with longer transfer duration and less payload, on the design are studied.

The alternative mission scenarios that are studied, are for a payload of 17 ton and 10 ton with a transfer time of 200, 400 or 800 days. The transfer time requirement changes the optimum specific impulse, initial acceleration and Δv-budgets of the corresponding missions. The new mission scenarios lead to less demanding designs (see table 0.2), from which it can be concluded, that relieving the transfer time requirement has a greater impact than diminishing the payload mass requirement. Also, an increase of the transfer time, results in a significant increase of the payload mass fraction. However, the relative payload mass fraction increase from 400 to 800 days is smaller than from 200 to 400 days. Therefore, it is advised to change the mission scenario to a 400 days scenario, having a payload mass of 17 ton.

Conclusion

The purpose of this study is to create a conceptual system design of a SEP stage for Earth-Moon cargo transfer missions. The mission objective is to transport a cargo of 17 ton from the Earth environment to LLO, within 200 days. The transfer is performed by electric thrusters, which results in a spiral trajectory. Simulations of this trajectory showed that a Δv of 8.5 km/s is required to go from a 500×500 km LEO to a 100×100 km LLO, having an initial acceleration of $4.8 \cdot 10^{-4}$ m/s^2. The Falcon Heavy launches the SEP stage and Payload Module separately into LEO, where the two dock and perform the transfer to LLO. After undocking, the Payload Module lands on the lunar surface and the SEP stage returns to LEO to meet with a second Payload Module. The SEP stage is designed for transporting three modules in total.

The design of the SEP stage is driven by the mission requirements, especially by the transfer time and payload mass requirement. They drive the propulsion system and electric power system and thus the overall stage's mass and architecture. The subsystems are designed by us-

ing well-established design methods and by applying a margin philosophy, to obtain a feasible and holistic design. Iterations were applied to converge to the final design, of which three in total were needed. The baseline SEP stage, employs Hall thrusters as type of propulsion, which provide a thrust of 31.3 N. The engines are powered by flexible solar arrays, which consists out of Inverted Metamorphic four junction solar cells, generating a total power, at EOL, of 608 kW. The operation point of the power system is controlled by the DDU in combination with the SSU.

A SEP stage can have various components failures, without endangering the mission objectives. A single engine failure will lead to a slightly longer transfer time of approximately one day, while a SADM failure will approximately double the transfer time, although it is expected that sufficient propellant is available to meet the other mission objectives.

The conceptual design meets all the top-level mission and system requirements, although a dual launch scenario was selected due to structural mass benefits and to meet the required payload mass. The complete spacecraft has a total mass of 68.1 ton and a payload mass fraction of 0.25. Compared to a chemical rocket, the SEP stage is capable of transporting approximately 32% more payload, while having the same initial mass. This can even increase to 90% in case the 400 days scenario is selected.

The SEP stage is a new and complex system, introducing technological challenges and critical issues. Multiple critical issues, with the DDU, SAs, SADM and deployable truss deployment, were identified. These systems require a significant engineering effort, to develop reliable space qualified components. For the high-voltage SA and DDU it is expected that a precursor mission is needed to validate the concept. The critical issues show that the current mission scenario reaches the limit of the technological possibilities, therefore less demanding missions and their impact on the design are studied. From the results, it is advised to change the mission scenario to a 400 days scenario, while having the same payload mass of 17 ton. For this advised new mission scenario, no optimization of the launcher selection is performed. For a more thorough analysis, the launcher selection has to be re-assessed and therefore there is a probability that the overall design will change. However, the rational of the performed parameter study is to show the impact of a different mission scenario on the design and to advice the customer to reconsider its initial requirements.

In conclusion, this study provides a conceptual design of a solar electric propulsion stage that can fulfill the mission objectives. Also, the effect of different mission scenarios on the design are researched, which results in the advice to change the transfer time requirement from 200 days to 400 days. For the future design phases it is advised to improve the mission analysis by improving the trajectory computation of the Spiral Program. Furthermore, the design of the subsystems can be performed in more detail, resulting in more accurate mass and power budgets.

Contents

List of Figures

List of Tables

Nomenclature

Latin Symbols

A	Area	m^2
a	Semi-major axis	m
Al	Albedo factor	–
B	Magnetic field strength	T
b	Semi-minor axis	m
b	Width	m
C	Specific heat	$J/m^2 \cdot K$
C	Specific orbital energy	m^2/s^2
c	Speed of light	m/s
C_D	Drag coefficient	–
c_e	Characteristic velocity	m/s
D	Distance Earth-Moon	m
d	Diameter	m
d	Distance	m
E	Young's modulus	N/m^2
e	Distance	m
e	Eccentricity	–
F	(View) factor	–
F	Force/Thrust	$kg \cdot m/s^2$
f	Frequency	Hz
FS	Factor of Safety	–

G	Gravitational constant	$\mathrm{m}^3/\mathrm{kg}\cdot\mathrm{s}^2$
g	Gravitational acceleration	m/s^2
g_0	Standard gravity	m/s^2
h	Height	m
I	Area Moment of Inertia	m^4
I	Current	A
I	Mass Moment of Inertia	$\mathrm{kg}\cdot\mathrm{m}^2$
i	Inclination	$^\circ$
I_{sp}	Specific impulse	s
J	Intensity	W/m^2
k	Boltzmann constant	J/K
k	Effective length factor	–
l	Length	m
$\dot{m}$	Mass flow	kg/s
M	Moment	$\mathrm{N}\cdot\mathrm{m}$
m	Mass	kg
Ma	Margin	–
MS	Margin of Safety	–
N	Number	–
P	Power	W
p	Pressure	N/m^2
p	Semi-latus rectum	m
Q	Heat	W/m^2
q	Electron charge	C
R	Planet radius	m
R	Resistance	Ω

r	Radius	m
s_σ	Specific strength	m
T	Temperature	K
T	Torque	Nm
t	Thickness	m
t	Time	s
U	Voltage	V
V	Volume	m^3
v	Velocity	m/s

Greek Symbols

α	Absorptivity	–
α	Angle	°
β	Angle	°
Δ	Increment	–
ε	Angle	°
ε	Emissivity	–
η	Efficiency	–
γ	Angle	°
γ	Reduction factor	–
λ	Patch point angle	°
μ	Standard gravitational parameter	m^3/s^2
ν	Poisson's ratio	–
ν	True anomaly	°
ω	Rotational speed	°/s
Φ	Irradiation	MeV/cm^2
ϕ	Flight path angle	°

ψ	Position angle	$^\circ$
ρ	Density	$\mathrm{kg/m^3}$
σ	Angle	$^\circ$
σ	Stefan-Boltzmann constant	$\mathrm{W/m^2 \cdot K^4}$
σ	Stress	$\mathrm{N/m^2}$
σ	Structural index	–
θ	Thrust angle	$^\circ$
φ	Geometric parameter	–
ϑ	Angle of incidence	$^\circ$
ζ	Angle	$^\circ$

Indices

0	Initial
ac	Active
Al	Aluminum
ax	Axial
b	Beam
bend	Bending
cab	Cabling
c	Circular
cg	Center of Gravity
CL	Current Losses
CoM	Center of Mass
D	Drag
des	Desired
E	Earth
EPS	Electric Power System

flex	Flexure
Gl	Gravity losses
HC	Hot Case
HET	Hall Effect Thruster
i	Input
i	Ion
IR	InfraRed
lat	Lateral
M	Moon
mp	Maximum Power
oc	Open Circuit
O	Output
p	Projected
pp	Panel Packing
prop	Propellant
ps	Propulsion System
rad	Radiation
rd	Redundant
req	Required
s/c	Spacecraft
sa	Solar Array
sc	Short Circuit
SEP	Solar Electric Propulsion stage
soi	Sphere Of Influence
sp	Solar Pressure
s	Structure

sys	System
thr	Thruster
tot	Total
VL	Voltage Losses
XFS	Xenon Feed System

Abbreviations

4J	**F**our **J**unction
ADAM	**A**ble **D**eployable **A**rticulated **M**ast
AOCS	**A**ttitude and **O**rbit **C**ontrol **S**ystem
a-Si	**A**morphous **Si**licon
ATV	**A**utomated **T**ransfer **V**ehicle
AU	**A**stronomical **U**nit
BCR	**B**attery **C**harge **R**egulator
BDR	**B**attery **D**ischarge **R**egulator
BGA	**B**eta **G**imbal **A**ssembly
BOL	**B**eginning **O**f **L**ife
CDV	**C**argo **D**elivery **V**ehicle
CFRP	**C**arbon **F**iber **R**einforced **P**lastic
CIGS	**C**opper **I**ndium **G**allium **D**iselenide
DDCU	**D**C-to-**D**C **C**onverter **U**nit
DDU	**D**irect **D**rive **U**nit
DET	**D**irect **E**nergy **T**ransfer
EOL	**E**nd **O**f **L**ife
EPS	**E**lectric **P**ower **S**ystem
ESA	**E**uropean **S**pace **A**gency
EVA	**E**xtra **V**ehicular **A**ctivity

FAST	**F**olding **A**rticulated **S**quare **T**russ
FCD	**F**low **C**ontrol **D**evice
GEO	**GE**ostationary **O**rbit
GMAT	**G**eneral **M**ission **A**nalyses **T**ool
GNC	**G**uidance **N**avigation & **C**ontrol
GPS	**G**lobal **P**ositioning **S**ystem
GTO	**G**eostationary **T**ransfer **O**rbit
HEFT	**H**uman **E**xploration **F**ramework **T**eam
HEMP	**H**ighly **E**fficient **M**ultistage **P**lasma
HEO	**H**ighly **E**lliptical **O**rbit
HET	**H**all **E**ffect **T**hruster
HiPER	**Hi**gh **P**ower **E**lectric propulsion: a **R**oadmap for the future
HVB	**H**igh **V**oltage **B**us
IADC	**I**nter-**A**gency Space **D**ebris **C**oordination Committee
IBDM	**I**nternational **B**erthing and **D**ocking **M**echanism
IMM	**I**nverted **M**eta**m**orphic
IMU	**I**nertial **M**easurement **U**nit
IR	**I**nfra**R**ed
ISECG	**I**nternational **S**pace **E**xploration **C**oordination **G**roup
ISS	**I**nternational **S**pace **S**tation
JPL	**J**et **P**ropulsion **L**aboratory
L1	**L**agrange point **1**
LEO	**L**ow **E**arth **O**rbit
LLO	**L**ow **L**unar **O**rbit
LVB	**L**ow **V**oltage **B**us
LVLH	**L**ocal **V**ertical **L**ocal **H**orizontal reference frame

MEO	**M**edium **E**arth **O**rbit
MJD	**M**odified **J**ulian **D**ate
MLI	**M**ulti **L**ayer **I**nsulation
MR	**M**ission **R**equirement
NASA	**N**ational **A**eronautics and **S**pace **A**dministration
NEO	**N**ear **E**arth **O**bject
OBDH	**O**n-**B**oard **D**ata **H**andling
OHB	**O**rbitale **H**ochtechnologie **B**remen
OTV	**O**rbital **T**ransfer **V**ehicle
PCDU	**P**ower **C**ontrol and **D**istribution **U**nit
PFCV	**P**roportional **F**low **C**ontrol **V**alve
PMA	**P**ropellant **M**anagement **A**ssembly
PPT	**P**eak **P**ower **T**racking
PPU	**P**ower **P**rocessing **U**nit
RMS	**R**oot **M**ean **S**quare
SADM	**S**olar **A**rray **D**rive **M**echanism
SARJ	**S**olar **A**lpha **R**otary **J**oint
SA	**S**olar **A**rray
SAW	**S**olar **A**rray **W**ing
SEP	**S**olar **E**lectric **P**ropulsion
SJ	**S**ingle **J**unction
SLS	**S**pace **L**aunch **S**ystem
SMU	**S**atellite **M**anagement **U**nit
SR	**S**ystem **R**equirement
SSU	**S**equential **S**hunt **U**nit
TBC	**T**o **B**e **C**onfirmed

TBC	**T**o **B**e **D**etermined
TBC	**T**hermal **C**ontrol **S**ystem
TJ	**T**riple **J**unction
TRL	**T**echnology **R**eadiness **L**evel
TT&C	**T**elemetry **T**racking & **C**ommand
VDA	**V**apor **D**eposited **A**luminum
WBS	**W**ork **B**reakdown **S**tructure
XFC	**X**enon **F**low **C**ontroller
XFS	**X**enon **F**eed **S**ystem

1. Introduction

Since the last Moon landing in 1972, the interest of human missions to the Moon faded. However, recently there is a renewed interest to go back. The International Space Exploration Coordination Group (ISECG), consisting out of 14 space agencies, updated a Global Exploration Roadmap in September 2011 [18]. This roadmap examines possible pathways in the next 25 years and developed two mission scenarios. One of these scenarios is the 'Moon Next' scenario, where it is planned to go to the Moon around 2028 and establish a long lasting human campaign. This human campaign needs to be supplied by resources, which will be provided by cargo freighters.

Transferring cargo from Earth to the Moon on a regularly basis by means of current technology is expensive. A potential solution for reducing cost is to transport the cargo by using a Solar Electric Propulsion (SEP) stage. A SEP stage can transfer significantly more payload compared to a chemical propelled transfer stage while having the same initial mass [1]. Secondly, a SEP stage can be made re-usable, which is another potential cost saver.

The goal of this study is to create a conceptual system design of such a SEP stage for Earth-Moon cargo transfer missions. The design of the transfer stage is limited to electric propulsion, which are powered by solar panels. Technological challenges, enabling technologies and requirements concerning the design will be identified. Comparable studies have been performed by NASA, although for different mission scenarios and diverse levels of detail. This study follows the ESA's design philosophy for concepts studies, to obtain a feasible design that can be compared with past studies. The study also incorporates the opportunity to evaluate other mission scenarios and their impact on the conceptual design.

The focus within the study will be on the design of the propulsion system and electrical power system. However, all other subsystems will be addressed as well in order to achieve a holistic system design. Though, the level of detail of these subsystems will be lower, since they do not drive the system architecture. The aim is the assessment of the system's mass feasibility and consistency, which is common for concept studies (phase 0). The resulting conceptual design shall serve as a reference for understanding the interaction of the subsystems and the system layout and will support further development of the mission.

Previously, a literature study was performed concerning electric propulsion and high power systems. Lessons learned from this literature study [1], in short, are:

- For every mission there is an optimum specific impulse from the mass point of view.
- Ion and Hall thrusters have profound flight heritage and are candidates for the mission.
- For High Power Hall thrusters a Direct Drive Unit (DDU) should be considered as power conditioning system.
- Solar cells have a big impact on the design and therefore a trade-off between different solar cells is required to come to a good selection.
- The dimensions of the large solar array yield to complications regarding its rotation and shadowing. Solutions for the solar array configuration will be evaluated.

The study will be done on behalf of OHB System AG located in Bremen, Germany. From now on they will be referred as being the customer. For designing the major aspects of the SEP stage, engineering software tools will be developed.

Together with the customer, the mission objectives and top-level requirements will be identified in chapter 2. To learn the approaches and specific issues concerning the design of a SEP stage, a literature study on comparable researches will be done in chapter 3. Chapter 4 contains the Mission Analysis, wherein initial orbits will be identified and Δv-budgets determined. Then the SEP stage itself will be designed in chapter 5, followed by an evaluation of its performance in chapter 6. Finally, a conclusion and recommendations will be given in chapter 7. The appendices contain the validation of the Mission Analysis program, data from components used for the stage's design, an overview of the requirements flow-down and the master thesis proposal.

2. Mission Objectives & Requirements

The mission objectives and requirements are defined in order to have a clear overview and direction in which the design is advancing. The study is currently in phase 0, meaning that only the top level objectives and requirements can be identified. First the mission objectives will be formulated, followed by the outline of the mission and system requirements.

2.1. Mission Objectives

The mission is considered to be an international cooperation (e.g. ISECG), due to the mission complexity and high amount of cost. The mission objective defined by the customer is as follows:

- Transportation of cargo (unmanned), at minimum 17 ton (TBC), from Earth environment to a Low Lunar Orbit (LLO), within 200 days, by means of a Solar Electric Propulsion stage and return to the Earth environment for a follow-up mission.

The study objective, defined by the customer, is:

- Improving system understanding of an Solar Electric Propulsion stage.

The mission need statement, derived from the introduction and objectives, is as follows: To realize a conceptual system design of a Solar Electric Propulsion transfer stage which is capable to transport cargo of minimal 17 ton from Earth environment to a Low Lunar Orbit within 200 days and return to the Earth environment for a follow-up mission.

2.2. Mission & System Requirements

In this section the mission and system requirements are deduced from the objectives. The requirements describe the need of what the end product should do and are the key to design and development. They ensure that the end result matches the envisaged outcome of the design.

Only the top level requirements are given, meaning that the total number of requirements is rather limited. This approach is chosen, since the complete design space, in which trades can be performed, can be covered to come to an optimum design. It is chosen to divide the requirements into two groups:

- Mission Requirements
- System Requirements

According to the ESA standards the mission requirements are related to tasks, functions, constraints, or the actions induced by the mission scenario [14]. ESA identifies a phase 0 study to focus on the system functional and technical requirements [15]. Since not many requirements are known at this point, these are grouped in the system requirements and they specify what the system as a whole must perform in order to meet the mission objective and mission need statement. The requirements are obtained in agreement with the customer:

Mission Requirements (MR)

1. The transfer stage shall transport a payload of minimal 17 ton (TBC) from Earth environment to a LLO of 100×100 km within 200 days (TBD).
2. The stage shall be reusable, meaning that the transfer stage shall return from LLO to the initial Earth orbit and perform at least two missions to LLO with the potential of extension to three missions.
3. The transfer stage shall primarily be propelled by electric propulsion.
4. The transfer stage shall be powered by solar panels as primary power source (nuclear power is excluded).
5. The transfer stage and cargo should be launched together (TBC) with one super heavy lift launch vehicle (TBD). The launcher has to be available in the next decade (i.e. SLS or Falcon Heavy).
6. The transfer stage shall dock and un-dock with the cargo, depending on the mission architecture.
7. The transfer stage shall follow End-of-Life regulations.

System Requirements (SR)

1. The transfer stage shall be able to operate in deep-space environment, specifically the environment surrounding the Earth and Moon. This includes the Van Allen belts, solar radiation, solar wind, cosmic radiation, debris and (micro-) meteoroids.
2. The transfer stage shall primarily be using electric propulsion.
   - 2.1 The electric propulsion shall be provided by Ion or Hall thrusters, since they have the most favorable characteristics for this mission type [1].
   - 2.2 The engine can provide thrust during eclipse.
3. The transfer stage shall be powered by solar panels.
   - 3.1 The solar array shall be deployed autonomously.

3.2 The critical systems shall be powered by batteries during eclipse time.

3.3 The EOL power generation of the solar panels shall be sufficient to maintain proper engine functionality.

4. The transfer stage shall have sufficient propellant capacity to perform the transfer.

4.1 The most suitable propellant from performance point of view shall be identified.

5. The transfer stage shall provide thermal control and radiate all excess heat to space.

6. The transfer stage shall provide a separation mechanism from its payload. Due to stage reusability, this shall be a docking mechanism to dock and un-dock with the payload.

7. The transfer stage shall provide 3-axis attitude control during the entire mission.

8. The transfer stage shall be able to communicate with an Earth based ground segment.

9. The transfer stage shall perform the mission automatically, meaning that the stage can perform some operations by itself (TBD) and for other commands can be given during the mission.

10. The transfer stage shall provide electric power to the payload during the transfer.

11. The transfer stage's configuration should be such that the direct impingement of the thrusters' exhaust on the solar arrays is limited (TBD).

12. The configuration shall be such that the thermal radiators, solar panels and the docking mechanisms have a unobstructed field of view.

13. The structure shall be rigid enough to withstand the launch loads and the frequencies that are imposed by the launcher.

These requirements serve as a basis for the phase 0 study and the conceptual design. Also, a first analysis is required to see if these top level requirements can be met. During the whole phase 0 study more thorough requirements will be deduced.

3. Former SEP-stage concepts

The use of an SEP stage to move cargo has only been studied at the conceptual design level. These conceptual designs have shown that SEP is an efficient way of moving large masses from LEO to GEO and beyond, although at the expense of trip time. First a general discussion about SEP-stages will be given here, followed by some results obtained by concept design studies. By studying earlier performed studies the (technical) challenges can be identified together with possible solutions.

There are a number of technical challenges associated with SEP stages. These are mainly the large, high power deployable solar arrays, power management, power architecture, multi-thruster operation, thruster life-time, optimized low thrust guidance and vehicle attitude control [31] [19]. On configuration level the challenge is to position the solar arrays of an SEP vehicle and electric thrusters such that harmful interactions of the arrays with the electric thruster plumes are avoided [19]. The plumes can cause sputtering and contamination of the arrays, which should be avoided. Besides, the arrays should be positioned such to obtain the most power. In case of more than two wings this can be problematic, since array shadowing can occur which reduces the power production. The arrays must also be designed such to avoid arcing and taking into account parasitic plasma electron current collection [31]. Another issue is that the cost and complexity of the solar array increases with a growing area, which influences the feasibility of the mission. Therefore there is a strong desire to keep the solar arrays as small as possible [31].

For a SEP stage usually a direct drive approach is considered for the power management. This Direct Drive power processing Unit (DDU) eliminates the traditional Power Processing Unit (PPU) and instead directly couples the solar array output to the electric thrusters [20] [19] [21]. Eliminating the PPU results in significant mass savings, although system complexity and operational stability becomes a point of concern. However, a number of ground test have demonstrated a stable direct drive operation with a single Hall thruster [31].

The design of an SEP stage compared to a chemical stage is more complicated, while the key systems are highly coupled and the electric power system driving much of the vehicle's design and concept of operations [31]. These challenges indicate that a big effort is required to design, construct, integrate and test an SEP stage.

All SEP concepts use either gridded ion engines or Hall thrusters as means of electric propulsion and typically they use Xenon as propellant. Since all SEP vehicles are con-

ceptual, mostly initial estimates are based on ratios or other simplified 'rule-of-thumb' techniques. The result can therefore be misleading and lead to optimistic estimates for the mass [31].

Reusability of an SEP stage is an asset, since it makes the stage cost effective compared to a cryogenic chemical stage. A logical consequence of the reusability is an increase in lifetime. Currently, the main life time limiters are the solar array degradation and high power Hall thrusters life time [19]. Further development in these areas are needed to obtain more radiation resistant solar arrays and longer lifetimes of Hall thrusters.

With these general results in mind, a closer look can be taken at some conceptual designs and their results. The discussion is limited to two NASA conceptual studies; the SEP Cargo vehicle from 2005 and the HEFT study from 2010 and 2011. The European HiPER program is investigating and developing the technologies required for these missions, but does not have an overall system design at this point.

3.1. SEP Cargo Vehicle to support NASA Lunar Exploration Program 2005

This study was performed to compare a traditional chemical transfer stage to multiple SEP designs. Also key technical challenges and critical technologies were investigated and developed. The information presented in this section is coming from reference [19].

The study researched a reusable variant of an SEP vehicle, which goes to the Moon and back to the Earth, and also a one-way variant, which stays in lunar orbit. The reusable variant consist of two separate vehicles; an Orbital Transfer Vehicle (OTV) and a Cargo Delivery Vehicle (CDV). All reusable components, like the solar arrays, thrusters, PPUs are on the orbital transfer vehicle. The cargo and main propellant tanks are on the cargo delivery vehicle. A disadvantage of the reusable variant is that for all the missions docking with the cargo is required in Earth orbit. Also each cargo spacecraft will be required to bring up the propellant for the transfer to the Moon.

The SEP vehicle is launched into a 550km circular orbit and the target orbit is a LLO of 100x100km. The Δv requirements for this mission are estimated between 7.83 and 8.34km/s. The power level of the SEP vehicle is determined at 600kW and Hall thrusters are selected for this mission because of their high thrust-to-power ratio and high level of technical maturity. The specific impulse of the selected thrusters is 2500s. Due to the high operation power the vehicle can not operate in eclipse, since the mass limitations prohibits a power storage system.

As a consequence of the huge solar array, in total 2400m^2, the drag area is also substantial. This area results in an atmospheric drag in low Earth orbits and therefore limits the orbital lifetime of the vehicle. An analysis showed that an orbit height of 375km should be a safe minimal operating altitude for a few days. However, failures might

occur in these few days and therefore a minimal height of 550km is chosen were the orbit lifetime is 1.5 years. At a height from 1,000km and above almost no drag is present, therefore this orbit is selected to be a parking orbit when no operations are necessary.

In table 3.1 the results for different cargo delivery configurations can be seen. For the multiple cargo design the first value is the cargo that can be delivered the first time, the second value corresponds to all the follow-up missions.

	Chemical	Multiple cargo	One-way
Power Level (kW)	N/A	600	600
Specific Impulse (s)	450	2500	2500
LEO-LLO Transit Time (month)	0.13	5.9/6.5	5.8
LLO-LEO Transit Time (month)	N/A	1.2/1.2	N/A
Thruster firing time (hrs)	N/A	5128/5698	4234
OTV On-orbit Mass (kg)	N/A	7996	7400
CDV dry mass w/o landing stage (kg)	N/A	1840/2120	N/A
Propellant Mass (kg)	42,900	23,001/25,553	18,990
Surface Cargo Delivered (kg)	11,900	19,690/22,439	23,210

Table 3.1.: Comparison of Cargo Delivery Configurations [19].

One of the conclusions from this study is that a high power SEP system is capable of delivering over twice the mass to the lunar surface as compared to a cryogenic chemical system, as can be seen in table 3.1. This comes at the expense of trip time and vehicle dry mass.

The one-way configuration illustrates the cost of having a reusable system compared to a disposable system. In this configuration there is no docking mechanism required and the OTV and CDV are integrated into one vehicle. The resulting increase in delivered cargo is minimal, which shows that the cost of returning the OTV to LEO is negligible to the system.

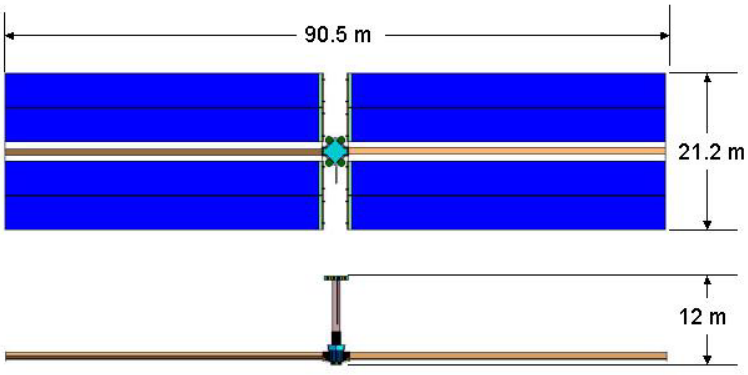

Figure 3.1.: Configuration of the SEP stage [19].

In this design of the SEP vehicle it is chosen to store the propellant cryogenic, at a temperature of -37°C, and at a low pressure of 1.7 MPa. At this pressure the boiling point of Xenon is raised to -35°C, which means that the thermal control system should keep the tank below this temperature. An initial analysis showed that this temperature requirement can be met when the propellant is sufficiently shielded from the rest of the relatively warm spacecraft and has a reasonable radiation view factor to space.

For the attitude control system, which has to perform the critical docking maneuvers, it is chosen to have a standard hydrazine attitude control system, while this system is well understood and has a low risk. The complete configuration of the SEP stage can be seen in figure 3.1.

3.2. Human Exploration Framework Team 2010

In 2010, NASA started to systematically evaluate human exploration mission and architectures. This team, called Human Exploration Framework Team (HEFT), completed some initial top-level studies. Their results will be discussed and can be found in reference [31].

One of the outcomes of the studies was that a Solar Electric Propulsion stage has the potential to be the most effective solution to perform deep space transfer for human missions to Near Earth Objects (NEOs). The study concluded that a SEP vehicle reduces launch mass by a factor of two. Besides, these architectures are robust with respect to mass growth when more Δv is required, because of the high specific impulse of the propulsion system [31].

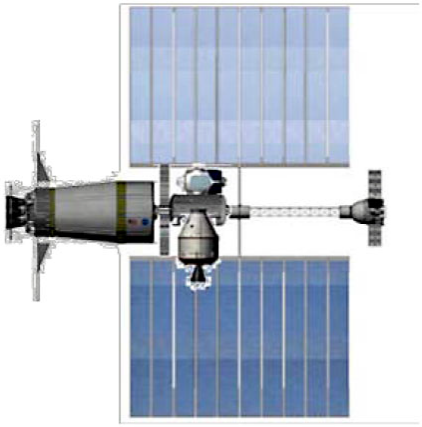

Figure 3.2.: SEP vehicle of the HEFT study [31].

The HEFT study examined the usage of a SEP vehicle to support a human mission to a near Earth asteroid. For this mission two 300-kW SEP stages would be used. The first would be launched to LEO and used to spiral cargo, a large cryogenic propulsion stage, to the Earth-Moon Lagrange point 1 (L1). The second SEP vehicle would bring a deep

space habitat, a space exploration vehicle and a propulsion kick stage from LEO to L1. A third launch would bring up a crew transfer vehicle and a second cryogenic propulsion stage, to transport the crew to L1 and dock to the deep space habitat. The second SEP stage would then be used to bring the crew, deep space habitat, space exploration vehicle and crew transfer vehicle to a near Earth asteroid and back within a year (see figure 3.2). The advantage of this mission is that the entire mission can be accomplished with only three heavy lift launches, which is half the number when using all-chemical propulsion [31].

For the solar array wings the Inverted Metamorphic (IMM) solar cells were identified as the leading candidate to become the next generation solar cell technology. These cells combine increased efficiency with a lower mass compared to conventional triple junction solar cells [31]. The solar array wings are consisting out of these IMM cells, which have an efficiency of 33% and an areal density of 260W/m^2 at array level. The specific power at array level is 200 W/kg, generating 390kW and 337Vdc at Beggining Of Life (BOL), having a total deployed area of 1,400 to 1,500m^2 [31].

To keep the trip time reasonable (within 1 year) for this mission the specific impulse was chosen to be 2,000s. A logical consequence of this relatively low specific impulse is that Hall thrusters are selected as propulsion type. The NASA-457M was indicated as a thruster that could meet the mission requirements with some modest amount of further development. A total of eight thrusters would be required, each operating at 37.5kW. The key remaining major challenges in this area are to demonstrate reliable thruster operation over the required lifetime and to ensure no adverse effects from multi-thruster operation [31].

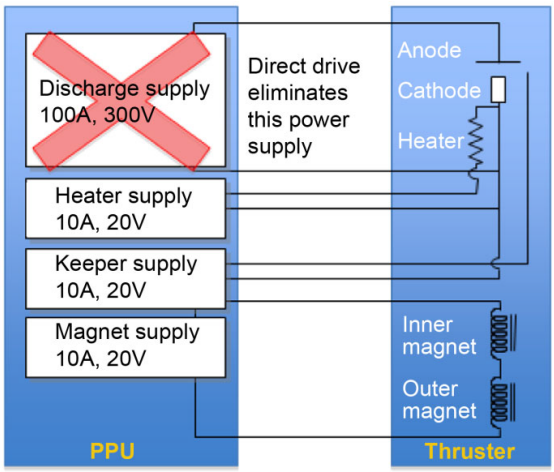

Figure 3.3.: A Direct Drive Unit, eliminating the discharge power supply of a Hall thruster [31].

The selection of a Hall thruster as propulsion system, leads to a interesting trade off concerning the power system. The discharge voltage of a Hall thruster typically operates at 300 to 400Vdc. If the solar array can function at these voltages, the need for an extra

PPU at the engine is eliminated (see figure 3.3). At these significant power levels, this results in a mass saving greater than 50% concerning the PPU, while also decreasing the cost and complexity [31].

Another benefit of the direct drive approach is that due to the higher operating voltage the losses in the cables are reduced, consequently reducing the cable mass. This study indicated that operating at 300Vdc could reduce the mass of the vehicle by more than 2,400kg compared to a voltage of 160Vdc. However, higher operating voltages increase the probability of solar array arcing and spacecraft charging, which need to be dealt with [31].

3.3. 300kW SEP stage for Human Exploration 2011

The continuation of the HEFT research, resulted in a preliminary design of a 300 kW SEP stage for Human Exploration of Near-Earth Asteroids (see figure 3.4). The information presented here is coming from reference [20].

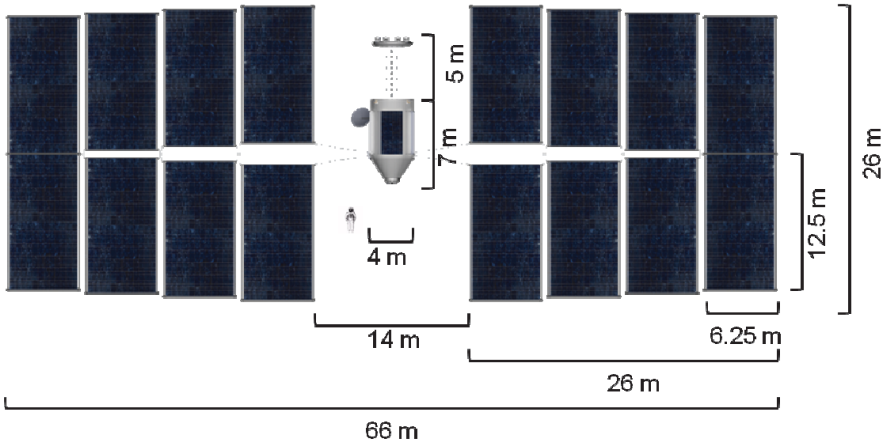

Figure 3.4.: 300kW SEP vehicle of the HEFT study [20].

The approach taken in designing this stage is to minimize the use of new technology where ever possible. This is done to obtain a more realistic cost budget, even though it resulted in a higher system mass. The main goal of the stage is to transport 40,000kg of cargo from LEO to high-perigee HEO (60,000x400,000km) within less than 2 years.

The solar cells selected for this mission are the Inverted Metamorphic (IMM) solar cells, which are assumed to have an efficiency of 33% and a thickness of only 10μm. The cells are mounted to a 5μm kapton substrate and the front and back glass covers are each 125μm thick, completing the blanket assembly (except for wiring). The glass covers reduce the total radiation dose on the cells induced by the radiation belts, resulting in a blanket consisting mostly out of glass.

To produce a total power of 350kW at 1 AU with these cells, a total area of 800m^2 is required, which means an area of 400m^2 per wing. One of the most significant require-

ments is the need for an autonomously deployable solar array with this area. In addition, the wings must be capable of withstanding a load of maximum 0.2-g due to the firing of a cryogenic kick stage. Also, the first-mode natural frequency must be greater than 0.1Hz when fully deployed. In a stowed configuration, the specific power density should be greater than 70 kW/m^3. The BOL specific mass of the solar array should be less than 5kg/kW (specific power of > 200W/kg). Furthermore, to minimize the moment of inertia around the roll axis of the spacecraft and to lower solar array and solar-array-gimbal bending moments, the array configuration should have an aspect ratio of approximately 1-to-1.

The electric propulsion system is consisting out of eight thrusters of which seven are operating simultaneously, with a total input power of 300kW. The PPUs must be capable of processing up to 43kW with input voltages over the range of 250 to 350V and an efficiency of $\geq 95\%$. Their maximum allowable operating temperature is $60°C$ and they have a specific mass of < 1.8kg/kW. The thrusters have a specific impulse of 2000 s and an efficiency of 60%. At 1 AU their minimum thrust level is 18N. The specific mass of the thrusters must be < 1.9kg/kW, while the gimbals shall not exceed 50% of the thruster mass. The thrusters operate on Xenon as propellant. In total the storage system stores up to 40,000kg of Xenon of which 37,000kg is used for the mission.

The heat produced by the PPUs needs to be rejected, which is done by the thermal control system. This system needs to radiate about 15kW of PPU heat at their maximum operating temperature. Therefore, a total radiator surface area of about $28m^2$ is required, assuming that the radiators do not see any warm bodies, with an IR emissivity of about 0.86 (white paint) and a fin effectiveness of about 90%. The vehicle has two radiators of $14m^2$ mounted to the spacecraft structure. Moreover, another 5kW of heat caused by other power loads need to be rejected by additional radiator area, which is currently not included in the design. The heat is transported by imbedded loop-heat pipes to the radiators, while having a specific mass for the total system of < 25kg/kW.

Instead of a PPU also a design with a DDU was considered. This design resulted in a slightly smaller solar array and significantly less waste heat. Therefore, potentially this system is much easier to develop. The DDU also has an input power of 43kW and is estimated to have a mass of 17kg. In total eight DDUs are required, saving a total mass of about 500kg compared to PPUs, not counting the structure and thermal subsystem mass savings and reduction in solar array size.

In case of a DDU system, the other loads of the spacecraft are supplied by a separate electric segment of the solar array. This segment of the array is operating at a different voltage level, eliminating the need for a high-voltage down converter.

As said, the SEP stage needs to store approximately 40,000kg of Xenon. This is done in seamless aluminum-lined composite overwrapped pressure vessels. Each tank has a diameter of 1m by 4.5m long and can store up to 4,900kg with a maximum design pressure of 10MPa. In total eight tanks are required to store the propellant.

With all the information presented a rough high level mass estimate was performed for the two concepts, see table 3.2. The concept with the DDU has a reduced vehicle dry mass of about 1.4ton and wet mass by 2.6ton. One of the main conclusions of this study was that by using SEP stages the number of heavy lift launches is halved into a total of three launches.

	Total Mass with margin (kg)	
Subsystem	PPU-concept	DDU-concept
Structures & Mechanism	2535	2305
Ion Propulsion	4376	3739
Electric Power	3391	3286
Reaction Control	230	230
Command & Data Handling	87	87
Attitude Control	19	19
Thermal Control	1049	659
RF Communications	41	41
Spacecraft Harness	365	365
Total Dry Mass	12095	10733
Xenon Mass	40150	39017
Wet Mass	52245	49663

Table 3.2.: Mass estimate of a 300 kW SEP stage for a PPU and DDU within the HEFT study [20].

4. Mission Analysis

The mission analysis plays a crucial role in the conceptual design study and poses a complex task. The analysis is needed to determine the Δv-budget, which is equivalent to the propellant mass for a given I_{sp}, and the mission duration. An optimization of the mission time is excluded, which means that no specific predefined launch date and arrival date are determined. In the current design phase only the overall mission time is relevant.

The thrust level of electric propulsion is very low compared to chemical, therefore a spiral transfer needs to be conducted to go to the Moon (section 4.1). The Δv and transfer time depends on the initial acceleration of the spacecraft and is thus depending on the performance of the propulsion system, which is again tightly coupled to the performance of the power system. This illustrates that there is a strong interdependency between the mission analysis and the design of a Solar Electric Propulsion stage, especially the propulsion and electric power system (see figure 4.1).

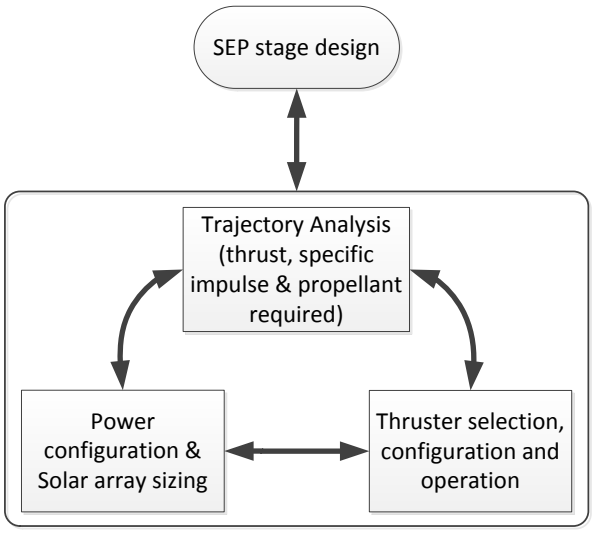

Figure 4.1.: The interdependencies in designing a SEP stage [22].

A heavy lift launcher has to transport the SEP stage and payload to an initial orbit, which are examined in section 4.2 about the mission architecture. Due to the high interdependencies, an initial mass budget is required to obtain results for the Δv, I_{sp}, initial acceleration and total mission time. Also, the total radiation dose upon the solar array will be evaluated within the environmental factors section (section 4.4). The overall analysis will be used in the design phase of the different subsystems (see chapter 5).

4.1. Spiral Transfer Strategy

As stated, the SEP stage will conduct a spiral transfer to the Moon. The general orbit geometry of a spacecraft within a two dimensional reference frame is described by the velocity $\bar{v}$, flight path angle ϕ, radius $\bar{r}$, true anomaly ν, semi-major axis a, eccentricity e, semi-minor axis b and the semi-latus rectum p (see figure 4.2). In figure 4.2 the Earth is in one of the focal points of the ellipse and has a radius R_E.

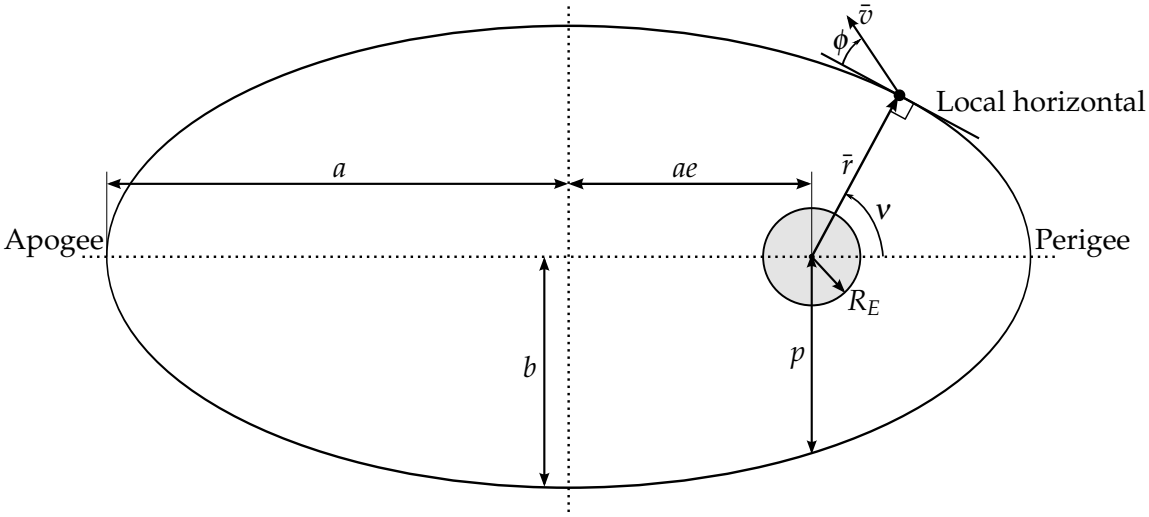

Figure 4.2.: Elliptical orbit with Keplerian Orbital elements, derived from reference [9].

The Δv-budget to accomplish the transfer needs to be determined in order to have a thorough mission analysis. A spiral transfer is from the Δv point of view not the ideal case, since losses occur. These losses can be explained by first having a look to the ideal HOHMANN transfer (see figure 4.3), in which the transfer from an initial orbit to a final orbit is done most efficiently from a Δv point of view [1].

The HOHMANN transfer states that the minimum change in velocity between orbits can be achieved by using two tangential burns (see figure 4.3). The flight path angle must be equal to zero at the point were the impulsive shot is applied, so in an elliptical transfer orbit this can only be done in the apogee or perigee. At this point the semi-major axis and eccentricity are changed exclusively. However, in reality there is no impulsive shot and a finite burn time is required to deliver a Δv. During this burn the flight path angle is only for a limited time equal to zero, in the duration that it is unequal to zero, energy will be lost. These energy losses are called gravity losses, Δv_{Gl}.

An ideal HOHMANN transfer to the Moon requires a Δv of 3.9 km/s [80]. In our case constant thrust is applied during the spiral transfer and the flight path angle is per orbit only briefly equal to zero. Therefore, a spiral transfer is from the Δv point of view very inefficient and results in high gravity losses.

[1] In some cases a bi-elliptic transfer is more efficient than a HOHMANN transfer [4].

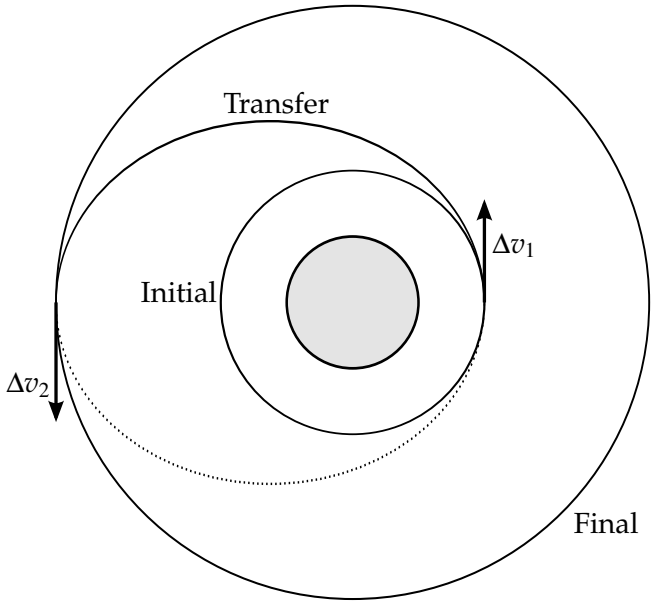

Figure 4.3.: Illustration of an ideal Hohmann transfer [4].

A launch from Cape Canaveral would result in a inclination of 28.5°. The Moon has an inclined orbit of 5.1° towards the ecliptic, while the Earth's equator is 23.5° inclined to the ecliptic. This configuration results in a Moon inclination between 18.3° and 28.6° with respect to the Earth, because the longitude of the ascending node and therefore the Moon's plane is changing over time. The period for this periodic movement is 18.6 years, meaning that with the right timing no inclination change is required. The maximum declination of the Moon is again reached in April 2025. This phenomenon is called the 'major lunar standstill' [45]. In case the mission is performed in this time period, no inclination and longitude of the ascending node change would be required neither by the solar electric stage nor by the launcher upper stage. Therefore it is assumed that the stage is spiraling in a two dimensional plane to the Moon and that neither the inclination nor the longitude of the ascending node of the stage need to be changed.

At this moment no reliable analytical solutions exists to solve a spiral transfer. Therefore, a program within the SCILAB environment is written, which solves the equations of motion numerically in order to reach an end-orbit with certain desired conditions. The program is based upon the following assumptions:

- The Earth and Moon are considered to be point masses
- The Earth and Moon stay at the same distance from each other.
- The Lunar sphere of influence is a perfect sphere.
- The problem is a two-body problem, meaning that first the spacecraft spirals in the Earth system up to the lunar sphere of influence and then spirals within the Moon system. No third-body perturbations are considered.
- Other perturbations, like solar radiation pressure and atmospheric drag, are not considered.

- The Moon is present when the spacecraft arrives at lunar sphere of influence radius.
- The Moon and the SEP stage are situated in the same orbital plane, i.e. they have the same inclination and longitude of the ascending node.

The SPIRAL PROGRAM is further elaborated in the next sections.

4.1.1. Equations of Motion

For the Earth and the Moon an inertial reference frame is selected. This means that the rotation of the Earth around the Sun and the resulting Coriolis force is neglected. The spacecraft is moving in these two reference frames, of which the velocity, $\bar{v}$, flight path angle, ϕ, radius, $\bar{r}$ and true anomaly, ν, are changing over time. This change is formulated within the equations of motion, which are taken from reference [9] and are given in the Local Vertical Local Horizontal (LVLH) reference frame. Within this frame the spacecraft's center of mass is the origin, the x-axis is perpendicular to the radius vector (local horizon) and in the direction of the velocity, the z-axis (local vertical) is perpendicular to the x-axis and the y-axis is perpendicular to the xz-plane. The time derivative of the velocity, $\dot{v}$, in the LVLH reference frame is depending on the thrust F, mass of the stage m_{SEP}, thrust angle θ, standard gravitational parameter μ, radius to the object r and the flight path angle ϕ:

$$\dot{v} = \frac{F}{m_{SEP}} \cos\theta - \frac{\mu}{r^2} \sin\phi. \tag{4.1}$$

The variation of the flight path angle with time is calculated with:

$$\dot{\phi} = \frac{1}{v}\left[\frac{F}{m_{SEP}} \sin\theta - \left(\frac{\mu}{r^2} - \frac{v^2}{r}\right)\cos\phi\right]. \tag{4.2}$$

The thrust angle within these two equations is used to define the direction of thrust. In general there are two possibilities:

- Spiral up: thrust angle of 0°.
- Spiral down: thrust angle of 180°.

The radius changes with the direction and magnitude of the velocity vector:

$$\dot{r} = v \sin\phi. \tag{4.3}$$

The propellant mass has to be computed, which is the change in mass integrated over time:

$$\dot{m} = -\frac{F}{c_e}. \tag{4.4}$$

Where c_e is the characteristic velocity, which is equal to the specific impulse, I_{sp}, times the standard gravity, g_0. This forms the set of ordinary differential equations which are necessary to determine the motion of the spacecraft in the LVLH reference frame. To determine the position of the spacecraft in the inertial reference frame, it is convenient to calculate the position angle for every time step:

$$\dot{\psi} = \frac{v \cos \phi}{r}. \tag{4.5}$$

The integration of this rotational angle is the position angle with respect to the start of the maneuver. Note that this angle is not the true anomaly. The state vector is then:

$$\bar{u} = \begin{bmatrix} \bar{v} \\ \phi \\ \bar{r} \\ m \\ \psi \end{bmatrix}. \tag{4.6}$$

And the set of ordinary differential equations which are used to solve the state vector:

$$\dot{\bar{u}} = \begin{bmatrix} \dot{\bar{v}} \\ \dot{\phi} \\ \dot{\bar{r}} \\ \dot{m} \\ \dot{\psi} \end{bmatrix} . = \begin{bmatrix} \frac{F}{m_{SEP}} \cos \theta - \frac{\mu}{r^2} \sin \phi \\ \frac{1}{v} \left[\frac{F}{m_{SEP}} \sin \theta - \left(\frac{\mu}{r^2} - \frac{v^2}{r} \right) \cos \phi \right] \\ v \sin \phi \\ -\frac{F}{c_e} \\ \frac{v \cos \phi}{r} \end{bmatrix} \tag{4.7}$$

These equations are applied in a propagator within the SPIRAL PROGRAM, which calculates for every time step the new velocity, flight path angle, position and mass of the spacecraft, such that the spiral transfer within the Earth and Moon system can be simulated.

4.1.2. Conditions at Lunar Sphere Of Influence

When the spacecraft reaches the lunar sphere of influence, a switch to the Moon system has to be made. To change the coordinates from the Earth system to the Moon system, a method is used from reference [8]. When the spacecraft reaches the lunar sphere of influence, the Moon is considered to be the central body. Hence, there has to be a method to calculate the new velocity, flight path angle and position in the Moon system, which is described in this section.

The sphere of influence of the Moon, r_{soi}, is depending on the mass ratio of the Earth

and the Moon and is calculated by using the definition of LAPLACE [8]:

$$r_{soi} = D\left(\frac{m_M}{m_E}\right)^{2/5}. \tag{4.8}$$

Where D is the distance from the Earth to the Moon, with a mean value of 384,399 km. When the spacecraft enters the lunar sphere of influence, the Moon is considered to be the central body. To go from the Earth- to the Moon-system, the speed and direction of the spacecraft relative to the center of the Moon has to be derived in the so-called 'Patch Point'. The patch point conditions can be seen in figure 4.4.

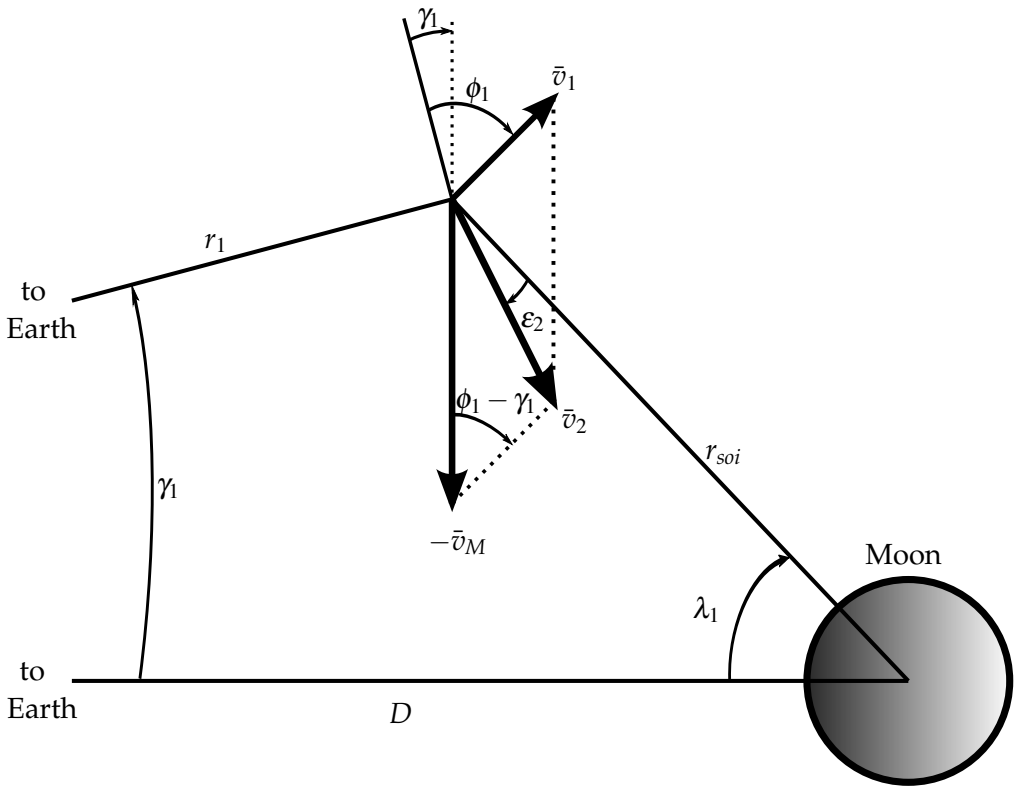

Figure 4.4.: Illustration of the patch point conditions [8].

The angle λ_1 in figure 4.4 specifies the point at which the geocentric trajectory crosses the lunar sphere of influence and is called the patch point angle. The value of λ_1 is set such that the spacecraft enters a bound orbit around the Moon. Negative λ-values results in a positive orbital energy of the spacecraft. Meaning that the spacecraft is unbound and performs a gravity assist, since it is accelerated by the Moon's velocity vector. For λ between 90 and 180°, the probability of overshooting the Moon system is increased and also a higher propellant mass is required. This shows that the patch point angle has to be in between 0 and 90°.

The radius to which the spacecraft has to travel within the Earth system, r_1, can be calculated by using the law of cosines:

$$r_1 = \sqrt{D^2 + r_{soi}^2 - 2Dr_{soi}\cos\lambda_1}. \tag{4.9}$$

The propagator integrates the equations of motion until r_1 is reached. From the law of sines the angle between r_1 and the distance D, γ_1, can be determined:

$$\sin\gamma_1 = \frac{r_{soi}}{r_1}\sin\lambda_1. \tag{4.10}$$

The speed of the Moon relative to the center of the Earth is equal to 1.018 km/s. The new speed when the lunar sphere of influence is entered, v_2, can be obtained using the law of cosines:

$$v_2 = \sqrt{v_1^2 + v_M^2 - 2v_1 v_M \cos(\phi_1 - \gamma_1)}. \tag{4.11}$$

The angle, ε_2 is needed to obtain the direction of the new velocity vector relative to the Moon's center. Equating the components of v_2 perpendicular to r_{soi} results in:

$$v_2 \sin\varepsilon_2 = v_M \cos\lambda_1 - v_1 \cos(\lambda_1 + \gamma_1 - \phi_1). \tag{4.12}$$

Solving for ε_2 gives:

$$\varepsilon_2 = \sin^{-1}\left[\frac{v_M}{v_2}\cos\lambda_1 - \frac{v_1}{v_2}\cos(\lambda_1 + \gamma_1 - \phi_1)\right]. \tag{4.13}$$

The new flight path angle, ϕ_2, in the Moon system is now:

$$\phi_2 = \varepsilon_2 - 90^\circ. \tag{4.14}$$

The new flight path angle and velocity within the Moon system can be inserted into the equations of motion as initial conditions. From here on, the numerical integration within the Moon system can be executed until the targeted Low Lunar Orbit is reached.

For a return from the Moon to the Earth system, the same approach is used and a λ angle must be chosen. When λ is in between 0 and 90°, the resulting flight path angle in the Earth system is positive, meaning that the stage is moving towards the apogee and therefore going into a undesired higher orbit. In case the angle is in between 0 and -90° (opposite direction as in figure 4.4), the resulting flight path angle is negative and the stage is moving towards a lower orbit. This is obviously the most desired case and therefore the conditions change to the one seen in figure 4.5. In here the subscript 1 is defining the velocity vector and flight path angle with respect to the Earth system, the subscript 2 is defining them with respect to the Moon system. For calculating r_1 and γ_1 the formulas 4.9 and 4.10 can be used respectively. The formula for calculating the velocity in the Earth system becomes:

$$v_1 = \sqrt{v_2^2 + v_M^2 - 2v_2 v_M \cos(-\lambda_1 - \phi_2)}. \tag{4.15}$$

And the new flight path angle in the Earth system is calculated by:

$$\phi_1 = \sin^{-1}\left[\frac{v_M}{v_1}\sin\gamma_1 - \frac{v_2}{v_1}\sin(\lambda_1 + \gamma_1 + \phi_2)\right]. \tag{4.16}$$

Now the new state within the Earth system is known and the numerical integration can be performed to spiral down to a predefined Earth orbit.

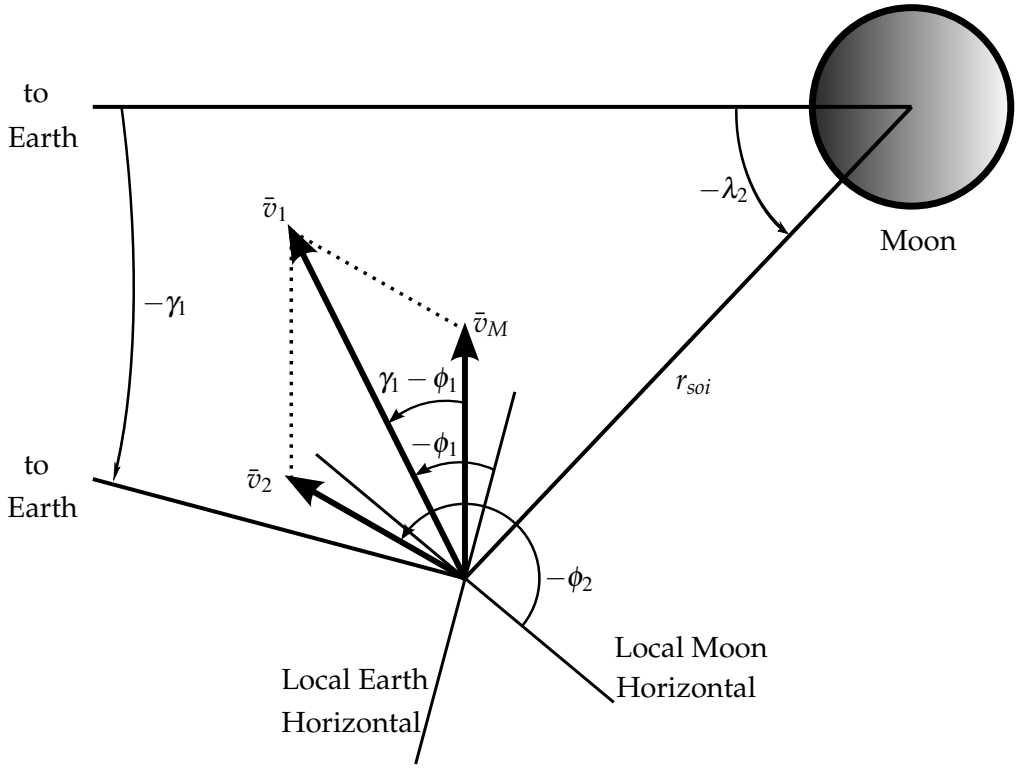

Figure 4.5.: Illustration of the patch point conditions when going back to the Earth system.

4.1.3. Model of the Earth and Moon shadow

During eclipse time, the thrusters will not be operated, simply because the mass of an energy storage system (batteries, fuel cells, etc.) is too demanding to supply this amount of power. The consequence of not applying thrust in eclipse is that it gives an impact on the trajectory and on the mission time.

The required power level of the SEP-stage is so high, that batteries can not be included into the design without exceeding the mass budget. As a consequence no thrust is applied when the satellite is in eclipse, which has an impact on the trajectory and mission time. Therefore, it is included within the propagator of the simulation.

The shadow is assumed to be positioned in a straight line behind the Earth and the

Moon respectively, see figure 4.6. It has to be noted that this model, though sufficient for our purposes, is certainly a simplification of the real circumstances. In reality, two shadow regimes will be present; penumbra and umbra.

The rotation speed of the planets determine the propagation of the shadow. The rotation of the Earth around the Sun and the Moon around the Earth equals [8]:

$$\omega_E = 1.991 \cdot 10^{-7} \text{rad/s} \tag{4.17}$$

$$\omega_M = 2.6459 \cdot 10^{-6} \text{rad/s} \tag{4.18}$$

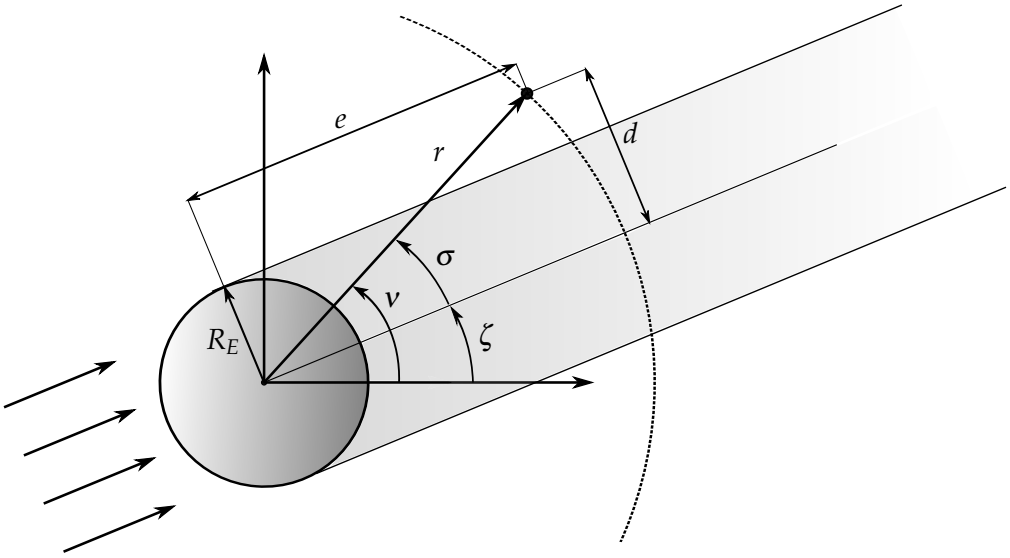

Figure 4.6.: Illustration of the Earth's shadow.

The Moon's reference frame is chosen to be a inertial (non-rotating) reference frame. This means that the shadow of the Moon is at exactly the same angle as the Earth's shadow and the shadow's rotation equals the Earth's rotation:

$$\omega_{M-shadow} = \omega_{E-shadow} = 1.991 \cdot 10^{-7} \text{rad/s} \tag{4.19}$$

In the simulation an angle, ζ, is defined which moves with the time integral of the angular velocity $\omega_{M-shadow}$. A second angle, σ, is defined, which is the angle between the true anomaly and ζ. The distance of the spacecraft to the center of the shadow can be calculated by using basic geometry:

$$d = r \sin \sigma \tag{4.20}$$

Now two conditions have to be fulfilled to test if the spacecraft is within the shadow. First the distance d has to be smaller than the radius of the Earth and secondly the distance e has to be positive. When both conditions are true, the spacecraft is in the shadow and the thrust is set to zero. At the point where the stage is moving out of the shadow, the thrust is set to its initial value.

4.1.4. Spiral Program

With all the information from the preceding sections, section 4.1.1 to 4.1.3, the SPIRAL PROGRAM can be made inside the SCILAB environment. The structure of this program is displayed in multiple flow charts. In figure 4.7 the flow chart of the main routine, called RUN.sce, can be found.

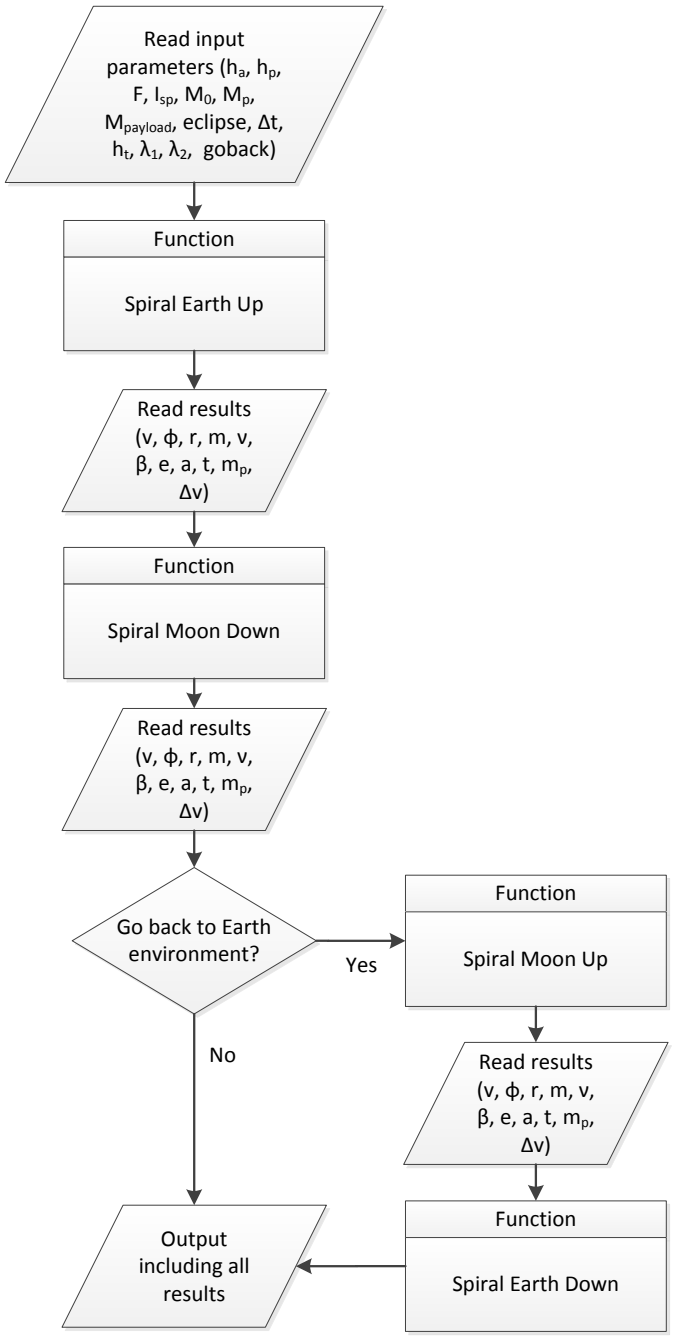

Figure 4.7.: Flow Chart of RUN.sce which is the main file of the program.

The main routine requires input parameters in order to run. Then it calls multiple sub-routines, which are functions, to simulate the transfer of the spacecraft. The flowcharts of these functions are displayed in the figures 4.8 to 4.11. Between the four functions,

there are not many differences. The main differences are the loop conditions and the initial calculations when going from the Earth reference frame to the Moon reference frame and vice versa.

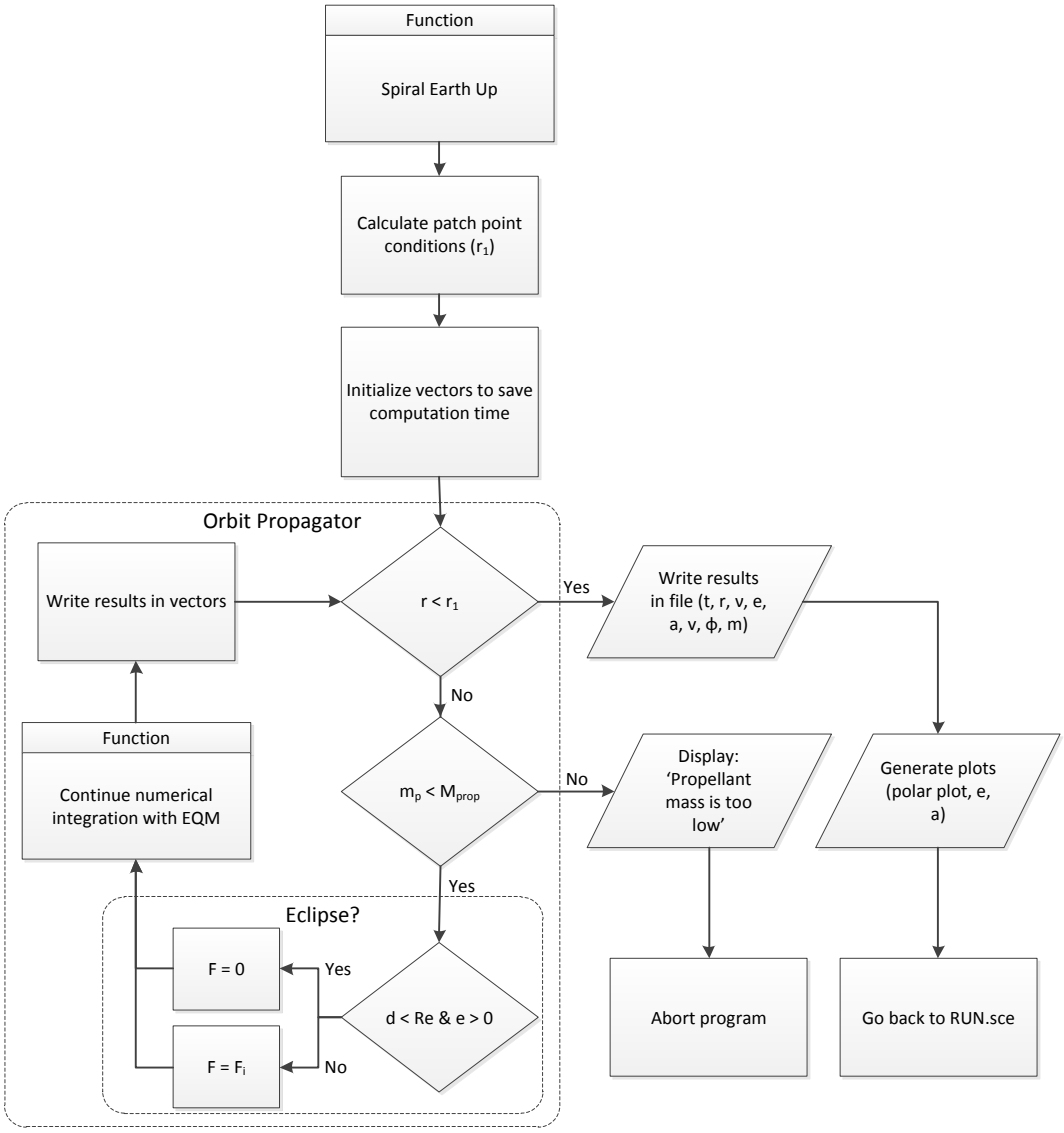

Figure 4.8.: Flow Chart of the function 'Spiral Earth Up'.

The initial eccentricity for the two spiraling down functions, figure 4.9 and 4.11, is very high and a strategy has to be chosen to cancel it out. Within these functions the orbit is lowered by applying a thrust direction opposite to the flight direction. The eccentricity is canceled out by not giving thrust when the radius is larger than the semi-major axis, thus in the apogee region. It is damped out to a value of 0.1, which is sufficient for the preliminary analysis.

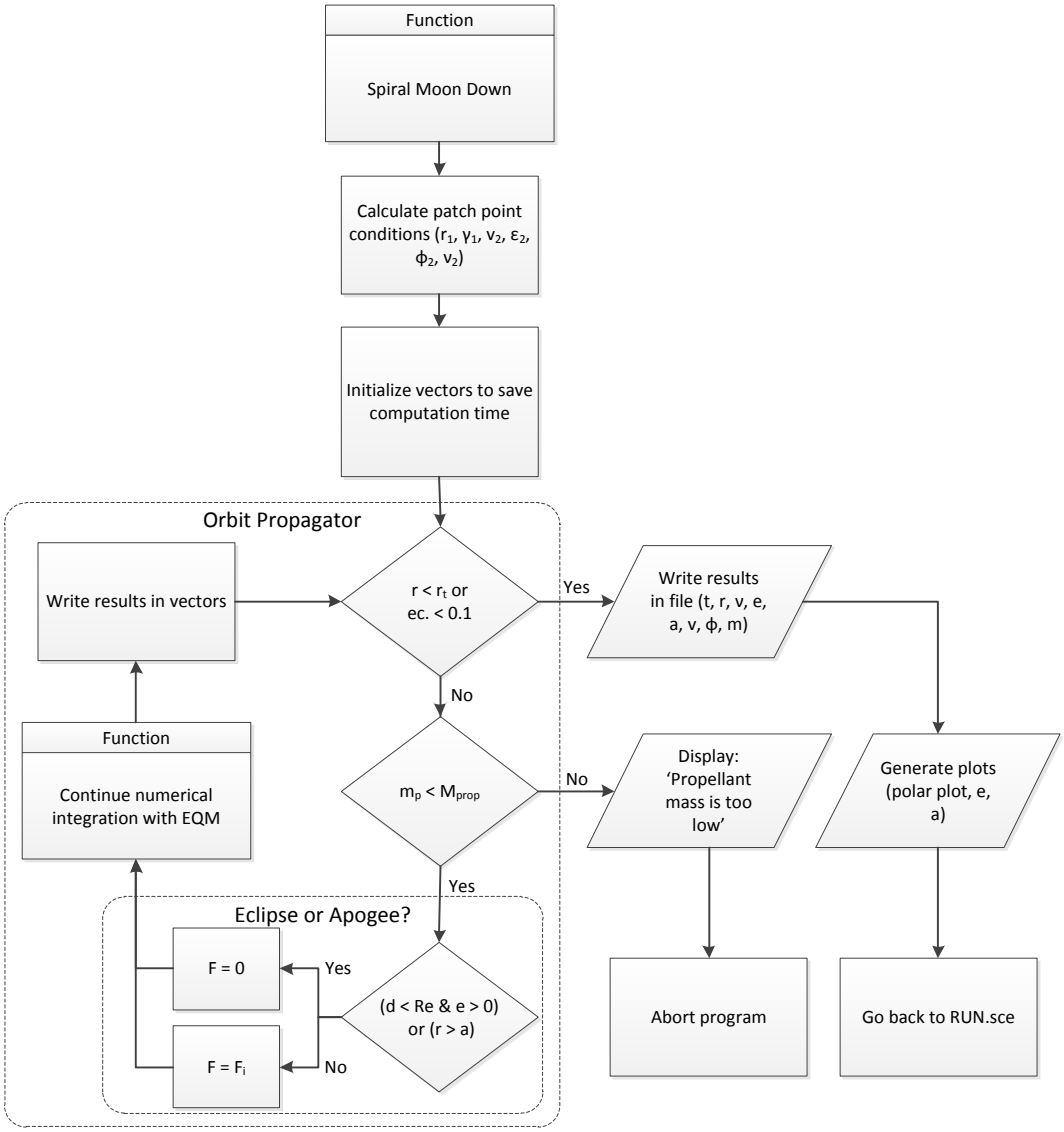

Figure 4.9.: Flow Chart of the function 'Spiral Moon Down'.

The equations of motion are also stored into one function, which is called by the main four functions when they perform the integration. No flowchart of this function is given, since it is very straightforward and only contains the equations of motion. The numerical integration is performed by the RUNGE-KUTTA-FEHLBERG method of order 4 and 5 is used, which is present within the SCILAB library.

Another simplification is the fact that continuous thrust is applied when the spacecraft is in the true anomaly region of 90° and 270°. In this area not all the energy is used in an efficient way, since an orbit is most efficiently raised when firing in an apogee and/or perigee. The energy inserted into the orbit near the semi-minor axis will be 'dissipated' into changing the argument of perigee, which is for a true anomaly of 0 to 180° larger than zero and for 180 to 360° smaller than zero. The sum after one orbit would equal to zero in case no eclipse is present. Since in this case an eclipse is present, there would be

a small change in the argument of perigee.

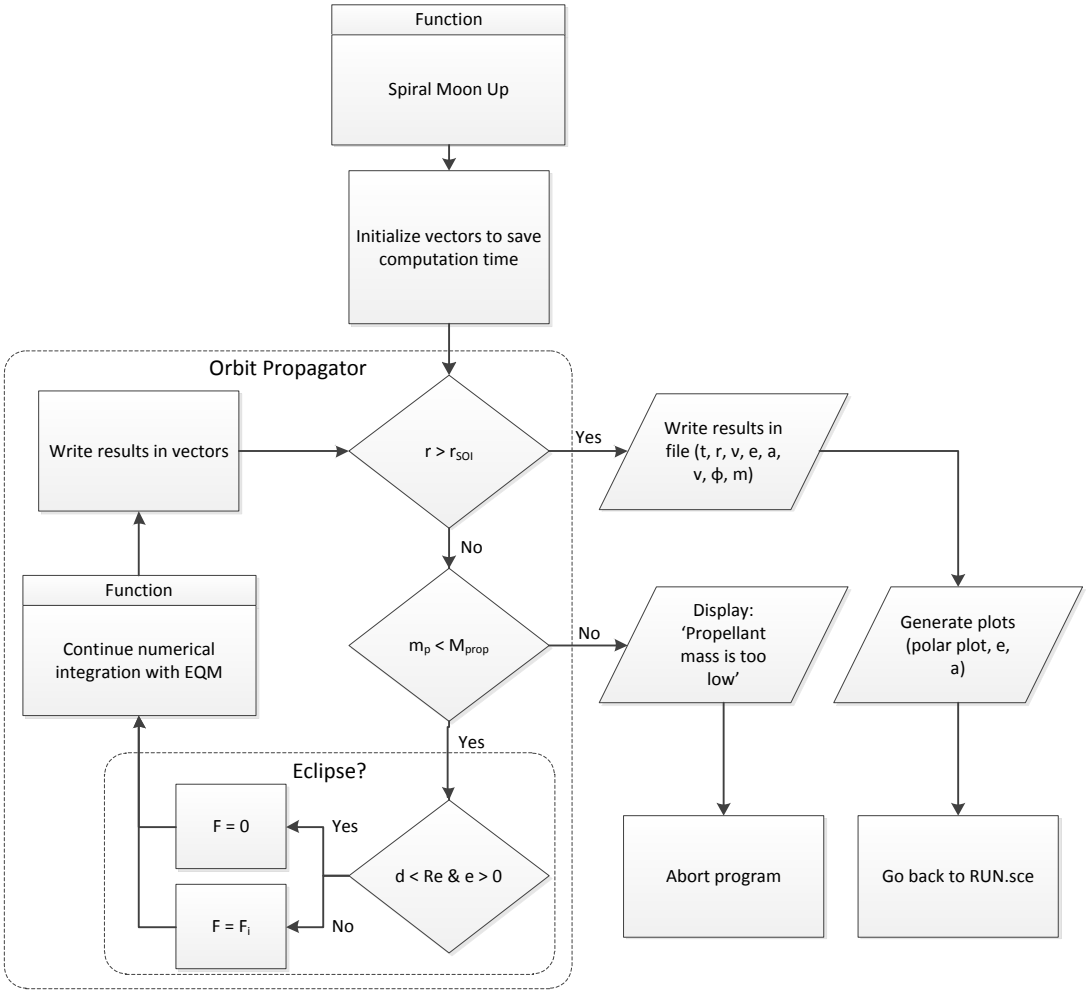

Figure 4.10.: Flow Chart of the function 'Spiral Moon Up'.

The method that is presented here is not sufficient for a complete detailed trajectory analysis, but it is perfectly sufficient for a first mission analysis to have a good initial Δv calculation (including gravity losses) and to have an indication of the mission time.

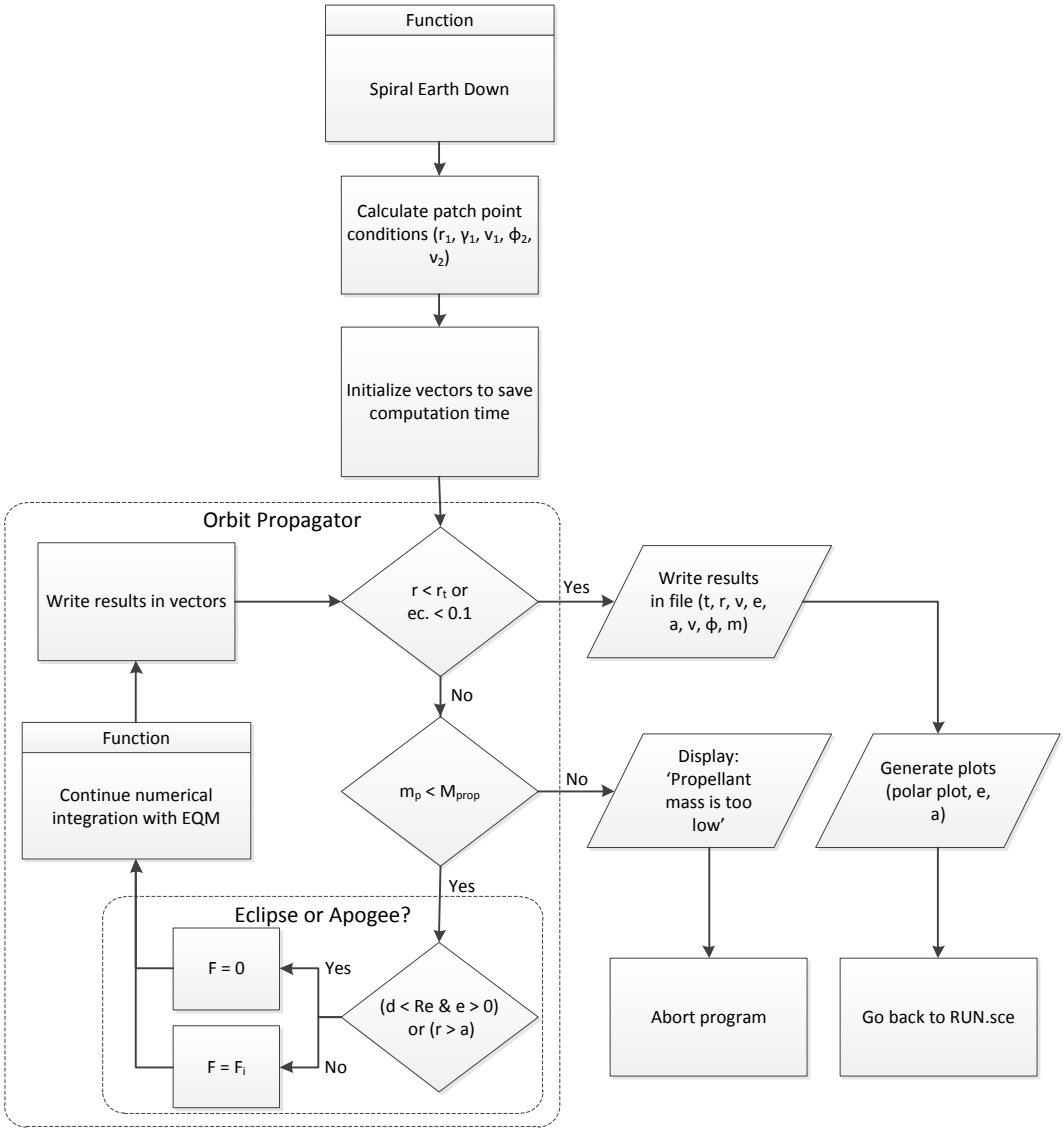

Figure 4.11.: Flow Chart of the function 'Spiral Earth Down'.

4.1.5. Patch point angle selection

The patch point angle specifies the point at which the geocentric trajectory crosses the lunar sphere of influence, see figure 4.4. As discussed in section 4.1.2, the angle has to be in between 0 and 90°. However, the program demonstrated that in many cases the velocity of the spacecraft at the patch point relative to the Moon was positive, meaning that the spacecraft is actually moving away from the lunar sphere of influence. However, in case the simulation would be propagated (with no thrust) and the spacecraft passes the Earth-Moon distance, the spacecraft will be slower than the Moon and can enter the sphere of influence from a patch point angle in between 90 and 180°. The last approach is more realistic, but from an energetic point of view does not differ from the first approach. Therefore, this is in the current design phase not considered to be of

major importance. Proper mission analysis in later design phases has to guarantee that the spacecraft can be overtaken by the lunar sphere of influence.

The patch point angle is set within the SPIRAL PROGRAM and has an impact on the outcome. This impact is evaluated by running multiple simulations for different initial accelerations:

- Initial mass: 49,613 kg
- Initial orbit: 500 x 500 km
- Time interval: 200 s
- Specific Impulse: 2800 s
- Eclipse: yes (Initial ζ: 180°)
- Initial thrust-to-mass ratios: $3.2 \cdot 10^{-4}$, $4 \cdot 10^{-4}$, $6.5 \cdot 10^{-4}$ and $1 \cdot 10^{-3}$ m/s^2

The simulations are performed for λ_1-values in between 10 and 80°. The resulting propellant mass, Δv and transfer time duration for one acceleration of $4 \cdot 10^{-4}$ m/s^2, can be found in table 4.1. The table shows that for different λ-values, different propellant masses and transfer time durations are obtained. It demonstrates that the conditions at the patch point determine how much extra propellant and time is required to obtain a LLO with an eccentricity of 0.1.

λ_1 (°)	M_p (kg)	ΔV (m/s)	t (days)
10	12075.2	7658.3	252.6
20	12141.3	7706.7	245.9
30	12172.2	7729.4	242.2
40	12180.2	7735.3	242.1
50	12180.6	7735.6	243.1
60	12182.6	7737.0	244.8
70	12194.6	7745.8	245.0
80	12208.2	7755.8	245.5

Table 4.1.: Impact of different λ-values on results, having an initial acceleration of $4 \cdot 10^{-4}$ m/s^2.

The outcomes for the different initial accelerations are shown in figure 4.12. The largest deviation can be found for an initial acceleration of $6.5 \cdot 10^{-4}$ m/s^2, which is 248 m/s, corresponding to 3.3%. This is considered to be negligible for the current mission analysis.

For future simulations it is desired to fix the patch point angle, such that the optimum or conservative value does not have to be found for every simulation. At this point in the design phase it is chosen to have a conservative patch point angle of 30°. As a consequence, a slightly different initial acceleration can result in a different Δv outcome,

within a range of $\pm 300\,\mathrm{m/s}$.

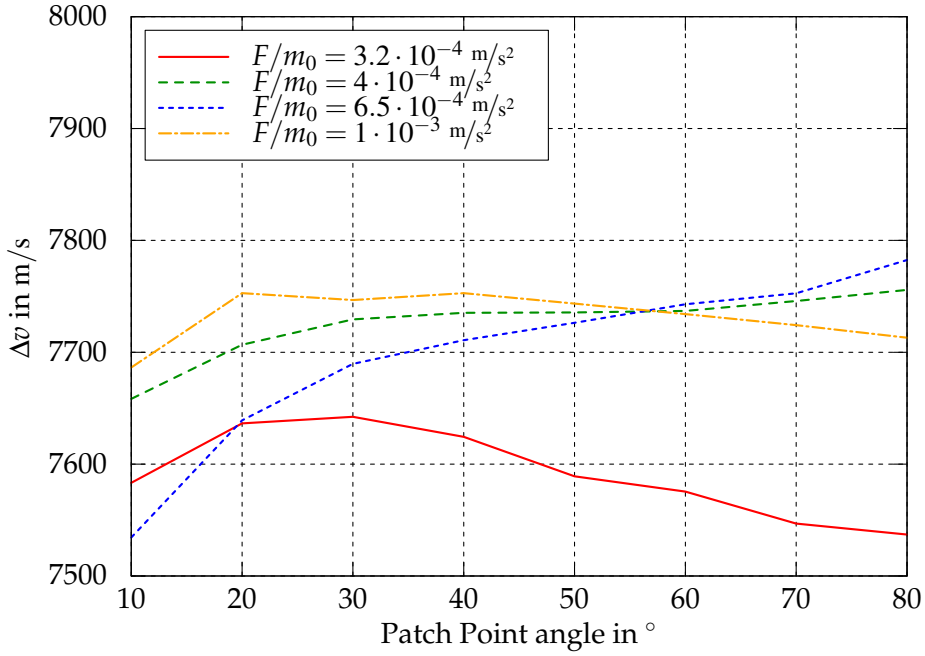

Figure 4.12.: Influence of patch point angle on Δv for different initial accelerations

4.1.6. Validation and Results

The program needs to be validated in order to conclude that it is giving reasonable results. This is done in a number of consecutive steps. First a closer look at the behavior of the keplerian parameters is taken. This is done by identifying five comparison cases and compare their simulations to each other and to analytical formulas. The outline of this comparison can be found in appendix A.1 and shows that the code is behaving as expected.

The code is now validated by comparing the outcomes to simulations performed by the General Mission Analysis Tool (GMAT) from NASA. The comparison between the planetary systems is done consecutively. First, the outcomes within the Earth system and Moon system are compared. Then a complete transfer from the Earth to the Moon is simulated and compared.

For the simulations within GMAT the normal Earth gravity model is used and the problem is calculated as a two-body problem. It also has to be noted that within GMAT it is not possible to have no thrust when the spacecraft is in eclipse, or this should be programmed by the user itself. However, GMAT is only used for validation purposes and therefore both programs are configured to have no eclipse. In this way both programs can be compared and the SPIRAL PROGRAM validated.

The first simulation cases within the Earth system are defined and can be seen in table 4.2. Case one is a simulation from an LEO orbit ($500 \times 500\,\mathrm{km}$) to a GEO orbit ($35,786 \times$

35,786 km) and the second case spirals form LEO up to 300,000 km.

Variable	Case 1	Case 2
Target height (km)	35,786	300,000
Initial mass (kg)	50,000	
Initial height (km)	500x500	
Thrust (N)	20	
Specific impulse (s)	2800	

Table 4.2.: Test cases for comparison of the SPIRAL PROGRAM to GMAT within the Earth system.

The results of the different simulations can be seen in table 4.3. For all simulations the spacecraft applies thrust until it reaches the target height. The outcomes are very similar and demonstrate the validity of the code within the Earth system.

	Case1			Case 2		
Variable	GMAT	Spiral Program	Δ (%)	GMAT	Spiral Program	Δ (%)
m_{prop} (kg)	7622.7	7623.2	0.007	10,546.6	10,547.2	0.006
Δv (m/s)	4541.93	4542.29	0.008	6505.0	6505.5	0.008
e (−)	0.004	0.004	0	0.2175	0.2177	0.09
a (km)	42,137	42,160	0.05	331,837	331,856	0.006
t (days)	121.2	121.1	0	167.6	167.6	0

Table 4.3.: Simulation results within the Earth system.

Secondly, a simulation case within the Moon system is defined, which can be seen in table 4.4. It is chosen to spiral down from the lunar sphere of influence to a low lunar orbit. The end condition in both programs is such that the simulation is ended when a semi-major axis of 1847 km is reached and the eccentricity is below 0.1. The results for these simulations can be seen in table 4.5 and show again very similar outcomes.

Variable	Case 1
Initial mass (kg)	50,000
Initial height (km)	66,183
Initial eccentricity (−)	0.8
Thrust (N)	20
Specific impulse (s)	2800
Target semi-major axis (km)	1847

Table 4.4.: Test cases for comparison within the Moon system

Variable	GMAT	Spiral Program	Δ (%)
Propellant mass (kg)	1916.6	1915.0	0.08
ΔV-budget (m/s)	1073.25	1072.35	0.08
Eccentricity (−)	0.10	0.10	0
Semi-major axis (km)	1844.2	1846.9	0.1
Time (days)	64.0	64.0	0

Table 4.5.: Simulation results within the Moon system.

After the validation within the Earth and Moon system, a complete simulation from the Earth system to LLO is performed. Note that the initial height indicated here, is not equal to the final selected LEO. The simulation case is shown in table 4.6. Within these simulations, GMAT is configured such that the problem is handled as a two body problem, which is the same as for the SPIRAL PROGRAM. The simulation is slightly different within the Earth system compared to the SPIRAL PROGRAM; it is set such that the spacecraft is not firing anymore after a radius of 280,000km.

Variable	Case 1
Initial mass (kg)	50,000
Initial height (km)	6,000x6,000
Thrust (N)	20
Specific impulse (s)	2800
Target Lunar height (km)	100

Table 4.6.: Test case for the total transfer from Earth to Moon.

The results for these simulations within GMAT, with different starting dates, can be seen in table 4.7. They show that a slightly different start date determines how the spacecraft is captured by the Moon and therefore gives completely different outcomes. Outside the specified date range, the spacecraft was not captured by the Moon. As discussed in section 4.1.2 it is very inefficient to approach the Moon from the backside, since then actually a swing-by is performed and a lot of extra Δv is required to reach a bound lunar orbit. The fact that this can not be controlled within GMAT results in very diverse Δv outcomes depending on the epoch date. For example, a difference of 1.5 days, results in a propellant mass variation of 15%.

The same simulation is run within the SPIRAL PROGRAM for different λ_1-values (see table 4.8). This table shows that concerning the propellant mass, Δv-values and transfer time the results overlap each other and are in the same order of magnitude. There are however differences, especially for the transfer time, which can be explained by lack of control within GMAT. In GMAT the transfer is depending on the epoch date, while in the SPIRAL PROGRAM the transfer can be controlled by setting a predefined

λ_1-value. Actually, within GMAT it is extremely difficult to find out how and at which point the spacecraft is entering the Moon system and requires a user very familiar with GMAT. Therefore, concerning the transfer time, the outcomes of the SPIRAL PROGRAM are considered to be more optimized and selected for the mission analysis.

Date (MJD)	$m_{prop}(kg)$	$\Delta v(m/s)$	$r(km)$	$e(-)$	$a(km)$	$t(days)$
27707.43	10154.1	6233.2	1835.2	0.1	2037.7	224.8
27707.63	10157.1	6235.3	1837.2	0.1	1962.4	220.7
27707.83	10448.3	6436.7	1822.1	0.1	1953.6	225.8
27708.03	10742.5	6641.7	1815.1	0.1	2017.3	229.2
27708.23	10537.1	6498.4	1819.6	0.1	1958.7	221.4
27708.63	10127.9	6215.2	1838.1	0.008	1823.5	217.3
27708.68	9714.4	5931.9	1834.5	0.1	2038.2	224.1
27708.73	9163.9	5559.2	1798.2	0.4	2830.9	212.1
27708.83	8880.0	5368.9	1409.5	0.7	3604	209.6

Table 4.7.: Results of multiple simulations within GMAT.

λ_1 $(^\circ)$	$m_{prop}(kg)$	$\Delta v(m/s)$	$r(km)$	$e(-)$	$a(km)$	$t(days)$
0	9106.9	5520.9	1836.3	0.1	2037.8	185.8
20	9445.6	5749.3	1831.5	0.1	2032.5	162.9
30	9455.4	5755.9	1837.1	0.1	2036.7	162.8
40	9436.9	5743.4	1834.6	0.1	2031.9	165.2
60	9350.2	5684.7	1836.2	0.1	2031.9	173.1
80	9338.3	5676.7	1836.2	0.1	2032.3	177.7
100	9479.7	5772.4	1836.7	0.1	2039.1	173.4
150	9610.8	5861.4	1834.5	0.1	2036.5	178.8
170	10455.3	6441.6	692.0	0.1	768.8	246.7

Table 4.8.: Results of multiple simulations for the Spiral Program.

GMAT also offers the possibility to run the simulations as a three-body problem, of which the results can be seen in table 4.9. The results are in the same order of magnitude as the two-body simulations and show again a very high dependency on the epoch date.

These control problems of entering into the lunar sphere of influence were also one of the main reasons to develop an own program, since it is independent and therefore easier to manipulate. The validation showed that the program is suitable for a first mission analysis and can be used in the rest of this study. However, in later design phases more sophisticated software must be used to acquire a more detailed trajectory analysis considering start and arrival date. From the comparison (see appendix A.1) it

can also be concluded, that if the engines are not firing in the orbit's apogee and it is located in the Earth's shadow, the orbit raising is more efficient from the energy point of view compared to firing all the time. The only benefit of applying continuous thrust throughout the mission, is a reduction in the transfer time.

Date (MJD)	$m_{prop}(kg)$	$\Delta v(m/s)$	$r(km)$	$e(-)$	$a(km)$	$t(days)$
27707.63	9749.7	5955.9	1833.4	0.1	1956.1	215.9
27707.83	10007.8	6132.6	1824.0	0.1	1978.4	213.2
27708.03	10164.1	6240.1	1838.1	0.1	1979.9	213.6
27708.23	10249.6	6299.1	1832.9	0.1	1970.5	213.6
27708.43	9014.3	5458.8	1833.4	0.51	3121.2	203.1

Table 4.9.: Results of multiple simulations within GMAT by having a 3-body problem.

4.2. Mission Architecture

Before an orbit analysis can be performed, more information about the mission architecture is required and in particular the specifications of the launch vehicles. The challenge in designing the SEP stage is to fit the whole system into the launcher, hence not violating their mass and volume budget. The goal of this section is to find a suitable launcher and an initial orbit, which fulfill the requirements.

4.2.1. Launcher & orbit discussion

For the mission it is required to use one super heavy lift launch vehicle to ultimately bring 17 ton of payload to the Moon. Currently, the Delta IV Heavy is the heaviest launcher available, capable of launching 23 ton in LEO [49]. This is not sufficient to deliver the required payload and therefore future heavy lift launchers are considered. At the present time there are two under development: SLS and Falcon Heavy (see table 4.10).

As stated, the SLS and Falcon Heavy are still in development, which means that limited information is available and some estimations have to be made, e.g. on the fairing dimensions. For SLS, the outer dimensions are 8.38×27.25 m, including the cone [47]. The inner dimensions of the payload fairing are at this point unknown. Therefore the fairing is compared to an Ariane 5 long fairing and an envelope of 44 cm at both sides of the payload is approximated [48]. The length is estimated at 26.0 m, so the inner dimension are 7.5×26.0 m.

The Falcon Heavy is based upon the Falcon 9 rocket and therefore the upper stage is expected to be the same. This upper stage is restartable [51] and can deliver the payload to a variety of orbits. However, for Falcon Heavy it is currently unknown how much

payload it can deliver to different orbits. The SLS block 1 configuration has 1.5 stages and thus no upper stage is present. Going to a different orbit than the parking orbit comes in this configuration at a very high cost and is therefore undesirable. SLS block 2 has a planned restartable cryogenic upper stage and a payload mass of 120 ton to LEO. However, this program is currently barely funded and therefore it is questionable if this configuration will ever be realized [47].

	SLS	Falcon Heavy
Payload mass to LEO (kg)	70,000	53,000
LEO Parking Orbit (km)	200x200	200x200
Payload mass to MEO (kg)	N/A	-
MEO Parking Orbit (km)	N/A	-
Payload mass to GTO (kg)	N/A	12,000
GTO Parking Orbit (km)	N/A	185x35,786[a]
Inner fairing diameter (m)	7.5[a]	4.6
Inner fairing height w/o cone (m)	16.5[a]	6.6
Inner fairing height with cone (m)	26.0[a]	11.4
Operational	in 2017	in 2013

a: These values are based upon estimations and should be checked when more design specifications become available.

Table 4.10.: Launchers and there specifications [47] [82].

From a mass point of view, it is expected that LEO is the optimum initial orbit. However, there are multiple reasons to go to a higher orbit. Firstly, the atmospheric drag is high at low altitudes and has to be considered. The influence can be determined with:

$$F_D = \frac{1}{2}\rho C_D A v^2. \tag{4.21}$$

The formula shows the dependency of the drag upon the density ρ, of the atmosphere, the drag coefficient C_D, the frontal area A and the velocity of the spacecraft. The velocity is calculated for a spacecraft in a circular orbit, by using the following formula:

$$v_c = \sqrt{\frac{\mu}{r}}. \tag{4.22}$$

When the whole stage is deployed, including solar arrays, the drag coefficient is extremely high. A first rough estimation of the total solar array area, is 2000 m^2, having a drag coefficient of 4 [19]. Together with an atmospheric model from the European Cooperation for Space Standardization [16], the drag force at different heights and solar and geomagnetic activities can be calculated (see figure 4.13). The solar cycle is 11 years and the next solar maximum is expected for April 2022 [16], while the mission is

planned for 2025, which means that the solar activity is in between the maximum and minimum and is therefore considered to be moderate. The parking orbit for such an solar activity shall at least be 250 km to compensate for the drag force. This is under the assumption that the stage can produce 20 N of thrust from the moment the solar arrays are deployed. However, in reality system check procedures are required before the thrusters can be fired. During the time that no thrust can be applied, the stage will loose height and in the worst case makes a reentry in the atmosphere. To prevent this catastrophe, the stage needs to be clear of almost all drag, which is the case at a height of 500 km where the drag force is reduced to 0.20 N for moderate solar activity.

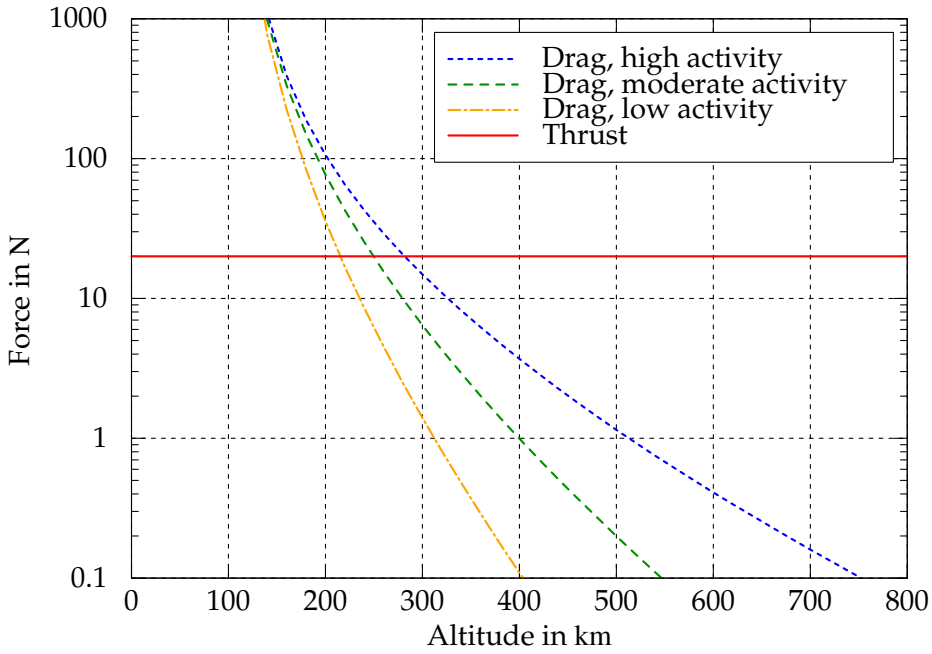

Figure 4.13.: Atmospheric drag of the SEP stage.

Nevertheless, the drag force still has an impact on the orbit, which has to be investigated. For one orbit at 500 km altitude the orbital period is 94.5 min and the spacecraft is 27.9 min in eclipse. The relative influence of the drag on the Δv for one orbit is then:

$$\frac{\Delta v_D}{\Delta v_{SEP}} = \frac{\frac{F_D}{m}\Delta t}{\frac{F_{SEP}}{m}0.7\Delta t} = \frac{0.20}{0.7 \cdot 20} = 1.4 \cdot 10^{-2} \tag{4.23}$$

This influence of the drag is considered to be negligible, which is certainly the case when the spacecrafts starts to spiral up to higher altitudes. Therefore this is not included in the SPIRAL PROGRAM. Furthermore, the 500 km orbit is considered to be a safe parking orbit, which is required for array deployment and system checks.

The atmosphere also contains atomic oxygen, which is eroding the solar arrays. The presence of atomic oxygen is decreasing with height and has an impact on the solar arrays between the altitudes of 180 to 650 km [96]. Another reason to go to a higher orbit are the radiation belts. These belts cause degradation of the solar arrays, reducing their

performance significantly. Especially the first Van Allen belt, which consists of high energy protons and is located between 700 and 10,000 km, has a high impact on the solar array performance. However, the SMART-1 mission experienced most of its degradation, of around 8%, in orbits below 6,000 km. Above this altitude the degradation was negligible [1]. Therefore, initial orbits of 6,000 km and 10,000 km are also considered.

A fourth reason to go to a higher initial orbit is the mission time. The lower the orbit the deeper the spacecraft is inside the potential well of the Earth. Spiraling up from LEO therefore requires much more time compared to an initial MEO orbit.

These reasons show the need for a higher initial orbit. As discussed earlier, SLS is not capable of bringing the payload to a higher orbit and for Falcon Heavy the performance at higher altitudes is unknown. To identify how much extra mass is required to bring the SEP stage to a higher orbit, a kick stage is introduced. In the end, this kick stage might not be needed, since the launcher can bring us to this higher altitude.

4.2.2. Impact of a kick stage on launcher payload mass

The main reason to introduce a kick stage is to identify how much extra mass is required if one of the two launchers, SLS or Falcon Heavy, brings us to a higher orbit. For SLS this kick stage might in fact be necessary, since it does not have an upper stage of its own. However, this can not be decided currently, since there are too many uncertainties in the launcher specifications.

For a kick stage three options are possible concerning liquid propellants: mono-, storable and cryogenic propellant. The performance of a monopropellant kick stage is very low and would result in a too conservative estimate. A cryogenic stage is very efficient from the mass point of view, which could result in a too optimistic mass estimate. Also, in case the cryogenic stage is really developed it would take more development time, be much more expensive and would require a lot more volume compared to a storable propellant kick stage. Therefore, a simple and cheap storable propellant kick stage is chosen, which results in a conservative mass estimate of the launcher performance loss. This kick stage is based upon the Ariane 5 EPS, which uses the Aestus engine, has N_2O_4/MNH as fuel and delivers 28.4 kN of thrust with an I_{sp} of 320 s.

To determine the Δv and corresponding propellant mass of the kick stage, a tool is used which has been developed in the frame of a chemical propulsion stage study at OHB system [2]. The tool calculates the transfer by applying two impulse maneuvers and includes the gravity losses. The initial orbit is 200 km and the target orbits are 500 km, 6,000 km and 10,000 km. The resulting Δv can be converted into the propellant mass by using TSIOLKOVSKY's equation [1]:

$$m_{prop} = m_0 \left(1 - e^{\frac{-\Delta v}{c_e}}\right). \tag{4.24}$$

Where c_e is the characteristic velocity, which is a function of the specific impulse, I_{sp}, and standard gravity, g_0. The structural mass of the kick stage can be estimated by using an empirical relation for bi-propellant stages, which gives the structural index as a function of the total propellant mass [1]:

$$\sigma = \frac{m_s}{m_{prop}} = 2.0753 m_{prop}^{-0.2953}. \tag{4.25}$$

With all the previous information, the mass of the different kick stages can be calculated for the two different launchers (see table 4.11).

	SLS			Falcon Heavy		
m_0 (ton)		70.0			53.0	
h_{target} (km)	500	6,000	10,000	500	6,000	10,000
Δv (m/s)	172	2,131	2,897	172	2,105	2,833
m_{prop} (kg)	3,732	34,792	42,960	2,826	26,032	31,891
m_s (kg)	683	3,292	3,819	561	2,683	3,096
m_{total} (kg)	4,415	38,093	46,779	3,387	28,715	34,987

Table 4.11.: Different kick stage masses to go from an initial height of 200 km to the target height.

4.2.3. Launcher & orbit selection

Now that the launcher performance loss is estimated, consequently the initial mass of the SEP-stage is known. This initial mass is inserted into the SPIRAL PROGRAM to calculate the required propellant mass to go to LLO. The following assumptions are made to determine a payload mass:

- The initial acceleration of the SEP stage is $4 \cdot 10^{-4}$ m/s^2.
- The subsystems mass of an SEP stage is 22% of the initial mass. This figure is based upon information provided in chapter 3.

With these assumptions the payload mass can be estimated for the different initial orbits and launchers (see table 4.12). These results are plotted for the SLS launcher in figure 4.14 and for Falcon Heavy in figure 4.15. From the results it can be concluded that, from a mass point of view, a 500 km orbit is the best orbit to enable the heaviest payload to the Moon. Therefore, the requirement to deliver at least 17 ton of payload to the Moon is fulfilled by both launchers for an initial orbit of 500 km. However, Falcon Heavy is a commercial project and SLS a governmental project. Past experience shows that a commercial project is much cheaper than a governmental one [10]. Also, for SLS it is currently unknown if it can deliver a payload to a 500×500 km orbit. In conclusion, Falcon Heavy is selected as the launcher of the SEP system.

	SLS			Falcon Heavy		
$h_{initial}$ (km)	500	6,000	10,000	500	6,000	10,000
m_0 (ton)	65.6	31.9	23.2	49.6	24.3	18.0
F/m_0 (m/s^2)	$4 \cdot 10^{-4}$	$4 \cdot 10^{-4}$	$4 \cdot 10^{-4}$	$4 \cdot 10^{-4}$	$4 \cdot 10^{-4}$	$4 \cdot 10^{-4}$
F (N)	26.2	12.8	9.3	19.8	9.7	7.2
$m_{subsystems}/m_0$ (−)	0.22	0.22	0.22	0.22	0.22	0.22
$m_{subsystems}$ (ton)	14.4	7.0	5.1	10.9	5.3	4.0
Δv (m/s)	7,668	5,799	4,992	7,605	5,800	4,992
m_{prop} (ton)	16.0	6.1	3.9	12.0	4.6	3.9
t_{burn} (hrs)	4,646	3,630	3,170	4,613	3,631	3,170
$t_{transfer}$ (days)	249	187	177	254	187	177
$m_{payload}$ (ton)	35.2	18.8	14.3	26.7	14.3	10.2

Table 4.12.: Results of how much payload the SEP stage can deliver to the Moon.

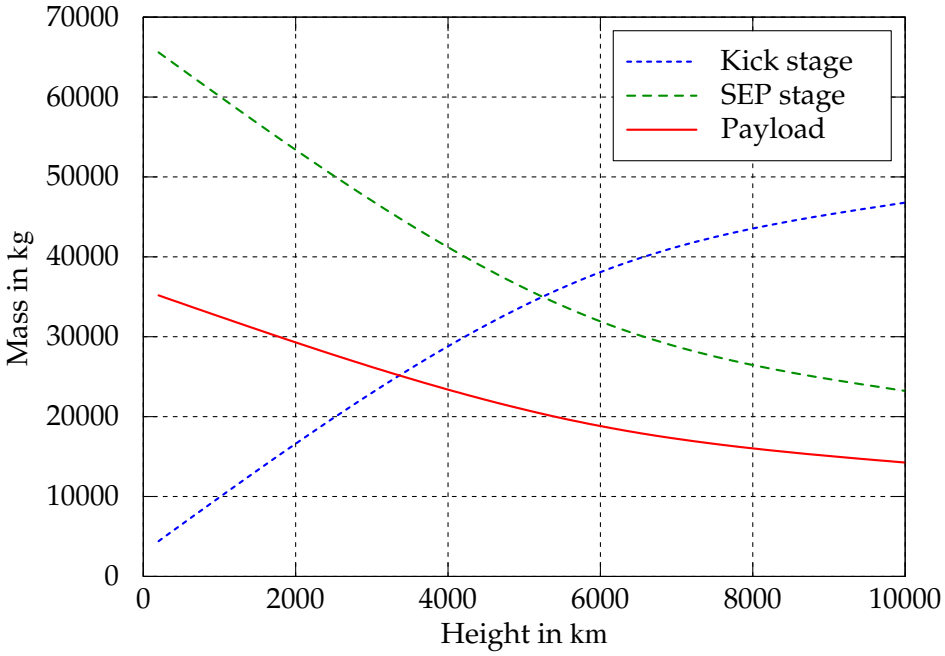

Figure 4.14.: Kick stage, SEP stage and payload mass for different initial orbits by using SLS as a launcher.

With the initial orbit and launcher known, a plot can be generated which displays the initial acceleration as function of time and Δv (see figure 4.16). The plot shows an irregular behavior considering the Δv. This can be explained by the eclipse (see appendix A.1) and the varying conditions at the patch point (see section 4.1.5). Both have an influence on the total outcome and therefore it is chosen to plot a trend line through the outcomes.

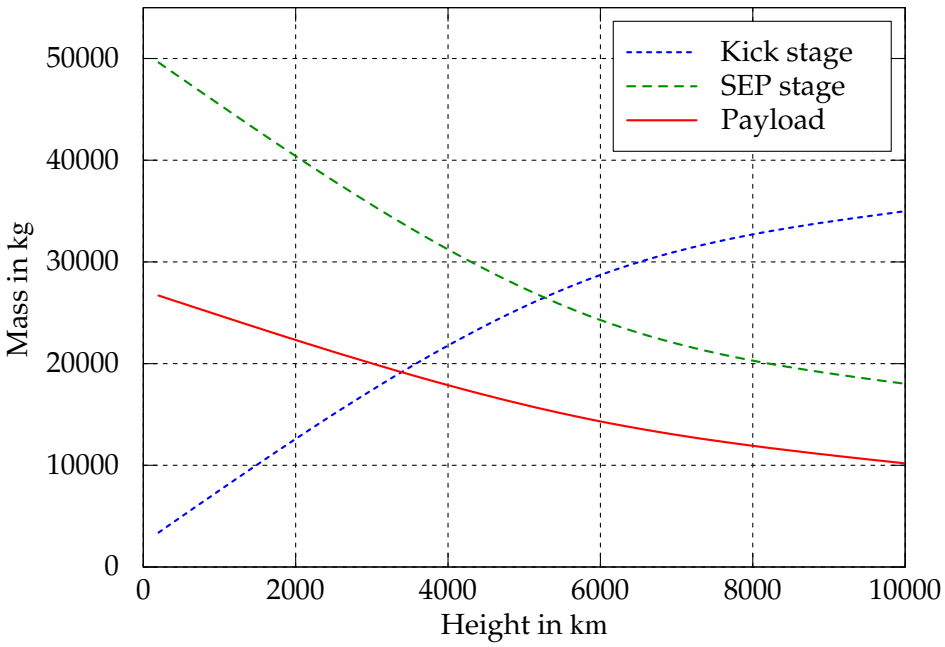

Figure 4.15.: Kick stage, SEP stage and payload mass for different initial orbits by using Falcon Heavy as a launcher.

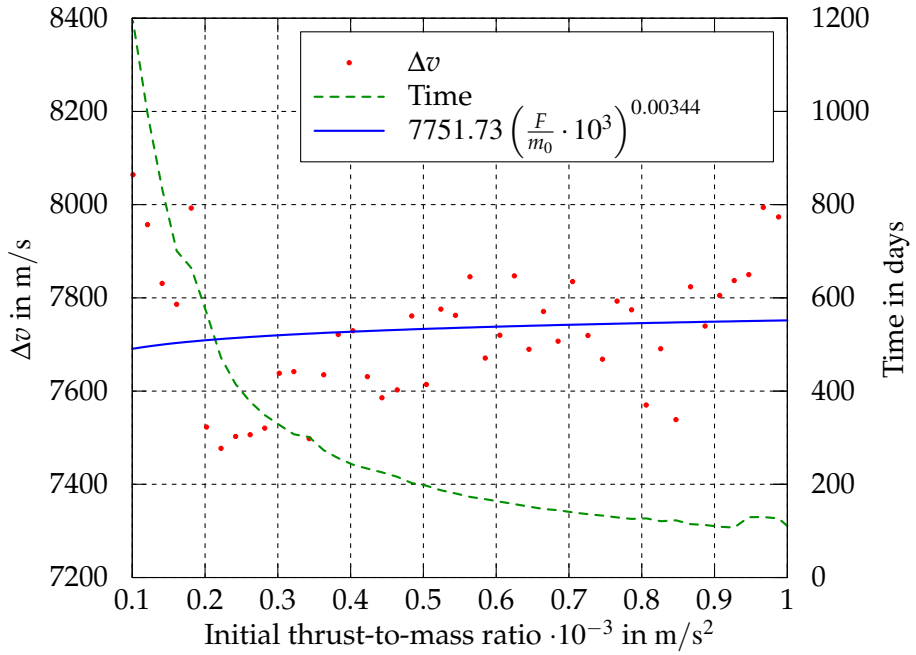

Figure 4.16.: The time and Δv as function of the initial acceleration for an I_{sp} of 2,800s.

The transfer from the Earth to the Moon should be performed within 200 days. This means that the initial acceleration should be $5 \cdot 10^{-4}\,\mathrm{m/s^2}$ (see figure 4.16). This corresponds to a thrust level of 25 N for a 50 ton SEP stage. The required Δv to go from LEO to LLO, is equal to 7733 m/s. For the preliminary analysis, a margin of 10% is included on the Δv according to the margin philosophy of reference [75], resulting in 8507 m/s. This

initial Δv is used for the preliminary analysis, in which the initial mass is obtained as function of the specific impulse, to select an optimum specific impulse for the specified mission.

4.2.4. End-of-Life procedures

When the SEP stage is nearing the end of its mission operations, procedures have to be in place that follow End-Of-Life (EOL) regulations. The Inter-Agency Space Debris Coordination Committee (IADC) set up guidelines for space debris related issues. The purpose of the committee is to share space debris information with the ten involved space agencies and to identify debris mitigation options. The guidelines for limiting the generation of space debris are [52]:

- Limitation of debris released during normal operations.
- Minimisation of the potential for on-orbit break-ups.
- Post-mission disposal.
- Prevention of on-orbit collisions.

In the guideline [52] measures are given for post mission disposal. These measures state that all energy stored on the spacecraft shall be eliminated, to reduce the chance of break-up. These passivation measures include venting or burning of excess propellant, discharging batteries and relieving pressure vessels.

Another guideline is to de-orbit the spacecraft for re-entry into the Earth's atmosphere, which eliminates the hazard it poses to other spacecrafts. If de-orbit is too costly for the spacecraft, re-orbit should be applied to bring the stage to a disposal orbit were it poses no threat to other missions.

For the SEP stage there are two possible locations where it can perform its last mission operations: at a LEO of $500 \times 500\,\text{km}$ or at a LLO of $100 \times 100\,\text{km}$. It is most logical that the SEP stage would bring, for its last mission, the largest amount of payload possible to LLO and perform there its EOL operations before disposal. A LLO of $100 \times 100\,\text{km}$ is a frequently used orbit for lunar missions, therefore to pose no threat to future missions, the stage should be placed in a different orbit. However, there is no space debris tracking system for the Moon, which means that the stage can not be tracked all the time and could pose an unknown threat to other satellites. Therefore it is most logical to de-orbit the SEP stage and let it impact on the Moon's surface. A simulation with the Spiral Program is performed for this de-orbit maneuver, for a 11 ton stage with an I_{sp} of 2800 s and thrust of 25 N. The Δv required to de-orbit the stage from LLO and let it impact on the Moon, is only $32.3\,\text{m/s}$, equivalent to $12.8\,\text{kg}$ of propellant.

The other possibility is that the SEP stage is in LEO when it is performing its last operations. In this case the orbit regulations of the Earth apply, which states that the LEO

region, up to an altitude of 2000 km, is protected to ensure their future use. The guideline states that the spacecraft should make a re-entry into the atmosphere within 25 years, although direct re-entry is preferred [52]. A direct re-entry can be accomplished by bringing the spacecraft from a 500×500 km orbit down to a 200×200 km. From there the atmospheric drag would cause the stage to make a direct re-entry (see section 4.2.1). The same 11 ton stage is considered, which results in a total Δv of 124 m/s for the de-orbit maneuver (49.2 kg of propellant).

Debris that survives and reaches the surface of the Earth should not pose a risk to people or property, which can be accomplished by limiting the amount of surviving debris or confining it to uninhabited regions, such as ocean areas. Also toxic substances or any other environmental pollutants should be prevented or minimized from making a re-entry.

As stated, the most logical choice to perform the EOL operations during the last mission, would be in LLO. Since there are still some uncertainties in the design, a margin of 100% on the required Δv is taken, resulting in a Δv of 64.6 m/s that is needed to de-orbit from LLO and impact on the Moon.

4.3. Preliminary Analysis

In this section a preliminary analysis is performed for the SEP stage. The first goal is to achieve the optimum operation point, in terms of I_{sp}, initial acceleration (total thrust) and power, followed by an initial mass budget. The mass of the SEP stage is estimated by using a model provided by JPL [32] and by estimates from literature. This mass is obtained to show the feasibility of the mission and to obtain an optimum specific impulse. Secondly, an analysis is performed on the fairing volume, resulting in an initial volume budget. The volume budget is derived from the launcher fairing and is considered to be critical, since the large solar arrays will require a substantial volume.

4.3.1. Initial Mass Budget

The preliminary analysis is based upon a method developed in the literature study [1] and from reference [32]. The analysis results in the mass of the SEP stage as function of the specific impulse. By choosing a specific impulse, a mass budget can be estimated for the systems. The largest contributors to the stage mass are the propellant mass, propulsion, thermal and power system mass.

The SEP stage transfers a payload from the initial 500×500 km LEO to a LLO of 100×100 km. The mission time for this transfer is 200 days. The corresponding Δv can be found in figure 4.16 and is 7733.3 m/s. A margin of 10% is included on the Δv, since the design is in a preliminary phase, so the Δv used to come to a propellant mass is equal to 8506.6 m/s.

The power is generated by solar arrays. The current state of the art triple junction Ga/As solar arrays have a specific power of up to 60 W/kg (1AU). However, research and development in this field is still ongoing and predicts that the highest achievable specific power of triple junction GaAs solar arrays is 100 W/kg [33]. Another possibility is to select thin-film cells, which currently obtain in laboratories specific power levels higher than 100 W/kg [33]. In this analysis the future triple junction GaAs solar arrays are considered (see table 4.13). During the power system design, a trade-off will be performed on all the solar array technologies, which might result in the usage of a different solar cell.

Solar array	
Cell efficiency EOL $(-)$	0.249
Specific mass $(\mathrm{kg/m^2})$	3.53
Specific Power $(\mathrm{W/kg})$	95.8

Table 4.13.: EOL characteristics of the triple junction GaAs solar arrays, as suggested by OHB experts.

For the propulsion, the NASA-457M hall thruster is used for the preliminary analysis [1]. This thruster can generate 2.5 N of thrust at a power level of 50 kW, total efficiency, η, of 0.56 and an I_{sp} of 2800 s. The efficiency of a Hall thruster is expressed as the kinetic thrust power (or jet power) as function of the input power. The jet power can be rewritten into the mass flow, $\dot{m}$, and the characteristic velocity [7]:

$$\eta = \frac{P_{jet}}{P_{in}} = \frac{\dot{m}c_e^2}{2P_{in}} = \frac{FI_{sp}g_0}{2P_{in}}. \tag{4.26}$$

Rewriting this formula, the power required for the propulsion system is obtained:

$$P = \frac{FI_{sp}g_0}{2\eta}. \tag{4.27}$$

The mass of the propulsion system is depending on the total system input power P_{sys}, of which the thrusters demand by far the most power. Also the number of active thrusters, N_{ac}, and the number of redundant thruster strings, N_{rd}, have an impact on the mass. Redundant thruster strings are used in the event of a failure. A robotic mission like this is typically single-fault tolerant, therefore there is one redundant thruster string ($N_{rd} = 1$). The number of active thrusters is determined by the total system input power divided by the operating power level of a single thruster. The thruster mass scales linearly with the power level [32]:

$$m_{thr} = (N_{ac} + N_{rd}) \left(2.4254 \frac{P_{sys}}{N_{ac}} \right). \tag{4.28}$$

This is an empirical formula from JPL based upon EP missions and discussions with manufacturers [32]. For the power system it is chosen to have a Direct Drive power processing Unit (DDU), which directly transfers the power from the solar arrays to the engine resulting in the lowest possible power loss. However, some losses will occur between the solar array and the engine (SADM, cables, etc.), which is estimated at 5%. The mass of the DDU is depending on the power level and described by [32]:

$$m_{DDU} = (N_{ac} + N_{rd}) \left(0.35 \frac{P_{sys}}{N_{ac}} + 1.9 \right). \tag{4.29}$$

The cable mass off the high-voltage system can also be determined by this model and is given by [32]:

$$m_{cab} = (N_{ac} + N_{rd}) \left(0.06778 \frac{P_{sys}}{N_{ac}} + 0.7301 \right). \tag{4.30}$$

The Xenon feed system is consisting out of pressure regulators, flow control valves, pressure transducers, thermocouples, latch valves, services valve, tubing, fittings, etc. The mass of this system is estimated by [32]:

$$m_{XFS} = (N_{ac} + N_{rd})\, 3.2412 + 4.5189. \tag{4.31}$$

The propellant mass is given by the rocket equation. The mass of the tanks is a fraction of this mass [32]:

$$m_{tank} = 0.04 m_p. \tag{4.32}$$

The total mass of the propulsion system is then [32]:

$$m_{ps} = 1.26 \left(m_{thr} + m_{DDU} + m_{cab} + m_{XFS} + m_{tank} \right). \tag{4.33}$$

Where the fraction 1.26 is a structural fraction to account for elements necessary to integrate the propulsion system into the spacecraft. The waste heat produced by the engines and the power system needs to be rejected to space, which can be estimated by:

$$Q_{thermal} = (1 - \eta_{EPS})\, P_{EPS}. \tag{4.34}$$

The heat is rejected by radiators of the thermal control system, of which the specific mass is currently estimated at 25 kg/kW [1]. The total structure mass, consists out of the sum of the propulsion, thermal and solar array mass:

$$m_s = m_{ps} + m_{thermal} + m_{sa}. \tag{4.35}$$

The propellant mass, using equation 4.24, and structure mass can now be calculated as a function of I_{sp} (see figure 4.17). The sum of the propellant and structure mass, has a mass optimum of 23.8 ton at an I_{sp} of 3,200 s. However, the required power production by the solar arrays is equal to 737 kW, which is more than two times of the current state of the art. Therefore it is chosen to go to a lower I_{sp} of 2000 s, at which the Hall thruster can still be efficient. If an even lower I_{sp} is selected, it will come at the cost of engine efficiency and again a higher power would be required. For this new I_{sp} of 2000 s, the total mass changes to 25.5 ton, the required power to 461 kW and the solar array area is equal to 1363 m^2.

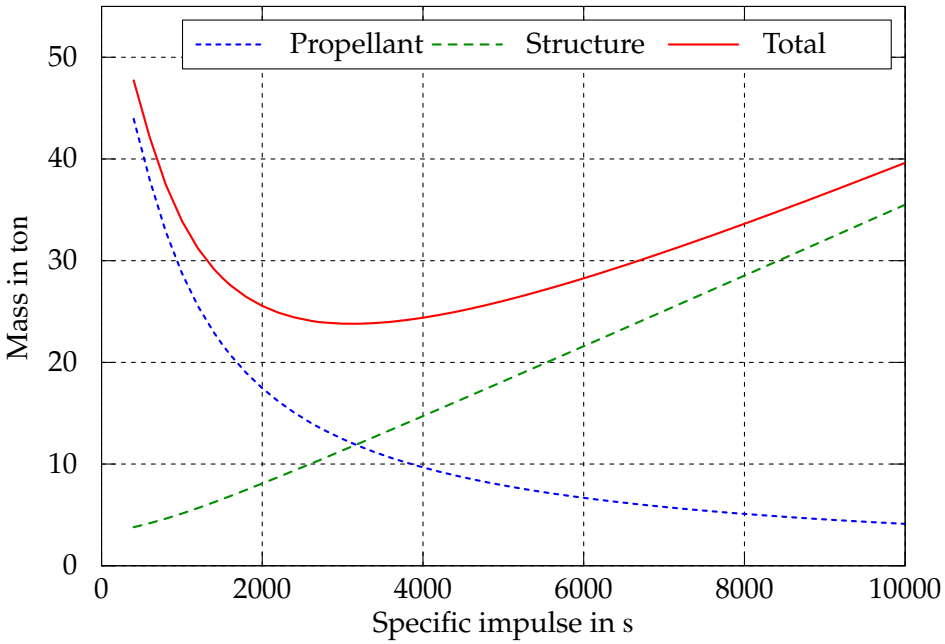

Figure 4.17.: The propellant, structure and total mass as function of specific impulse, for a thrust of 25 N and Δv of 8507 m/s.

Due to this new I_{sp}, the transfer time and required Δv change (see figure 4.18). It shows that the required initial acceleration is decreased to a value of $4.8 \cdot 10^{-4}$ m/s^2, equivalent to a thrust level of 24 N. The resulting Δv to go from LEO to LLO, including a 10% margin [75], is equal to 8498 m/s.

It is required that the SEP stage returns from LLO back to LEO to perform at least one more mission. For this return a Δv is needed, which is simulated in the SPIRAL PROGRAM (see figure 4.19). The initial acceleration in this figure still corresponds to the one given in LEO at the start of the mission and is thus the same as the initial acceleration of figure 4.18. For the earlier specified initial acceleration of $4.8 \cdot 10^{-4}$ m/s^2, a Δv of 7395 m/s is required to perform the transfer in a time of only 53 days. A margin of 10% is included for the design, resulting in a Δv of 8134 m/s.

The total mission duration to perform a complete transfer from LEO to LEO, is approximately 250 days, in which the thrusters operate for a duration of 4658 hrs. A mar-

gin of 20% is included to cover for uncertainties and to include time for docking and un-docking procedures, which means that the total transfer shall be performed within 300 days and that the thrusters are designed to fire 5590 hrs per mission.

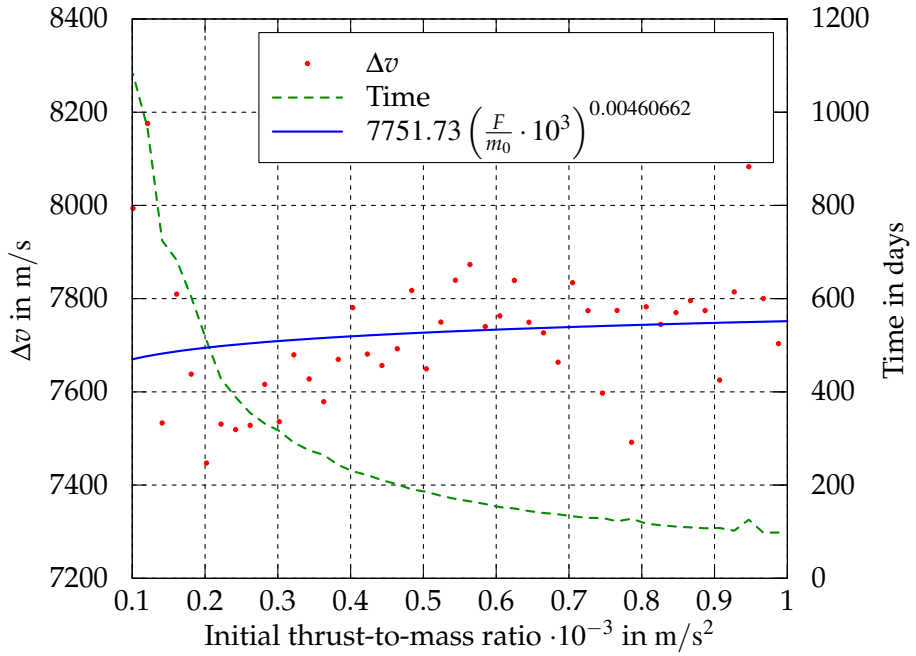

Figure 4.18.: The time and Δv as function of the initial acceleration for an I_{sp} of 2,000s.

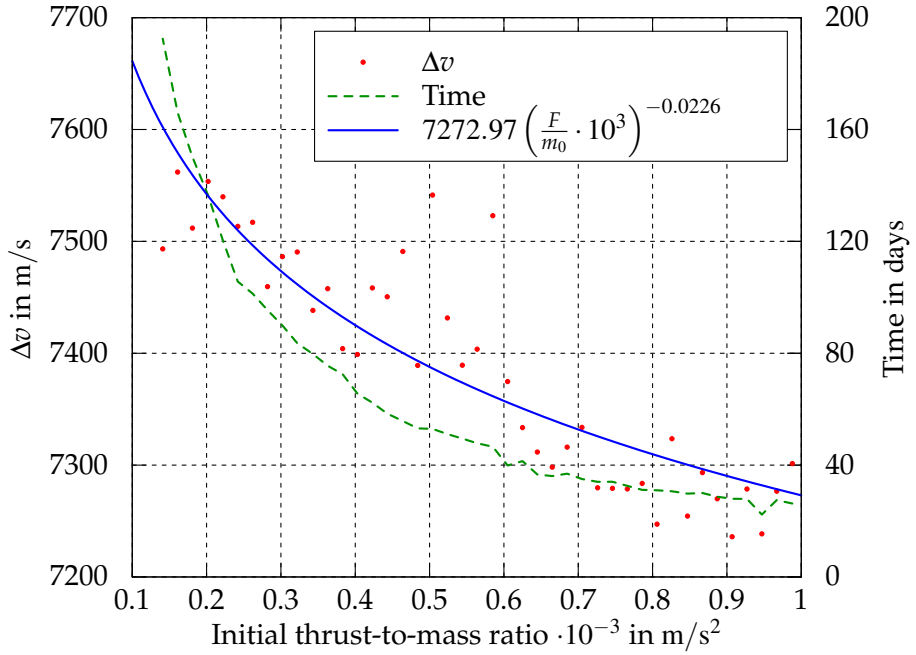

Figure 4.19.: The time and Δv to return from LLO to LEO, as function of the initial acceleration for an I_{sp} of 2,000s.

For this chosen operation point a mass budget can be constructed by using the mass relations and information from literature (see table 4.14). On the subsystems mass a

margin of 20% is applied, which corresponds to the margin philosophy of ESA [75]. The mass for the Attitude and Orbit Control System (AOCS), On-Board Data Handling (OBDH), Telemetry, Tracking and Command (TT&C) system and harness are estimates coming from table 3.2 and literature [1]. A better estimate of these subsystems will be determined in the design phase in chapter 5.

The stage shall be reusable and thus propellant is required to transfer the SEP stage from LLO to LEO, which corresponds to $5,928\,\text{kg}$. As a consequence, the payload mass is reduced to $14.7\,\text{ton}$ and thus the payload requirement of $17\,\text{ton}$ is not met. However, for the last mission this extra propellant is not needed and thus the payload mass can be enlarged to $20.6\,\text{ton}$. Therefore, for this launcher scenario, the payload requirement is partially met from the mass point of view. It is expected that the volume budget will have an impact on the mass budget, therefore an initial analysis on the volume budget is required, before a final decision on the scenario can be made.

On the presented mass analysis, the impact of space radiation is not evaluated. It is expected that the space radiation will enlarge our solar array area and mass. This is further analyzed when the solar array technology is selected in the design phase and the resulting radiation on the solar array is estimated (see section 4.4).

Subsystem	Total mass (kg)
$m_{propulsion}$ (kg)	2,702
m_{power} (kg)	4,811
$m_{thermal}$ (kg)	576
m_{AOCS} (kg)	520 (TBD)
m_{OBDH} (kg)	87 (TBD)
$m_{TT\&C}$ (kg)	41 (TBD)
$m_{harness}$ (kg)	876 (TBD)
$m_{subsystems}$ (kg)	11,535 (20%)
$m_{payload}$ (kg)	14,705
m_{dry} (kg)	26,240
$m_{prop,LEO-LLO}$ (kg)	17,445
$m_{prop,LLO-LEO}$ (kg)	5,928
m_0 (kg)	49,613

Table 4.14.: Resulting initial mass budget of an SEP stage with an thrust level of 24 N, I_{sp} of 2000 s and a margin of 20% on the subsystems mass.

4.3.2. Initial Volume Budget

An initial analysis is performed to examine if the stage fits in the selected Falcon Heavy fairing. The launcher is using the same fairing as the Falcon 9, while Falcon 9 is only launching 13 ton of payload into LEO. Obviously, this fairing is too small for 53 ton and, since SpaceX offers the possibility to adjust the fairing size [82], it is chosen to alter its dimensions to reasonable values. This is performed by comparing the fairing dimensions of different launchers (see table 4.15). The usable volume of the fairing is estimated by calculating the volume of the cylindrical section and by approximating the volume of the conical section as a cone:

$$V_{fairing} = V_{cylinder} + V_{cone} = \pi \left(\frac{d_{inner}}{2}\right)^2 l_{cylinder} + \frac{1}{3}\pi \left(\frac{d_{inner}}{2}\right)^2 \left(l_{total} - l_{cylinder}\right). \quad (4.36)$$

For the comparison, a new parameter is introduced, called the fairing density, $\rho_{fairing}$, which expresses the ratio between the payload mass, $m_{payload}$, and the available fairing volume, $V_{fairing}$:

$$\rho_{fairing} = \frac{m_{payload}}{V_{fairing}}. \quad (4.37)$$

The fairing density for the standard Falcon Heavy fairing is very high (see table 4.15), which indicates that the fairing is relatively small. When adjusting the fairing size the technical feasibility has to be taken into account. This would introduce complex calculations concerning aerodynamics and structural integrity, therefore it is chosen to make a qualitative comparison to other launcher fairings to see what has been done so far (see table 4.15).

	SLS	Falcon Heavy	Delta IV Heavy	Ariane 5-LF	Atlas V-5m
$m_{payload}$ (kg)	70,000	53,000	22,977	21,000	18,510
d_{inner} (m)	7.5[a]	4.6	4.57	4.57	4.57
$l_{cylinder}$ (m)	16.5[a]	6.6	11.268	10.04	12.19
l_{total} (m)	26.0[a]	11.4	15.995	15.6	16.49
$\left(\frac{l}{d}\right)_{cylinder}$	2.2	1.4	2.5	2.2	2.7
$\left(\frac{l}{d}\right)_{total}$	3.5	2.5	3.5	3.4	3.6
$V_{cylinder}$ (m^3)	728.9[a]	109.7	185	164.7	200.2
V_{total} (m^3)	868.8[a]	136.3	210.9	193.9	223.7
$\rho_{fairing}$ (kg/m^3)	80.6	388.8	108.9	108.3	82.8

a: These values are based upon estimations and should be checked when more design specifications become available.

Table 4.15.: Fairing specifications of multiple launchers [47] [82] [49] [48] [50].

For adjusting the payload fairing of Falcon Heavy it would be convenient to adjust the payload diameter, since it has a large impact on the total volume. However, the diameter of the fairing can not be increased unlimited, since there are expansion waves at the back of the fairing which causes high pressure variations at the fairing surface. Therefore it is statistically researched what is currently feasible by taking the $\frac{d_{fairing}}{d_{core}}$-ratio of other launchers. It turns out that Falcon Heavy, together with Atlas V, already have the highest ratio (1.42 and 1.41 respectively). Therefore it is chosen not to extend the diameter any further and fix the outer diameter at 5.2 m and the inner usable diameter at 4.6 m.

The only possibility that remains to enlarge the fairing volume is to increase the length of the fairing. Also this can not be performed unlimited, because the fairing endures, among other things, bending moments. Therefore, it is again statistically researched what is currently possible by having a look at the $\frac{l}{d}$-fractions for the cylindrical part and the total length. Once more the Atlas V has the largest ratios, hence these ratios are used for the adjustment of the Falcon Heavy fairing (see table 4.16). The resulting fairing still has a relatively large fairing density compared to others, despite the fact that it is made as large as what is currently assumed to be technical feasible. This is very unfavorable for an SEP stage, where the EPS requires a substantial volume.

	Falcon Heavy fairing
$m_{payload}$ (kg)	53,000
d_{outer} (m)	5.2
d_{inner} (m)	4.6
$\left(\frac{l}{d}\right)_{cylinder}$	2.7
$\left(\frac{l}{d}\right)_{total}$	3.6
$l_{cylinder}$ (m)	12.42
l_{total} (m)	16.6
$V_{cylinder}$ (m^3)	206.4
V_{total} (m^3)	229.6
$\rho_{fairing}$ (kg/m^3)	230.8

Table 4.16.: Adjusted fairing of the Falcon Heavy.

The resulting volume budget equals 229.6 m^3. One of the largest contributor to the volume budget, is the payload. The payload volume can be estimated by using the Automated Transfer Vehicle (ATV) as a reference (see table 4.17). The mass of the payload is compared to the ATV mass and scaled by maintaining the same density. The first payload requires a volume of in total 126.7 m^3, leaving 113.5 m^3 for the SEP stage. It is expected that the SEP stage, together with the propellant, requires more volume than the available volume. As a consequence, the payload mass will drop further below the

required 17 ton. Therefore, it is chosen to introduce two alternative mission scenarios:

- Launch the complete vehicle with SLS.
- Adopt a dual-launch scenario with Falcon Heavy, in which the SEP stage and payload are launched separately.

In a single launch scenario with SLS, the 17 ton payload will be mounted on top of the SEP stage. During launch this payload will start to vibrate and, as a consequence, the structure of the SEP stage needs to be strong enough to transfer these loads to the adapter. Therefore, the SEP's structure in this scenario will have a mass which is significantly larger than in a dual launch scenario. Secondly, it is expected that two Falcon Heavy launches are less expensive than one SLS launch [10] [34]. These structural and economical reasons show that the dual-launch scenario with Falcon Heavy is preferred.

	ATV	Payload 1	Payload N (final mission)
m_{total} (kg)	20,750	14,705	20,633
d_{outer} (m)	4.5	4.6	4.6
l_{total} (m)	10.3	7.0	9.8
V_{total} (m^3)	163.8	116.1	162.9
ρ (kg/m^3)	126.7	126.7	126.7

Table 4.17.: Estimated payload dimensions using ATV as a reference [83].

The transition to a dual launch scenario changes the mission analysis drastically and should therefore be revised. However, due to a chain of events, the mission analysis was performed as presented. Especially, the discovery of the impact on the structure mass in case the payload is placed on top of the stage (see chapter 5.5), drove the decision to select a dual-launch scenario. Because of time restrictions and the expectation that another analysis will not affect the outcome, the mission analysis is not performed allover again.

Due to the transition to a dual launch scenario, the volume and mass budget are doubled. As a consequence, there is much more flexibility in the design variables. However, due to the already very high power demand of 461 kW, which is twice the state of the art value, it is decided to make the mission reusable and keep the target payload mass at 17 ton. During the stage design phase, the sizing is performed such that this payload requirement is met.

4.4. Environmental Factors

The Van Allen Belts will be passed multiple times during the transfers, as a consequence the total radiation dose will be relatively high for such a relatively short mission. The

most significant influence of space radiation is on the solar array efficiency and the resulting loss in performance. Other subsystems can be designed to be radiation hard by means of shielding and thus the radiation dose upon these subsystems is in the current design phase not of interest.

For solar cells the total radiation dose is converted into a equivalent electron fluence[2] ($1\,\mathrm{MeV/cm^2}$). These equivalent values can be used, in combination with a solar cell datasheet, to estimate the cell performance at EOL and for different operating temperatures. The equivalent electron fluence is determined by using SPENVIS, which is a tool developed by ESA [96].

The tool has as shortcoming that not a complete trajectory can be imported. Instead, the user can insert five trajectory segments with a maximum time duration of 30 days per segment. Therefore, a segmentation has been applied, which is done for:

- Spiraling up in the Earth environment.
- Spiraling down and up again in the Moon environment.
- Spiraling down in the Earth environment.

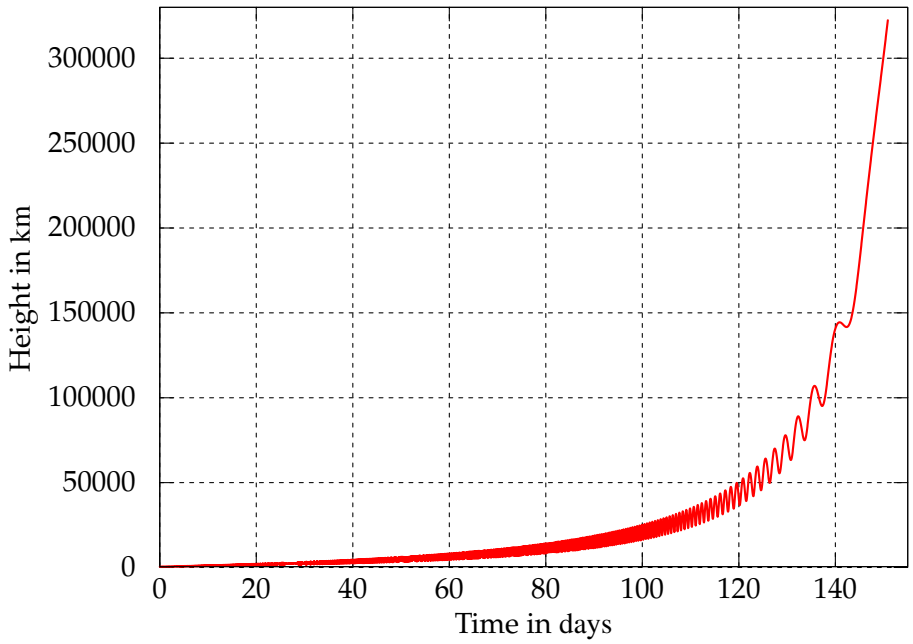

Figure 4.20.: Altitude of the spacecraft with respect to time for spiraling up within the Earth environment.

The altitude of the spacecraft with respect to time is used to determine the segments. For the Earth up simulation, two segmentations are applied to investigate the impact of the segmentation on the end result (see figure 4.20 and table 4.18). A single segment within SPENVIS can have a maximum simulation time of 30 days, therefore a factor of

[2] In the equivalent electron fluence, all radiation components of the space environment are combined in a single term of a selected mono-energetic particle, commonly the 1 MeV electrons [46].

two is applied between real time and the simulation time. This is corrected in the end, by multiplying the total radiation dose by a factor of two. Also, the segments are defined as ellipses, with a perigee height equal to the lower bound of the orbit and the apogee height being the highest position in the specified period.

Segmentation 1		
Orbit height (km)	Real time (days)	Simulation time (days)
500 - 3,467	0 - 52	26
3,467 - 18,601	52 - 96	22
18,601 - 51,508	96 - 122	13
51,508 - 142,032	122 - 142	10
142,032 - 322,404	142 - 152	5
Segmentation 2		
Orbit height (km)	Real time (days)	Simulation time (days)
500 - 1,062	0 - 32	16
1,062 - 7,423	32 - 62	15
7,423 - 19,584	62 - 92	15
19,584 - 51,508	92 - 122	15
51,508 - 322,404	122 - 152	15

Table 4.18.: The two different orbit segmentations for spiraling up in the Earth environment.

With the segmentation in place, all the other models within SPENVIS can be run. It was advised by experts within OHB systems to use the standard models for all the appropriate calculations. To obtain the equivalent radiation fluence, also the solar cell shielding must be known. The solar cell can be shielded against space radiation by using a cover glass. The cover glass is glued to the solar cell by an adhesive and finally embedded on the flexible Kapton substrate. All these layers contribute to the protection of the solar cell. The shielding in the SPENVIS environment is modeled with Aluminum ($\rho_{Al} = 2.2\,\mathrm{g/cm^3}$) as shielding material. Therefore, all the layers of the solar cell have to be translated into an aluminum equivalent shielding thickness $t_{Al-equivalent}$, by using:

$$t_{Al-equivalent} = \frac{\rho_{material}}{\rho_{Al}} t_{material}. \tag{4.38}$$

The complete solar cell is specified in section 5.4.7 and the resulting equivalent shielding, which is inserted into SPENVIS, can be seen in table 4.19. For this shielding the resulting radiation is computed by SPENVIS for all the different segments. As stated, the end result of spiraling up in the Earth environment, is multiplied by two in order to obtain the total accumulated radiation during the real transfer time. The end results of

all the segmentations are expressed in the equivalent 1 MeV electron fluence (see table 4.20). The difference between the results is approximately 30% and can be explained by having different orbit segmentations with different Van Allen belt crossings.

Shielding	Material thickness (μm)	Material density (g/cm^3)	Equivalent shielding thickness (μm)
Cover glass	250	2.605	296
Cover glass adhesive	20	1.080	10
Total front side shielding			306
Cover glass adhesive	20	1.080	10
Cover glass	250	2.605	296
Kapton substrate	25	1.42	16.1
Total rear side shielding			322.1

Table 4.19.: Equivalent shielding thickness of the solar cell.

This discrepancy between the two segmentations is too large and therefore it is chosen to introduce a new segmentation with ten segments and thus the SPENVIS model will be set up twice (see table 4.21). The boundaries of the segments are chosen such that they coincide with the Van Allen belts, with the proton belt from 700 to 10,000 km and the electron belt from 13,000 to 65,000 km.

Flux component	Segmentation 1		Segmentation 2	
	Φ(I) (MeV/cm^2)	Φ(V) (MeV/cm^2)	Φ(I) (MeV/cm^2)	Φ(V) (MeV/cm^2)
Front side	$1.401 \cdot 10^{14}$	$1.930 \cdot 10^{14}$	$2.046 \cdot 10^{14}$	$2.586 \cdot 10^{14}$
Rear side	$1.381 \cdot 10^{14}$	$1.906 \cdot 10^{14}$	$2.000 \cdot 10^{14}$	$2.538 \cdot 10^{14}$
Total flux Earth up	$2.782 \cdot 10^{14}$	$3.836 \cdot 10^{14}$	$4.046 \cdot 10^{14}$	$5.124 \cdot 10^{14}$

Table 4.20.: Irradiation encountered when spiraling up in the Earth environment.

The results for the third segmentation (see table 4.22) shows an increase of the radiation in comparison to the second segmentation. Interestingly, approximately 97% of this segmentation's radiation is encountered in the proton belt when spiraling in the Earth environment. This segmentation has a higher resolution compared to the others and therefore the end result is used to compute the total accumulated irradiation.

Another drawback of SPENVIS is, that no simulation can be performed in the Moon environment. Therefore the radius is expressed with respect to the Earth, with two segments for spiraling down and one for spiraling up (see table 4.23). The segmentation for spiraling down in the Earth environment is defined such that segment two coincides with the electron belt and segment four coincides with the proton belt (see table 4.23).

Segmentation 3		
Orbit height (km)	Real time (days)	Simulation time (days)
500 - 700	0 - 2.76	2.76
700 - 2616	2.76 - 23.81	21.05
2616 - 5411	23.81 - 44.83	21.02
5411 - 10,000	44.83 - 66.78	21.95
10,000 - 13,000	66.78 - 76.75	9.97
13,000 - 26,739	76.75 - 92.75	16
26,739 - 40,314	92.75 - 109.11	16.36
40,314 - 65,000	109.11 - 127.04	17.93
65,000 - 110,285	127.04 - 138.04	11
110,285 - 322,404	138.04 - 150.87	12.83

Table 4.21.: The third orbit segmentation for spiraling up in the Earth environment.

Segmentation 3		
Flux component	Φ(I) (MeV/cm^2)	Φ(V) (MeV/cm^2)
Front side	$2.590 \cdot 10^{14}$	$3.356 \cdot 10^{14}$
Rear side	$2.360 \cdot 10^{14}$	$3.062 \cdot 10^{14}$
Total flux Earth up	$4.950 \cdot 10^{14}$	$6.418 \cdot 10^{14}$

Table 4.22.: Irradiation encountered for the third segmentation.

Segmentation Moon environment		
Orbit height (km)	Real time (days)	Simulation time (days)
322,404 - 384,499	152 - 155.6	3.6
353,452 - 384,499	155.6 - 184.9	29.3
384,499 - 322,404	184.9 - 195.3	10.4
Segmentation Earth Down environment		
Orbit height (km)	Real time (days)	Simulation time (days)
322,404 - 71,371	195.3 - 205.4	10.1
71,371 - 19,371	205.4 - 217.4	12
19,371 - 16,371	217.4-219.4	2
16,371 - 6,869	219.4 - 230.9	11.5

Table 4.23.: Orbit segmentation in the Moon environment and for spiraling down in the Earth environment.

Due to the crossing of the Van Allen belts, the resulting radiation in the Moon environ-

ment is more than a factor ten lower compared to the radiation obtained in the Earth environment (see table 4.24).

Irradiation Moon		
Flux component	Φ(I) (MeV/cm^2)	Φ(V) (MeV/cm^2)
Front side	$2.453 \cdot 10^{12}$	$3.486 \cdot 10^{12}$
Rear side	$2.418 \cdot 10^{12}$	$3.446 \cdot 10^{12}$
Total flux Moon	$4.871 \cdot 10^{12}$	$6.932 \cdot 10^{12}$
Irradiation Earth Down		
Flux component	Φ(I) (MeV/cm^2)	Φ(V) (MeV/cm^2)
Front side	$2.275 \cdot 10^{13}$	$2.810 \cdot 10^{13}$
Rear side	$2.226 \cdot 10^{13}$	$2.757 \cdot 10^{13}$
Total flux Earth down	$4.501 \cdot 10^{13}$	$5.567 \cdot 10^{13}$

Table 4.24.: Irradiation encountered within the Moon environment and when spiralling down the Earth environment.

The summation of all the irradiation in the different phases, results in an estimate on the total encountered radiation (see table 4.25). These values are used to predict the impact on the solar cell efficiency and size the solar array such that it produces the required amount of power at EOL (see section 5.4.7).

Flux component	Φ(I) (MeV/cm^2)	Φ(V) (MeV/cm^2)
Total flux Earth up	$4.950 \cdot 10^{14}$	$6.418 \cdot 10^{14}$
Total flux Moon	$4.871 \cdot 10^{12}$	$6.932 \cdot 10^{12}$
Total flux Earth down	$4.501 \cdot 10^{13}$	$5.567 \cdot 10^{13}$
Total flux one transfer	$5.449 \cdot 10^{14}$	$7.044 \cdot 10^{14}$
Total flux three transfers	$16.347 \cdot 10^{14}$	$21.132 \cdot 10^{14}$

Table 4.25.: The total irradiation that the SEP stage endures during its lifetime.

4.5. Mission Analysis Results

The results from the mission analysis that are of importance for the design phase, are transformed into requirements (see table 4.26), flowed down from the original requirements of section 2.2. Also, the section where the requirement is acquired can be found in the table. The complete requirement flow-down, including the design phase, can be seen in appendix C.

	Mission Requirement	Created
1.1	The initial orbit within the Earth environment shall be a LEO of $500 \times 500\,\text{km}$.	Sec. 4.2.3
1.2	To transfer from LEO to LLO, a Δv of $8498\,\text{m/s}$ shall be provided by the engines.	Sec. 4.3.1
1.3	The initial acceleration in LEO shall be $4.8 \cdot 10^{-4}\,\text{m/s}^2$.	Sec. 4.3.1
2.1	To transfer from LLO to LEO, a Δv of $8134\,\text{m/s}$ shall be provided by the engines.	Sec. 4.3.1
2.2	The total transfer from LEO to LEO of a single mission shall be performed within $300\,\text{days}$.	Sec. 4.3.1
5.1	The transfer stage and cargo shall be launched by Falcon Heavy to a $500 \times 500\,\text{km}$ orbit.	Sec. 4.2.3
5.2	The transfer stage and cargo shall be launched separately.	Sec. 4.3.2
7.1	During the last mission the SEP stage shall be disposed by de-orbitting it from LLO to impact with the Moon's surface, which requires a Δv of $64.6\,\text{m/s}$.	Sec. 4.2.4
	System Requirement	**Created**
1.1	The solar arrays shall be sized to endure, during its lifetime, a total current irradiation of $16.347 \cdot 10^{14}\,\text{MeV/cm}^2$ and voltage irradiation of $21.132 \cdot 10^{14}\,\text{MeV/cm}^2$.	Sec. 4.4
2.1.1	The specific impulse of the engine shall be $2,000\,\text{s}$.	Sec. 4.3.1
2.1.2	The initial acceleration in LEO shall be $4.8 \cdot 10^{-4}\,\text{m/s}^2$.	Sec. 4.3.1
2.1.3	A single engine shall operate $5,590\,\text{hrs}$ per mission for at least two missions with the potential of extension to three missions.	Sec. 4.3.1
3.5	The solar array shall fit inside the launcher fairing.	Sec. 4.3.2

Table 4.26.: The mission and system requirements following from the mission analysis.

5. Stage Design

The design of the Solar Electric Propulsion stage shows strong interdependencies between the Mission Analysis, Propulsion System and Electric Power System. The main system design drivers for the SEP stage and their interdependencies, are represented in figure 5.1. Note that the sketch is on top level, such that not all interdependencies and design drivers are indicated. The design is directly driven by the mission requirements, especially the transfer time and the initial acceleration have a significant impact on the thrust, power, propellant and finally on the initial mass.

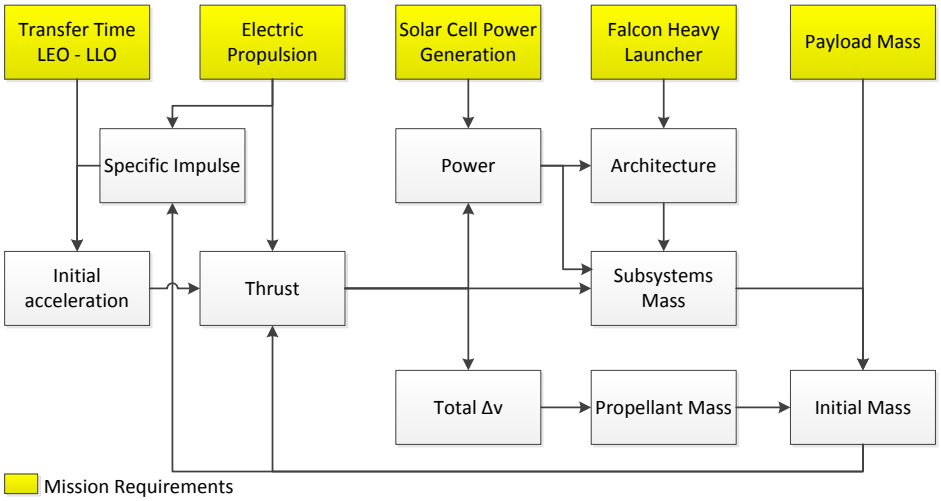

Figure 5.1.: Main system design drivers for the SEP stage.

To obtain a holistic and feasible design, the subsystems are designed by using well-established design methods, in which conventional and new technologies are used. The new technologies are especially applied in the two critical subsystems; the propulsion and electric power system. Also, a margin philosophy is applied on component and on system level. On system level, a margin of 20% is applied on the subsystems mass [75]. On component level, the magnitude of the margin depends on the heritage of the used part and is divided into three categories [75]:

- 5% for Off-The-Shelf items.
- 10% for Off-The-Shelf items that require minor modifications.
- 20% for new designed or developed items, or items requiring major modifications or re-design.

In this chapter, the decisions, models and tools, to come to the final design, are presented. The tools converge to the final design in an iterative manner by following an

iteration methodology, as described in section 5.1. To reduce the number of design options, an initial trade-off is performed on the stage architecture, resulting in a system baseline (section 5.2). Then, the Propulsion System will be designed and the power it requires analyzed (section 5.3), followed by an extensive analysis of the Electric Power System (section 5.4). The power system impacts the Configuration, Structures and Mechanisms of the stage, which will be discussed in section 5.5, and produces excess heat that needs to be rejected by the Thermal Control System (see section 5.6). Also, the agility of the stage is analyzed, resulting in a design of the Attitude and Orbit Control System (section 5.7). Finally, conservative designs are presented for the Telemetry, Tracking and Command and On-Board Data Handling systems (section 5.8). Per subsystem, the requirements that drive the subsystem design, are listed at the beginning of their sections.

5.1. Iteration Methodology

The tools that are developed in this chapter, converge to the final design in an iterative manner by following an iteration methodology (see figure 5.2). Experience learns that the mass budget of a phase 0 study has an accuracy of $\pm 10\%$. Due to this accuracy, it is chosen to apply iterations until the new initial mass budget is within 5% of the previous initial mass budget. A change in initial mass has the highest impact on the propulsion and EPS mass, followed by the structure and TCS. The initial acceleration, specific impulse and required Δv are kept constant, aswell as the AOCS, TT&C and OBDH mass. Three iterations had to be applied before the new initial mass was within 5% of the previous initial mass. The values presented in this chapter are of the last iteration step.

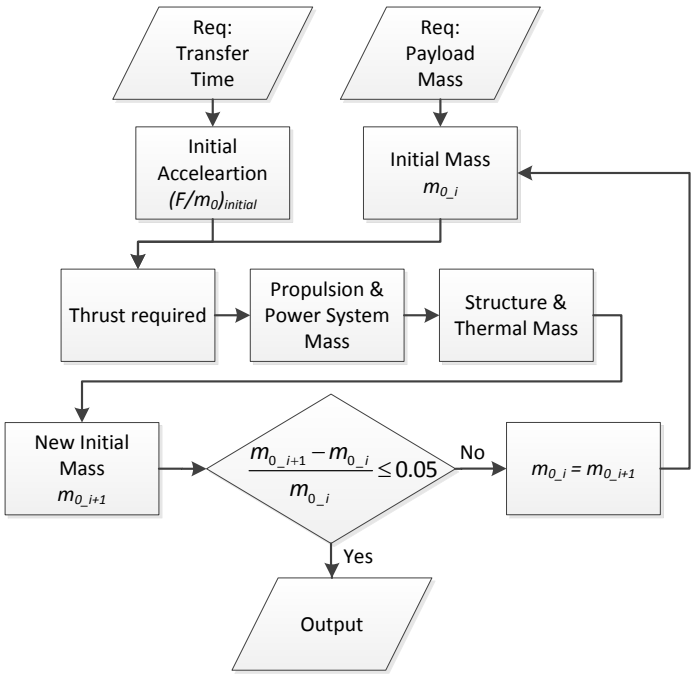

Figure 5.2.: Methodology for applying iterations to the design.

5.2. Stage Architecture Trade-off

For the SEP stage, three systems will drive the stage architecture: propulsion system, electric power system and truss structures. Especially the Electric Power System (EPS) is the driving factor for the configuration of the spacecraft due to the high power demand. This calls for a thorough trade-off on the solar array, where future and conventional technologies are considered to develop a reliable system which enables the stage to meet the mission objectives. The identified possibilities for the system architecture can be seen in the trade tree of figure 5.3, with a total number of possible system configurations of 7,200. This number of possibilities is too extensive to cover in a thesis and in order to make the trade-off feasible, a baseline is chosen through a qualitative discussion in sections 5.2.1 to 5.2.4.

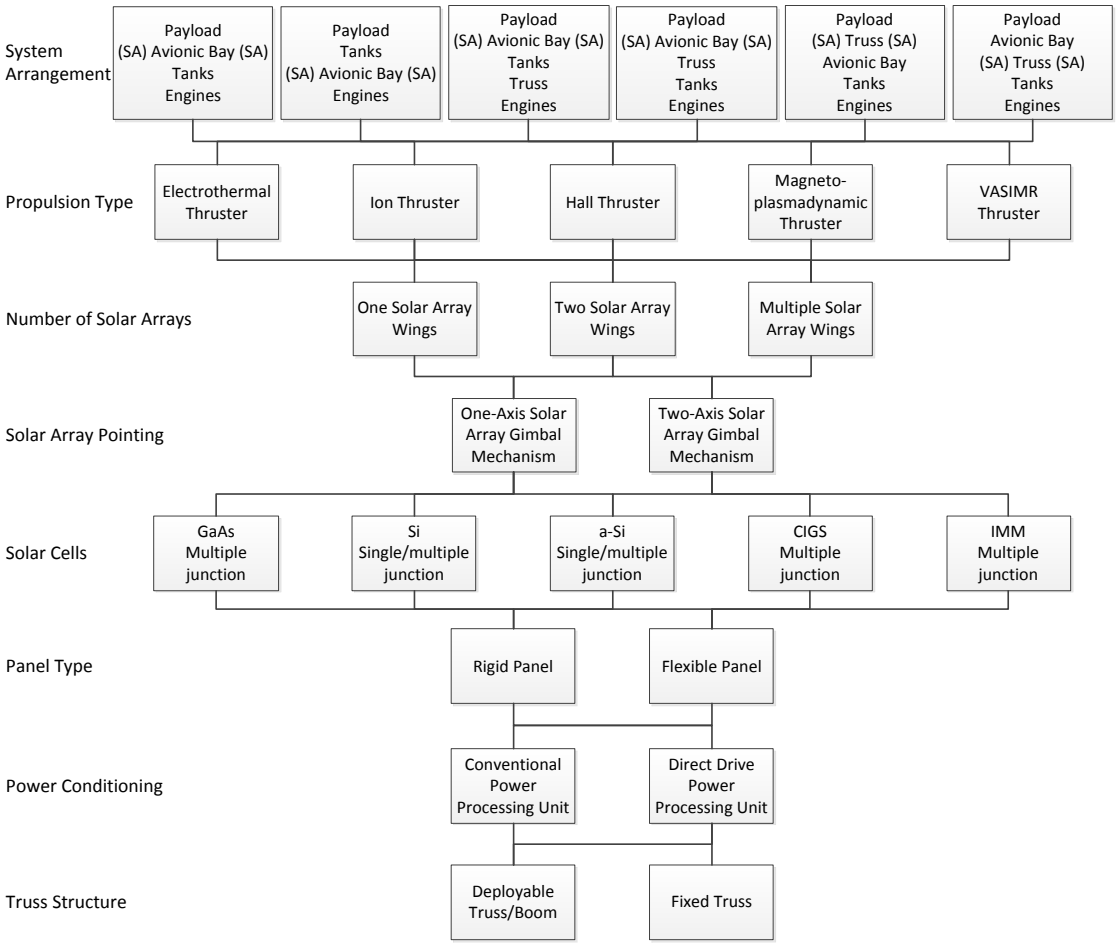

Figure 5.3.: Trade Tree for System Architecture

5.2.1. System Arrangement

The arrangement of the subsystems can be divided into six segments: engines, truss, avionics bay, payload, solar arrays and the tanks (see figure 5.4). The avionics bay contains the Power Control and Distribution Unit (PCDU), On-Board Data Handling

(OBDH) computer and Telemetry, Tracking & Command (TT&C) system. The main criteria to exclude some configurations are the position of the center of mass, subsystem dimensions, structural aspects and technological considerations.

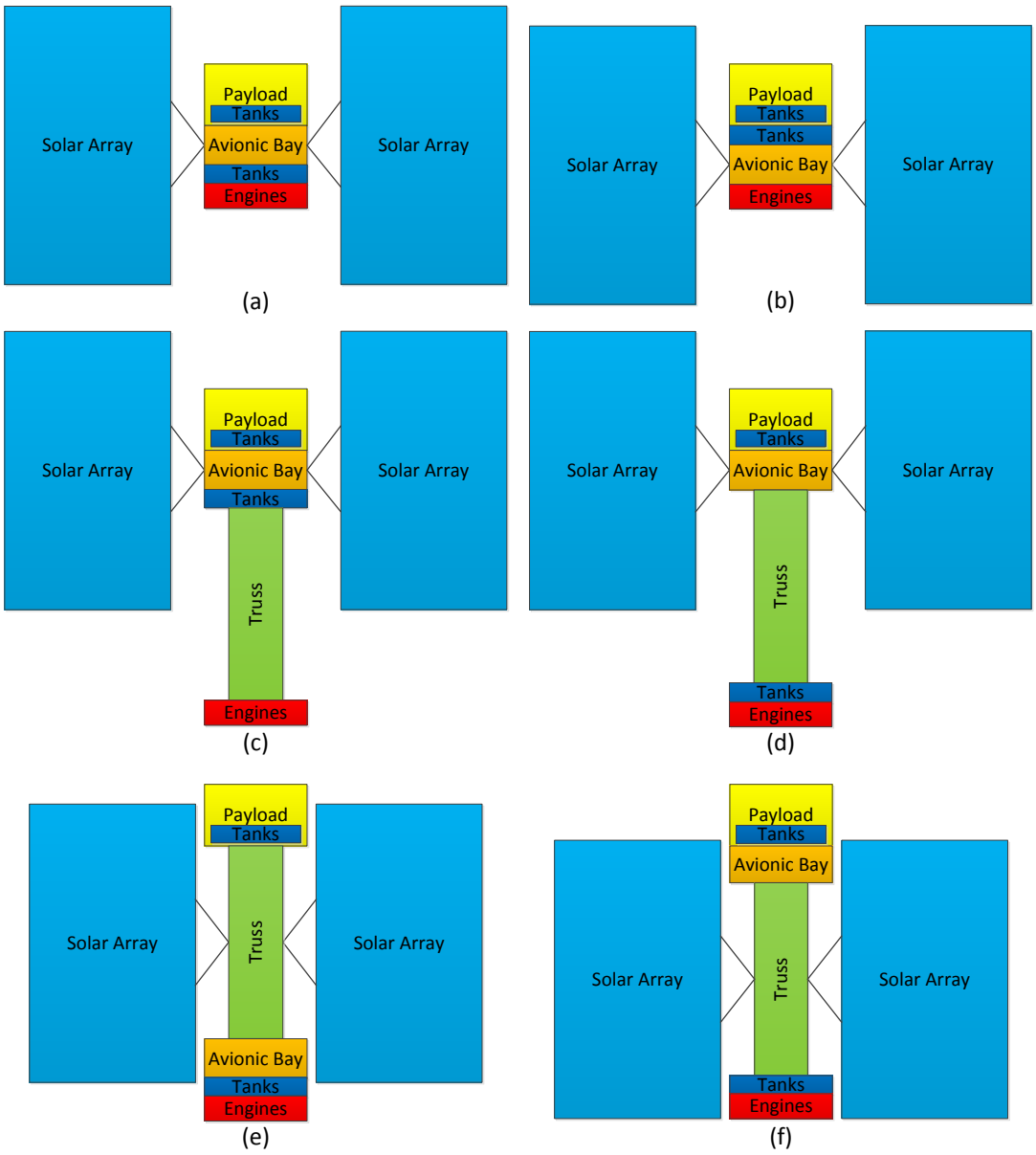

Figure 5.4.: Conceivable System Arrangements

It is required to make the stage reusable, which means that propellant is needed to perform the mission multiple times. There are two ways to achieve this: by having the complete propellant demand at the start of the mission or by refueling the stage once it is back in LEO. The first option would results in a massive stage with more than 50 ton of propellant, not mentioning the increase in power, propulsion and structural mass. This results in an unrealistic stage which does not fit into the selected launcher. The second option, to refuel the SEP stage, is more realistic. Refueling will take place when the stage returns from one mission and is in LEO. Since also a payload has to launch and

dock with the SEP stage, it is chosen to incorporate the fuel tanks within the payload, such that only one extra launch is required to perform the mission another time. The payload will be disconnected in LLO and therefore the stage itself also requires tanks to return from the Moon to the Earth. Between these tanks there has to be a propellant transfer system (see section 5.3).

From the mission analysis it was concluded to launch the SEP stage and payload separately. The stage's launcher adapter can therefore be at the engines side or at the avionic bay side. During the launch it is preferred to have the center of mass placed as low as possible in order to reduce the mechanical loads due to launcher vibrations (see section 5.5.4). So it is advisable to have the heaviest subsystems as close to the adapter as possible. For the SEP stage the propellant tanks and solar arrays are more massive than the thrusters, thus it is chosen to have the adapter at the avionic bay or tank side. The design phase shall point out how the tanks and avionic bay should be placed with respect to each other.

In configuration (a) and (b), the engine thruster plume will cause degradation of the solar arrays. This can be compensated by increasing the solar array size, but since the solar array area is already critical, this is not desired. Therefore these two options are not considered to be optimal.

Concerning the solar array wings, it is highly favorable to have two wings in order to prevent shadowing. This poses technological challenges on the Solar Array Drive Mechanism (SADM) and the solar array structure, which should therefore be studied in more detail (see section 5.4.2 & 5.5.2). In configuration (a) to (d), the Solar Array Wings (SAWs) are connected to the avionics bay and thus close to the PCDU system which is beneficial for the spacecraft harness. In case a multiple of two SAWs are required, configuration (a) to (d) become obsolete, since it is assumed that the avionic bay is not long enough to support more than one SAW each side.

In configuration (e) and (f) the truss structure also enables the possibility to have a multiple of two SAWs, in case it is not possible to have two SAWs. Configuration (e) is preferred above (f) due to harness considerations, since the high power cables have to run along the truss structure 1.5 times in configuration (f), compared to 0.5 times in configuration (e). However, the supporting truss structure in both configurations must be very stiff and therefore requires a relatively large mass. Thus, these configurations are excluded from the baseline and only come into interest when more than two SAWs are deemed necessary.

As stated, due to launcher volume limitations and center of mass considerations, the truss structure should preferably be deployable after launch. The truss structure, as placed in configuration (c) and (d), has as main purpose to ensure enough spacing between the solar array and the engines, which mitigates solar array degradation by the electric thruster exhaust plume. In option (d), the combination of tanks and engines results in a heavy tip mass and the load-carrying truss has to provide enough stiffness,

which can result in a heavy truss and should therefore be investigated.

The engines are connected to the tanks by fuel lines. The longer the fuel lines, the higher the pressure loss. However, for electric thrusters, a very high fuel pressure at the inlet of the thruster is not desired and thus configuration (c), which has long fuel lines, is not considered to impact the stage's performance. In case a deployable truss structures is used in configuration (c) or (d), flexible propellant lines are required. Flexible lines are used frequently in space industry and therefore it is expected not to be highly problematic, although a significant development effort for flexible lines along a deployable truss is foreseen.

This leaves configuration (c) and (d) as a baseline for the rest of the design phase. Also the thermal control system is a driving factor for the SEP stage, since the system needs to reject a large amount of waste heat. This is done by radiators, which are preferably positioned close to the avionics bay and engines, perpendicular to the solar array plane.

5.2.2. Propulsion Type

For the electric propulsion of the stage, five possible thruster technologies are identified:

- Electrothermal thruster
- Ion thruster
- Hall thruster
- Magnetoplasmadynamic thruster
- VASIMR thruster

Another possible thruster technology would be the Highly Efficient Multistage Plasma (HEMP) thruster, which is a new development within Europe. This new technology has the potential to perform better than Hall thrusters, but is currently performing less. The immaturity of the thruster and the fact that it is not considered to be scaled up for operation at higher power levels in the near future, make it not suitable for the mission.

The mission analysis showed that a specific impulse of around $2,000\,\mathrm{s}$ is required for the engine. The various electric propulsion technologies have different points of operation, see figure 5.5. For the required specific impulse, the Hall thruster and Magnetoplasmadynamic thruster are the main candidates. The Electrothermal and Ion thrusters typically operate at a different specific impulse and thus can not be used for the mission.

Of the VASIMR thruster only a few designs were tested, which means that the technology is still very immature and therefore it is not present in figure 5.5. The advantage of this engine is the possibility to thrust over a wide specific impulse range. In the $2,000\,\mathrm{s}$ range, the engine's performance is comparable to a conventional Hall thruster, while having a much higher complexity and mass [1]. Thus, this engine is not considered for the design phase.

The Magnetoplasmadynamic thruster fulfills the requirement considering the specific impulse. However, this type of thruster still has a very low lifetime of below $1,000\,\text{hrs}$, which is not sufficient to perform a whole mission.

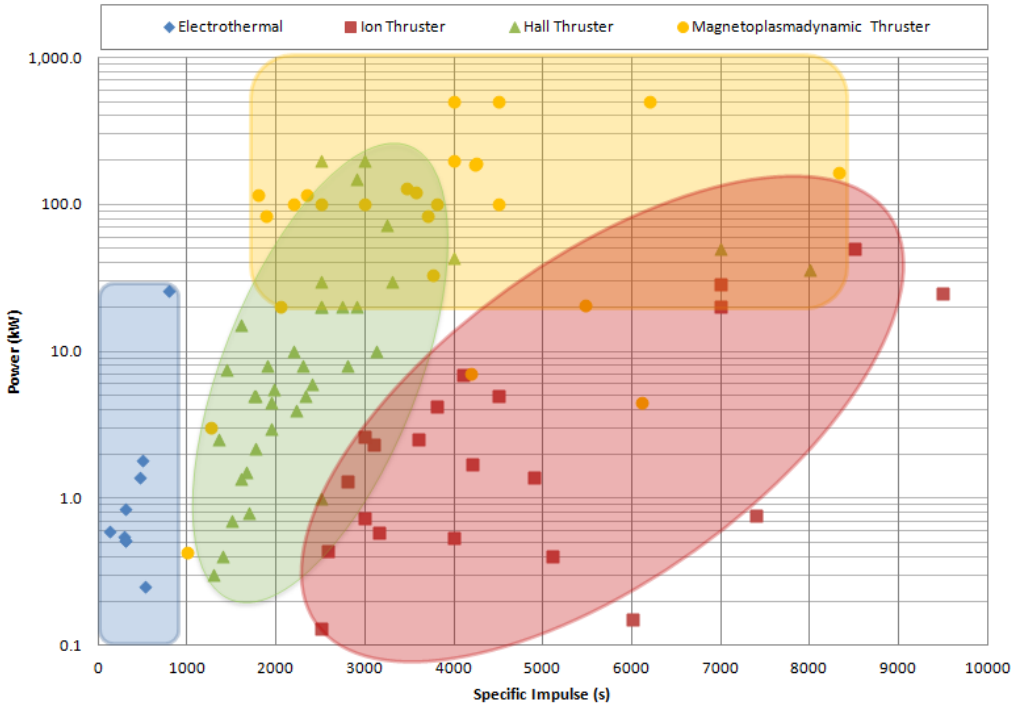

Figure 5.5.: Typical operation regions of different electric thrusters [1].

A Hall thruster can operate at the required specific impulse of $2000\,\text{s}$ and has as benefit of having a lower mass and volume compared to Ion thrusters. Compared to a Magnetoplasmadynamic thruster, the advantage of a Hall thruster is the higher level of maturity and therefore lower risk. In conclusion, the Hall thruster is chosen as baseline.

5.2.3. Solar Arrays & Power

For solar arrays there are two possible configurations: body-mounted or wing-mounted. Due to the high power requirement, a body-mounted solar array is impossible, so only wing-mounted arrays are considered. In case of a single wing-mounted array, the center of mass of the spacecraft is not in line anymore with the engines and the rest of the structure. Therefore, it is desirable to have a symmetric approach, in which the center of mass is located in line with the thruster engines. So, for the number of solar array wings, the one-wing possibility is not considered and only two or multiples of two in a symmetric wing-mounted configuration are examined. As stated in section 5.2.1, two solar array wings are preferred due to shadowing and is therefore chosen as a baseline.

The gimballing mechanism or Solar Array Drive Mechanism (SADM) is responsible for transferring power from the solar array to the spacecraft and pointing the solar array to the Sun. At least one gimbal is required to rotate the solar array in one axis and

keep it pointed at the sun. Using a one- or a two-axis gimbal has consequences for the size and complexity of the solar array and/or the Attitude Orbit Control System (AOCS) of the spacecraft. An one-axis gimbal is lighter and a simpler mechanisms than a two-axis gimbal, although one gimbal can lead to pointing errors resulting in less produced power. In section 5.4.1, a further investigation will be performed and one option selected.

The solar cell material with single or multiple junctions, in combination with a rigid or flexible panel make up the solar array. Multiple junction solar cells are more efficient than single junction cells, although they are in general thicker and thus heavier. The conventional Silicon single and multiple junction cells are ruled out, since their efficiency is too low ($< 17\%$) compared to other cells and are relatively heavy. Amorphous Silicon and CIGS also have a low efficiency, but are very thin and lightweight and are thus considered in the trade-off. Flexible solar arrays have as advantage that they can be stored in a rolled or folded configuration. The numerous possibilities require a thorough analysis in order to come to the right selection from a systems engineering point of view (see section 5.4).

The solar cells could also be combined with concentration techniques, which concentrates the sunlight unto a smaller solar cell. This technique requires a high pointing accuracy for the refractive optics in at least one axis. In combination with one gimbal, this is considered to be very difficult. Besides, concentration technology makes the design and especially deployment of the array more complex and therefore it is considered not suitable for large solar array areas [1].

The solar array, together with the power conditioning type, defines the complete EPS. For the power conditioning there are two possibilities: a conventional Power Processing Unit (PPU) or a Direct Drive power processing Unit (DDU). Using a DDU instead of a PPU eliminates the costly and massive high power converters, which leads to a significant reduction in mass. Besides, the direct drive approach increases the overall efficiency and reduces waste heat, thereby reducing the size and mass of the spacecraft thermal radiator system [19]. Also, the distance of the spacecraft with respect to the Sun is, throughout its lifetime, close to one astronomical unit. As a result, the solar array voltage is expected to stay within acceptable boundaries for the Hall thruster. Thus the DDU is ideal for the mission and selected as a baseline for the design phase.

The solar array is area and mass critical. The maximum possible area that can be obtained, depends, in case of rigid panels, on the volume limitation of the launcher fairing. In case of flexible panels, the possibilities of deployable technologies determine the maximum area that can be achieved. The silicon solar cell has a low efficiency and is commonly applied in rigid panels, which results in a significant area and mass. The other considered cells have the advantage of being either very efficient, or very lightweight. Therefore, only the conventional Si cell is omitted from the trade in section 5.4.5.

5.2.4. Truss Structure

A deployable truss is a compelling technology to save volume inside the launcher and to potentially save structural mass. The deployable structures are primarily important for the deployment of a flexible solar array. Also, a deployable structure can be considered to distance the electric thrusters from the rest of the spacecraft, in order to prevent contamination and solar array degradation. Due to these benefits, the deployable truss is selected as baseline.

5.2.5. Preliminary System Baseline

The discussion of section 5.2.1 to 5.2.4 results in a chosen baseline for the system architecture (see figure 5.6). The green boxes indicate the options that have been selected as baseline and they will be further elaborated during the design phase. The yellow boxes show that more study is required or a trade-off needs to be performed to select a final baseline at the end of the design phase. The number of possible system architectures is reduced from 7,200 to 32.

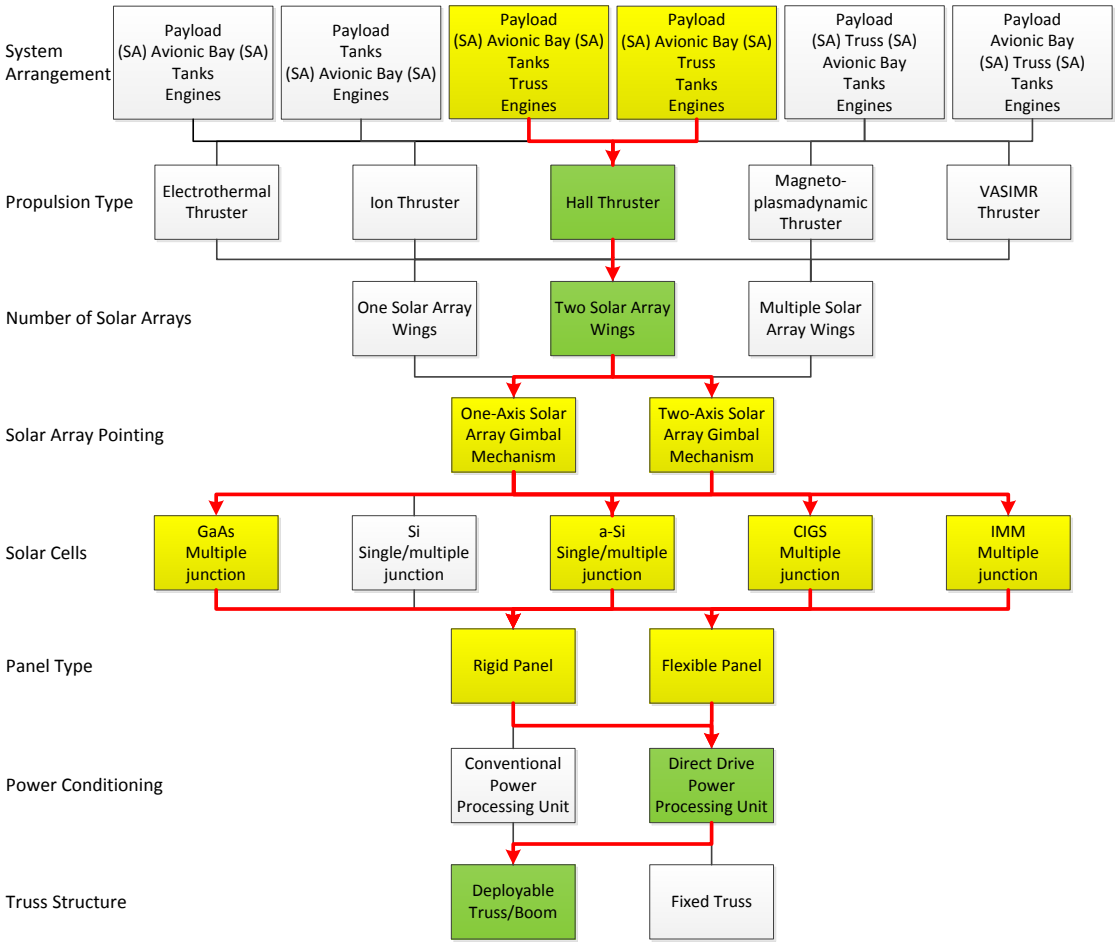

Figure 5.6.: Baseline for the System Architecture

5.3. Propulsion System

The propulsion system is essential to enable the transfer from LEO to LLO and fulfill the mission requirements. The Hall thruster is identified as the best candidate for the mission (see section 5.2.2) and the working principle will be shortly described in combination with the electric characteristics and the thruster plume interactions. Then a trade-off is made on the propellants, followed by a discussion on the tank design and the propellant feed system. Finally, a description of the mass model, a thruster selection and a propulsion system mass estimation is given.

The propulsion system has to comply with the following requirements:

	Mission Requirement	Created
1.2	To transfer from LEO to LLO, a Δv of 8498 m/s shall be provided by the engines.	Sec. 4.3.1
2.1	To transfer from LLO to LEO, a Δv of 8134 m/s shall be provided by the engines.	Sec. 4.3.1
2.2	The total transfer from LEO to LEO of a single mission shall be performed within 300 days.	Sec. 4.3.1
3.	The transfer stage shall primarily be propelled by electric propulsion.	Sec. 2.2
7.1	During the last mission the SEP stage shall be disposed by deorbitting it from LLO to impact with the Moon's surface, which requires a Δv of 64.6 m/s.	Sec. 4.2.4
	System Requirement	**Created**
2.	The transfer stage shall primarily be using electric propulsion.	Sec. 2.2
2.1.1	The specific impulse of the engine shall be 2,000 s.	Sec. 4.3.1
2.1.2	The initial acceleration in LEO shall be $4.8 \cdot 10^{-4}$ m/s^2.	Sec. 4.3.1
2.1.3	A single engine shall operate 5,590 hrs per mission for at least two missions with the potential of extension to three missions.	Sec. 4.3.1
2.1.4	The electric propulsion shall be provided by Hall thrusters.	Sec. 5.2.2
2.2	The engine can provide thrust during eclipse.	Sec. 2.2
2.3	The engines should be placed such that the thruster exhaust plume is not in contact with the solar array surface, to mitigate solar array degradation.	Sec. 5.2.1
4.	The transfer stage shall have sufficient propellant capacity to perform the transfer.	Sec. 2.2
4.1	The most suitable propellant from performance point of view shall be identified.	Sec. 2.2

	System Requirement (continued)	Created
4.2	The payload shall incorporate the propellant to transfer from LEO to LLO, for the first and final mission. For other missions, the payload shall incorporate propellant to perform the complete mission, from LEO to LEO.	Sec. 5.2.1
4.3	The SEP stage's tanks shall have enough capacity to store the propellant required to transfer from LLO to LEO.	Sec. 5.2.1

5.3.1. Hall Thruster Fundamentals

The working principle of a Hall Effect Thruster (HET) is based upon the Hall effect (see figure 5.7). First Xenon gas is fed at the anode into the discharge chamber. The electrons, coming from the cathode, are captured by a magnetic field into a helicoid near the thruster exit. Some of these electrons are attracted by the anode, spiral down into the discharge chamber and ionize the Xenon. The positive Xenon particle is now accelerated by the electric field, which is present between the anode and cathode, and provides thrust. Underway the Xenon particles pick up negative electrons which neutralizes the overall plasma beam [1].

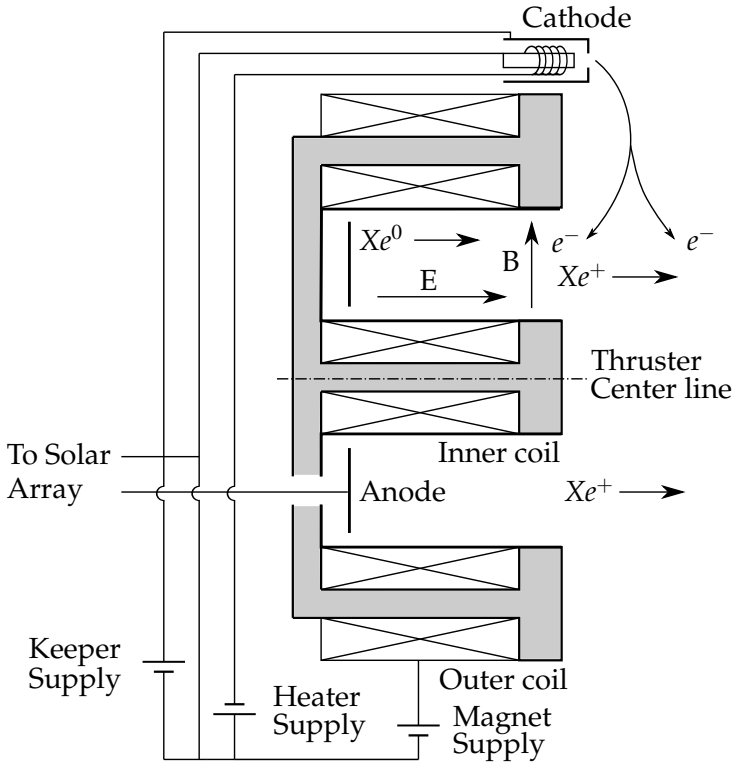

Figure 5.7.: Hall Thruster Schematic.

A Hall thruster has multiple electric supplies to control the functionality of the thruster (see figure 5.7). The heater and keeper supply are connected to the cathode and are both required to raise the temperature of the emitter and to start the electron emission and

ignition of the thruster. After start-up, the heater supply is typically turned of and the keeper supply maintains the cathode temperature to ensure a stable electron emission. The keeper supply is positively charged and therefore also functions as protection to high-energy ion bombardment from outside the cathode. The magnet supply controls the outer and inner coils to create a magnetic field [7]. These three supplies are powered by the PCDU (see section 5.4.6). Normally, a discharge supply is present between the anode and cathode. Since the DDU approach is chosen as a baseline, the discharge supply is removed and replaced for a physical connection to the solar array (see figure 5.7).

The thrust of a Hall thruster depends on the beam current, the beam voltage present between the anode and cathode and the mass of the ion. The beam current is used for ionizing the mass flow, while the beam voltage is the potential through which the ions are accelerated. The thrust is proportional to the beam current, I_b, times the square root of the acceleration voltage, U_b, and ion mass, m_i [7]:

$$F_{HET} \propto I_b \sqrt{U_b m_i}. \tag{5.1}$$

The specific impulse of the thruster depends on the exit velocity of the ions and the mass of the ion particle. The ions within a Hall thruster are accelerated under influence of the electric field, which is created by the potential difference between the anode and cathode. The level of acceleration depends on the mass of the particle. The specific impulse is therefore directly proportional to the square root of the beam voltage divided by the square root of the ion mass [7]:

$$I_{sp_{HET}} \propto \frac{\sqrt{U_b}}{\sqrt{m_i}}. \tag{5.2}$$

The lifetime of current state of the art Hall thrusters is approximately $8,000$ hrs, while for the mission a lifetime of $16,770$ hrs is required to perform three missions. However, some breakthroughs are about to be realized in which magnetic shielding should result in so-called 'immortal Hall thrusters' [68]. The lifetime of a Hall thruster is primarily limited by erosion of the discharge chamber walls, which is mostly localized near the exit plane. In this region the ions have enough energy to sputter erode the walls, which can lead to failure when eventually the magnets are affected. The magnetic shielding needs to limit this erosion, by having a balance between the thruster shape and magnetic field strength (see figure 5.8). In this configuration the erosion can be stopped and the lifetime can be extended to the next failure mode, which is, due to ion bombardment, expected to be the cathode. The lifetime of a typical cathode is demonstrated to be at least $30,000$ hrs [19].

When a Hall thruster is operated at higher powers, the power density within the discharge chamber increases. To prevent the erosion from limiting the lifetime, the thruster

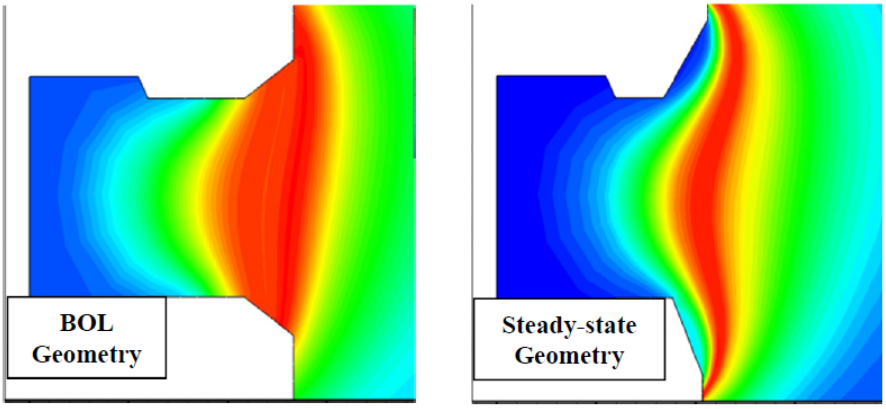

Figure 5.8.: A thruster with the magnetic shielding principle; erosions stops once the steady-state geometry is obtained [68].

needs to be scaled up, which will increase the size, mass and exhaust footprint of the thruster. The conventional way is to either increase the discharge channel of a single Hall thruster or to cluster a number of thrusters together. A new development is the nested Hall thruster, in which concentrically nesting of two or more channels are used to scale up the thruster. This approachs proofs to be beneficial for the size, mass and exhaust footprint compared to the conventional way and increases the thruster specific power and operational range [1]. Currently, only one of these thrusters exists and further development is ongoing to make it flight ready. Due to this reason it is decided not to use this technology, although it is advised to monitor the developments closely, since the anticipated performance improvement is significant [1].

5.3.2. Hall Thruster Characteristic

It is necessary to discuss the electric characteristic of the Hall thruster in order to understand the operation of the thruster within an electric circuit. The V-I characteristic of a Hall thruster for one operation point (constant mass flow and magnetic field strength) is shown in figure 5.9 [7]. The full description of the HET V-I curvature requires a profound understanding of plasma physics and is actually still a subject of debate among experts. Within the plasma, there will be potential and density variations near the thruster walls. This region of potential and density change is called the sheath and is an important region in explaining the thruster behavior.

The first region in the characteristic (see figure 5.9) shows that a certain amount of power is required to get the mass flow ionized. While increasing the potential, the ionization level is also increased until it reaches a maximum at which the ion current reaches its saturation point. The sheath voltage at these low discharge voltages is high, resulting in almost no electron flow to the discharge channel wall [63].

In the second region the total discharge current drops. There are three physical possibilities for this phenomenon. First the ions are accelerated faster with the increasing

potential, causing it to pick up more electrons that go out of the thruster. Secondly, new electrons coming from the cathode hit old electrons that are captured in the magnetic field and due to the collision the electron energy is reduced. The first option seems illogical, since it is assumed that the flow at the thruster exit is quasi-neutral at all times. The second option might be possible, but then the same effect on the total current should also be seen at higher potentials, which is not the case. A third possibility, which is found in literature [63], is that there is a high electron leakage to the discharge channel wall. This seems to be the most reasonable cause of the drop, since the rise in potential, results in an increase of the electron temperature and, hence, the kinetic energy of the electron. The energy of the electron is at this point high enough to penetrate the sheath voltage and get lost to the wall. As a consequence, the sheath potential drops and many electrons are lost to the wall. These losses increase strongly with the voltage in this regime until the electron loss to the wall saturates and the lower boundary in region two of the characteristic is reached.

In the third region the discharge voltage is high enough to saturate the sheath potential. Models predict that in this region a linear increase of total current has to occur, which corresponds to stabilization of the ion current and to a steady increase of the electron current due to Ohm's law. However, in reality the total current reaches a saturation value, which is still a non understood phenomenon [63].

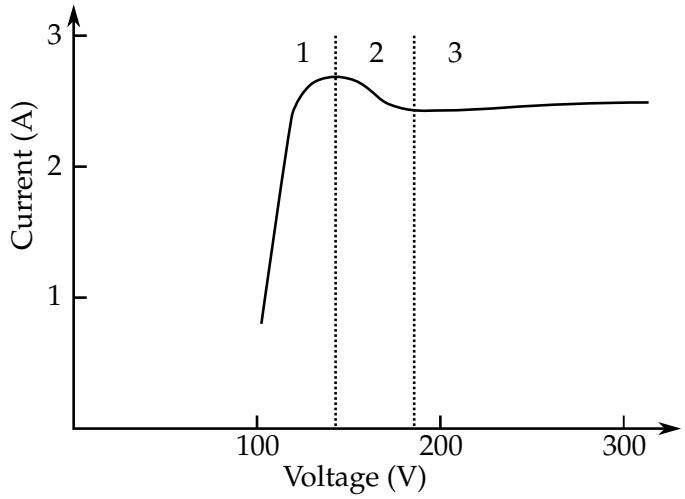

Figure 5.9.: Typical V-I characteristic of a Hall thruster [7].

The plasma that is present between the anode and cathode, can be seen as a load impedance. This plasma impedance changes under the influence of the mass flow and magnetic field strength [7]. In case the Hall thruster has no mass flow, there is a vacuum in between the anode and cathode and the impedance is infinitely high. This means that there is an open circuit and the current is zero. When the mass flow is initiated, the electrons coming from the cathode are initially all captured by the magnetic field. While increasing the voltage at the anode, the pull on the captured electrons becomes higher. At some point, they drift into the discharge chamber, create the plasma, close

the circuit and a current starts to flow. During this process also the impedance in between the anode and cathode drops. The impedance of the plasma is therefore related to the mass flow as:

$$R_{plasma} \propto \frac{1}{\dot{m}^c}. \tag{5.3}$$

Where c is a parameter, determined by experiment. As stated, the magnetic field in a Hall thruster captures the electrons in a helix near the thruster exit. Some of the electrons are attracted by the anode and spiral back. In case the magnetic field strength is stronger, less electrons will fall back to the anode. In this situation, when the discharge voltage is kept constant, the current is decreased and the impedance of the plasma is increased ($R = U/I$). The magnetic field strength is therefore proportional to the plasma impedance:

$$R_{plasma} \propto \bar{B}^d. \tag{5.4}$$

Where d is a parameter, determined by experiment. The real behavior of the plasma impedance is difficult to be modeled quantitatively, but the discussion shows that the V-I characteristic can be manipulated by changing the mass flow and/or the magnetic field strength. When the magnetic field strength is increased, the curve will shift down and to the right. The same effect occurs when the mass flow is decreased. There are models existing to create the characteristic of a specific Hall thruster, although a significant effort is required to make them more accurate [63]. Further study of the characteristic is beyond scope, due to the complexity of all the effects and the system engineering character of this work. In subsequent design phases the characteristic should be determined by detailed modeling and intensive testing of the selected thruster.

5.3.3. Thruster Plume Interactions

A Hall thruster has a wide exhaust plume, which causes problems for the spacecraft. The issues that arise due to the thruster plume are [6] [19]:

- Erosion of surfaces, especially the solar arrays, by the high energy ions.
- Contamination of (solar array) surfaces due to re-deposition of sputtered material.
- Interference of spacecraft communication within the S-band.
- Spacecraft charging and electrostatic discharge.

Especially the first two issues are of importance, since they have an effect on the solar array performance. To investigate the impact, the geometry of the plume has to be modeled and researched. Due to the complexity of such a model, the thruster plume is discussed qualitatively in order to come to an initial design decision.

The highest ion concentration of the plume can be found along the thruster centerline. Typically, the ion density for Hall thrusters decreases gradually for an increasing plume angle to an angle of 80°, thereafter it decreases rapidly. Experiments showed that a small fraction of high-energy ions are still present at plume angles from 90° to 110° [59].

As stated, sputtered material from the thruster discharge channel can contaminate the solar array. The sputtered material comes out at large angles and can fall back to the spacecraft surfaces. Thin layers of the deposited material can change the properties of the spacecraft surfaces and lower the performance of the solar array. This deposition occurs for plume angles far from the thrust direction [7].

The effect of the plume on the communications is considered to be a minimal problem. A conventional S-band antenna should be sufficient for communication, although the plume will cause a phase shift within the signal (see section 5.8) [7].

The spacecraft charging and electrostatic discharge can be prevented by having a smart design. For the stage this entails to have a proper grounding scheme and to use plasma contractors to lower the spacecraft potential. The last task can be performed by the Hall thruster cathodes, which should therefore also operate during eclipse. This can be achieved by providing Xenon to the cathode and power to the heater and keeper supply, which is estimated at 200 W per cathode [22]. The cathodes help to control the charge on the spacecraft and reduce the possibility of arcing events. More importantly, leaving the cathodes on, also keeps the engine in a configuration that will allow for a quick start to return as fast as possible to nominal operations when the stage comes out of eclipse [1]. This on-off cycling is critical, since maximizing the duration of full thrust will maximize the vehicle performance [31].

The most straightforward solution to protect the solar array from the ions and the sputtered material, is to position the thrusters such that the plume and sputtered material does not interact with the solar cells. This means that, due to the large plume angle of 110°, the thruster should be positioned approximately 10 to 20 meters away from the solar array blankets, which is an unacceptable distance due to the volume limitation of the launcher. Therefore it is chosen to size the solar array, such that it accounts for the plume impingement loss. Consequently, the thrusters can be placed in line with the solar array width, meaning that some ions at plume angles of 90° to 110° have a probability of hitting the solar arrays and erode its surface. Also, the array will be exposed to some of the sputtered material coming from the thruster. These effects will be taken into account in the solar array design, by having redundant solar cell strings and loss factors. Further analyses are required in subsequent design phases to evaluate the effect of the thruster plume on the stage performance.

5.3.4. Hall Thruster Propellant

Multiple propellants have been tested and used for Hall thrusters, of which the ionization potential and atomic weight are important properties (see table 5.1). The ionization potential is the amount of energy which is required to ionize the propellant. It is preferred to have a low ionization potential to achieve a high thruster efficiency. The square root of the atomic weight is proportional to the thrust and inversely proportional to the specific impulse (see equations 5.1 and 5.2).

Every propellant has different performance characteristics, handling properties and accessibility (see table 5.2). Mercury and Cesium were initially tested as propellant, but became obsolete due to their high toxicity and difficult handling characteristics. Argon has a low performance and is therefore not considered to be an option, which leaves Xenon and Krypton as the only feasible options.

Fuel	Ionization potential (eV)	Atomic weight (−)
Argon	15.8	39.95
Cesium vapor	3.9	132.9
Krypton	14.0	83.8
Mercury vapor	10.4	200.59
Xenon	12.1	131.3

Table 5.1.: The ionization potential and atomic weight of typical Hall thruster propellants [1].

Currently, Xenon is mostly used as propellant, since it has a good performance and handling characteristics. Compared to Krypton, the efficiency of a Hall thruster operating on Xenon is typically 5 to 15% higher than for the same thruster operating on Krypton [1]. So due to the conventionality and higher performance, Xenon is selected as propellant.

Fuel	Advantages	Disadvantages
Argon	Cheap Abundant	Low performance
Cesium vapor	Easy to ionize High vapor pressure	Toxic, highly reactive Difficult to handle
Krypton	Cheap, chemical inert	Average performance
Mercury vapor	Relatively low ionization potential	Toxic, highly reactive Poor storage properties
Xenon	Nontoxic, rel. low ionization potential Reliable, good storage properties	Relatively high cost Low availability

Table 5.2.: Advantages and disadvantages of Hall thruster propellants [1].

However, it must be noted that Xenon has a low availability and therefore relatively high costs. The global production of Xenon in 2008 was around 71 ton [85], while approximately 30.9 ton is required to perform the mission once. This is 44% of the total production in 2008, which shows that a Xenon buying strategy of multiple years is required to safeguard the required amount of Xenon propellant. In case this cannot be realised, Krypton can be used as a back-up, since it is more widely available. Recently, a new propellant, Iodine, is discovered which has the same performance as Xenon, a lower plume divergence and is more widely avalaible [74]. This development could result in a better alternative than Krypton and should be followed closely.

5.3.5. Propellant Tanks

The tanks are required to store the propellant, without having any leakage. The Xenon is stored in multiple tanks, within the SEP stage and in a separate section of the payload. The payload has to store 22.8 ton of Xenon for at least 200 days and the SEP stage approximately 8.1 ton for at least 900 days, having a total of 30.9 ton. The tank has an interface to the Xenon Feed System (XFS), which typically can accept a maximum pressure of 18.6 MPa (see section 5.3.6).

A decision has to be made at which temperature and pressure the Xenon shall be stored. The Xenon phase diagram indicates at which temperatures and pressures the fluid is in liquid, gaseous or supercritical phase (see figure 5.10). The critical point of Xenon is at a temperature of 289 K and a pressure of 5.8 MPa [86]. Above the critical point, Xenon is a supercritical fluid in which a distinction between gas and fluid cannot be made.

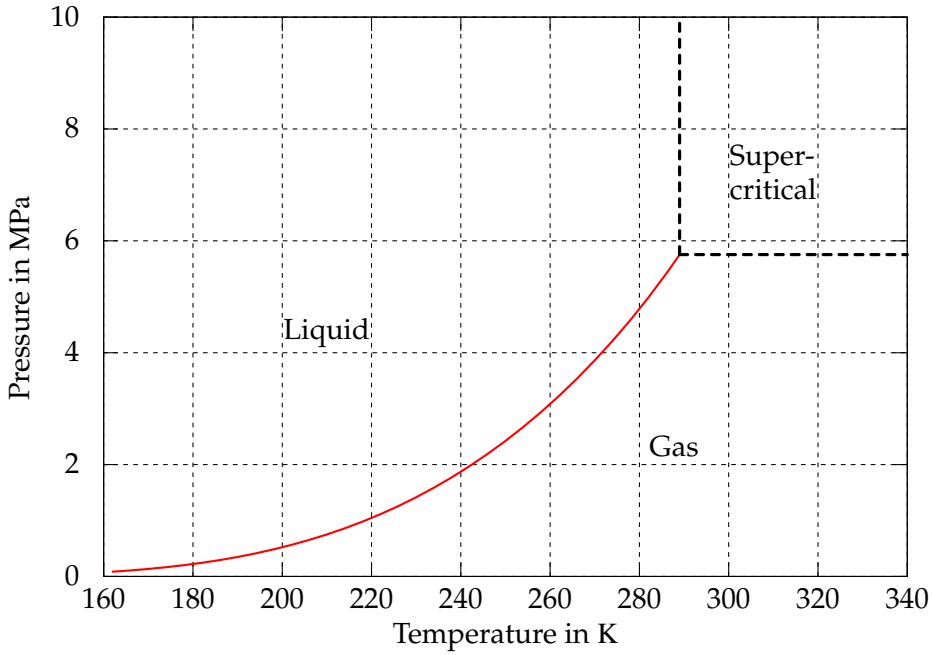

Figure 5.10.: The Xenon Phase Diagram showing the liquid, gaseous and supercritical phase [86].

The Xenon tanks of the SMART-1 and Dawn missions both store the propellant at 15 MPa in the supercritical regime [72] [73]. For these systems it was not allowed that the fluid would condense and liquefy and such the tanks were equipped with powered thermal blankets to keep the temperature above 294 K. However, from the density point of view it is preferable to store the Xenon in the liquid phase. Figure 5.10 indicates that the temperature should then be below 289 K, including a safety margin this can typically be 274 K. Comparison with the inside of the spacecraft, which will be in between 273 K and 303 K (see section 5.6), indicates that thermal insulation of the tanks will be required to shield it from the rest of the relatively warm spacecraft and keep it at a temperature of ≤ 274 K. Also, the Xenon must be supplied to the Xenon Feed System in the gaseous state and thus it must be heated to boil in a separate volume, which requires a heater of approximately 230 W [19]. Besides, a liquid fuel is more dense than a gas and therefore requires more structural mass to carry for example sloshing loads during launch. This system is therefore relatively complex and a trade-off on the storage point, has to be done.

The required tank volume to store the propellant, is depending on the pressure and temperature of the Xenon (see figure 5.11). For $T = 274$ K, the phase change from liquid to gas can be seen at the point where the volume suddenly increases. This indicates that the least required volume for storing Xenon is in the liquid phase. For temperatures above the critical point ($T = 294$ and 304 K), the fluid is at high pressures supercritical and makes a more gradual transition to gas.

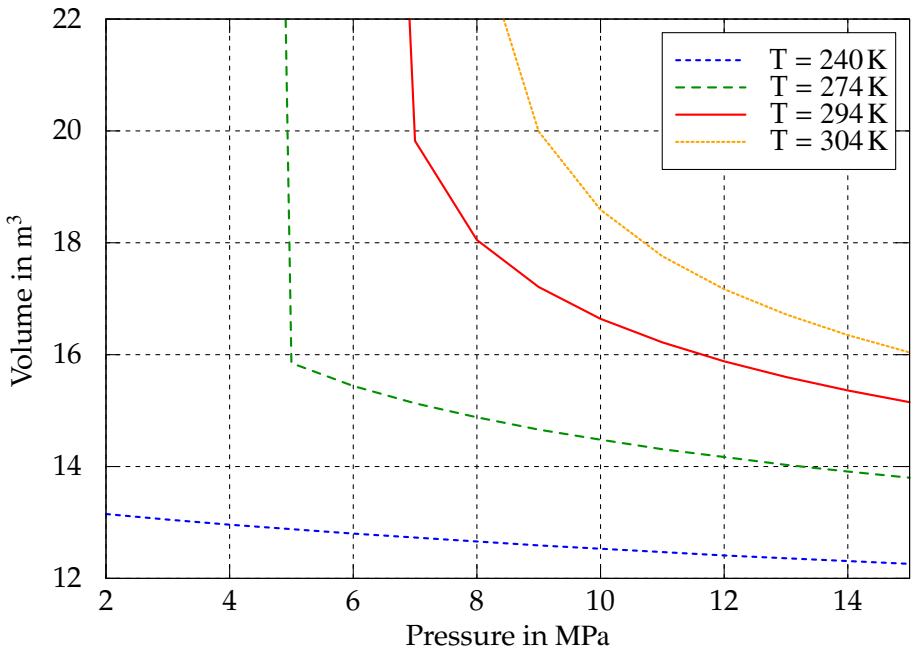

Figure 5.11.: The required tank volume for a propellant mass of 30.9 ton and different storage temperatures [86].

The dual launch mode releases the volume budget considerably and such reducing the

tank volume from $16\,m^3$ to around $12\,m^3$ is not a decisive parameter. Another important decision parameter would be the mass of the system. The two following storage conditions are considered [32] [19]:

1. Conventional option: $P = 12\,MPa$, $T = 294 - 304\,K$, $\rho_{Xe} = 1797 - 1943\,kg/m^3$
2. Cryogenic option: $P = 2\,MPa$, $T = 240\,K$, $\rho_{Xe} = 2346.2\,kg/m^3$

The Xenon densities for these pressures and temperatures are obtained from reference [86]. The first option is a conventional option, comparable to Dawn and SMART-1, although the tank pressure is reduced from 15 MPa to 12 MPa. The second option is considered in reference [19] and stores the Xenon in liquid phase at a pressure of 2 MPa and a temperature of 240 K. The lower storage pressure logically results in a lighter storage tank compared to option 1. However, the higher density of the fluid will cause it to initiate relatively high sloshing loads during launch and could possibly be the sizing case that drives the tanks mass. On the other hand, due to the low storage temperature, the complexity of the thermal control system and Xenon feed system are increased.

The tank mass for the different options can be expressed as a fraction of the total propellant mass, for option one this is equal to 0.04 [32] and for option two 0.02 [19]. The resulting tank volume and mass can be found in table 5.3. It shows that the cryogenic storage is 617 kg lighter compared to the conventional storage option, which means a reduction of approximately 1% on the total vehicle mass. However, as stated, the cryogenic option requires a higher complexity for the thermal control system, structure and Xenon feed system. Besides, since propellant storage at the payload is required, it will also increase the complexity of the payload's thermal control system and structure. Although there is a reduction of 1% in mass, this increase in complexity is not considered to be practical and, most likely, will reduce the mass benefit. Therefore, the simpler option, i.e. the conventional one, is selected for the storage of the propellant.

Characteristic	Option 1	Option 2
Pressure (MPa)	12	2
Temperature (K)	294-304	240
Density (kg/m^3)	1797-1943	2346.2
Tank Volume (m^3)	17.2	13.2
Propellant Mass (kg)	30,853	30,853
Mass Fraction ($-$)	0.04	0.02
Tank Mass (kg)	1,234	617
Complexity	Average	Above average

Table 5.3.: Comparison of the two suggested Xenon storage points.

The Xenon high pressure tanks are typically constructed out of large composite overwrapped pressure vessels with a titanium liner and graphite-epoxy overwrap [72] [19].

To determine the mass of these tanks, an approach from reference [13] is adopted. The mass of a spherical pressure vessel can be calculated by [13]:

$$m_{spherical} = 1.5\frac{pV}{s_\sigma}. \tag{5.5}$$

Where p is the pressure in Pa, V the volume in m^3 and s_σ is the specific strength of the material in m. The specific strength for a composite pressure vessel can be in between 110 to 390 km [13]. A value was chosen for which the tank mass of the Dawn and SMART-1 mission could be reconstructed and resulted in a specific strength of 250 km. The tanks can also be made up of cylindrical sections and elliptical domes. The chosen mass relation for the elliptical dome, has a configuration in which the height is 60% of the circular base radius. The mass of a cylindrical section in between two spherical domes and the mass of a eliptical dome, is estimated by [13]:

$$m_{cylindrical-section} = 2\frac{pV}{s_\sigma}. \tag{5.6}$$

$$m_{elliptical} = 3\frac{pV}{s_\sigma}. \tag{5.7}$$

The following equations are required to calculate the volumes and identify the tank dimensions:

$$V_{sphere} = \frac{4}{3}\pi r^3. \tag{5.8}$$

$$V_{cylinder} = \pi r^2 h. \tag{5.9}$$

$$V_{ellipsoid} = \frac{4}{3}\pi abc. \tag{5.10}$$

For the ellipsoid the base area is circular, meaning that a and b are equal to the radius of the tank and the height of the ellipsoid is c. The total propellant storage shall be equal to 30.9 ton. In practice, the tanks cannot be emptied completely and some residuals remain in the tank, therefore a margin of 2% is applied on the propellant mass [75]. Also, during fuelling of the tank, some gas will remain inside the tank, called ullage. A margin of 10% is included on the volume of the tanks to account for this ullage [75]. The propellant residuals increase the overall propellant mass to 31.5 ton, this value combined with the accounted ullage, increases the total volume to 19.3 m^3. In case one spherical tank is selected, it requires a diameter of 3.3 m. When four cylindrical tanks with spherical domes are used, with a radius of 0.74 m, the total height will be 3.3 m. The cylindrical tanks can be easier attached to the structure and have thus structural benefits, therefore,

four cylindrical tanks are chosen, that have to be attached to every payload. For the SEP stage it is beneficial, from the structural point of view, to have a single tank. To limit the height of the tank, a elliptical tank is chosen which has a sufficient cylindrical section to provide an interface with the load bearing structure (see table 5.4).

	SEP stage	Payload 1	Payload N
Number of tanks	1	4	4
Geometry	Cylindrical+ Elliptical domes	Cylindrical+ Spherical domes	Cylindrical+ Spherical domes
Radius (m)	1.14	0.74	0.74
Height cylinder (m)	0.33	1.08	1.82
Total height (m)	1.69	2.56	3.30
Total volume (m^3)	5.05	14.21	19.26
Tank mass (kg)	663.4	1202.1	1686.7
Propellant mass (kg)	8,248	23,222	31,470

Table 5.4.: Final tank configuration for SEP stage and payload, by taking into account 2% propellant residuals and 10% ullage volume.

For the last mission, an incremental Δv of 64.6 m/s is required for disposal, which is, with the current architecture, equal to 53 kg of extra fuel. During the last mission, the fuel to return from LLO to LEO does not have to be incorporated and therefore there is more than enough space to incorporate the fuel for disposal.

The tank masses are obtained by taking the pressure and volume as the sizing case. However, Xenon has a very high density and thus the mass inside the tanks is very high. Therefore, it has to be evaluated in subsequent design phases if the tank's strength is sufficient to carry the propellant mass, especially during launch.

5.3.6. Xenon Feed System

The Xenon Feed System (XFS) is responsible for supplying the Hall thrusters with propellant. The propellant comes from the high pressure tanks and needs to be conditioned to a lower pressure, to finally deliver a low pressure gas to the anode and cathode of the thrusters. The mass flow needs to be accurately adjusted for every anode and cathode to be able to have enough control concerning the Hall thruster characteristic and DDU operation. The XFS presented here is based upon lessons learned from the Dawn and SMART-1 mission and follows the approach of reference [71].

It is required that the XFS has to function for at least 900 days, while preventing internal and external propellant leakage. In case the maximum amount of power is fed to the thrusters, the XFS should be able to provide a maximum mass flow of 6.4 g/s (using equation 4.26 and applying a margin of 100% to account for power variation), which is

distributed to all the functioning engines. To maximize the stage performance, the start up time and transition times between throttle levels should be as low as possible.

The propellant which is fed to the anode and cathode of the thrusters, does not require a high pressure level. A pressure regulated system, which maintains the high pressure in the propellant tank, is therefore not required. However, the pressure in between the tank and thruster is regulated to a lower level that is acceptable for the engine.

The Dawn and SMART-1 vehicles store the Xenon propellant at 15 MPa and use a so called 'bang-bang' regulation method to condition the pressure down to 0.68 MPa and 0.2 MPa respectively, into plenum tanks. Two solenoid valves, with a small volume in between, control the pressure reduction of the system. Downstream of the valves, the two plenum tanks act as a buffer, of which one is connected to the anode and the other to the cathode of the thrusters. Flow controllers near the thruster regulate the low pressure flow, such that the thruster anode and cathode are supplied with the desired mass flow. The controller regulates the flow using a thermothrottle, which contains thermally constricting capillary tubes, such that an increase in temperature results in a decrease of Xenon flow [71]. In the design of Dawn and SMART-1, Xenon is fed to the plenum tank until a certain pressure is reached and the solenoid valves are closed. When the pressure reaches a lower bound, the solenoid valves are opened again to fill up the plenum tanks. This sawtooth flow behavior caused a 1% higher Xenon flow rate to the thrusters than required. Also, the plenum tanks have a long transition time, from a few to ten minutes, from one flow condition to another, especially when throttling down. These long throttling times result in long startup transients, which leads to wasted propellant and a loss in performance. This is undesirable, especially in LEO and LLO, and therefore JPL developed a new standard architecture for XFS [71], which is used as a baseline for this mission.

The new architecture consists out of a common high-pressure regulation module (PMA) combined with a distributed low-pressure throttling module (XFC, see figure 5.12). The high-pressure module consists out of a single Propellant Management Assembly (PMA), which allows for the propellant distribution to all the engines at low pressures. This regulation approach has an interface with the OBDH of the spacecraft. The PMA consists out of pressure transducers, temperature sensors, fill and drain valves and two parallel redundant regulator-isolation-latch-valve strings. The strings contain a gas regulator, which has two stages. The fist stage releases the gas at a constant rate, despite the pressure upstream of the gas regulator. The second stage of the regulator controls the pressure reduction from the high pressure to a constant low pressure. The maximum inlet pressure of the complete PMA is typically 18.6 MPa and the regulated outlet pressure in between 0.245 to 0.265 MPa [71].

The low-pressure flow throttling module is located near every engine and is called the Xenon Flow Controller (XFC). It has an electronic interface with the Xenon Thruster Unit within the DDU and consists out of a latch valve, Proportional Flow Control Valve

(PFCV) and Flow Control Device (FCD). The PFCV actively controls the pressure upstream of the FCD. The FCD is located near the thruster anode or cathode [71] and consists out of a thermothrottle. Such a thermothrottle changes under the influence of changing temperature to regulate the mass flow. The temperature can be controlled by the power that is provided by the DDU. The combination of PFCV and FCD can therefore control the pressure and temperature and thus provide a precise mass flow regulation. The PFCV also provides shut-off capability to close off the anode while cathodes are still running, as required for the eclipse phase.

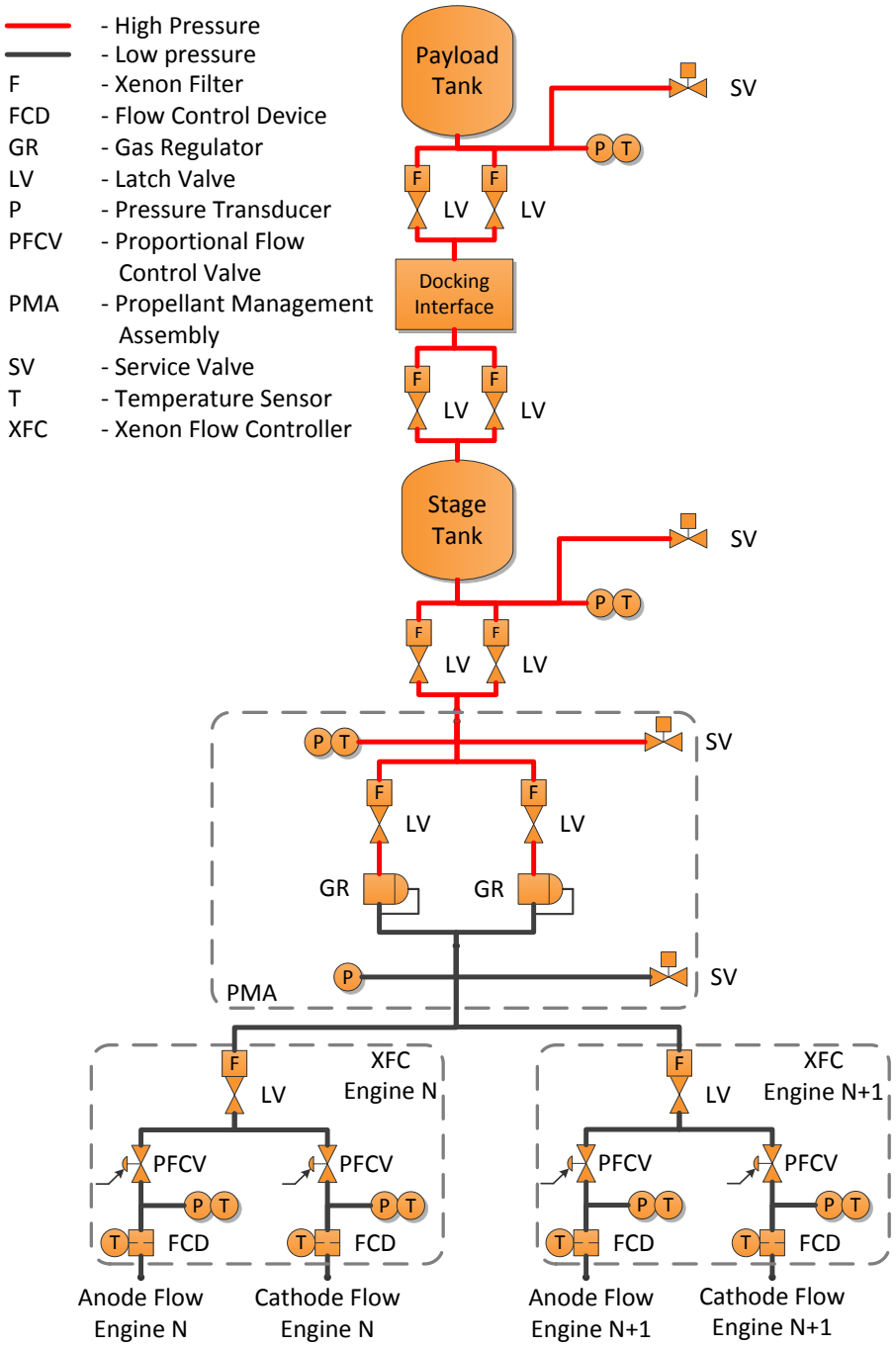

Figure 5.12.: Conceptual design of the Xenon Feed System.

The failure of a component within an XFC, will result in the failure of one thruster string, which can be separated from the rest of the system by closing the latch valve. This is accounted for by having one redundant thruster string and thus this part of the system is single-fault tolerant. Upstream of the XFCs, the PMA and tank valves have each a redundant string, which can take over the complete functionality in case one string fails.

Compared to the Dawn and SMART-1 mission, the transition times between throttle levels is reduced from more than ten minutes, down to typically 90 to a maximum of 200 seconds for this type of architecture [71]. This system will therefore ensure quick start up times and maximize the performance of the SEP stage, especially in lower orbits.

The XFS also has to provide propellant transfer from the payload tanks, through the docking interface, to the SEP stage propellant tanks. Also service valves are required for filling and draining of the tanks. The XFS, as proposed here, functions as a conceptual design for subsequent design phases, which means that changes can still be applied to the PMA, XFC and tank valves.

5.3.7. System Mass Model

The complete propulsion system is existing out of the Xenon tanks, Xenon feed system, DDUs, gimbals and thrusters (see figure 5.13). The suggested solar electric propulsion stage is an unconventional design, which requires a high power and a high thrust compared to already realized electric propulsion systems. Therefore there are almost no off-the-shelf components available for the system and thus small EP systems are scaled up to come to a mass estimate for our system. For these estimations, the model of reference [32] is adopted, where known systems and discussions with manufacturers were used to come to empirical formulas for high power EP systems.

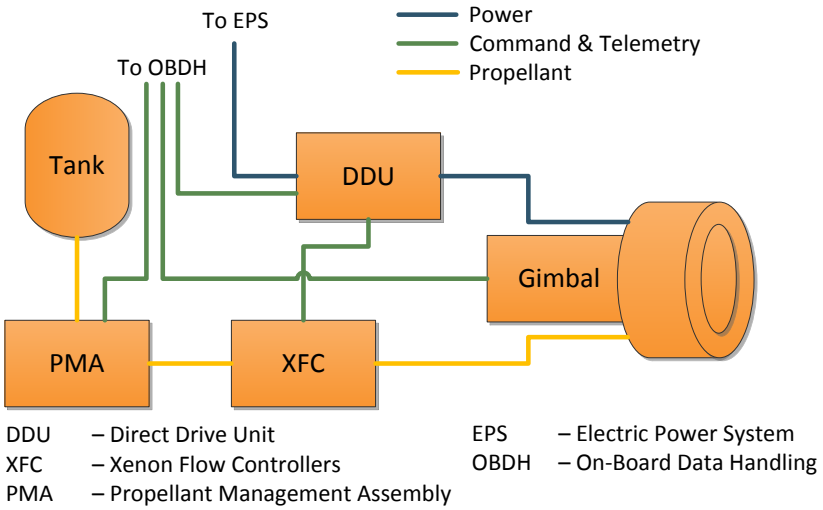

Figure 5.13.: A complete thruster string of the propulsion system.

The presented mass equations are based upon the assumption that each thruster string is able to operate independently. In this case only the propellant tank is shared with the other thruster strings. The mass of all the system components is scaling with the thruster power, P_{thr}, and the total number of thrusters, N_{tot}. The total number of thrusters is consisting out of the active, N_{ac}, and redundant ,N_{rd}, thrusters [32]:

$$N_{tot} = N_{ac} + N_{rd}. \tag{5.11}$$

Redundant thruster strings are used when a thruster or complete string fails. For a robotic mission, the system is typically single-fault tolerant and therefore one redundant thruster sting is included in the system ($N_{rd} = 1$, see section 6.1.1). The thruster power is depending on the total system power, P_{sys}, divided by the number of active thrusters [32]:

$$P_{thr} = \frac{P_{sys}}{N_{ac}}. \tag{5.12}$$

Where the thruster power and system power are in kW. The total system power is the required discharge power for the Hall thrusters (see section 4.2). The power delivered by the solar array, shall therefore be higher, since the electric power system has an efficiency below one.

It is assumed that the thruster mass scales linearly with power [32] and such a linear curve can be plotted through Hall thruster data, to obtain the thruster mass as function of the thruster power (see figure 5.14). The total thruster mass equals:

$$m_{thr} = N_{tot}\left(1.4572 P_{thr} + 0.7241\right) = \left(N_{ac} + N_{rd}\right)\left(1.4572 \frac{P_{sys}}{N_{ac}} + 0.7241\right). \tag{5.13}$$

Where the mass is in kg. This relation is established out of a database with ten Hall thrusters (see appendix B.2). To allow for steering during the flight, gimbals are required. A gimbal provides a pivoted support that allows the thruster to rotate about its axis and thus tilts the thrust vector to a required angle. The thruster gimbal mass can be expressed as a ratio of the thruster mass. From the flown missions, like NSTAR and NEXT, it can be concluded that the gimbal mass is approximately 50% of the thruster mass. Not all thrusters have to be gimbaled and thus a gimbal factor f_{gim} is included in the gimbal mass equation [32]:

$$m_{gim} = 0.5 f_{gim} m_{thr}. \tag{5.14}$$

The DDU mass scales linearly with increasing power [32]:

$$m_{DDU} = N_{tot}\left(0.35 P_{thr} + 1.9\right). \tag{5.15}$$

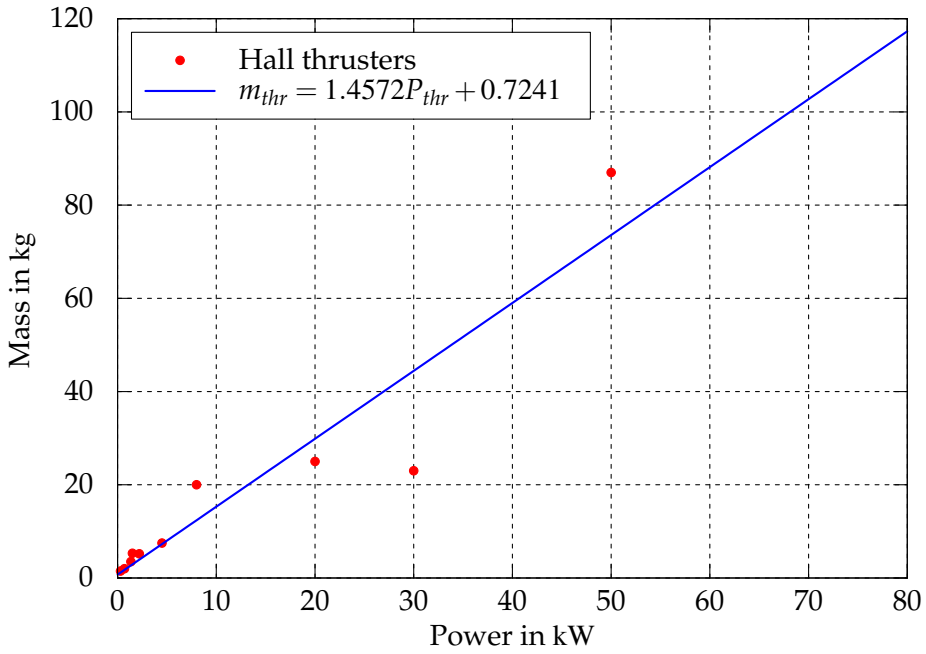

Figure 5.14.: Hall thruster mass as function of power (data from appendix B.2).

The mass of the cables in between the thruster and DDU can be expressed as [32]:

$$m_{cab} = N_{tot}\left(0.06778P_{thr} + 0.7301\right). \tag{5.16}$$

The mass of the Xenon feed system is only a function of the total number of thrusters and determined by [32]:

$$m_{XFS} = 3.2412N_{tot} + 4.5189. \tag{5.17}$$

The tank mass is calculated in section 5.3.5. The total mass of the propulsion system is the summation of all the components. Also, a fraction (1.26) is included which accounts for the structural mass necessary to integrate the propulsion system into the spacecraft [32]:

$$m_{ps} = 1.26\left(m_{thr} + m_{gim} + m_{DDU} + m_{cab} + m_{XFS} + m_{tank}\right). \tag{5.18}$$

This model is used to determine the mass of the propulsion system.

5.3.8. Hall Thruster Selection

Earlier identified requirements are used to select Hall thruster candidates and perform a trade-off. From the mission analysis it was derived that the initial acceleration shall be at least $4.8 \cdot 10^{-4}\,\mathrm{m/s^2}$, the specific impulse $2,000\,\mathrm{s}$ and the Hall thruster lifetime at least $16,770\,\mathrm{hrs}$. The Hall thruster database (see appendix B.2) and references [64] and [65] are used to select a high power thruster that fulfills all the requirements (see table 5.5).

As the name suggest, the NASA-400M and NASA-457M are development projects from NASA. They were initiated in the year 2000 and stopped in 2006, because of budget cuts. However, there is renewed interest in developing high power Hall thrusters, which can also be concluded from the new development of the NASA-457Mv2, X2 and X3 nested Hall thruster [67] [1]. In Europe, the highest power thruster currently designed is the HT-30 (Alta SpA, Italy, 2011) [69], followed by the operational and tested 20 kW PPS-20k ML (Snecma, France, 2011) [70].

Characteristic	Requirement	HT-30	NASA-400M	NASA-457M
Power (kW)	529	30	38.5	50
Thrust (N)	31.3	1.55	1.75	2.5
Specific Impulse (s)	$2,000$	$2,500$	$2,500-3,300$	$1,700-3,000$
Lifetime (hrs)	$\geq 16,770$	-	-	$8,000$
Operating Voltage (V)	$300-500$	500	$300-500$	$300-600$
TRL		4	6	6

Table 5.5.: Hall thruster requirements and candidates for the mission (see appendix B.2) [64] [65].

The mass model of section 5.3.7 is applied on the thruster candidates (see table 5.6), assuming one redundant thruster string for all the thrusters. The total propulsion system mass for the different thrusters is almost equal and thus no selection can be made by solely looking to the mass.

	HT-30	NASA-400M	NASA-457M
Number of active thrusters	21	18	13
Redundant thruster string	1	1	1
Mass thrusters (kg)	823.1	827.0	839.8
Mass gimbals (kg)	411.5	413.5	419.9
Mass DDU (kg)	235.7	231.4	225.9
Mass cables (kg)	53.6	51.7	48.8
Mass XFS (kg)	75.8	66.1	49.9
Mass tank (kg)	663.4	663.4	663.4
Structural factor	1.26	1.26	1.26
Propulsion system mass (kg)	2851.5	2838.9	2832.2

Table 5.6.: Propulsion system mass calculation for thruster candidates.

For the selection, the other requirements are also taken into consideration (see table 5.5). All the thrusters violate the specific impulse requirement, except for the NASA-457M. This thruster only violates the lifetime requirement, which is a common problem for current state of the art Hall thrusters, since their lifetime is around $8,000$ hrs. However,

some breakthroughs are about to be realized in which magnetic shielding will result in so-called immortal Hall thrusters (see section 5.3.1) [68]. This shows that the design of the NASA-457M requires an iteration in which magnetic shielding is applied and such the lifetime is extended to an expected duration of 30,000 hrs. This updated version of the thruster will be perfectly suited to fulfill the mission and is selected.

During operation, the NASA-457M's heater, keeper and magnet supply, require approximately 3% of the total power, while the thruster operates at a total efficiency of 58% [65]. Using equation 4.26, the total power demand of the thrusters equals 528.7 kW. The thruster falls under ITAR regulations and the outer dimensions of the thruster are given in table 5.7 [66]. From reference [25] it could be derived that the thruster mass equals 87 kg, while equation 5.13 gives a result of 66 kg. Since an iteration of the thruster test model is required in which the magnetic shielding is applied, it is assumed that excessive mass can be taken away and such the thruster mass equation is chosen.

Figure 5.15.: The NASA-457M Hall thruster [65].

NASA-457M	
Radius single thruster (cm)	29.0
Depth single thruster (cm)	16.0
Operation power (kW)	40.7
Single Thruster mass (kg)	66
Thruster total efficiency (−)	0.58
Active thrusters	13
Redundant thruster string	1
Total thrusters	14
Gimbaled thrusters	4
Total thrust (N)	31.3
Total power demand (kW)	528.7

Table 5.7.: Hall thruster information and configuration for SEP stage [66].

For the SEP stage, the total number of engines is equal to 14 (see table 5.7). It is assumed that four gimbaled thrusters are enough to provide steering in all directions effectively and to provide compensation in case one thruster fails (see section 6.1.1).

5.3.9. Propulsion System Results

From the selected propulsion system configuration, the complete mass (see table 5.8) can be derived by using the model presented in section 5.3.9. The structure mass factor is included to account for the extra mass that is required to integrate all the components into the spacecraft. Also, margins for the mass and volume are applied according to the margin philosophy. The thrusters and gimbals are further developments of already existing systems and therefore a margin of 10% is applied. The DDU, composite overwrap

tanks and XFS are relatively new developments and thus a margin of 20% is applied. Cabling is standard in spacecrafts, so only the smallest margin of 5% is selected. The total mass estimate of the propulsion system for the SEP stage can be seen in table 5.8. The payload module contains propellant tanks and the mass required for these tanks can be seen in table 5.9.

SEP stage	Mass	Margin	Mass w margins
Thruster mass (kg)	839.8	10%	923.8
Gimbal mass (kg)	120.0	10%	132.0
DDU mass (kg)	225.9	20%	271.1
Cable mass (kg)	48.8	5%	51.3
Tanks mass (kg)	663.4	20%	796.1
XFS mass (kg)	49.9	20%	59.9
Total components mass (kg)			2234.1
Structure mass factor			1.26
Total mass (kg)			2814.9

Table 5.8.: Final mass estimate of the SEP stage's propulsion system, including margins.

Payload	Mass	Margin	Mass w margins
Tanks mass (kg)	1202.1	20%	1442.5
Structure mass factor			1.26
Total mass (kg)			1817.5

Table 5.9.: Final mass estimate for the propellant tanks inside the payload module.

The largest contributor to the propulsion system volume are the propellant tanks (see table 5.10). The DDU volume is derived by taking the specific mass of the PPS 1350 HET PPU, and scaling the volume with the DDU mass [88]. A gimbal of an electric thruster requires roughly twice the volume of the engine [73]. The complete volume estimate can be seen in table 5.10.

SEP stage	Volume	Margin	Volume w margins
Thruster volume (m^3)	0.59	10%	0.65
Gimbal volume (m^3)	0.17	10%	0.19
SEP tank volume (m^3)	5.05	10%	5.55
DDU volume (m^3)	0.30	20%	0.36
Total volume (m^3)			6.75

Table 5.10.: Final volume estimate of the SEP stage's propulsion system.

5.4. Electric Power System

The Electric Power System (EPS) is the most critical subsystem of the SEP stage, because the functionality of this system determines not only the performance but also the feasibility of the mission. Therefore, an extensive analysis for the EPS is performed.

The power for all systems on the SEP stage, is generated by solar arrays. They need to be positioned perpendicular toward the Sun in order to generate the maximum amount of power. The arrays are connected to the spacecraft through the Solar Array Drive Mechanisms (SADM), which diverts the power coming from the solar arrays to the Hall thrusters. A small fraction of the power is converted, regulated and distributed by the Power Control and Distribution Unit (PCDU). In the following, all these elements and their trade-offs will be discussed, including a mass and power estimation.

The Electric Power System has to comply with the following requirements:

	Mission Requirement	Created
4.	The transfer stage shall be powered by solar panels as primary power source (nuclear power is excluded).	Sec. 2.2
	System Requirement	**Created**
1.1	The solar arrays shall be sized to endure, during its lifetime, a total current irradiation of $16.347 \cdot 10^{14}\,\mathrm{MeV/cm^2}$ and voltage irradiation of $21.132 \cdot 10^{14}\,\mathrm{MeV/cm^2}$.	Sec. 4.4
2.1.5	The thrusters shall require a total power of 529 kW. The heater, keeper and magnet supply require 3% of this power.	Sec. 5.3.8
2.2	The engine can provide thrust during eclipse.	Sec. 2.2
2.3.2	The solar array shall be designed such that it accounts for the ion impingement losses.	Sec. 5.3.3
2.4	The thruster's cathode shall operate continuously to prevent spacecraft charging, also in eclipse. A minimum power of 200 W per cathode is required.	Sec. 5.3.3
3.	The transfer stage shall be powered by solar panels.	Sec. 2.2
3.1	The solar array shall be deployed autonomously.	Sec. 2.2
3.2	The critical systems shall be powered by batteries during eclipse time.	Sec. 2.2
3.3	The EOL power generation of the solar panels shall be sufficient to maintain proper engine functionality.	Sec. 2.2
3.4	The solar array should consist out of two Solar Array Wings.	Sec. 5.2.1
3.5	The solar array shall fit inside the launcher fairing.	Sec. 4.3.2
3.6	The power system shall operate with a Direct Drive power processing Unit.	Sec. 5.2.3

	System Requirement (continued)	Created
3.7	The power system should deliver a voltage of $300-600\,\mathrm{V}$ to the thrusters.	Sec. 5.3.8
5.1	During eclipse, a heater shall operate at 320 W to keep the stage's temperature above 0°C	Sec. 5.6.4
7.2	The attitude sensors shall operate at a total power of 90 W.	Sec. 5.7.1
8.1	The Telemetry, Tracking and Command system shall operate at a total power of 105 W.	Sec. 5.8
9.1	The On-Board Data Handling shall operate at a total power of 63 W.	Sec. 5.8
10.	The transfer stage shall provide electrical power to the payload during the transfer.	Sec. 2.2

For the design of the EPS, well established methods are used that are available within reference [3] and [6]. This approach is chosen to come to a feasible and conventional design of the system. Also, the margin philosophy introduced at the beginning of the chapter will be applied to the power, mass and volume of the system.

5.4.1. Solar Array pointing

The SEP stage employs continuous thrust to make a spiral transfer to the Moon. During the transfer the power generation needs to be kept at maximum by maintaining the solar arrays pointed at the sun. However, this must be performed while keeping the SEP stage's thrusters pointed along the velocity vector, which can be accomplished in three ways [31]:

- A two-axis gimbal[1].
- A one axis gimbal in combination with a roll-steering maneuver.
- A one axis gimbal and sizing the solar array for off-pointing errors.

The first option, having a two-axis solar array gimbal, compensates for the pointing error in two angles: the α and β angle. The α angle represents a rotation caused by the orbit around the Earth, whereas the β angle defines the angle between the orbit plane and the solar vector (or ecliptic), see figure 5.16. Such a two-axis gimbal is complex, requires a high volume and adds a considerable amount of mass to the overall system [31].

A second and alternative method is to use a typical single-axis array gimbal and employ a roll steering maneuver. In this case, the single-axis gimbal is compensating for the α angle and the spacecraft roll steering maneuver for the β angle, which employs one full revolution per orbit. Thus the orientation of the spacecraft is used to point the solar arrays. This maneuver has to be applied continuously and affects the Attitude Orbit

[1] A gimbal is a pivoted support that allows an object to rotate about a single axis.

Control System (AOCS), which carries out this maneuver [31].

If roll steering is not applied, the solar array will experience off-pointing errors equal to the solar β angle and potentially shadowing, which is the third considered method. The power production in this case will at least be reduced by the cosine of the β angle and should be taken into consideration when designing the solar array. Therefore, the orbit parameters are of importance to select a pointing method.

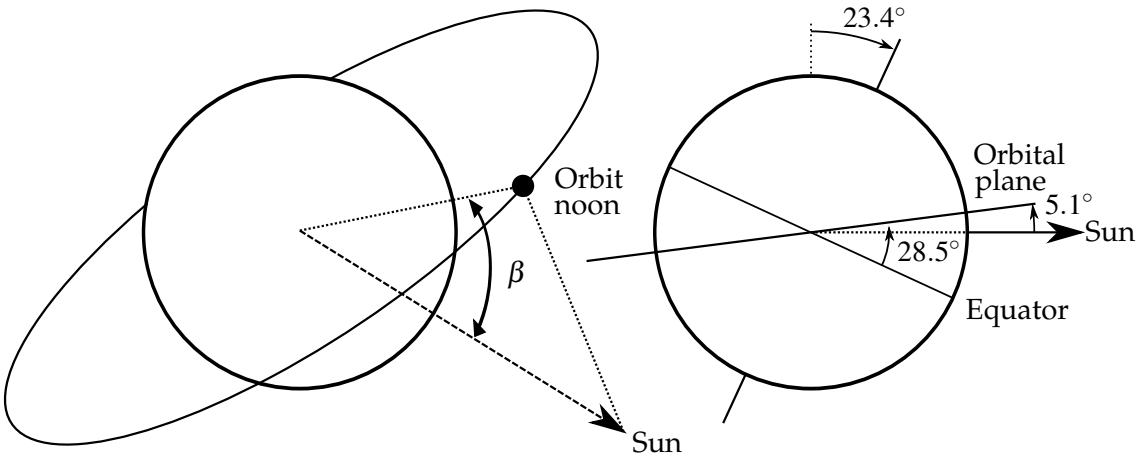

Figure 5.16.: A 3D illustration of the solar β-angle (left) and a 2D representation of the β-angle during the mission (right).

From the mission analysis it was derived that the mission will be performed during a major lunar standstill (see section 4.1). The SEP stage is launched into a 28.5° inclination, such that the orbital plane coincides with the lunar plane. The lunar plane has a stable orientation towards the ecliptic, at an angle of 5.1° to the Sun (see figure 5.16). Thus, in this configuration the β angle is constantly 5.1°, which results in a power loss of only 0.4%. This loss is very minimal and can be taken into account by increasing the solar array area slightly. Therefore the third method is selected in favor of the two-axis gimbal, which increases complexity, and the roll-steering maneuver, which increases the AOCS propellant demand.

5.4.2. SADM availability and sizing

The Solar Array Drive Mechanism (SADM) is driving the solar array wing and is a crucial part within the EPS. During the flight, it has to guarantee that the solar arrays stay pointed perpendicular to the Sun direction, such that the maximum amount of power is produced. Secondly, it has to transfer all power from the solar arrays to the spacecraft. Also, the SADM shall be able to transfer signals. A SADM is a single point of failure device, which shows how critical the component actually is. There are two main technologies to transfer power to the spacecraft: by a slip ring or a roll ring.

The power within a slip ring assembly is transferred from an inner rotating conductive ring, through a brush to the spacecraft (see left side of figure 5.17). The brushes form

a slipping contact with the ring, which causes wear and requires some form of lubrication. A roll ring assembly (see right side of figure 5.17) contains rolling flexures, which transfer power between the outer conductive ring and the inner rotating conductive ring. These flexures are made of conducting materials, typically gold plated Beryllium Copper [53]. They are separated by non-conductive idlers, which rotate in the idler guide tracks and ensure that no short circuiting occurs. This configuration provides a rolling contact between the spacecraft and the solar array, resulting in almost no friction and wear. As a consequence, the lifetime of a roll ring assembly is much higher than a slip ring assembly. Also, the reduced friction forces results in a 5 to 20 times lower torque to turn the assembly [54].

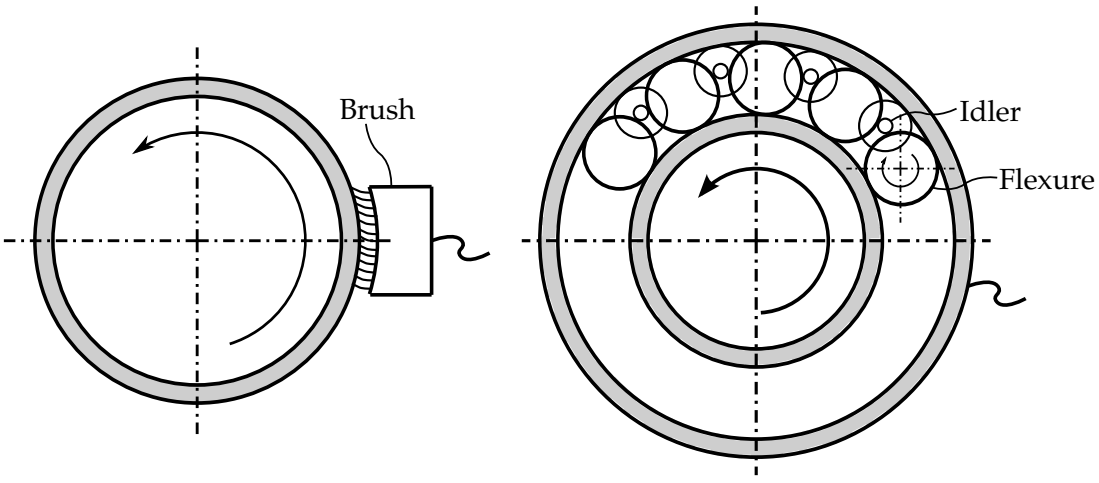

Figure 5.17.: The working principle of the slip ring (left) and roll ring (right).

The contact area of a roll ring is larger compared to a brush contact, enabling it to transfer more current and have a compact design. A slip ring can typically transfer up to 12 A [56], while one roll ring with ten flexures can transfer 100 A [55]. In both configurations, multiple rings can be stacked above each other to reach higher power levels. The flexures and brushes do not support the array mechanically. This is normally provided by ball bearings. Also, rotation of the SADM is driven by a motor, typically a stepper motor.

The SADM completes one full rotation when one orbit is performed. The number of rotations is therefore equal to the amount of orbits, which can be obtained by the SPIRAL PROGRAM. For the specified mission (including return to Earth), the number of rotations is equal to 1126. Margins are required to account for operations at LEO and LLO. During these operations, the thrusters are not fired and thus the total power demand is reduced. However, power is still required for the avionic bay and payload and such the panels need to be rotated. To account for this, a margin of 20% is included. Assuming that the mission is performed at least three times, the required number of rotations should at least be 4054.

In a later design phase, it has to be researched if it is possible to generate enough power

in LEO parking orbit when the panels are oriented towards the Earth, using only the Albedo radiation. If this is the case, the solar arrays can stay in a fixed position with respect to the spacecraft and such no extra rotations have to be applied, reducing the required amount of rotations and especially the moment that is applied upon the spacecraft.

The rotational speed of the SADM needs to be high enough to ensure that the solar array is pointed towards the Sun at all times. This speed is equal to the rotation speed of the spacecraft, which is the highest in low orbits and therefore the most demanding. For the current mission the most demanding case is either in LEO or LLO:

$$\omega_{LLO} = \frac{v}{r} = \sqrt{\frac{\mu_M}{r^3}} = 8.89 \cdot 10^{-4}\,\mathrm{rad/s}. \tag{5.19}$$

$$\omega_{LEO} = \frac{v}{r} = \sqrt{\frac{\mu_E}{r^3}} = 1.11 \cdot 10^{-3}\,\mathrm{rad/s}. \tag{5.20}$$

The calculations show that the most demanding case occurs in LEO and that the corresponding rotational speed of the SADM should at least be $1.11 \cdot 10^{-3}\,\mathrm{rad/s}$ or $0.064^\circ/\mathrm{s}$. No problems are foreseen in fulfilling these two requirements, since current state of the art roll ring SADMs are capable of having a maximum rotation speed of $0.067^\circ/\mathrm{s}$ and a total number of revolutions of more than 35,000 (see appendix B.1).

The number of SADMs is linked to the number of solar array wings. A total of two solar array wings is preferred in order to prevent array shadowing. This means that two SADMs need to transfer the total required power from the solar array wings to the spacecraft, equal to 569 kW each at maximum BOL power. Because such high power levels have never been applied in space missions so far, there is no SADM existing for these power levels.

With a peak power of 256 kW [1], the ISS is up until now the spacecraft with the highest power production. The SADM of the ISS, called Beta Gimbal Assembly (BGA), is qualified for transferring 33 kW from the solar array wing to the truss structure. The Solar Alpha Rotary Joint (SARJ) connects the truss structure to the rest of the space station and is qualified at 60 kW, which is obviously not enough for the proposed mission. However, within the development program of the Space Station, the initial power levels were higher and also the devices were tested at these higher power levels [54]. In the program, three different roll ring assemblies were designed, with 4, 8 and 12 roll rings (see figure 5.18). The 4 and 8 circuit assemblies were extensively tested, even to a point were 200 A and 500 Vdc (100 kW) were transfered through one single circuit [54]. The roll ring assembly offers a great flexibility due to the modularity of the design. Modules containing sets of circuits can be added or removed easily to meet system requirements [54]. Also the roll ring datasheet from Diamond Roltran [55] shows that the assembly can be fitted to our needs.

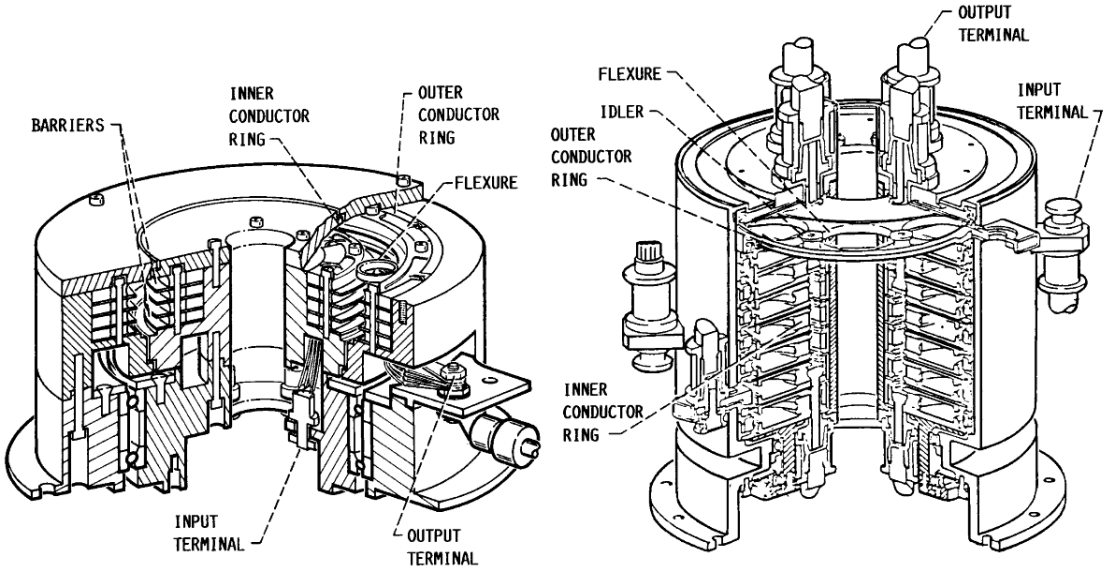

Figure 5.18.: A four circuit roll ring assembly (left) and an eight circuit roll ring assembly (right) [53].

Table 5.11 compares the slip ring and roll ring assembly. The roll ring is selected due to its longer life time, lower torque and especially its higher power density. This last benefit results in a smaller sized SADM and is therefore the preferred solution.

Characteristic	Slip Ring	Roll Ring
Torque	T	0.05-0.2 T
Power density	P	> P
Demonstrated power level (kW)	≤ 20	≤ 60
Modularity	Yes	Yes
Lubrication	Yes	No
Wear	Yes	Very low
Life (rev)	$\leq 40,000$	$> 300,000$
TRL	9	9

Table 5.11.: Trade off between different SADM types.

The design of the SADM can be based upon heritage coming from ISS (see figure 5.19). The power module, secondary power module and signal module are all constructed out roll ring assemblies. The power module is consisting out of five roll rings, that provides four power crossings and one ground. Each roll ring has a total estimated thickness of 5 cm and contains eleven flexures with a diameter of 8 cm. This BGA, with a total mass of 24 kg, was designed to be accessible during an Extra-Vehicular Activity (EVA) of an astronaut and is therefore more spacious in its design [54]. This is not required for the current mission and therefore this space can be used for a larger power module.

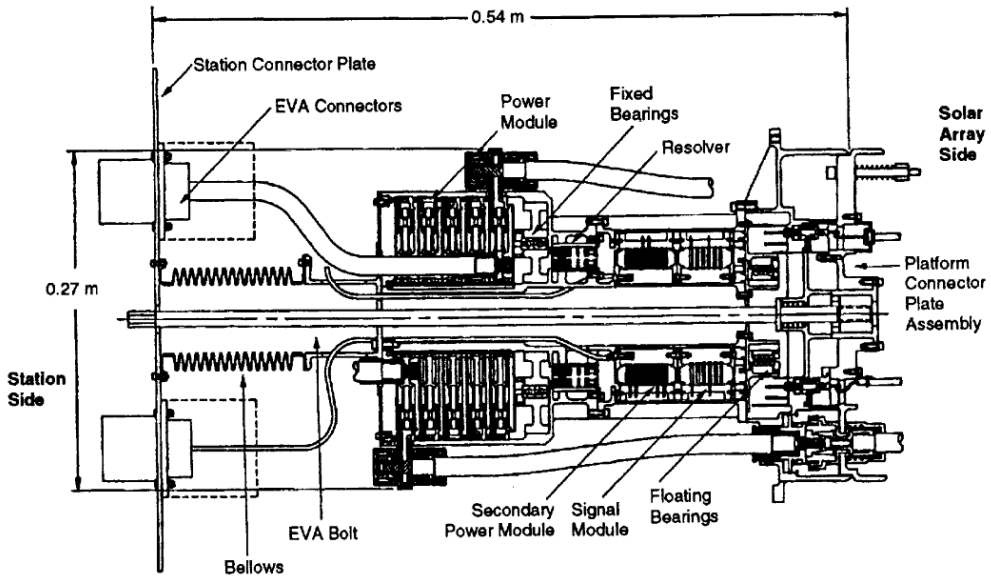

Figure 5.19.: Cross section of the BGA of ISS [54].

The flexures within a roll ring assembly are designed to carry 20 A of current and 500 V [53] and are qualified at 10 A and 250 V [55]. The power system is operating at 400 V and is therefore transferred across one ring. The power a single ring can transfer, equals:

$$P_{ring} = U_{EPS} I_{flex} N_{flex}. \tag{5.21}$$

Due to the configuration of the stage (see section 5.5), the length of the SADM is more critical than the diameter. Therefore, the diameter of the power rings is increased, such that it can contain more flexures of the same diameter and the complete ring can transfer more power. The new SADM radius is determined by the following formula:

$$r_{req} = \frac{d_{flex} N_{flex}}{2\pi} + d_{flex}. \tag{5.22}$$

The power rings are scaled up to contain 22 flexures, which requires a diameter of 0.72 m, with a total power capability of 88 kW per ring. The maximum power capability of a single SADM should be 569 kW (see section 5.4.7) and therefore requires seven power transferring rings. Two more rings are required, one for being the neutral return line and another one for the ground. The length of the SADM is estimated by having a base length of 0.25 m (derived from ISS BGA) and adding the number of rings multiplied by their thickness:

$$l_{req} = l_{base} + N_{rings} t_{ring}. \tag{5.23}$$

The mass of the SADM is estimated by comparison to the ISS BGA, which has a specific mass of $1.29 \cdot 10^{-3}\,\mathrm{m^3/kg}$. The calculated specifications of a single SADM can be found

in table 5.12. A margin of 10% is applied on both the mass and volume, since the SADM is a further development of existing technology, which is proven in space.

Characteristic	Specification
Power transfer technology	Roll Ring
Rotation speed (°/s)	0.064
Lifetime (rev)	4,054
Power transferred (kW)	569
Number of power rings	7
Number of rings	9
Maximum power transfer capability (kW)	616
Diameter (m)	0.72
Length (m)	0.7
Volume, including 10% margin (m^3)	0.31
Mass, including 10% margin (kg)	243.5

Table 5.12.: Specifications of a single SADM.

5.4.3. Types of Solar Cells

The mass and volume limitations, by the launcher fairing envelope, make the specific power (W/kg) and the stowed power (kW/m^3) two critical parameters for the selection of a solar cell for the array. Therefore a thorough trade off is required to select the most suitable solar cell type for this specific mission. In this section, the potential solar cell options and their technical properties are presented, while the trade is performed in section 5.4.5.

There are many types of solar cells, which are build up of one or more layers of different materials. The theoretical maximum energy conversion efficiency of three common materials is [6]:

- Germanium (Ge): 16%
- Silicon (Si): 24%
- Gallium Arsenide (GaAs): 29%

Silicon and Gallium Arsenide rigid solar panels are commonly applied. These materials can also be combined in multi-junction cells, where the cell is build up by different material layers. By using concentration techniques, the efficiencies of double and triple junction cells can currently reach 35% and 40%, repectively, while the theroretical limit of a triple junction cell equals 50% [1].

The traditional solar cells are crystalline cells, meaning that the atoms and molecules in the cell are arranged in a regular manner. Any dislocation or defect in the structure

of the cell, results in a reduction of the performance. A new development are thin-film solar cells, which are amorphous instead of crystalline. These amorphous cells have a random atomic structure that can not be misaligned (no performance loss), which makes them in general more radiation resistant. In a crystalline cell, even the slightest damage to the well-aligned structure degrades the power generation [6] [34].

The thin-film cell is a few micrometers thick ($< 5\,\mu$m) and consists out of a certain semiconducting material, mostly in amorphous or polycrystalline form and as single or multi-junction cell. The cell is deposited on a substrate, which can be aluminum, glass, ceramic, stainless steel, polyimide or other compatible substrate materials. There are multiple types of thin-film cells currently under development, of which the most promising are:

- Amorphous Silicon (a-Si)
- Copper Indium Gallium Diselenide (CIGS)

The efficiency of a CIGS thin film solar cell is higher than a-Si based cell, which are around 12-14% and 9-12% respectively. However, a-Si has the advantage of being deposited at lower temperatures, allowing the use of lighter polymer substrate and therefore of having a higher specific power. Typically, a-Si single junction has a substrate thickness of around $6\,\mu$m and CIGS $30\,\mu$m [34]. Advances in this field enabled the possibility to embed CIGS thin film onto Kapton flexible polymer and reduce substarte thickness to around $25\,\mu$m [35].

The temperature degradation of a-Si triple junction cells is half of that of conventional crystalline Silicon cells, therefore a-Si is expected to perform better at high temperatures found in LEO and GEO [6]. However, a disadvantage is that the a-Si cell efficiency is low at the beginning and degrades by about 20% in the first months of operation before stabilizing. After this period the cell suffers less radiation damage [6]. Also, tests showed that after more than 33,000 thermal cycles between +150°C and -110°C, there was no change in performance, nor after exposure to atomic oxygen with a concentration of $1.3 \cdot 10^{20}$ atoms/cm^2 [6].

Conventional solar panels are typically 2 cm thick, which makes them relatively heavy and such they have a low specific and stowed power. In case high power levels are required, this would result in a fairing that is mostly filled by solar panels. Therefore there are initiatives to develop thin panels, where the supporting honeycomb structure is removed and the solar cell is made as thin as possible. This is also a new trend in current development programs, where the goal is to make the GaAs triple junction cells as thin as possible. Initially the aim is to go to a thickness of 80μm and eventually down to 10-20μm [44] [34]. These GaAs next generation cells will be manufactured from inverted metamorphic structures and are called Inverted Metamorphic Multijunction (IMM) cells. They are expected to have efficiencies of 33-35% and are so thin that they are flexible, allowing fold-out or roll-out configurations [34]. Test flights with these cells

are already performed on the ISS (MISSE-7 & MISSE-8, see figure 5.20), having a cell thickness of around 15 μm. These cells, in combination with the ultraflex lightweight panel of ATK (see appendix B.3), are selected to make up the solar panel of the Orion crew vehicle. In order for an array, consisting out of these cells, to be flexible, the protecting covers and the substrate, on which the solar cell is deposited, have to be flexible. In case for example a glass cover is used, the flexibility of the panel is (partially) lost. Currently the IMM cell is not commercially available, but multiple companies (NREL, Emcore, Spectrolab) started developing commercial versions of the IMM cell, which will come available in the next years [37].

Figure 5.20.: The Materials International Space Station Experiment (MISSE-8) investigates long-term exposure of materials and performance of new solar cells.

A database is created where the characteristics of the considered solar cells can be found on cell level and on panel level (see appendix B.3). Mostly, the characteristics are stated under AM0 conditions, which is equal to the conditions in space at a distance of 1 AU. For some cells also the performance under AM1.5 conditions[2] were stated in case not much information was found for AM0. The typical performance levels of the cells on panel level under AM0 conditions are summarized in table 5.13. Some of the values are based upon estimation, e.g. the a-Si triple junction (TJ) and CIGS solar cells are twice the thickness as the a-Si single junction (SJ) cell and therefore their stowed power is halved. The IMM TJ and a-Si SJ are both tested on the ISS and therefore have a TRL of 7 on cell level. Also, IMM cells with four junctions are currently under development and a roadmap exists to go even to five and six junctions [39]. Not much is known about these five and six junction IMM cells (TRL $\leq$ 3) and therefore they are not considered for the design. The trade-off for selecting the cell type will be done in section 5.4.5.

[2]Corresponding to the performance under one atmosphere and a solar zenith angle of 48.2°.

Cell type	Efficiency (%)	Specific power (W/kg)	Areal density (W/m^2)	Stowed power (kW/m^3)	Radiation resistance	Scalability	TRL
c-Si	8-10	20-40	100	1-2	Low	Limited	9
GaAs TJ rigid panel	24-30	45-108	270-300	8-15	High	Limited	9
GaAs TJ flexpanel	24-30	118-180	270-300	30-40	Medium	Limited	9
GaAs SLA	24-30	150-500	300-400	**20-80**	High	Difficult	9
a-Si SJ	9-12	**1200**	95-160	100	**Superior**	**Easy**	7
a-Si TJ	9-13	770	95-170	50[a]	High	**Easy**	4
CIGS	12-14	500[a]	145-180	50[a]	High	Medium	4
IMM TJ	**28-33**	200-500	**360-450**	50	High	Limited	7

a: These values are based upon estimations

Table 5.13.: Typical performance of solar cells when integrated into flexible or rigid panels (see appendix B.3).

5.4.4. Solar Cell V-I Characteristic

The solar cell voltage-current (V-I) characteristic is different for every solar cell type and also changes under variable conditions. The shape of a typical V-I characteristic can be seen in figure 5.21. The following factors that influence the solar cell behavior are taken into account:

- Operative absolute temperature
- Degradation by cosmic radiation

The intensity of the incident light is assumed to be constant at 1367 W/m^2 (1 AU).

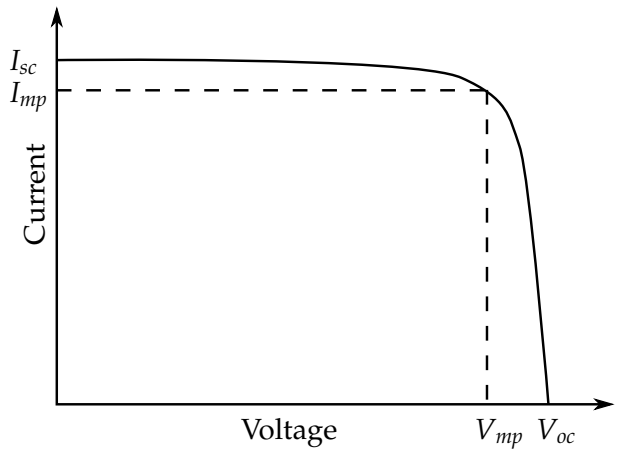

Figure 5.21.: Typical V-I characteristic of a solar cell [46].

The solar cell V-I characteristic can be derived from the specifications provided by the data sheet. On solar cell data sheets the following information, for AM0 and $T_{ref} = 301.15\,\mathrm{K}$, is in general provided:

- Short circuit current, I_{sc}.
- Maximum power current, I_{mp}.
- Maximum power voltage, V_{mp}.
- Open circuit voltage, V_{oc}.
- Short circuit current temperature coefficient, dI_{sc}/dT.
- Maximum power current temperature coefficient, dI_{mp}/dT.
- Maximum power voltage temperature coefficient, dV_{mp}/dT.
- Open circuit voltage temperature coefficient, dV_{oc}/dT.

A solar cell can be modeled as a current source with a diode in parallel and a shunt and series resistance. The equivalent electronic circuit of the solar cell (see figure 5.22) together with Kirchhoff's law are used to obtain an equation for the output current, i_O, and output voltage, V_O, of the solar cell [46]:

$$i_O = i_L - i_D\left[\exp\left(\frac{qV_D}{kT}\right) - 1\right] - i_R\left[\exp\left(\frac{qV_D}{2kT}\right) - 1\right] - \frac{V_D}{R_P}. \tag{5.24}$$

$$V_O = V_D - R_S i_O. \tag{5.25}$$

Where k is the Boltzmann constant, q the electron charge, i_L, i_D and i_R are respectively the current due to illumination and the reverse current of the diodes, V_D the voltage drop across the diodes, R_S the series resistance and R_P the shunt or parallel resistance. For a triple junction cell, the series resistance is usually around $300\,\mathrm{m\Omega}$ and the parallel resistance around $500\,\Omega$. In a first approximation these resistances can be considered constant in the operating temperature range of the cell.

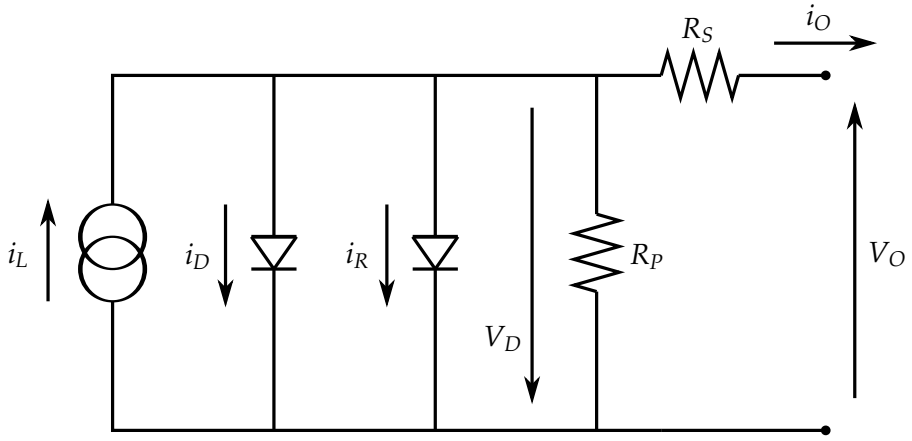

Figure 5.22.: Equivalent electronic circuit of a solar cell [46].

As stated, the data sheet provides information of three typical operating points on the V-I curve: short circuit, maximum power and open circuit. These points are used to solve the equations 5.24 and 5.25 for the three unknowns (i_L, i_D and i_R) that are not provided on the datasheet, by applying the least square method:

$$x = \left(A^T A\right)^{-1} A^T y. \tag{5.26}$$

Now that these variables are known, the voltage-current curve can be plotted for the reference temperature. For other operating temperatures, the temperature coefficients can be used to calculate the new typical short circuit current, maximum power current, maximum power voltage and open circuit voltage as follows:

$$I_{sc_{T1}} = I_{sc_{ref}} + \frac{dI_{sc}}{dT}\left(T_1 - T_{ref}\right). \tag{5.27}$$

$$I_{mp_{T1}} = I_{mp_{ref}} + \frac{dI_{mp}}{dT}\left(T_1 - T_{ref}\right). \tag{5.28}$$

$$V_{mp_{T1}} = V_{mp_{ref}} + \frac{dV_{mp}}{dT}\left(T_1 - T_{ref}\right). \tag{5.29}$$

$$V_{oc_{T1}} = V_{oc_{ref}} + \frac{dV_{oc}}{dT}\left(T_1 - T_{ref}\right). \tag{5.30}$$

These values can be used, in combination with the procedure as described in this section, to obtain the solar cell characteristic.

5.4.5. Solar Arrays Concepts and Trade Off

The solar array concepts are based upon heritage and multiple options that can be realized within this design, are identified:

- Rigid panels
- Flexible panels
  - Deployable truss structure
  - Coilable boom
  - Shape memory composite

An explanation of all the different deployable mechanisms, that are suggested in combination with the flexible panel, can be found in section 5.5.2. The size of a rigid panel is limited by the dimensions of the launcher. To overcome this problem it is common practice to stack multiple rigid panels on top of each other. Once in space, the panels are deployed to obtain the required solar array area (see figure 5.23, concept (a)). The

configuration of concept (a) is chosen such that the panels close to the SEP stage are at a safe distance from the thruster plume, combined with a length to width ratio that is as close to one as possible. The Falcon Heavy is selected as launcher and limits the size of a single rigid panel to $4 \times 12\,\text{m}$, due to the height and diameter of the fairing.

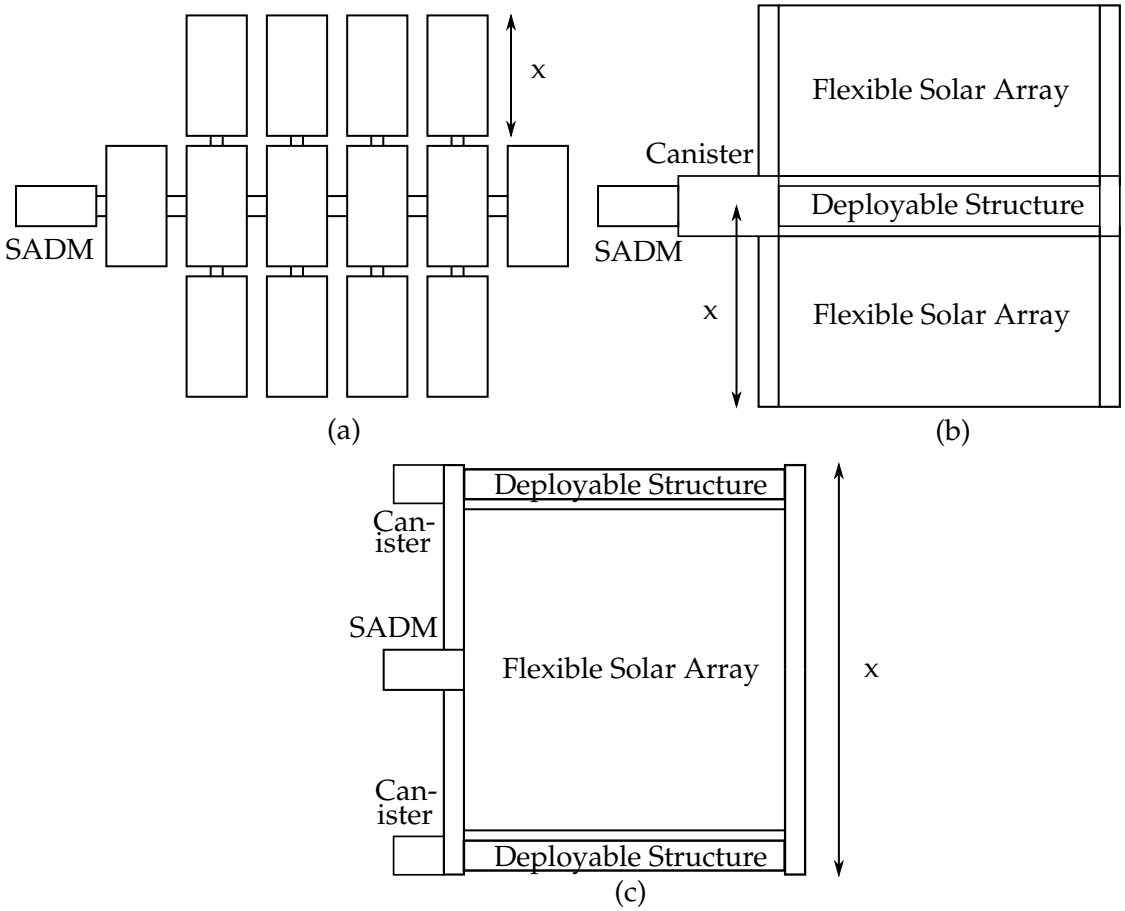

Figure 5.23.: Solar array concepts, with a rigid panel concept, (a), and two flexible solar array concepts, (b) & (c).

Concept (b) and (c) (see figure 5.23) contain flexible solar arrays and deployable structures that are folded in the launch configuration and deployed once in space. The deployable mechanism can be a deployable truss structure, coilable boom or a shape memory composite (see section 5.5.2). The width of configuration (c) is limited to 12 m due to the launcher fairing dimensions. In configuration (b) the booms, at which the flexible solar arrays are attached, can be folded together in the stowed configuration and therefore this configuration has an expected maximum solar array width of 20 m (including a margin of 4 m for the canister). The concept that is selected in the end, depends on the length and stiffness that is required for the solar array.

In section 5.3 it was derived that at least 529 kW of power is required to operate the engines. In combination with the performance of the solar cells (see table 5.13), the size, mass and stowed volume can be estimated (see table 5.14). This first estimation is without taking power margins and solar array performance losses into account. Con-

ventional silicon and stretch lens arrays are excluded from the trade-off, due to the low performance of silicon and the complexity of stretch lens arrays, which makes them unsuitable for large solar array areas.

Cell type	Mass (kg)	Area (m^2)	Number of rigid panels	Flexible panel (m) Width	Length	Volume stowed (m^3)
GaAs TJ RP	13,225	1,763	37	-	-	66
GaAs TJ FP	3,648	1,763	-	20	44.1	17.6
a-Si SJ	**441**	4,336	-	20	108.4	**5.3**
a-Si TJ	529	3,977	-	20	99.4	10.6
CIGS	1058	3,623	-	20	90.6	10.6
IMM TJ	1,763	**1,469**	-	20	**36.7**	10.6

FP: Flexible Panel SJ: Single Junction
RP: Rigid Panel TJ: Triple Junction

Table 5.14.: Approximated dimensions of the solar array, using different solar cells.

The rigid panel concept requires in total 37 panels of its maximum possible size ($4 \times 12\,m$), to meet the power demand. The mechanisms and supporting structure to deploy and support all these panels will be significant. Even if the GaAs TJ cell are replaced by the more efficient IMM TJ cells, still 31 panels will be required. The conventional rigid panels are therefore considered to be impractical considering the mass and stowage volume within the launch vehicle and thus the flexible panel concept is preferred.

The a-Si and CIGS cells are favorable from the mass and volume point of view. However, they require huge areas which have to be created by the deployable mechanisms. For both concept (b) and (c), this seems to be highly problematic, since only very long coilable booms ($\geq 90.6\,m$) can be considered in order to create the required area (see figure 5.32). These booms are less stiff than a deployable truss structure and only one boom of 10 m has been flown in space [42]. Therefore, this option entails a relatively high risk and is not deemed suited for the mission.

This leaves the GaAs TJ and IMM TJ as the final candidates, which can be incorporated in concept (b) or (c). For concept (c) this would require a deployable truss with a length of 61.2 m for IMM or 73.5 m for GaAs compared to 36.7 m or 44.1 m for concept (b). For the maneuverability of the system it is advised to have a length to width ratio of 1:1. Therefore concept (b) is preferred above concept (c). Also, the usage of IMM cells results in a lighter and smaller design compared to GaAs. From this discussion and table 5.14 it can be concluded that the IMM TJ cells, incorporated into flexible blankets, are the best option in combination with concept (b).

5.4.6. Power Management and Distribution

The power generated by the solar array can be controlled with the Direct-Energy-Transfer (DET) or the Peak-Power-Tracking (PPT) approach. In the DET approach, the solar array is regulated by shunt regulators that are in parallel with the solar array. This Sequential Shunt Unit (SSU) controls the solar array current by shunting array strings and therefore reducing the number of operational strings. In the PPT approach the operation point is regulated such that the current and voltage are located at the peak power point of the I-V curve, irrespective of temperature variations.

For the mission a Direct Drive power processing Unit (DDU) is chosen as baseline (see section 5.2.3). In a direct drive system, the power created by the solar arrays is directly transferred to the Hall thrusters, which eliminates the need for voltage conversion. The solar array is the current source (see section 5.4.4) and the Hall thruster is the load. This load can be seen as an impedance and its V-I characteristic can be controlled by adjusting the mass flow and magnetic field strength (see section 5.3.2). In case that the Hall thruster has no mass flow, the impedance is infinitely high, which means that there is an open circuit and the current is zero. When the mass flow is initiated and a plasma is formed, a current can start to flow. This will be at the open circuit voltage point of the solar array V-I characteristic. In order to move the operation point upwards, either the mass flow needs to be increased or the magnetic field strength need to be decreased or a combination of the two. In this manner the operation point can be shifted and the thruster can be operated near the maximum power point (see figure 5.24). In case the current and/or the voltage at this point is too high, the SSU can shunt solar array strings and reduce the current and voltage of the operation point. Consequently, there is full control in selecting the point of operation on the V-I characteristic and the operation point can be selected at the maximum power point, just as with a PPT and without loss of efficiency.

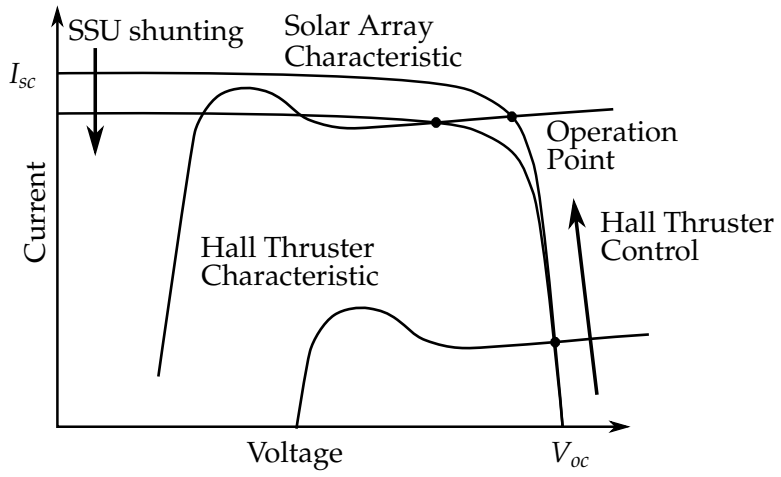

Figure 5.24.: Operation point of the solar cell in combination with the Hall thruster load.

The starting up and shutting down of the the thruster, can also be explained with the aid of these characteristics. Shutting the thruster down can be achieved by removing the propellant flow at the anode of the thruster. Starting up the system is more problematic, since the current cannot be easily turned on and off. Typically, the impedance of the thruster temporarily drops when the initial ions are created. The resulting current surge can collapse the array (0 V) and potentially affect other components [60]. This needs to be prevented by having the right startup method. One method to control the startup is to slowly increase the anode flow rate during startup and additionally controlling the magnet current [60].

This means that for the DDU principle, there are two ways in controlling the operation point. Adjusting the Hall thruster mass flow and magnetic field strength is considered to be a slow control loop, while the SSU can control the operation point in a quick manner. The design of these loops shall be such that the two do not counteract each other. Extensive testing is foreseen to obtain a reliable control philosophy for a controlled start up and stable DDU operation. The Jet Propulsion Laboratory is currently performing tests with a 10 kW Hall thruster in a DDU set-up. The tests showed that Hall thruster operation and control is simple and not much different than operation on conventional power supplies [61].

Power Control Strategy

There are three strategies for controlling the Hall thruster and solar array output power during the lifetime of the spacecraft:

- Constant Voltage
- Constant Current
- Peak Power Tracking (PPT)

The constant voltage and constant current strategy fall within the DET approach. This type of regulation has an efficiency of approximately 99% [84]. The PPT approach will result in a higher specific impulse and thrust, especially at the beginning of the mission. The drawback of this power conditioning method, is the low efficiency of 93 to 96% [1] and would therefore undo the high efficiency of the DDU. Therefore this way of power conditioning is not desired and the DET approach is selected in combination with a Sequential Shunt Unit (SSU), where the SSU has and efficiency of 99% [84].

The constant voltage control strategy fixes the specific impulse of the Hall thruster (see equation 5.2). The solar array current output will decline during the mission due to solar array degradation. To keep the voltage constant during the mission, the impedance is increased by increasing the magnetic field strength or by reducing the mass flow. This approach does not take advantage of all the available power, especially at BOL. However, control of the operating voltage is possible (see figure 5.24), which enables the possibility to select a higher operating voltage at BOL. Thus, the DDU can operate at the maximum power point [61], resulting in a higher specific impulse and thrust

and consequently in a shorter trip time and reduction of propellant mass. This is based upon the assumption that the thruster efficiency will vary little with a changing operating voltage.

The simplest strategy in terms of operation would be to select constant current, fixing the propellant mass flow rate and the current. However, in this case both the specific impulse and thrust vary, complicating the trajectory analysis in consequent design phases. Also, in case the solar array can no longer support the total current due to degradation, the system has to switch to a constant voltage approach. The constant voltage approach thus simplifies the trajectory analysis (constant I_{sp}) and enables the possibility to operate at higher power levels at BOL. These advantages make that the constant voltage approach is selected.

Electric Power System Design

The power is controlled by DET in combination with an SSU (see figure 5.25). Since the other subsystems within the SEP stage require a lower voltage for their electronics, the power distribution is broken up into a high voltage bus and a low voltage bus. The high voltage bus is directly connected to the Hall thrusters, which typically operate in a voltage range of $300 - 600\,\mathrm{V}$. The voltage the solar array has to provide at EOL shall be $400\,\mathrm{V}$ (see section 5.4.7). The high voltage bus is converted to the low voltage bus by a DC-DC power converter in the PCDU, which is providing power to the other subsystems, payload and to the magnet, heater and keeper supply of the thruster.

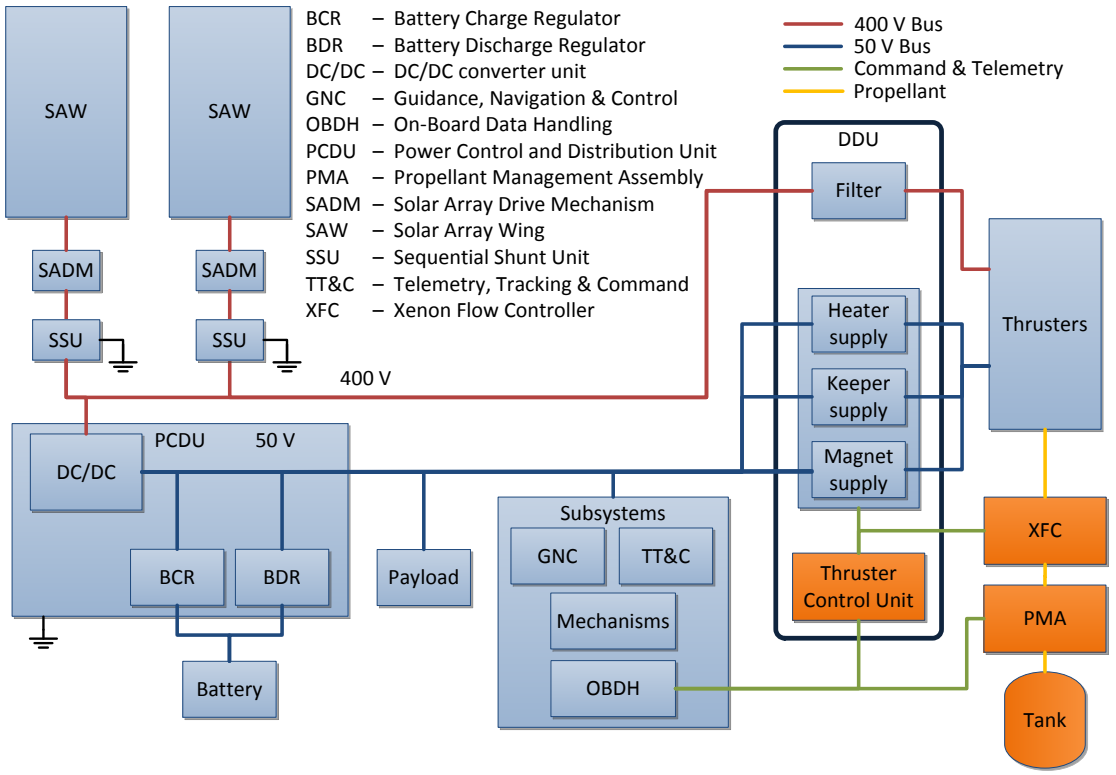

Figure 5.25.: Schematic of the electric power system.

For the low voltage bus a voltage level needs to be chosen. Typical bus voltages are 28, 50, 70, 100 and 120 V. A higher bus voltage, results in a reduction of the harness mass and conversion losses, on the other hand it increases the battery mass and volume significantly. As a consequence, studies showed that a 100 V bus is not significantly lighter than a 50 V bus [6]. Commonly, low power spacecrafts have a bus voltage of 28 V, thus such a buss will allow the usage of existing spacecraft components without the need to re-design them for higher voltage levels. Also, the magnet, heater and keeper supply of the thruster operate typically at 20 V [31], although their designs can be modified to operate at higher voltage levels [60]. However, recently voltage buses of 50 V are adopted more and more due to increasing power demands of (telecommunication) satellites. Therefore the amount of available systems for this voltage level will increase and 50 V bus is chosen as a baseline. More information about the bus systems and their operation voltage is required to make a final decision, so the possibility to change to a 28 V is left in the open. At this point the decision is considered to be less important, since the low voltage bus only uses approximately 5% of the total power demand. It is also chosen to have a fully regulated low voltage bus, such that the mass and power estimate of the secondary bus is conservative. The efficiency of the PCDU during sunlight phase is estimated at 94% and during eclipse, when the batteries are discharged, at 90% [3]. The complete electric power system schematic can be seen in figure 5.25.

During operation, a Hall thruster produces current oscillations with typically frequencies of around 10 to 30 kHz [1]. These oscillations, in combination with the direct connection to the solar array, can potentially cause power stability issues. These instabilities need to be compensated by using a filter, which incorporates an appropriately sized capacitance with possibly some additional filtering. This isolates the thruster oscillations from the power bus and the arrays and therefore not affect the operation of the solar array [60] [61].

The thruster control unit of the DDU provides an interface between the On-Board Data Handling and the heater, keeper and magnet supply and the Xenon Flow Controller. The latter unit controls the mass flow to the anode and cathode separately, which is required to operate the cathode during eclipse and for added control during startup.

Subsystem	Power (W)
Thermal Control	320
Attitude, Orbit and Control System	90
On-Board Data Handling	63
Telemetry, Tracking and Command	105
Payload	1,000 (TBC)

Table 5.15.: Power demand of the subsystems and payload, including margins.

The power demand of all the subsystems can be seen in table 5.15. The total power

demand of the thrusters is 529 kW, of which the heater, keeper and magnet require 3% (see section 5.3.8). A 10% margin is included on this power, since the thruster is a further development of an existing one, changing the power demand to 582 kW. During eclipse, the thruster cathodes are still operated and require in total 2.6 kW (see section 5.3.3). The power that has to be provided by the solar array during the sunlight and eclipse phase can be seen in table 5.16 and is divided into two operation modes:

- Mode 1: The SEP stage is in the Sun and the solar arrays provide power to the High Voltage Bus (HVB) and Low Voltage Bus (LVB). The DDU requires power both from the HVB, for the thruster discharge, and the LVB, for the heater, keeper and magnet supply.
- Mode 2: The SEP stage is in eclipse and the battery provides power to the Low Voltage Bus (LVB), thus only the LVB is operating. The heater is in operation to keep the spacecraft above 0°C and the thruster cathodes are operating to keep the engines in quick start mode and to prevent spacecraft charging.

	Mode 1		Mode 2
	HVB	LVB	LVB
P_{DDU} (kW)	564	17.5	2.6
$P_{Subsystems}$ (kW)	-	1.3	1.6
$P_{required}$ (kW)	564	18.7	4.2
η_{SADM} (%)	99	99	-
η_{SSU} (%)	99	99	-
η_{filter} (%)	100	-	-
$\eta_{harness}$ (%)	99.5	99.5	99.5
η_{PCDU} (%)	-	94	90
$\eta_{Battery-charge}$ (%)	-	-	97
$\eta_{Battery-discharge}$ (%)	-	-	90
η_{total} (%)	97.5	91.7	78.2
Margin (%)	0	20	20
$P_{total-required}$ (kW)	578	24.5	6.4

Table 5.16.: Efficiencies and power demand of the different parts within the EPS system during Sun and Eclipse.

For the LVB, an additional margin of 20% to the power demand is applied, as according to the margin philosophy [75]. On the HVB, no extra margin is applied, which is contradictionary to the philosophy. The HVB is consisting only out of the power demand from the thrusters, which is derived from the thrust. The thrust is again derived from the initial mass, which already has a 20% margin on subsystem level. This indicates

that there is already a margin included on the thruster power, due to the margins on the mass. Besides, the power demand from the thrusters is derived from physics, so it is expected that the eventual power demand is not much different and no additional margin is included. The total required power for the different modes, including a margin Ma, is calculated with:

$$P_{total-req} = \frac{P_{req}}{\prod(\eta_i)} Ma. \tag{5.31}$$

The batteries supply the stage with power during eclipse and need to be charged during the sunlight phase. Thus the solar array has to provide this extra power for charging. The power, in kWh, that should be provided during sunlight or eclipse, can be determined by:

$$P_{sunlight} = P_{mode1} t_{sunlight}. \tag{5.32}$$

$$P_{eclipse} = P_{mode2} t_{eclipse}. \tag{5.33}$$

The power that shall be generated by the solar array, can be calculated with the following formula:

$$P_{SA-required} = \frac{P_{total}}{t_{orbit}}. \tag{5.34}$$

At low orbits, the eclipse and sunlight duration is shorter than at higher orbits. The sizing case for the solar array is at LEO (not LLO), while the sizing case for the battery capacity is at high Earth altitudes. The impact on the power demand can be seen in table 5.17, which shows that the power produced by the solar arrays should be at least 607 kW at EOL and the battery capacity 19.9 kWh.

Altitude (km)	500	300,000
Sunlight duration (hrs)	0.98	465.6
Eclipse duration (hrs)	0.59	3.10
Orbit duration (hrs)	1.57	468.7
Power Demand		
$P_{sunlight}$ (kWh)	590.6	280,750
$P_{eclipse}$ (kWh)	3.8	**19.9**
P_{total} (kWh)	594.4	280,770
Solar Array Power Production Required		
$P_{SA-required}$ (kW)	**606.8**	603.0

Table 5.17.: The amount of power that the solar array needs to generate.

The second sizing case of the battery occurs when the SEP stage is launched. During this time until the unfolding of the solar array, the battery has to provide enough power to the spacecraft. This sizing case is not treated here, since in the current design phase too much is unknown about this procedure and its required power. Therefore, it has to be analyzed in future design phases.

In the requirements definition, it was suggested also to provide thrust during eclipse. In this case, the batteries should store around 2140 kWh. If an lithium-ion battery is selected and a very optimistic energy density of 250 Wh/kg [1] is assumed, a total battery mass of 8.6 ton would be required, which is almost 50% of the total subsystems mass. Obviously, this mass is too high and their is no increased performance due to the high mass increase and thus it is chosen not to fire the thrusters in eclipse.

For the battery, current state of the art lithium-ion batteries are selected, due to their high specific energy and high energy density. The space qualified rechargeable VES-180 lithium battery of SAFT is chosen [87], which has to provide an operating voltage of 50 V. As a result, 20 cells are required in series and in total 160 cells are needed to provide a capacity of 28.8 kWh, with a total mass of 195.4 kg (see table 5.18).

Battery	SAFT VES 180 Li-Ion
$P_{Battery-required}$ (kWh)	19.9
Nominal voltage (V)	3.6
Lowest discharge voltage (V)	2.57
Nominal capacity (Ah)	50
Diameter (mm)	53
Height (mm)	250
Mass (kg)	1.11
Cells in series	20
Parallel strings	8
Number of cells	160
Min. Operating voltage (V)	50
Max. Operating voltage (V)	72
Max. storage capability (kWh)	28.8
Volume, with 10% margin (m^3)	0.0971
Mass, with 10% margin (kg)	195.4

Table 5.18.: Battery required to power SEP stage during eclipse.

For the PCDU one of the modular approaches of Astrium, Terma Space or Thales Alenia should be adopted. During the LEO sunlight phase, the PCDU has to regulate a maximum amount of power of 36.5 kW. Currently, the highest power PCDU is from Thales Alenia and can regulate 21 kW [88]. When this unit is scaled up, it can be concluded that

a mass of 97.9 kg and a volume of 0.15 m^3 should be sufficient to provide a PCDU with a DC/DC converter, BCR and BDR regulator at an operating voltage of 50 V. Both the mass and volume include a margin of 10%.

There are two SSUs to switch solar array strings and control in total a maximum power of 1,138 kW (see section 5.4.7). The SSU with currently the highest power level is the one of ISS, which can control 38.5 kW and has a mass of 84.4 kg. In case this is scaled up for the SEP system, the expected SSU mass should be around 2,744 kg with an estimated volume of 4.6 m^3, both including a 10% margin (see table 5.19).

	PCDU	SSU
Maximum operating power (kW)	36.5	1,138
Specific volume (m^3/kW)	0.0037	0.0037
Volume, with 10% margin (m^3)	0.15	4.6
Specific mass (kg/kW)	2.44	2.19
Mass, with 10% margin (kg)	97.9	2,744

Table 5.19.: Mass and volume estimations for the PCDU and SSU.

At this stage of the design it is challenging and unrealistic to determine the harness mass. Therefore, the margin philosophy of ESA prescribes that the harness mass shall be considered to be at least 5% of the total subsystems mass [75]. Since the mission is requiring a substantial amount of power, it is chosen to doulbe the fraction to 10% of the total subsystems mass. This also includes harness for the transfer of data and communication signals. The total harness mass will be given in the final mass budget (see section 6.2).

5.4.7. Solar Array Design

Now that the required power demand is known and the solar cell and array concept are selected, the complete solar array can be designed. Currently, there are no existing commercial IMM cells and such their performance is derived from experimental data, coming from reference [58], [37] and [38]. Companies are developing commercial versions of the IMM, which are expected to come available in the next couple of years [38].

Flexible solar panels can be stored in a rolled or folded configuration. In the folded configuration there is more freedom in selecting the cover glass thickness and solar cell substrate compared to the rolled configuration [36]. Embedding the cell within a cover glass is used to reduce the total radiation dose on the cells. Typically, GaAs TJ cells are embedded in 100 or 125 μm thick cover glass. However, due to the multiple passes through the Van Allen belts, the effect of the radiation on the solar cell performance was higher than expected. Therefore it was chosen to take a thicker cover glass of 250 μm.

The chosen solar cell is the IMM4J cell from reference [37], which is engineered with a

radiation-resistant structure. As a result, the estimated performance loss due to a radiation flux of $16.35 \cdot 10^{14}\,\mathrm{MeV/cm^2}$ and $21.13 \cdot 10^{14}\,\mathrm{MeV/cm^2}$ (see section 4.4), is on the current 0.98 and on the voltage 0.95 respectively (see table 5.20). The temperature coefficients are from reference [38], although no information is given how the coefficients change under the influence of radiation, therefore an estimate is made based upon the similarity with GaAs triple junction cells.

Characteristic	BOL	η_{rad}	EOL
Cell area (cm^2)	27.6	-	-
Cell length (cm)	6.3	-	-
Cell width (cm)	4.6	-	-
η_{cell} (%)	34.5	0.93	32.1
I_{sc} (mA)	468.4	0.98	459.0
I_{mp} (mA)	429.5	0.98	420.9
V_{mp} (mV)	3000	0.95	2850
V_{oc} (mV)	3236	0.95	3074
dI_{sc}/dT (mA/K)	0.163	1.29	0.21
dI_{mp}/dT (mA/K)	0.163	1.23	0.2
dV_{mp}/dT (mV/K)	-6.44	1.07	-6.9
dV_{oc}/dT (mV/K)	-6.44	1.06	-6.8

Table 5.20.: Characteristics of IMM4J solar cell [37] [38] and radiation impact (see section 4.4).

The pointing accuracy of the solar arrays is assumed to be $\pm 5^\circ$ of the desired position. The beta angle is at maximum 5°, which also causes a loss. Other degradation factors that influence the array performance are cell mismatch, micrometeoroids and debris impacts. Also a random loss factor is included that covers losses due to bypass diode failure and thermo-elastic stress cycles [6]. All the different losses on the current and voltage can be seen in table 5.21.

	Current losses		Voltage losses	
Characteristic	η_{CL_i}	BOL/EOL	η_{VL}	BOL/EOL
Cell mismatch	0.99	BOL	-	-
Off-pointing error loss	0.996	BOL	-	-
Beta angle loss	0.996	BOL	-	-
Plume impingement	0.98	EOL	0.99	EOL
Micrometeorites	0.98	EOL	-	-
Random loss	0.97	EOL	-	-

Table 5.21.: Current and voltage losses on the solar cell [6].

The EOL current of one cell is then the product of all the losses, multiplied by the radiation loss and cell current at BOL. The same applies for the voltage, which is expressed in the following formulas:

$$I_{EOL} = \prod (\eta_{CL_i}) \eta_{rad} I_{BOL}. \tag{5.35}$$

$$V_{EOL} = \eta_{VL} \eta_{rad} V_{BOL}. \tag{5.36}$$

The performance of the cell under different temperature conditions can be calculated with equations 5.27 to 5.30. The solar array hot case and cold case are 106 °C and −193 °C, respectively (see section 5.6.1). With this information, the performance of the cell at BOL, EOL and under different operation temperatures are completely known (see table 5.22). Therefore, different solar array designs can be evaluated to come to a final selection. It is required that the solar array produces 606.8 kW under hot conditions at EOL.

	Cold case		Hot case	
Characteristic	BOL	EOL	BOL	EOL
I_{sc} (mA)	424.64	377.51	472.50	434.96
I_{mp} (mA)	386.39	344.62	434.26	399.33
V_{mp} (mV)	4423.2	4331.2	2497.7	2288.7
V_{oc} (mV)	4659.2	4531.2	2733.7	2518.4

Table 5.22.: Performance of a single solar cell under different temperature conditions for BOL and EOL.

Solar cells of neighboring strings should have the same electric potential to limit arcing. The length of a string is shorter than the width of all the strings combined. Therefore, the strings are placed in the flight direction of the stage. They will be subject to erosion caused by the thruster and thus require a number of redundant strings. In order to keep the blankets equal in design, one redundant string per blanket is chosen, having a total of four redundant strings that compensate for the performance loss due to ion impingement (see section 5.3).

Due to the placement of the strings, the required voltage level determines the width of one blanket. The length of the blanket can then be determined in combination with the total power requirement. For attitude control considerations, it is advisable to keep the length and width of one complete SAW in the same order of magnitude. Also, the length of deployable structures is taken into consideration together with the voltage that is required for Hall thrusters. High power Hall thrusters typically operate in a voltage range of $300 - 600$ V. The blanket dimensions for different operation voltages can be seen in table 5.23, while the SAW dimensions are two blankets placed side-by-

side (see concept (b) of figure 5.23).

Characteristic	300 V	400 V	500 V
Blanket width (m)	6.1	8.1	10.1
Blanket length (m)	84.5	63.3	50.7
SAW width (m)	12.2	16.2	20.2
SAW length (m)	84.5	63.3	50.7
Length:width	6.9:1	3.9:1	2.5:1
$V_{oc,BOL-cold}$ (V)	615	815	1,020

Table 5.23.: SAW dimensions, without deployable truss, for different operational voltages.

The maximum allowable length of the blanket is 10 m, which is slightly violated by a 500 V bus. However, more important is the open circuit voltage when the solar array is coming out of eclipse and thus in the cold state of approximately $-193\,^{\circ}$C (see table 5.23), since the Hall thruster has to provide stable operation at this high voltage level. The selected NASA-457M is tested for operation voltages up to 650 V and is expected to allow for stable operation up to 1000 V [65]. A 500 V bus therefore slightly violates this requirement and is not selected, leaving the 300 V and 400 V bus as the remaining options. The 300 V bus requires a very long deployable boom (84.5 m), which can only be achieved by a not very stiff coil-able boom. Besides, the length to width ratio is 6.9:1, which is not beneficial for the AOCS. The 400 V bus has a maximum open circuit voltage of 815 V, length of 63.3 m and a length to width ratio of 3.9:1. This length allows for the usage of a deployable truss structure and as conclusion, the 400 V bus is selected. The bus requires 175 cells in series and in total 3,804 parallel strings (4 redundant strings included) to produce the required power of 606.8 kW at EOL. The characteristics of the complete solar array under different temperature conditions at BOL and EOL can be determined (see table 5.24) and the corresponding V-I and V-P characteristics are created (see figure 5.26 and 5.27).

	Cold case		Hot case	
Characteristic	BOL	EOL	BOL	EOL
I_{sc} (A)	1615.3	1436.1	1797.4	1654.6
I_{mp} (A)	1469.8	1310.9	1651.9	1519.1
V_{mp} (V)	774.1	758.0	437.1	400.5
V_{oc} (V)	815.4	793.0	478.4	440.7
P_{mp} (kW)	1,138	993.6	722.0	608.4

Table 5.24.: Performance of the complete solar array under different temperature conditions for BOL and EOL.

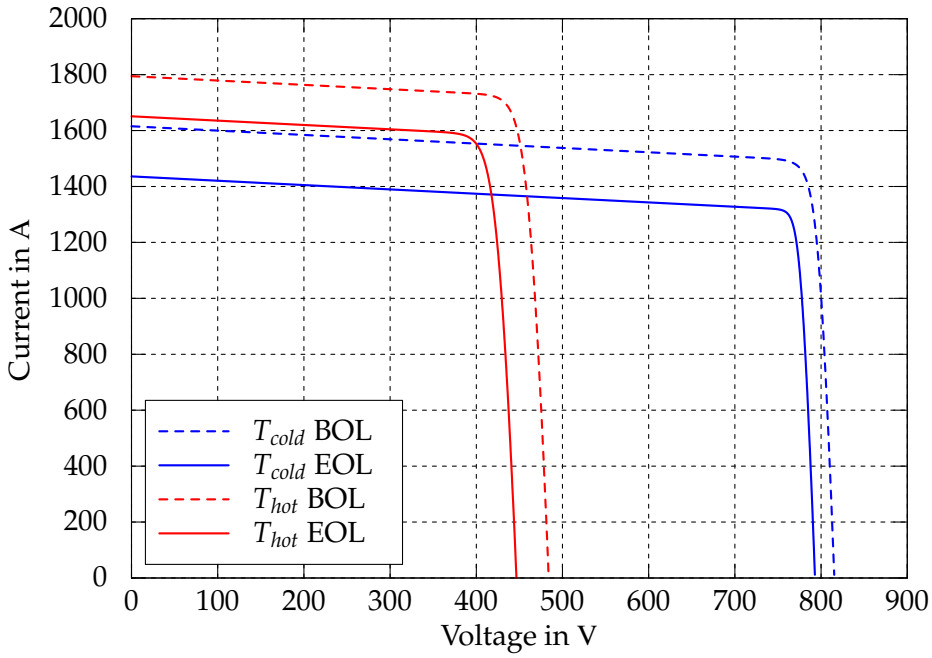

Figure 5.26.: Voltage-current characteristic for the Solar Array at BOL, EOL and for the hot and cold case.

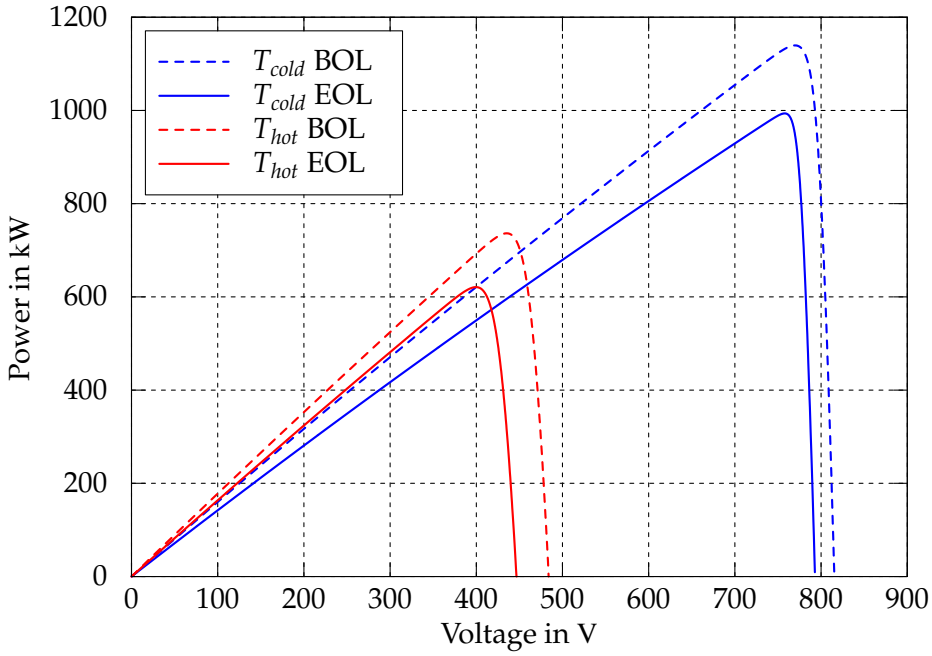

Figure 5.27.: Voltage-power characteristic for the Solar Array at BOL, EOL and for the hot and cold case.

The dimensions of one solar array blanket can be specified by taking the size of the solar cell (see table 5.20) and including spacings for fold lines and neighboring strings. This spacing between the solar cell strings is required in order to prevent arcing in case the potential difference of adjacent cells is high. Theoretically, the maximum potential difference occurs when a single string is shadowed and the neighboring string is fully operational, resulting in a maximum potential difference of 400 V. The dielectric strength of 25 μm thick Kapton is about $256.1 \cdot 10^6$ V/m [6] and thus a spacing of at least

1.56 mm is required to avoid arcing. The spacing for the fold lines is estimated at 1.8 cm and the number of strings per section at nine. As a result the total length of a single blanket is 63.3 m (see table 5.25). To validate the design, a check is made by considering the panel packing factor, F_{pp}, which is calculated by:

$$F_{pp} = \frac{N_{cells} A_{cell}}{A_{total}}. \tag{5.37}$$

Typically, the panel packing factor for a solar array is equal to 0.9 [57], which is also the result for our designed solar array.

Solar Array Blanket	
Cells in string	175
String length (m)	8.05
Parallel strings	951
Length blanket w/o spacing (m)	59.9
String spacing (mm)	1.6
Fold line spacing (cm)	1.8
Strings per section	9
Total spacing length (m)	3.43
Section width (m)	0.6
Total length single blanket (m)	63.3
Panel packing factor	0.9

Table 5.25.: Dimensions of one solar array blanket.

The high operating voltage of the solar array gives rise to spacecraft charging and arcing. Ground tests of the solar array at these high voltage are required to identify problems concerning arcing and potential charging and apply design changes where needed. Also, tests should be done to determine the lifetime of the solar array under high voltages in the space environment.

Layer	Thickness (μm)	Density (g/cm^3)	Mass (g)
Cover glass	250	2.605	1.797
Cover glass adhesive	20	1.08	0.0596
IMM4J cell	20	0.012	0.331
Cover glass adhesive	20	1.08	0.060
Cover glass	250	2.605	1.797
Kapton substrate	25	1.42	0.098
Total	585		4.143

Table 5.26.: Configuration of the solar cell layers and their properties.

The solar cell is build up in layers, with the substrate functioning as the base of the flexible blanket. The selected substrate is Kapton with a thickness of 25 μm [6] [20] and the IMM4J cell is embedded in 250 μm thick cover glasses for protection against radiation. The density of an IMM solar cell is not specified, therefore it was estimated by taking the density of a GaAs TJ cell of 140 μm, 84 mg/cm^2, and reducing the thickness to 20 μm, resulting in an estimated density of 12 mg/cm^2. The resulting total mass of the solar cell is estimated at 4.14 g (see table 5.26). The blanket mass is determined by multiplying the cell mass with the number of cells. The final dimensions and mass of a single blanket can be seen in table 5.27.

Characteristic	Solar array blanket
Width (m)	8.05
Deployed length (m)	63.3
Area (m^2)	509.9
Stowed length (m)	0.6
Stowed height (m)	0.25
Stowed volume, with 20% margin (m^3)	1.44
Mass, with 20% margin (kg)	827.5

Table 5.27.: Specifications of a single solar array blanket.

The deployable structure in between the solar array blankets has to provide stiffness to the complete wing, of which the selection is done in section 5.5.5. A tension mechanism is to supply tension to the blanket as it reaches complete deployment. This mechanism also has to keep the blanket level when the solar array comes out of eclipse and thermal snap occurs, which has to be evaluated in subsequent design phases. The entire wing is tied structurally to the transverse boom by means of the canister and SADM.

5.4.8. Electric Power System Results

The Electric Power System is described in detail throughout the sections 5.4.1 to 5.4.7. The resulting volume and mass estimates can be seen in table 5.28. Note that the DDU and its components is included in the propulsion mass budget.

Component	Volume (m^3)	Mass (kg)
2xSAW	5.7	3,310
2xSADM	0.6	487.0
2xSSU	4.6	2,744
PCDU	0.15	97.9
Battery	0.10	195.4
Total EPS	11.3	6,834

Table 5.28.: Mass and volume budget of the EPS, including margins.

5.5. Configuration, Structures & Mechanisms

All the spacecraft components need to be arranged into a suitable configuration. This is performed by first identifying configuration driving components, followed by a discussion of different mechanisms. Then a structure design model is introduced to size all the different structures. Finally, within the results, a configuration is suggested, the whole structure and mechanisms are selected and sized accordingly the models.

The Configuration, Structures and Mechanisms have to comply with the following requirements:

	Mission Requirement	Created
5.2	The transfer stage and cargo shall be launched separately.	Sec. 4.3.2
6.	The transfer stage shall dock and un-dock with the cargo, depending on the mission architecture.	Sec. 2.2
	System Requirement	**Created**
2.3.1	To limit the plume impingement, the thrusters shall be placed in line with the solar array width.	Sec. 5.3.3
6.	The transfer stage shall provide a separation mechanism from its payload. Due to stage reusability, this shall be a docking mechanism to dock and un-dock with the payload.	Sec. 2.2
6.1	The docking mechanism shall provide propellant transfer.	Sec. 5.2.1
6.1.1	At a pressure of 12 MPa.	Sec. 5.3.6
10.2	The docking mechanism shall provide power transfer between the payload and SEP stage.	Sec. 5.4.6
11.	The transfer stage's configuration should be such that the direct impingement of the thrusters' exhaust on the solar arrays is limited (TBD).	Sec. 2.2
12.	The configuration shall be such that the antennas, thermal radiators, solar panels and the docking mechanisms have a unobstructed field of view.	Sec. 5.5
13.	The structure shall be rigid enough to withstand the launch loads and the frequencies that are imposed by the launcher.	Sec. 5.5
13.1	The structural design shall aim for simple load paths and maximize the use of conventional materials.	Sec. 5.5
13.2	The structure shall protect all systems, excluding solar array and radiators, to the radiation and debris of the space environment.	Sec. 5.5
13.3	The structure shall fit into the adjusted Falcon Heavy fairing, with inner diameter of 4.6 m, cylindrical height of 12.4 m and total height of 16.6 m.	Sec. 5.5
14.	The deployable mechanisms shall be designed to withstand a natural frequency of 0.1 Hz (TBC) in the deployed state.	Sec. 5.5

5.5.1. Configuration driving components

The preliminary system baseline, suggested two possible system arrangements (system arrangement (c) or (d), see figure 5.4 and 5.6). As stated, the payload and SEP stage are launched separately, therefore the focus in this section will be on the SEP stage.

In order to avoid large structural stresses during launch and, consequently, a heavy structure, the center of mass should be located as close as possible to the launcher adapter. The driving components are therefore, primarily, the components that have a high mass. Secondly, the size of components are important in order to compose a suitable configuration. The following driving components are identified:

- Propellant tank, mass of $> 8\,\text{ton}$.
- Solar Array Wings assembly, mass of $3.8\,\text{ton}$ and considerable dimensions.
- Canister length of the solar array deployable boom, which is $2.2\,\text{m}$ (see section 5.5.5).
- The EPS power conditioning equipment, e.g. the SSU, mass of $> 2.8\,\text{ton}$.
- Thrusters and DDU, mass of $1.2\,\text{ton}$.
- Radiators, mass of $0.9\,\text{ton}$.

The propellant tank is the heaviest component during launch and is therefore located directly above the launcher adapter. The tank has a radius of $1.14\,\text{m}$, while the fairing has a radius of $2.3\,\text{m}$. Therefore, around the tank there is sufficient space to place the electronic equipment of the avionic bay. This means that configuration (c) of figure 5.4 is selected, where it has to be noted that the tank is placed inside the avionic bay.

Above the tank and avionic bay, the next heaviest element is placed, which is the solar array wing assembly. The deployable boom of the solar array is stored inside a canister, which has a length of $2.2\,\text{m}$. Due to this length, the two SAWs can not be placed on the same rotational axis, since it would require a fairing with a diameter larger than $4.4\,\text{m}$. Therefore the SAWs have to be placed off-axis, side by side.

On top of the SAWs, the engines and radiators are located. They have to be supported by a structure that goes around the SAWs. It is chosen to place this supporting structure along the longitudinal axis of the spacecraft, such that it can be connected to the load carrying structure of the tank and in this way transfer the loads to the adapter. The suggested configuration can be seen in figure 5.28.

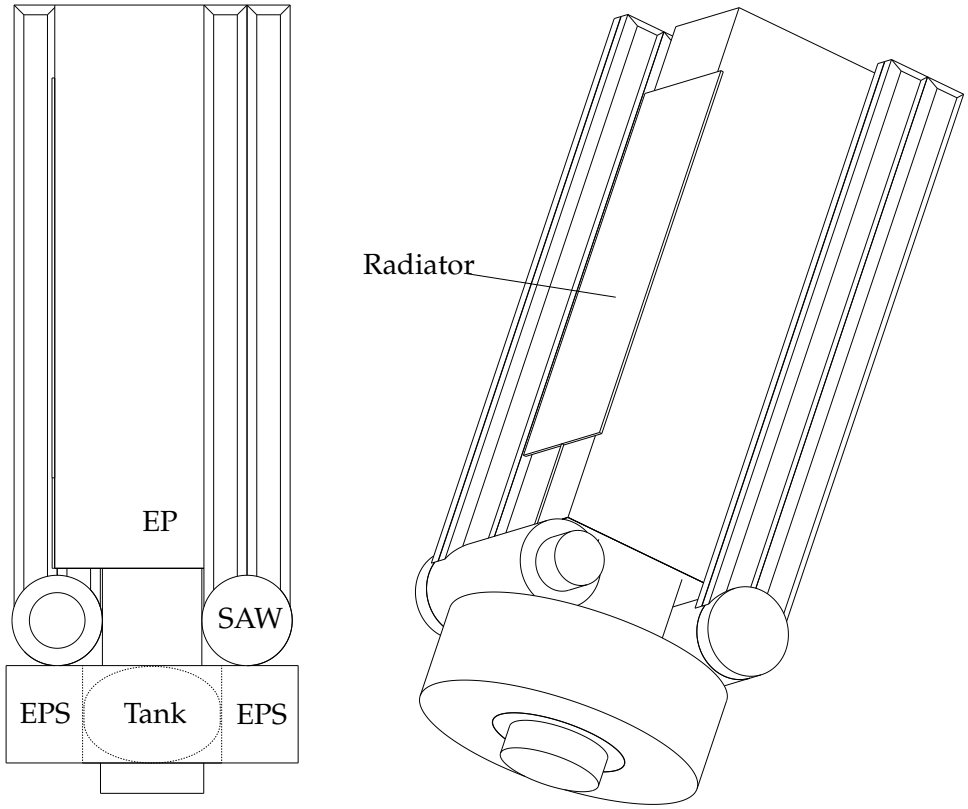

Figure 5.28.: The configuration of the SEP stage with a front view (left) and isometric view (right).

5.5.2. Deployment Mechanisms

Structural deployment technologies are evaluated for usage on the SEP stage. These technologies can separate the engines from the rest of the vehicle and/or for deploy the solar array. Especially for solar arrays, deployment technologies can potentially save significant amount of volume, since a common rigid panel is typically 2 cm thick. Therefore, flexible panels in combination with deployment technologies are studied for the design. Relevant deployment technologies that are currently available and have a TRL of ≥ 6, are [34] [42]:

- Inflatable booms
- Telescopic booms
- Shape memory composites booms
- Articulated booms
- Deployable truss structures
- Coil-able booms

Inflatable booms are unfolded by inflation and need to be rigidized after deployment in order to ensure a longer lifetime. These booms cannot deploy heavy structures, have a low deployment accuracy and low stability. The main advantage is that they are

extremely lightweight and have a very high packaging ratio [42].

The telescopic boom consist of a series of thin-walled cylindrical tubes that are nested inside one another and can be extended (see figure 5.29). They are precise, stable and more stiff compared to the inflatable booms. However, they are considerably heavier and have a relatively low packaging ratio [42] [43].

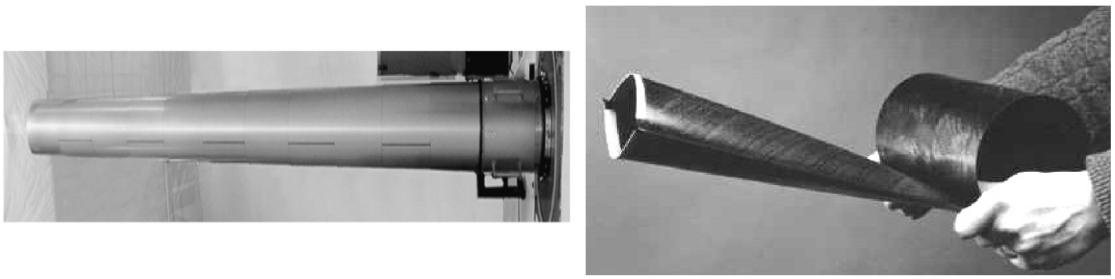

Figure 5.29.: A telescopic boom (left) [42] and a shape memory composite boom (right) [43].

A shape memory composite boom (see figure 5.29) is a thin-walled tubular boom that makes use of the elastic deformability of thin-walled shells. The booms are typically made out of stainless steel, Copper-Beryllium or Carbon Fiber Reinforced Plastic (CFRP) composites and are flattened and rolled up in their stored configuration. The advantage of this technology is the low weight and the low power which is required for deployment. In spite of these advantages, they have a relatively low deployment accuracy, cannot deploy heavy structures and have a low stability [42] [43].

Articulated booms consist out of solid booms with multiple motorized joints, like the robotic arm of the ISS. The advantage of such a deployment system is the flexibility in moving, even when the solar array is deployed. In theory, it could cancel out the β-solar angle. However, this system is the heaviest of all considered mechanisms and also has the lowest packaging ratio [42].

A truss structure can be made foldable by having a number of pinned joints instead of rigid joints and by replacing the diagonal members with cables. Multiple deployable truss structures exist, like the tensegrity mast, the Folding Articulated Square Truss (FAST) and Able Deployable Articulated Mast (ADAM) [42]. To prevent a too thorough discussion on all the possible options, only the structures with a TRL of ≥ 6 are considered, which are the FAST and ADAM system.

The FAST mast (see figure 5.30) has hinges along the four longitudinal booms, called the longerons, and two pairs of diagonal cables on each side of a module. The cables are prestressed by four lateral bows, which can bend to make the cables slack and fold the truss. Eight FAST masts are used on the ISS, with a diameter of 1.09 m and a length of 34.75 m. The canister, in which the folded truss is stored, is 2.3 m long [43] [34]. One ISS mast deploys and provides structural strength to one complete solar array wing.

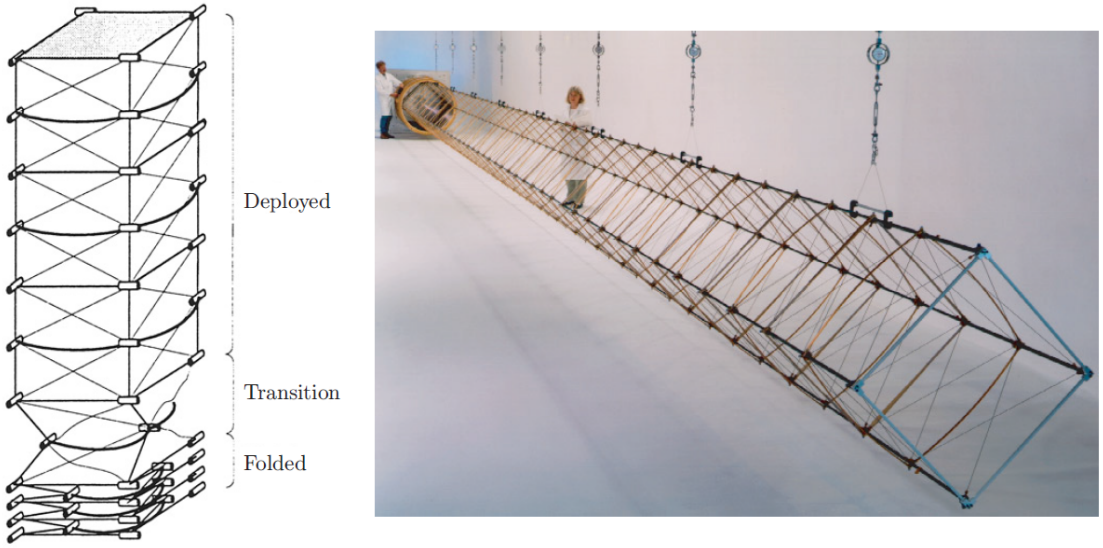

Figure 5.30.: The principle of the FAST mast (left) and the truss in a deployed state (right) [43].

The ADAM mast (see figure 5.31) has a longeron, which is pinned together to obtain a complete module. The diagonal cables latch to stiffen each module once deployed. The truss has a low eigen frequency of around 0.1 Hz [42] and the bending stiffness of the system can be adjusted by changing the mass. This type of truss was flown on a Space Shuttle STRM mission (2000) and on the NuSTAR mission (2012). The ADAM mast on the STRM mission had a diameter of 1.12 m, a stowed height of 1.42 m, canister length of 2.92 m and a total deployed length of 60 m [43]. This truss is the longest deployable mast ever flown in space [34], since the NuSTAR mast is only 10 m long.

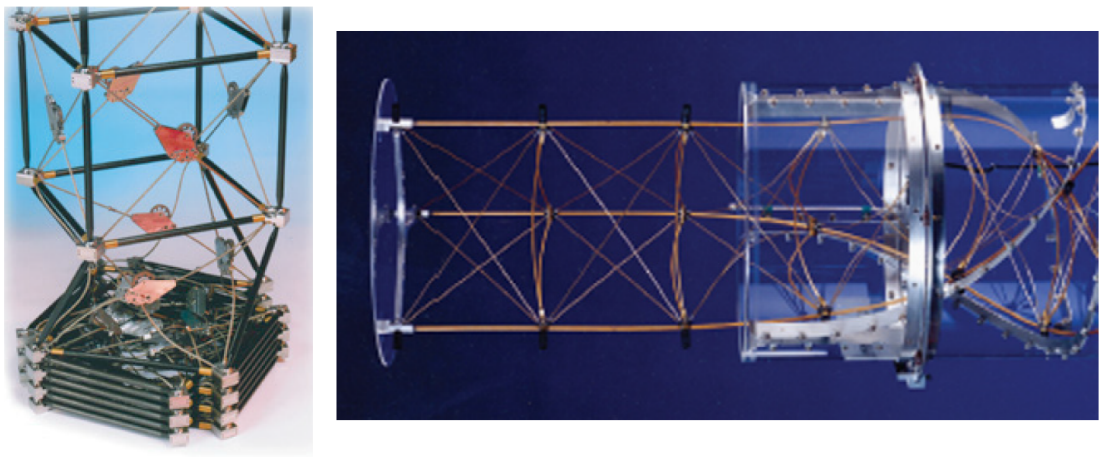

Figure 5.31.: To the left the ADAM truss [43] and to the right a coil-able boom [42].

Coil-able booms are comparable to deployable truss systems, with the main difference that the longeron is running over the full length. When stowed, the longeron is coiled as a spring which provides the energy necessary for their deployment. This configuration makes the tip of the boom rotate during deployment, an issue which is not present in the

ADAM boom. The storage is very compact and the stiffness and weight can be chosen by modifying the boom's diameter. The resulting mast is less stiff than an ADAM truss. This technique can potentially achieve the longest possible deployable boom of about 100 m [42].

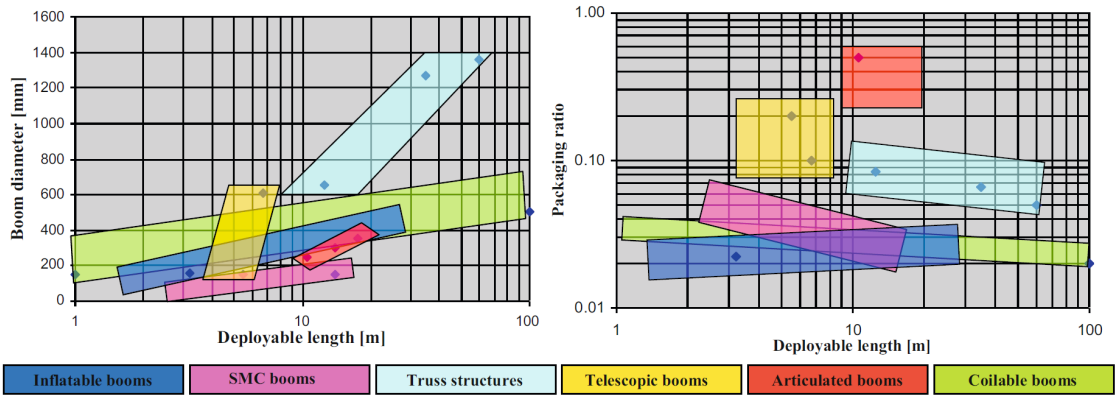

Figure 5.32.: Characteristics of deployable systems: boom diameter (left) and packaging ratio (right) as function of deployable length [42].

Every discussed boom type has different characteristics of which the most important are the deployable length, boom diameter, mass, packaging ratio and bending stiffness (see figure 5.32 and 5.33). The packaging ratio is the stored length divided by the deployed length. The stored length is equal to the canister length in which the deployment system is stored. Together with the diameter they make up for the total volume that needs to be accommodated on the spacecraft [42]. The bending stiffness describes how much deflection could occur at the tip of the boom under certain stress conditions, e.g. docking loads and vehicle acceleration. These types of deployable booms are usually less stiff in bending than they are in torsion and under axial loading [42].

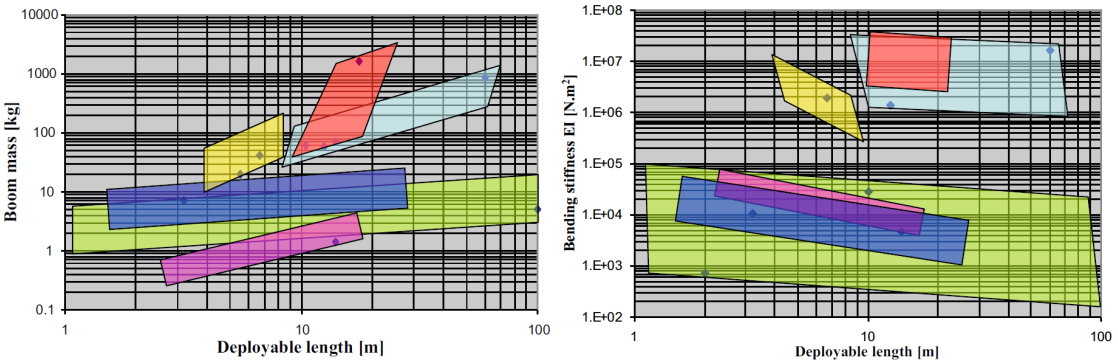

Figure 5.33.: Characteristics of deployable systems: boom mass (left) and bending stiffness (right) as function of deployable length [42].

As stated, due to the launcher volume limitations, these technologies need to be considered to enable the mission objectives. The most important characteristics of these deployable technologies are therefore the boom diameter, packaging ratio, mass, deployable length and TRL (see table 5.29), which are used for later trade-offs.

Deployment type	Deployable length (m)	Boom diameter (m)	Packaging ratio	Mass (kg)	TRL
Inflatable booms	1.6-28	0.04-0.5	0.018-0.028	2.2-25	7
Telescopic booms	3.8-7	0.15-0.65	0.075-0.16	10-200	8
Shape memory composite booms	1.5-18	0.01-0.24	0.018-0.072	0.18-4.2	6
Articulated booms	9-22	0.19-0.43	0.24-0.6	40-3400	9
Deployable truss structures	8-68	0.6-1.4	0.042-0.14	28-1040	9
Coil-able booms	1-100	0.1-0.72	0.02-0.04	0.9-20	9

Table 5.29.: Characteristics and performance of different deployment technologies [42].

Most of the expertise for these deployment structures can be found in the American or Japanese industry. Articulated booms are under study for space applications in Europe, but are at a TRL of 4. Regarding deployable truss structures or coil-able booms, there is no expertise available in Europe. On the other hand, there is experience in Europe considering the inflatable and shape memory composite booms [42].

5.5.3. Docking Mechanism

A docking mechanism is required to make the system reusable and enables the SEP stage to perform the mission multiple times. The mechanism shall provide an mechanical interface between the payload and SEP stage and is able to transfer propellant, power and data.

Within a docking procedure, there is typically an active vehicle and a passive vehicle. The active spacecraft makes the approach and docks, while the passive vehicle can be cooperative or non-cooperative during the docking. Cooperative means that the spacecraft is capable of maintaining its attitude, while for a non-cooperative system it can not. Logically, the active vehicle is the most agile spacecraft, which is in our case the payload and thus the SEP stage is passive. Also, due to the magnitude of the SEP stage, it is deemed necessary that it maintains its position and is thus cooperative during the docking procedure.

For all docking maneuvers, the solar arrays will be deployed. The deployment of the solar array after launch, is required to fire the thrusters and cancel out any rotation rate or axis off-pointing caused by the launcher. Due to the fact that the stage is in the deployed configuration, missing the docking mechanism will most probably result in a collision with the spacecraft and thus the risk involved is relatively high. However, the heritage concerning docking is substantial and therefore no significant problems are expected.

Their is an international effort between NASA and ESA to develop an international docking system, called International Berthing and Docking Mechanism (IBDM), that should be operational on the ISS in 2014 [91]. This docking system provides a mechanical connection and is able to transfer propellant, electric power and data. The system is therefore able to fulfill all the SEP requirements and is therefore selected (see table 5.30).

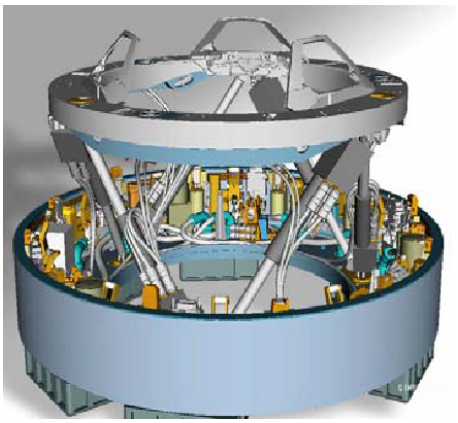

Figure 5.34.: The IBDM in a deployed configuration [90].

IBDM	
External diameter (m)	1.485
Height (m)	0.437
Volume (m^3)	0.757
Mass (kg)	340.2

Table 5.30.: Specifications of the International Berthing Docking Mechanism [90] [91].

5.5.4. Structure design model

The structure has to withstand all mechanical loads the spacecraft encounters during its lifetime and provide support to all the components. The spacecraft's most severe mechanical loads are experienced during the launch, in which the supporting structure has to provide enough strength. A simple analysis is performed to size the primary load carrying structure, by taking into account the stiffness, strength and buckling. For further design phases, once the baseline layout is consolidated, it is advised to perform finite-element-methods, which is a very complex and time consuming analysis, but offers a more accurate and optimized result. For the preliminary design phase, it is important to asses the structural mass in a fast manner and such a tool within EXCEL is created and a simple analysis is performed. This tool computes the required wall thickness of the different spacecraft's elements, by considering the strength, stiffness and buckling of the structure. From the resulting required wall thickness, the overall mass can be calculated.

Load Bearing Cylinder

The basic load carrying structure, which is connected to the launcher adapter, consists out of a thin-walled cylinder. On top of the cylinder, masses are attached that consists out of the solar array wings and thrusters. The cylinder is modeled as a cantilever beam with a mass on top. The cross-sectional area and moment of inertia of a thin-walled

cylinder is equal to:

$$A_{cylinder} = 2\pi rt. \tag{5.38}$$

$$I_{cylinder} = \pi r^3 t. \tag{5.39}$$

Where r is the radius and t is the wall thickness, both in m. The mass of the thin-walled cylinder can be calculated by:

$$m_{cylinder} = \rho Al. \tag{5.40}$$

Where ρ is the density of the chosen material in kg/m^3. The cylinder is modeled as a mass carrying cantilevered beam (see figure 5.35).

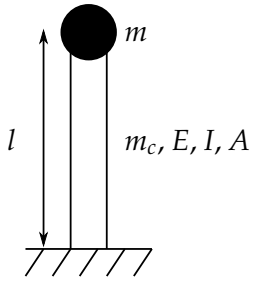

Figure 5.35.: Mass carrying cantilevered beam.

The launcher imposes certain frequencies on the spacecraft and the first lateral and axial mode frequencies of the spacecraft have to be above this threshold. The lateral and axial frequency, f_{lat} and f_{ax}, of the beam can be calculated by [3]:

$$f_{lat} = 0.276\sqrt{\frac{EI}{ml^3 + 0.236m_c l^3}}. \tag{5.41}$$

$$f_{ax} = 0.160\sqrt{\frac{AE}{ml + 0.333m_c l^3}}. \tag{5.42}$$

Where E is the material's Young's modulus, m the mass on top of the cylinder and m_c the mass of the cylinder. The minimum required thickness of the cylinder can be determined by using equations 5.38 to 5.42:

$$t_{lat-min} = \left(\frac{ml^3 + 0.236m_c l^3}{\pi r^3 E}\right)\left(\frac{f_{lat}}{0.276}\right)^2. \tag{5.43}$$

$$t_{ax-min} = \left(\frac{ml + 0.333m_c l}{2\pi rE}\right)\left(\frac{f_{ax}}{0.160}\right)^2. \tag{5.44}$$

The outcome that has the largest thickness, is the dimensioning case and, hence, se-

lected. The next step is to evaluate the strength of the cylinder with the obtained wall thickness. The sizing case again occurs during launch, where the acceleration factors are largest. The maximum lateral and axial force can be calculated by:

$$F_{lat} = (m + m_c)\, g N_{lat}. \tag{5.45}$$

$$F_{ax} = (m + m_c)\, g N_{ax}. \tag{5.46}$$

Where N_{lat} and N_{ax} are the maximum acceleration factors occurring during launch. The lateral force introduces a bending moment, M, which is of importance for the stress in the structure:

$$M = F_{lat} l_{cg}. \tag{5.47}$$

Where l_{cg} is the length to the center of gravity, measured from the bottom of the cylinder. It can be determined with:

$$l_{cg} = \frac{ml + \frac{1}{2} m_c l}{m + m_c}. \tag{5.48}$$

The axial and bending stress imposed on the structure can be calculated with [3]:

$$\sigma_{ax} = \frac{F}{A} = \frac{F_{ax}}{2\pi r t}. \tag{5.49}$$

$$\sigma_{bend} = \frac{Mr}{I} = \frac{M}{\pi r^2 t}. \tag{5.50}$$

A summation of both stresses, results in the maximum possible stress:

$$\sigma_{max} = \sigma_{bend} + \sigma_{ax}. \tag{5.51}$$

The maximum stress occurring in the structure is compared with the allowable stress of the material and expressed with the margin of safety, MS [3]:

$$MS = \frac{\sigma_{allow}}{FS \sigma_{max}} - 1 > 0. \tag{5.52}$$

Where FS is a factor of safety. The margin of safety has to be above zero in order to guarantee that the load bearing structure has enough strength. When this is not the case, the wall thickness has to be increased until this requirement is met.

The last possible failure mode of the structure can occur due to buckling in the thin-walled cylinder. For the cylinder, an isotropic material should be used and thus the buckling theory for isotropic materials is applied. The buckling stress for a cylinder

under axial compression can be calculated with [3]:

$$\sigma_{allow,buck} = \frac{\gamma E}{\sqrt{3\,(1-\nu)}}\frac{t}{r}. \tag{5.53}$$

Where ν is the Poisson's ratio, depending on the chosen material. The reduction factor, γ, is used to correlate theory to test results and depends on a geometric parameter, φ. The geometric parameter, for a wall thickness ratio (r/t) smaller than $1,500$ and a slenderness ratio (l/r) smaller than five, can be determined by [3]:

$$\varphi = \frac{1}{16}\sqrt{\frac{r}{t}}. \tag{5.54}$$

$$\gamma = 1 - 0.901\left(1 - e^{-\varphi}\right). \tag{5.55}$$

In case the maximum stress (equation 5.51) is higher than the allowable buckling stress, the wall thickness has to be increased to the point where a margin of 15% between the two is acquired.

Load bearing thin-walled rectangular box

For a thin-walled rectangular box, with outer width B, height H, inner width b and inner height h, the cross-sectional area, moment of inertia are and mass can be determined with [3]:

$$A_{box} = BH - bh. \tag{5.56}$$

$$I_{box} = \frac{1}{12}\left(BH^3 - bh^3\right). \tag{5.57}$$

$$m_{box} = \rho A l. \tag{5.58}$$

The lateral and axial frequency can now be determined with equation 5.41 and 5.42. The strength of the box can be resolved by applying equations 5.45 to 5.52. The allowable buckling stress is for a thin-walled box a function of the critical force, F_{cr}, and the cross-sectional area A [3]:

$$\sigma_{allow,buck} = \frac{F_{cr}}{A} = \frac{1}{B^2 - b^2}\frac{\pi^2 EI}{kl^2}. \tag{5.59}$$

Where k is the effective length factor, which is equal to two for a cantilever beam that is fixed on one end and free on the other. With all the presented formulas, the different failure modes of the structure can be analyzed and the minimum wall thickness of the structure can be determined.

5.5.5. Configuration, Structures & Mechanisms Results

The configuration of the SEP stage shall be such that the center of gravity is located as close as possible to the launcher's adapter. The heaviest identified parts are the propellant tank, solar array wings and the electronics (see section 5.5.1). All the subsystems, are mechanically supported and attached to the spacecraft by the structure. The primary structure, indicated in red (see figure 5.36), is connected to the adapter, carries the spacecraft's major loads and supports the components that are present within the spacecraft body. The primary cylinder is sized such that the propulsion tank fits into it. The electronic systems are attached to the primary cylinder, while the solar array wings, thrusters and radiators are all connected to the top of the primary cylinder. The secondary cylinder encloses all the electronic components and such protect them from the harsh space environment. The top of the cylinder is locally stiffened to provide support to the solar array wings and the primary load bearing thin-walled rectangular box, indicated in red. The box supports the radiators, DDUs and Hall thrusters.

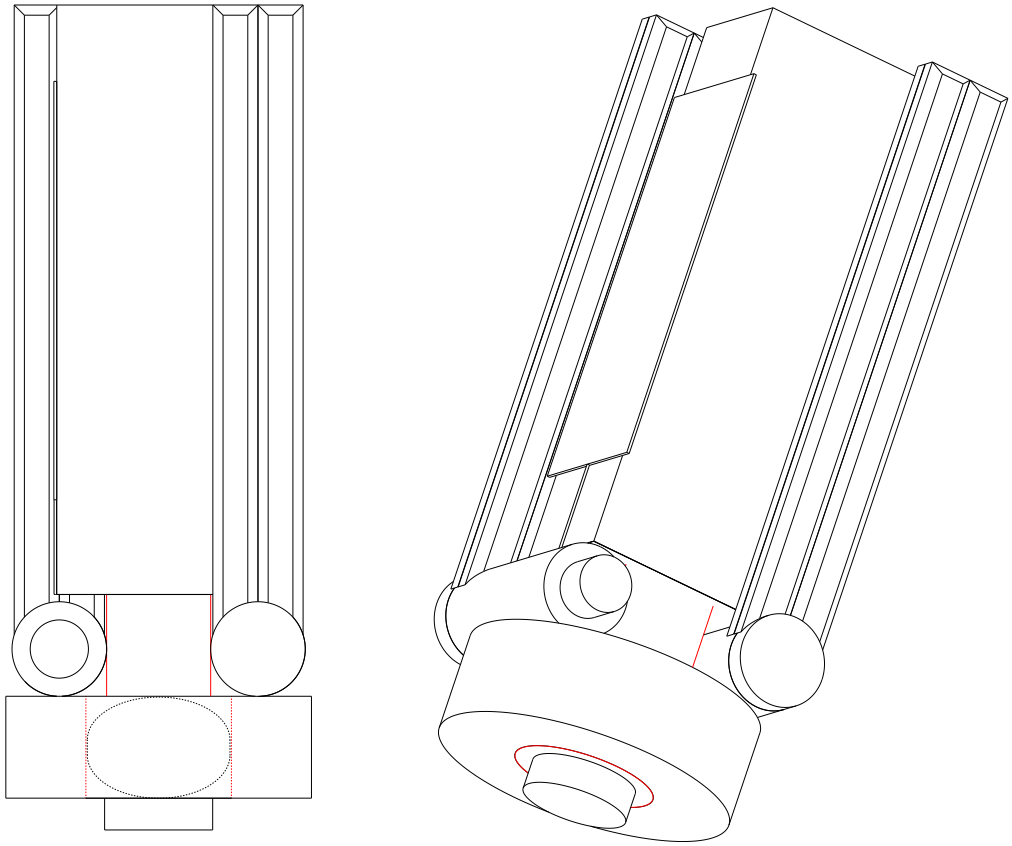

Figure 5.36.: The SEP stage in the folded configuration with a front view (left) and isometric view (right). The primary load carrying structure is indicated in red.

The materials commonly used in space industry for the structure, are aluminum alloys. Due to the high level of heritage, such an alloy is selected. The selected alloy for this mission is AL7075-T73, which has a density of $2,800\,\mathrm{kg/m^3}$, a Young's modulus of 71 GPa, compressive yield strength of 380 MPa and a Poisson's ratio of 0.33 [3] [89].

Primary structures

The primary load carrying structure consists out of a cylinder and a box connected to the top of the cylinder (see figure 5.36). The cylinder is directly attached to the launcher's adapter, which forms the direct connection to the launcher. The loads imposed by the launcher define the sizing case for the primary structures. Currently, the maximum loads produced by Falcon Heavy, are unknown. However, launchers have comparable maximum loads and therefore it is decided to take one from the same launcher family as reference, namely the Falcon 9 (see table 5.31).

	Lateral	Axial
Maximum load factor (G)	2	6
Frequency mode (Hz)	≥ 10	≥ 25

Table 5.31.: The maximum load factors and frequencies imposed by the Falcon 9 rocket [51].

The load bearing cylinder has masses directly connected to the cylinder and on top. It is assumed that the masses along the cylinder are evenly distributed. The model for a cantilever beam with a mass on top is used and the structural analysis is performed for the natural frequencies, strength and buckling of the cylinder. In the analysis, the buckling failure mode was identified as the sizing case, which can be seen by the fact that the allowable margin on buckling, is just met (see table 5.32).

	Lateral	Axial
Natural frequency (Hz)	86.3	66.6
Maximum force (N)	$3.6 \cdot 10^5$	$1.1 \cdot 10^6$
Bending moment (Nm)	$4.1 \cdot 10^5$	-
Stress (MPa)	24.8	37.7
Maximum stress (MPa)	62.5	
Factor of Safety $(-)$	2	
Margin of Safety $(-)$	2.04 (> 0)	
Allowable buckling stress (MPa)	71.9	
Margin allowable buckling on max. stress (%)	15.04 (> 15)	

Table 5.32.: Results of the structural analysis of the load-bearing cylinder.

The tanks and electronic systems are attached to the load bearing cylinder and is in table 5.33 described by the mass attached to the cylinder. The thrusters, solar array wings and radiators are all connected to the top of the primary cylinder and combined in the tip mass in table 5.33.

Load-bearing cylinder	
Length (m)	1.7
Radius (m)	1.15
Wall thickness (mm)	4.01
Tip mass (kg)	6,235
Mass attached to cylinder (kg)	12,321
Length to center of gravity (m)	1.14
Mass cylinder (kg)	137.9

Table 5.33.: Specifications of the load bearing cylinder.

The top of the cylinder is locally stiffened to provide support to the solar array wings and the primary box. The primary box supports the radiators, DDUs and Hall thrusters. It is stiffly connected to the cylinder and is modeled as a cantilever beam with a mass on top. The sizing case of the primary box is again the launch loads. It is required to place the thrusters in line with the solar array width, meaning that the length of the load bearing box has to be approximately 9.5 m. Due to this long length, the lateral forces are the designing case and the resulting wall thickness and mass are, respectively, 30.5 mm and 4,542 kg. This mass is unacceptably high and there is a more efficient solution. This solution entails that the thruster pallet, in its launcher configuration, is located just above the solar array canisters. Once in space, the thruster pallet along with the DDUs, are deployed by a deployable mechanism. As a result, the length of the secondary supporting rectangular box can be reduced to above the solar array canisters. The structural analysis of this shorter primary box can be seen in table 5.34.

	Lateral	Axial
Natural frequency (Hz)	27.6 / 40.2	43.1
Maximum force (N)	$4.83 \cdot 10^4$	$1.45 \cdot 10^5$
Bending moment (Nm)	$6.7 \cdot 10^4$	-
Stress (MPa)	142 / 40.3	41.5
Maximum stress (MPa)	183	
Factor of Safety $(-)$	2	
Margin of Safety $(-)$	0.04 (> 0)	
Allowable buckling stress (GPa)	1,930	
Margin allowable buckling on max. stress (%)	$1.05 \cdot 10^7$ (> 15)	

Table 5.34.: Results of the structural analysis of the load-bearing thin-walled box.

The corners of the box are connected to the primary load bearing cylinder, which means that the dimensions of the box is a function of the cylinder's radius. In the second direction, the length of the box is limited by the fairing radius and canister radius to a length of 1.2 m. The width of the box can be determined with:

$$l = \sqrt{\left(r_{cyl}\right)^2 - l_{req}^2}. \tag{5.60}$$

At the top of the load bearing box, the radiators, DDUs and thrusters are located and grouped within the tip mass (see table 5.35). Due to the shorter box, the wall thickness could be reduced drastically to 1.1 mm and the mass to 27.4 kg.

Load-bearing box	
Height (m)	1.4
Length required (m)	1.2
Width (m)	1.98
Wall thickness (mm)	1.1
Tip mass (kg)	2,436
Length to center of gravity (m)	1.4
Mass box (kg)	27.4

Table 5.35.: Specifications of the load bearing box.

Secondary structures

The secondary structures are not load bearing and their structural integrity can not be modeled in a simple way. More time-consuming analysis with Finite Element Methods would be required to optimize these structures, which is not desired for a phase zero study, as the secondary structure neither drives the architecture nor does it determine the concept feasibility. Therefore it is decided to give non load bearing aluminum panels a standard thickness of 0.5 mm, which is based upon OHB system's experts opinion. The secondary structures of the spacecraft consist out of a cylinder enclosing the primary load bearing cylinder and a secondary thin-walled box, that provides structural stability to the solar array booms and radiators. This secondary box forms an exception and can be modeled in a simple way. As stated, this box does not support other subsystems and thus only has to provide enough structural integrity.

	Bottom plate	Middle section	Top plate
Radius (m)	2.1	2.1	2.1
Area (m^2)	13.85	22.43	13.85
Height (m)	-	1.7	-
Thickness (mm)	0.5	0.5	1.0
Mass (kg)	19.40	31.4	38.79

Table 5.36.: Secondary structures of the cylindrical bottom section.

The electric system is enclosed by a cylinder around the primary load carrying cylinder. The cylinder has a bottom plate and top plate. The top plate is connected to the solar array wings and the box shaped primary structure. Therefore, it is load carrying and

decided to be thicker (1.0 mm) than the other structures (see table 5.36). The radius of the cylinder is depending on the size of the canisters that are placed on top.

The secondary box is sized and analyzed with a thickness of 0.5 mm. The analysis, see table 5.37, shows that the thickness is sufficient to fulfill all the requirements.

	Lateral	Axial
Natural frequency (Hz)	25.8 / 40.2	106.9
Maximum force (N)	$2.63 \cdot 10^3$	$7.90 \cdot 10^3$
Bending moment (Nm)	$1.07 \cdot 10^4$	-
Stress (MPa)	18.0 / 4.1	2.8
Maximum stress (MPa)	20.8	
Factor of Safety (−)	2	
Margin of Safety (−)	8.13 (> 0)	
Allowable buckling stress (GPa)	11,800	
Margin allowable buckling on max. stress (%)	$5.7 \cdot 10^7$ (> 15)	

Table 5.37.: Results of the structural analysis of the secondary thin-walled box.

The thruster plate is, in the launch configuration, located inside the secondary box just above the primary box. Due to the fact that the thruster pallet has to support the Hall thrusters and DDUs, the thickness is set at 1.0 mm (see table 5.38).

	Thruster plate	Secondary Box
Length (m)	3.6	3.6
Width (m)	2.0	2.0
Height (m)	-	8.1
Area (m^2)	7.2	95.9
Thickness (mm)	1.0	0.5
Mass (kg)	20.16	149.9

Table 5.38.: Secondary structures connected to primary box.

Deployable mechanism

There are two deployable mechanisms identified for the SEP stage:

1. A deployable mechanism that deploys and provide stiffness to the solar array wing.
2. A deployable mechanism that deploys the thruster pallet from the folded configuration into the deployed configuration.

The deployable structure in between the solar array blankets has to provide stiffness to the complete wing. For a deployed solar array the natural frequency is typically above 0.10 Hz [6] for lateral bending loads. Assuming that the connections between the

blankets and deployable structure are stiff, the whole structure can be modeled as a cantilever beam with a uniform mass distribution. The natural frequency, f_{nat}, of such a structure can be calculated with equation 5.41, where the tip mass equals zero. From this formula, the required stiffness is derived (see table 5.39). Only deployable truss structures can deliver this stiffness (see section 5.5.2 and figure 5.33) and are selected to support the solar array blankets. The dimensions of the canister are, in the selected configuration, limited by the fairing diameter and approaches the upper limit. Therefore, a significant engineering effort is required to meet the requirements concerning the stiffness and dimensions. This issue can be solved by relieving the power demand.

Requirements for deployable truss structure	
Required natural frequency (Hz)	≥ 0.10
Required stiffness (Nm^2)	$1.6 \cdot 10^7$
Selected deployable truss structure	
Diameter (m)	1.2
Deployed length (m)	63.3
Packaging ratio	0.035
Packaging length (m)	2.2
Stowed volume (m^3)	2.51
Mass (kg)	600
Bending stiffness (Nm^2)	$1.6 \cdot 10^7$

Table 5.39.: Requirements and specifications of the deployable truss structure supporting the solar array [42].

The thruster plate is connected to a deployable mechanism, which is deployed once the stage is in space. The different sizing cases for these deployable mechanisms are:

- The Hall thruster oscillations, having typical frequencies of 10 to 30 kHz.
- Maximum axial forces from the thrusters (31.3 N).
- Maximum lateral forces from the thrusters (2.4 N).

The deployable mechanism has to be fixed at one end to the load-bearing thin-walled box and at the other end to the thruster plate. This requirement eliminates the shape memory composite and inflatable boom. A telescopic boom, articulated boom or truss structure will result in a relatively heavy mechanism, which eliminates the mass benefit of this configuration. Therefore, from the mass point of view, a coilable boom is the most promising choice and is sized using figure 5.32 and 5.33 (see table 5.40). A benefit of this type of boom is that the elastic strain within the boom provides passive deployment. However, the stiffness is relatively low and therefore a configuration with four deployable booms, attached to the corners of the primary load carrying box, is selected. A risk of such a configuration is that the end-length of all the beams might be slightly different. In subsequent design phases a finite element model is needed to analyze if the

stiffness, provided by the deployable beams, is sufficient and to optimize their design.

Coilable boom	
Length deployed (m)	8.1
Diameter (m)	0.25
Packaging ratio (−)	0.025
Packaging length (m)	0.2
Stiffness single boom (Nm^2)	$1 \cdot 10^4$ (TBC)
Mass single boom (kg)	4
Mass four booms (kg)	16

Table 5.40.: Deployment mechanism to deploy the thruster plate.

Results overview

An overview of the resulting structure and mechanisms can be seen in table 5.41 and 5.42. The total mass, including margins, of the structure, deployable mechanisms and docking mechanism is 2308 kg.

	Primary Cylinder	Primary Box	Secondary Cylinder	Secondary Box	Total
Radius (m)	1.15	-	2.1	-	
Length (m)	-	1.2	-	3.6	
Width (m)	-	1.98	-	2.0	
Height (m)	1.7	1.4	1.7	8.1	
Wall thickness (mm)	4.01	1.1	0.5-1.0	0.5-1.0	
Mass (kg)	137.9	27.4	89.6	154.4	409.3
Margin	20%	20%	20%	20%	20%
Mass (kg)	165.5	32.9	107.5	185.3	491.2

Table 5.41.: The resulting structure of the SEP stage.

	Mass (kg)	Margin	Mass (kg)
Docking Mechanism	340.2	5%	357.2
Deployable Truss Solar Array	1200	20%	1440
Coilable Boom Thruster Plate	16	20%	19.2
Total			1816.4

Table 5.42.: The (deployable) mechanisms for the SEP stage.

5.6. Thermal Control System

A thermal analysis is very complex and normally performed by numerical software tools like ESATAN. However, a thermal analysis performed by these tools is time consuming and hence expensive. Besides, such an analysis requires a finished mission analysis and design, which are not realized at this point. Therefore, a more preliminary analysis is performed, which considers a hot case and a cold case to evaluate their impact on the design.

The Thermal Control System has to comply with the following requirements:

	System Requirement	Created
4.3.1	The propellant tanks should be kept at a temperature in between 20°C and 30°C.	Sec. 5.3.5
5.	The transfer stage shall provide thermal control and radiate all excess heat to space.	Sec. 2.2

The thermal environment during the stage's lifetime shall be analyzed. The stage undergoes certain phases where it experiences different environments:

- Pre-launch environment
- Launch environment
- Space environment

Within the pre-launch environment no major problems are foreseen. Typically, electronics can operate in a temperature range of -15°C to 50°C, rechargeable batteries between 0°C and 20°C and mechanisms between 0°C and 50°C [11]. The propellant tank should be kept at a temperature in between 20°C and 30°C. It is assumed that the temperature of the stage within this thermal environment can be controlled in between 0°C and 40°C, which means that for the batteries and tanks additional measures might be necessary to keep them at their required temperature. Once the stage is integrated into the rocket fairing, thermal control can be achieved by blowing conditioned air or nitrogen through the fairing enclosure.

During launch, the fairing will heat up due to friction. This heat is partly passed upon the stage and therefore undergoes heating. After fairing jettisoning, the stage will be subjected to free molecular heating. The point at which the fairing is jettisoned is a trade-off between the desire to save weight and the need to protect the spacecraft to atmospheric heating [12]. The thermal analysis of this launch phase is complex and should be performed in a subsequent design phase.

Within the current analysis the focus is on the space environment, where the spacecraft is heated by radiation and also radiates heat back into space. The environmental in-

fluences are solar radiation, albedo radiation and infrared radiation (IR). The overall interaction between them is expressed in the heat balance [11]:

$$mC\frac{dT}{dt} = Q_{internal} + Q_{solar} + Q_{IR} + Q_{albedo} - Q_{rad}. \tag{5.61}$$

Where m is the mass, C is the specific heat and Q all the various heat contributions in the form of internal heat, solar radiation, infrared radiation, albedo radiation and radiation that is emitted by the spacecraft. In case there is thermal equilibrium, the first term of equation 5.61 equals zero and the incoming heat equals the outgoing heat [11]:

$$Q_{in} = Q_{out}, \tag{5.62}$$

$$Q_{internal} + Q_{solar} + Q_{IR} + Q_{albedo} = Q_{rad}. \tag{5.63}$$

Solar radiation is coming from direct sunlight and is a very stable energy source. The intensity of sunlight reaching Earth varies approximately $\pm 3.5\%$, with the minimum at aphelion of $1322\,\mathrm{W/m^2}$ and the maximum at perihelion of $1414\,\mathrm{W/m^2}$ [12]. The heat coming from the solar radiation can be calculated by [11]:

$$Q_{solar} = \alpha A_p J. \tag{5.64}$$

Where A_p is the projected area, α the absorptivity of the surface material and J the intensity from the Sun.

When sunlight reaches a planet it is partially reflected back into space, this is known as albedo radiation. It is usually expressed as a fraction of the incident sunlight [12]:

$$Q_{albedo} = \alpha A_p F_{albedo} J. \tag{5.65}$$

Where F_{albedo} is the fraction of the incident sunlight, which is reflected. The absorbed heat of this reflected albedo changes with altitude, according to the inverse-square law, and the orientation of the spacecraft to the Earth. Both influences are expressed within the albedo factor:

$$F_{albedo} = Al\left(\frac{R_E^2}{r^2}\right). \tag{5.66}$$

Where Al is the albedo factor, r the radius of the orbit and R_E the radius of the Earth. The albedo factor is an experimental value, which is highly depending on the position of the spacecraft above the planets surface, i.e. longitude and latitude. Reflectivity is namely greater over continental regions than oceanic regions and also depends on cloud, snow and ice coverage. The chosen values are selected from measurements documented in

reference [12], which are adjusted to the top of the atmosphere at 30 km above Earth's surface and thus to an Earth radius of 6408 km. These experimental values have a standard deviation of 3.3-σ, which means that they will only be exceeded for 0.04% of the time. The values, for Earth typically in between 0.13 and 0.6, depend on the temperature case (hot or cold case), the inclination, the solar β angle and the time period. For our case, the inclination of the spacecraft is 28.5°, the solar β angle is 5.1° and for the time period the longest period is chosen, which represent the average over a whole orbit, resulting in an Earth albedo factor of 0.24.

Sunlight that is not reflected as albedo by a planet, is initially absorbed and eventually reemitted again as infrared (IR) energy. The position of the spacecraft above Earth has an influence on the amount of IR energy that is absorbed from the planet. Infrared radiation has the same wavelength as the one emitted by the spacecraft and therefore the emissivity factor, ε, determines in what degree IR radiation is absorbed and also the amount of radiation that is radiated to space. For example, a surface with a low emissivity does not absorb IR radiation, but is also not able to radiate the spacecrafts heat to space. The amount of planet IR radiation that is received by the spacecraft is determined by [11]:

$$Q_{IR} = \varepsilon A_p J_{IR}. \tag{5.67}$$

The infrared intensity that reaches the spacecraft varies with height according to the inverse-square law and with the temperature case. For the Earth and Moon, the hot case it is equal to [12]:

$$J_{IR_E} = 260\,\mathrm{W/m^2} \cdot \left(\frac{R_E^2}{r^2}\right). \tag{5.68}$$

$$J_{IR_M} = 1314\,\mathrm{W/m^2} \cdot \left(\frac{R_M^2}{r^2}\right). \tag{5.69}$$

The spacecraft also radiates its heat to space, which can be determined by [11]:

$$Q_{rad} = \varepsilon \sigma A \left(T^4 - T_{space}^4\right). \tag{5.70}$$

Where σ is the Stefan-Boltzmann constant ($5.67051 \cdot 10^{-8}\,\mathrm{W/m^2K^4}$), A the surface area and T the surface temperature. The space temperature is often neglected in this formula, since it is 2.8 K and such it has a negligible impact on the outcome.

During the transfer, the orbit altitude increases and the environmental loads from Earth (IR and albedo) will decrease rapidly. From an altitude of 36,000 km the albedo and IR radiation will be negligible and the stage will only be heated by solar radiation. When the stage starts to approach the Moon, it will come under the influence of lunar albedo and IR. The Moons surface is as absorptive as black paint and therefore only has an

albedo factor of 0.073 [12]. Also, due to the lack of an atmosphere, the Moon cannot retain its heat, which causes a very low IR radiation on the shadow side and consequently a low stage temperature in eclipse. On the Sun side the planets temperature is very high (high absorptivity) and, therefore the received radiation is dominated by IR ($1314\,W/m^2$) [12]. In a Moon orbit, the temperature extremes are therefore greater than in an Earth orbit.

5.6.1. Solar Array Thermal Model

It is desirable to keep solar array temperatures as low as possible, such that the electrical efficiency, and thus power production, is as high as possible. Therefore, this basic analysis is performed to evaluate the impact of the temperature on the solar cell performance.

Usually, the back-side of an array is painted with high-emittance black or white paint. White paint is primarily used in LEO, where albedo illuminates the back side of the array [12]. The front side of the panel is covered by solar cells, which have typically high absorptance and high emittance characteristics. In combination with the large area and relatively low mass, the solar arrays cycle through wide temperature variations. In LEO, this typically ranges from -75°C to +65°C and in GEO from -145°C to +55°C [12]. The model represented here is especially meant to find the maximum temperature, since it affects the electric efficiency. The model is based upon the following simplifying assumptions:

- The deployed solar array does not exchange heat with the outer surfaces of the satellite body.
- The wing mounted solar panel is adiabatically isolated from the rest of the satellite body.
- The panel surface temperature is considered as uniform.
- The panel has reached its heat equilibrium.

Solar cells perform differently under various temperatures. To analyze the impact the hot case and the cold case are examined. The cold case occurs when the stage is in eclipse and the solar array panels are not facing the Earth or Moon. In this situation, the panels are almost receiving no heat and will ultimately reach the space temperature $T_{space} = 2.8\,K$. However, in practice this will not occur, since the solar array is still exposed to radiation from the spacecraft and due to its finite heat capacity will cool down slowly. Of interest is also the solar array temperature when it comes out of eclipse in LEO or LLO. In these orbits, the highest effort is required to come out of the potential well of the Earth and Moon respectively. Thus, the following cases are analyzed:

- Hot case 1: The stage is positioned between the Sun and Earth at LEO, where the solar panels have an incidence angle of 0° and the back-side of the panels face

Earth's albedo and IR.

- Hot case 2: The stage is positioned between the Sun and Moon at LLO, where the solar panels have an incidence angle of 0° and the back-side of the panels face Moon's albedo and IR.
- Cold case 1: The stage is at LEO and the panel is pointed towards the Earth in order to receive IR radiation and retain some heat. While coming out of eclipse the panel should be oriented towards the Sun.
- Cold case 2: The stage is at LLO and the panel is pointed towards the Moon in order to receive IR radiation and retain some heat. While coming out of eclipse the panel should be oriented towards the Sun.

The solar panel is converting solar radiation into electricity. The amount that is converted depends on the solar cell efficiency, η, and the incidence angle, ϑ. Therefore, the absorbed heat, under influence of the solar radiation (equation 5.64), changes to:

$$Q_{solar} = \alpha\,(1-\eta)\,AJ\cos\vartheta. \tag{5.71}$$

The absorbed solar heat is higher when the solar cell efficiency is lower, therefore the EOL efficiency is used for the analysis. The other formulas for the albedo, IR and spacecraft radiation (equation 5.65, 5.67 and 5.70) are left unchanged. As stated, a thermal equilibrium is assumed and such equation 5.63 can be rewritten to solve for the surface temperature:

$$T_{SA} = \left(\frac{Q_{solar} + Q_{albedo} + Q_{IR}}{\sigma\varepsilon A}\right)^{1/4}. \tag{5.72}$$

The characteristics of the front side of the panel is determined by the solar cells. The backside characteristics can be controlled and are preferred to have a low absorptivity and high emissivity, since it is beneficial for the cell temperature in LEO. The following properties for the solar cell are assumed:

- $\alpha_{cell} = 0.91$
- $\varepsilon_{cell} = 0.81$
- $\alpha_{back-side} = 0.17$
- $\varepsilon_{back-side} = 0.82$
- $\eta_{cell} = 0.28$

The back side is assumed to be white paint and is selected to limit the hot case temperature. The Solar Array Thermal Model is written with SCILAB and the results for the different cases are:

- LEO: $T_{hot} = 64.4\,^{\circ}\text{C}$, $T_{cold} = -59.5\,^{\circ}\text{C}$

- LLO: $T_{hot} = 105.7\,^{\circ}\text{C}$, $T_{cold} = -193.3\,^{\circ}\text{C}$

As expected, the hot case is in LLO and it is desirable to reduce this high temperature. The main contributions to this hot case are the IR radiation and the solar radiation, so a logical conclusion would be to reduce the received IR radiation and consequently reduce the emissivity of the back side. However, in this case also the backside cannot radiate its heat anymore towards space. Therefore, changing the $\varepsilon_{back-side}$ to a value of e.g. 0.1, results in approximately halved incoming heat, but since the radiation area is now only the panel front side and thus also halved, the temperature stays approximately the same. This is also seen in the model, where changing the $\varepsilon_{back-side}$ from 0.1 to 0.9 only has an influence of $1\,^{\circ}\text{C}$. The only way to influence this LLO hot case temperature to a great extent, is to reduce the absorptivity on the cell side. For example, when α_{cell} is reduced to 0.51, the resulting temperature is $-189.6\,^{\circ}\text{C}$. This demonstrates that the absorptivity of the front panel should be as low as possible, without affecting the solar cell efficiency.

When a flexible solar array comes out of eclipse, the front side is heating up quickly, while the back side is still cold. The resulting thermal gradient across the blanket makes it to bend and thus reduces the power output. The duration of this effect depends on the thermal expansion coefficient and blanket design, which should be such to limit this effect and should be analyzed in subsequent design phases [1].

5.6.2. Spacecraft Thermal Model

A basic spacecraft thermal model is required to determine the desired outside properties of the spacecraft, which are needed for the radiator thermal model. The properties, i.e. the emissivity and absorptivity of the spacecraft, are determined by assessing the cold case of the stage. The model is based on the following assumptions:

- Interactions with other spacecraft surfaces is neglected.
- The spacecraft has reached its thermal equilibrium.
- The solar panels and radiators are adiabatically isolated from the rest of the satellite body, so there is no heat transfer from the panels and radiators to the spacecraft and vice versa.

The cold case occurs when the spacecraft is in eclipse at a higher lunar orbit. In this situation the infrared radiation can be neglected, thus the heat balance equation becomes:

$$Q_{rad} = Q_{internal}. \tag{5.73}$$

The heat balance equation can be solved for the emissivity of the spacecraft:

$$\varepsilon_{s/c-required} = \frac{Q_{internal}}{\sigma A_{s/c} T^4}. \tag{5.74}$$

The minimum allowable temperature is set at 0°C (see section 5.6). During eclipse the low voltage bus is operating and produces 1,245 W of internal heat (see section 5.4.6), which means that an emissivity of 0.03 is required. There is no material that can guarantee such a low emissivity, therefore a material with a typical emissivity is applied in combination with a heater. The selected material is MLI with an outer layer of Vapor Deposited Aluminum (VDA), which has an emissivity of 0.04 and absorptivity of 0.17 [3]. With this material, a heater of 320 W is required to maintain the spacecraft's temperature at the minimum of 0°C, which is a driving the battery of the power system.

5.6.3. Radiator Thermal Model

Radiators need to reject the heat created by the power system. The radiating power of a radiator is a function of the temperature and is given by the Stefan-Boltzmann equation [3]:

$$Q_{radiator} = \varepsilon \sigma A T^4. \tag{5.75}$$

The temperature has a significant influence on the radiation capability of the panel. The emissivity of the panel should be as high as possible, while the absorptivity is low. The actual sizing of the radiator is done by considering the desired operating temperature, worst-case waste heat and environmental heating of the spacecraft. The model is based on the following assumptions:

- Interactions with other spacecraft surfaces is neglected.
- The radiator panel temperature is considered as uniform.
- The panel has reached its heat equilibrium.
- The solar panel is adiabatically isolated from the rest of the satellite body, so there is no heat transfer from the solar panels to the spacecraft.

The hot case scenario is assessed to ensure that sufficient radiator area is available to maintain acceptable temperatures. The hot case occurs when the spacecraft is in the Sun and positioned at LLO. In Moon orbit the IR radiation is significant and affects the spacecraft radiator surface [12]. Therefore the spacecraft and radiator should be positioned such that the radiator view is minimized towards the Moon surface. It is even better to point the radiator area towards the Sun than to the lunar surface, since most radiators have a low solar absorptance and a high IR emittance. For the hot case, three orientations of the spacecraft can be considered:

- Hot case 1: The stage is positioned in between the Sun and Moon and the radiators are body-mounted and oriented such that they are facing the Sun, the stage's projected area is at maximum.
- Hot case 2: The stage is positioned in between the Sun and Moon and the radiators are wing-mounted and oriented such that they do not see the Moon and Sun. The stage's projected area is at maximum.
- Hot case 3: The stage is positioned 'at the side' of the Moon and one side of the wing-mounted radiator is facing the Sun. The stage's projected area is at minimum, meaning that only the front side of the spacecraft is facing the Sun.

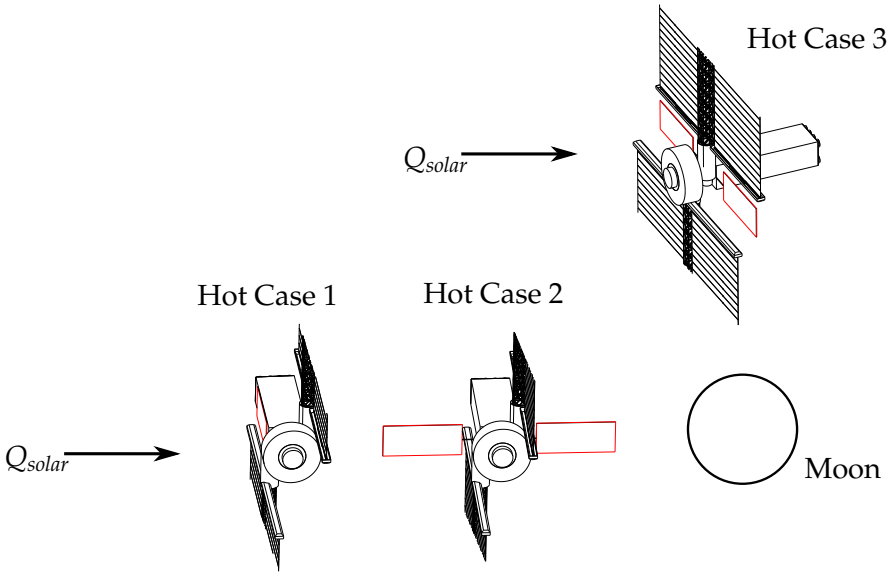

Figure 5.37.: The hot cases and radiator configurations (indicated in red).

The first hot case is the most severe one and is performed to evaluate if one body-mounted radiator is sufficient to provide thermal control. In case this is not sufficient, a wing-mounted radiator shall be considered according to hot case two and three. For all the hot cases, the internal dissipation of the power systems is considered to be at its maximum. For the first hot case, the heat balance can be expressed by:

$$Q_{radiator} = Q_{internal} + Q_{solar} + Q_{albedo} + Q_{IR}. \tag{5.76}$$

Solving the equation for the radiator area, results in:

$$A_{rad-HC1} = \frac{Q_{internal} + \alpha_{s/c} A_p J + \alpha_{s/c} A_p F_{albedo} J + \varepsilon_{s/c} A_p J_{IR} - \varepsilon_{s/c} \sigma A_{s/c} T^4}{\sigma T^4 \left(\varepsilon_{rad} - \varepsilon_{s/c}\right) - J\left(\alpha_{rad} - \alpha_{s/c}\right)}. \tag{5.77}$$

From the resulting radiator area it can be concluded if a body-mounted radiator can be used. When this is not the case, wing-mounted radiators are required and hot case two and three become valid. The required radiator area for the second and third hot case

can be calculated by:

$$A_{rad-HC2} = \frac{Q_{internal} + \alpha_{s/c} A_p J + \alpha_{s/c} A_p F_{albedo} J + \varepsilon_{s/c} A_p J_{IR} - \varepsilon_{s/c} \sigma A_{s/c} T_{s/c}^4}{\varepsilon_{rad} \sigma T_{rad}^4}. \tag{5.78}$$

$$A_{rad-HC3} = \frac{Q_{internal} + \alpha_{s/c} A_p J + \alpha_{s/c} A_p F_{albedo} J + \varepsilon_{s/c} A_p J_{IR}}{\varepsilon_{rad} \sigma T_{rad}^4 - \frac{1}{2} \alpha_{rad} J}. \tag{5.79}$$

These equations are programmed within SCILAB to solve for the dimensioning hot case.

5.6.4. Thermal Control System Results

The high power levels of the SEP stage results in high thermal loads that have to be rejected to space. Normal thermal management techniques, like a radiating panel incorporated in the spacecraft's structure, becomes challenging and has to be evaluated by the radiator thermal model. In case a body-mounted radiator is not feasible, wing-mounted radiators are required.

The characteristics of the thermal control system can be seen in table 5.43. In lower orbits, the spacecraft is always oriented with its longitudinal axis parallel to the planet's surface. The area that in this orientation is projected to the planet is called the side projected area in table 5.43. The frontal projected area, is the area of the flat surface of the secondary cylinder. The complete outside area is a summation of all the spacecraft's surface that radiates heat to space.

The maximum internal dissipation, calculated with equation 4.34, occurs when the power system is providing its maximum power at BOL and for the cold case. The radiator rejects the waste heat at a temperature of 60°C [20] and contains heat pipes that provide the heat transport from the inner body of the spacecraft to the radiators. The radiator's surface finish is selected to be Z93 white paint, with an emissivity of 0.92 and absorptivity of 0.17 [3]. For this typical surface finish, the outcome of hot case two and three results in a minimum radiator area.

S/C Thermal Control System	
S/C minimum temperature (°C)	0
S/C maximum temperature (°C)	40
S/C side projected area (m^2)	55.2
S/C frontal projected area (m^2)	16.62
S/C outside area (m^2)	106.1
S/C material	VDA
S/C absorptivity	0.17
S/C emissivity	0.04
Maximum internal dissipation (kW)	32.3
Minimum internal dissipation (W)	1,245
Heater dissipation (W)	320
Radiator	
Selected surface finish	Z93 white paint
Absorptivity	0.17
Emissivity	0.92
Radiator temperature (°C)	60

Table 5.43.: The characteristics of the thermal control system that are used for the thermal model.

For the first hot case a total radiator area of $90.5\,m^2$ is required (see table 5.44). In case these are body-mounted, 85% of the spacecraft's shell will be covered by radiators. These radiators will then also face the Moon, which alters the thermal balance and causes the radiator area to grow even larger. Therefore, this option is considered to be impossible from the structural point of view and not a suitable solution.

The second option is to have wing-mounted radiators, which increases the complexity of the spacecraft by adding flexible joints in the heat transport tubes. From the analysis it can be concluded that the radiator requires no rotary joint, since it can fully face the Sun and still radiate all the internal dissipation.

	Hot case 1	Hot case 2	Hot case 3
Radiator area (m^2)	90.5	67.6	73.6

Table 5.44.: Thermal Model outcome.

Since hot case one is eliminated, the sizing case is hot case three and thus a wing-mounted radiator is required with an area of $73.6\,m^2$. This is provided by two wing-mounted radiators, each 2.5 m wide and 7.36 m long (see table 5.45). A heavy deployable radiator and its support and deployment structure weights around $12\,kg/m^2$ [3],

consequently the total mass of the radiators is 972 kg (see table 5.47). Variable conductance heat pipes, filled with Ammonia, have typically a mass of 0.15 kg/m [3] and the required length is estimated at 20 m. A heater weights around 0.3 kg/kW [12] and MLI 0.73 kg/m^2 [3]. Also, margins are applied on these values. On the radiator and MLI a margin of 10% is included and on the heat pipes and heater a margin of 20% is included. The total mass, including margins, of the thermal control system is estimated at 1074.9 kg.

Radiators	
Number of radiators	2
Radiator width (m)	2.5
Radiator length (m)	7.36
Total radiator area (m^2)	73.6
Operation Temperature (°C)	60
Surface finish	Z93 white paint
Absorptivity	0.17
Emissivity	0.92

Table 5.45.: The radiators of the thermal control system.

SEP stage	
Temperature range (°C)	0 - 40
Insulation	MLI
Outer layer	VDA
Absorptivity	0.17
Emissivity	0.04
Heater (W)	320

Table 5.46.: The design of the SEP's thermal control system.

Mass budget	
MLI mass (kg)	99.3
Heat pipes mass (kg)	3.6
Heater mass (kg)	0.12
Radiator mass (kg)	971.9
Total mass (kg)	1074.9

Table 5.47.: Mass budget of the thermal control system, including margins.

5.7. Attitude and Orbit Control System

The Attitude and Orbit Control System (AOCS) has the task to control the orientation of the spacecraft during all the mission phases. The system does not drive the stage's architecture and therefore it is not treated at the same level of detail as the mission analysis, propulsion and EPS. The AOCS has to comply with the following requirements:

	System Requirement	Created
7.	The transfer stage shall provide 3-axis attitude control during the entire mission.	Sec. 2.2
7.1	Four gimbaled thrusters should provide enough agility for the stage.	Sec. 5.3.9

To control the orientation, sensors first need to fully resolve the position of the spacecraft. In case the position of the spacecraft needs to be changed, thrusters and/or actuators have to adjust the orientation to the desired one. The following sizing cases for the AOCS are identified and discussed in more detail:

1. The launcher releases the spacecraft in its predefined orbit with a certain separation accuracy. Errors in the attitude and rotation rate might occur and have to be corrected. Next, the spacecraft needs to control its orientation in the orbital plane. The longitudinal axis of the spacecraft is in line with the orbital path and makes a full revolution every orbit. The amount of propellant required for this steering, needs to be analyzed.
2. The solar pressure on the solar arrays cause a moment on the spacecraft. In almost all configurations the two opposite solar arrays cancel out the effect of the solar pressure. There is only one configuration in which this does not occur. In this configuration, the solar array is in line with the longitudinal axis of the spacecraft and the force exerted on the solar arrays, cause a moment around the lateral y-axis (see figure 5.39). This moment has a sinusoidal character due to the rotation of the solar arrays with respect to the spacecraft. The position of the center of mass is essential to determine the magnitude of the moment exerted on the spacecraft.
3. The rolling torque of the vehicle is determined to identify the maneuverability of the stage around the longitudinal axis. No requirements are imposed on the maneuverability around this axis.
4. The stepper motor of the SADM has to deliver enough torque to turn the solar array and is analyzed.

The spacecraft also has to perform the docking procedure, in which the SEP stage is a cooperative target and the payload executes the docking. This means that the SEP stage has to maintain its position in orbit and does not have to adjust its orientation actively. Therefore this is not considered to be a sizing case for the AOCS.

5.7.1. Attitude Sensors

The spacecraft is 3-axis controlled and the following sensors are needed to determine the position of the stage:

- Sun Sensor
- Star Tracker
- Inertial Measurement Unit (IMU)
  - Gyroscopes
  - Accelerometers
- GPS

The GPS sensor is mostly useful in the LEO phase, in which also the docking procedure with the payload is performed. The GPS receiver that is also used for ATV, the ATV-GPSA Receiver from Thales, is selected. No other instruments for this maneuver are required, since the SEP stage is a passive element which should remain at its position until the payload is docked. The other sensors are part of the basic equipment that a satellite requires for determining its position. Based upon experts opinions at OHB System a set of sensors is selected. Together with data from reference [3] a total mass and power budget can be determined (see table 5.48).

	Number (−)	Total mass (kg)	Total power demand (W)
Sun Sensor	6	6	0
Star Tracker	2	8	20
IMU	2	30	50
GPS (ATV-GPSA)	1	4	15
Total, with 5% margin		50.4	89

Table 5.48.: Selected sensors for the AOCS.

5.7.2. AOCS Model

To perform AOCS calculations on a spacecraft, the center of mass and mass moment of inertias of the spacecraft have to be known. This also requires a coordinate system and therefore a body-fixed reference frame is introduced (see figure 5.38), with:

- x-axis: the longitudinal axis of the SEP stage.
- y-axis: the lateral axis of the stage, in direction of the solar array wings.
- z-axis: vertical axis of the stage, in direction of the radiators.
- Origin: located in between the docking mechanism and primary load carrying cylinder on the longitudinal axis of the stage.

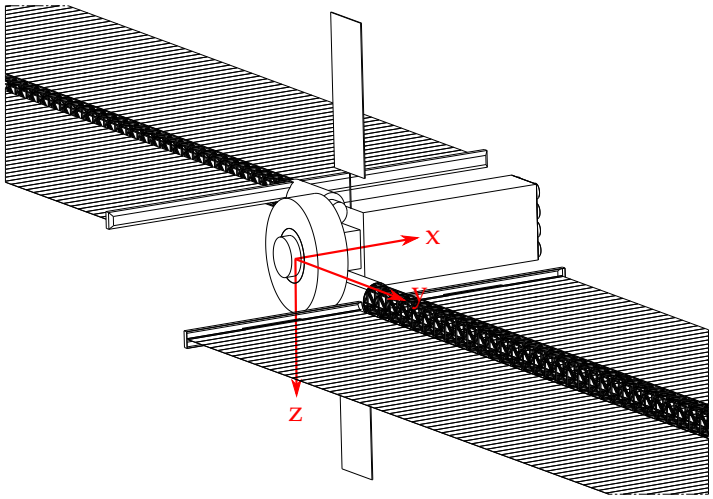

Figure 5.38.: The body-fixed reference frame of the SEP stage.

With the aid of this reference system and the locations of all the different components and their masses, the center of mass can be calculated for x, y and z:

$$x_{CoM} = \frac{\sum m_i x_i}{\sum m_i}. \tag{5.80}$$

$$y_{CoM} = \frac{\sum m_i y_i}{\sum m_i}. \tag{5.81}$$

$$z_{CoM} = \frac{\sum m_i z_i}{\sum m_i}. \tag{5.82}$$

The mass moment of inertias around the different axis, can be calculated with [3]:

$$I_{xx} = \sum \left(y_i^2 + z_i^2\right) m_i. \tag{5.83}$$

$$I_{yy} = \sum \left(x_i^2 + z_i^2\right) m_i. \tag{5.84}$$

$$I_{zz} = \sum \left(x_i^2 + y_i^2\right) m_i. \tag{5.85}$$

The torque that is required when a certain angular rate, ω, is given, depends on the mass moment of inertia, I. While the torque delivered by a thruster is a function of the force it produces and the arm length, l, to the center of mass [3]:

$$T = \dot{\omega} I = \frac{\Delta \omega}{\Delta t} I = Fl. \tag{5.86}$$

Where the angular rate is defined as a change of an attitude angle, θ, in a certain amount of time, t:

$$\omega = \frac{d\theta}{dt}. \tag{5.87}$$

The four gimballed thrusters produce a lateral force that act on the stage to create the torque. These forces also cause a secondary effect, i.e. a lateral shift of the SEP stage. This effect is neglected in the current design phase but should be included in subsequent phases.

In case a maneuver about a certain angle is required, a so-called 'bang-bang' maneuver is performed. In this maneuver first a torque is applied to start rotating to the new desired attitude, secondly a torque in the opposite direction is applied to cancel out this rotation. When equation 5.87 is filled into equation 5.86, the torque for a bang-bang maneuver can be determined as a function of the desired attitude angle change and time [3]:

$$T = \frac{4\Delta\theta I}{\Delta t^2}. \tag{5.88}$$

The formula can be rewritten to evaluate the time that is required to make a certain attitude angle change, while the engines deliver the maximum torque:

$$\Delta t = \sqrt{\frac{4\Delta\theta I}{T}}. \tag{5.89}$$

The solar pressure exerted on a body, F_{sp}, is a function of the solar intensity, I, the speed of light, c, the reflection factor of the surface, r and the area of the surface, A [3]:

$$F_{sp} = -\frac{I}{c}(1+r)A. \tag{5.90}$$

From these equations, the identified sizing cases can be analyzed.

5.7.3. AOCS Results

The center of mass of the spacecraft changes its position during the different phases. A distinction is made between four situations:

1. The SEP stage is completely fueled and the payload module is not attached.
2. The SEP stage is empty and the payload module is not attached.
3. The SEP stage and payload module are docked, both are fueled.
4. The SEP stage and payload module are docked, the fuel at the payload side is consumed.

For these different configurations, the center of mass can be determined by using the equations 5.80 to 5.82 and figure 5.38 as reference frame. The components and their location that are considered for the calculation can be seen in table 5.49. The results of the calculation show that the payload causes a significant shift in the center of mass of the spacecraft (see table 5.50). The two extremes of the center of mass occur for configuration 2, where the SEP stage is alone and empty, and 3, where the two are docked and fueled. The difference between the two cases, results in a shift of the center of mass of 7 m. With the position of the center of mass known, the mass moment of inertia of the spacecraft can be determined by using equations 5.83 to 5.85 (see table 5.50).

		Position (m)		
Component	Mass (kg)	x	y	z
Docking Mechanism	340.2	-0.2185	0	0
Primary Cylinder	165.5	0.85	0	0
Secondary Cylinder	107.5	0.85	0	0
Xenon Tank	9,044	0.85	0	0
Primary Box	33	2.4	0	0
Secondary Box	185	7.15	0	0
SADM 1	243.5	2.3	0	-1.2
SADM 2	243.5	2.3	0	1.2
SAW 1	2,375	2.3	27	-1.2
SAW 2	2,375	2.3	-27	1.2
Radiator 1	489	3.1	0	5.575
Radiator 2	489	3.1	0	-5.575
Thruster Plate	1,736	11.2	0	0
EPS cylinder	3,037	0.85	0	0
Payload	19,181	-6.5	0	0
Payload tanks	23,222	-6.5	0	0

Table 5.49.: The components' mass and location used for the computation of the Mass Moment of Inertia.

	x (m)	y (m)	z (m)	I_{xx} (kgm^2)	I_{yy} (kgm^2)	I_{zz} (kgm^2)
Configuration 1	2.22	0	0	$3.50 \cdot 10^6$	$2.08 \cdot 10^5$	$3.63 \cdot 10^6$
Configuration 2	3.39	0	0	$3.50 \cdot 10^6$	$1.84 \cdot 10^5$	$3.61 \cdot 10^6$
Configuration 3	-3.62	0	0	$3.50 \cdot 10^6$	$12.72 \cdot 10^5$	$4.70 \cdot 10^6$
Configuration 4	-1.96	0	0	$3.50 \cdot 10^6$	$9.69 \cdot 10^5$	$4.39 \cdot 10^6$

Table 5.50.: The center of mass and mass moment of inertia for different configurations of the spacecraft.

Sizing case 1: Steering maneuver

The first sizing case, is compensation of the separation errors caused by the launcher and the movement of the spacecraft around its y-axis within the orbital plane. The separation errors of the Falcon Heavy are currently unknown, therefore the Falcon 9 is used as reference. Compensation of these errors occurs just after launch, so in the configuration where the SEP stage is fueled and undocked (situation 1). For compensation of the rotation error, equation 5.86 is used to calculate the required torque. The resulting thrust can be translated to a propellant demand (see table 5.51). The four gimbaled thrusters deliver a maximum lateral force of 1.7 N and such the time a certain maneuver requires depends on this maximum thrust. The results show that especially for compensation of the roll around the x-axis, a long time is required of 100 min. For compensation of the attitude error, equation 5.88 is used to calculate the required torque, which can again be translated into a propellant demand (see table 5.52).

Axis	ω_{error} (rad/s)	Δt (s)	T_{req} (Nm)	F_{req} (N)	m_{prop} (kg)
x	0.0044	7200	2.1	1.68	0.62
y	0.0035	60	12.1	1.35	0.004
z	0.0035	840	15.1	1.68	0.07
Total					0.69

Table 5.51.: The rotation errors of the launcher [51] and the propellant that is required for compensation.

Axis	θ_{error} (rad)	Δt (s)	T_{req} (Nm)	F_{req} (N)	m_{prop} (kg)
x	0.024	420	1.9	1.5	0.03
y	0.024	360	0.2	0.02	0.0003
z	0.024	360	2.7	0.3	0.006
Total					0.034

Table 5.52.: The attitude errors of the launcher [51] and the propellant that is required for compensation.

The amount of propellant that is required for the steering maneuver, depends on the configuration of the spacecraft. The most demanding orbit is the LEO orbit, which has an orbital period of 1.572 hrs and requires a rotation rate of 0.0011 rad/s. After launch, the rotation first has to be initialized and during the orbit raising, the rotation rate is slowly reduced and approaches zero again at very high altitudes. This event occurs four times per mission. The torque that is required for this maneuver, can be calculated with equation 5.86 and the resulting propellant demand can be seen in table 5.53. For adjusting the rotation, the mass moment of inertia of configuration 3 around the y-axis is used, which is the most demanding case.

	ω_{des} (rad/s)	Δt (s)	T_{req} (Nm)	F_{req} (N)	m_{prop} (kg)
Initialize rotation	0.0011	100	2.3	0.3	0.001
Adjust rotation	≈ 0	$1.4 \cdot 10^7$	$1.0 \cdot 10^{-4}$	$7.0 \cdot 10^{-6}$	0.005
Total ($\times 4$)					0.021

Table 5.53.: Propellant required to initialize the rotation and for adjusting the rotation rate while raising the orbit.

The total propellant demand for sizing case 1 is 0.75 kg. This is a very small fraction of the total Xenon propellant (0.002%).

Sizing case 2: Solar Pressure

The second sizing case that is discussed, is the solar pressure on the spacecraft that causes a rotation around the y-axis (see figure 5.39). The force that is exerted on the solar arrays can be calculated by equation 5.90 (see table 5.54). The reflection factor of an absorptive surface, like the solar array, is equal to zero. The total torque the solar pressure force exerts on the spacecraft, depends on the position of the center of mass and thus the worst case occurs in configuration 3. The torque caused by this force has a sinusoidal character due to the rotation of the solar arrays with respect to the spacecraft. The propellant demand is estimated by using the root-mean-square (RMS) radius, for this orbit the total angular momentum is calculated. Multiplying by the total number of orbits for a single mission, gives the total propellant mass for compensation of the solar pressure (see table 5.54).

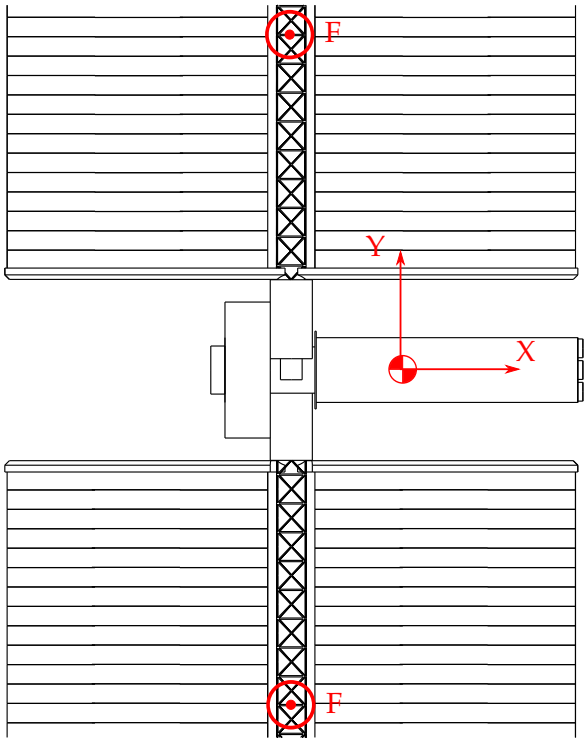

Figure 5.39.: The solar pressure on the solar arrays creates a moment around the y-axis.

Solar Pressure	
Radius RMS (m)	$6.95 \cdot 10^7$
Maximum Sun intensity (W/m^2)	1414
Reflection factor ($-$)	0
Total solar array area (m^2)	2038
Maximum solar pressure force (N)	$9.61 \cdot 10^{-3}$
Maximum torque on S/C (Nm)	$5.69 \cdot 10^{-2}$
Angular Momentum (Nms)	$3.3 \cdot 10^3$
Propellant mass for RMS orbit (kg)	$1.1 \cdot 10^{-2}$
Number of orbits per mission ($-$)	1300
Total propellant mass (kg)	14.78

Table 5.54.: The solar pressure force exerted on the solar arrays, the resulting angular momentum and the propellant required for canceling out the angular momentum.

Sizing case 3: Spacecraft rolling

The third sizing case is evaluated to identify the maneuverability of the stage around the longitudinal x-axis. The mass moment of inertia around this axis is for all the configurations the same (see table 5.50). The four gimbaled thrusters are located at the four edges of the thruster plate. The torque the thrusters can generate around the x-axis is significantly lower compared to the other axes, due to the small arm (see table 5.55). As a result, a relatively long time, of 11.1 min, is required to make a roll maneuver of 5°.

Spacecraft Rolling	
Thrust (N)	1.7
Thruster y-position (m)	0.67
Thruster z-position (m)	1.46
Maximum torque (Nm)	2.73
Rotation angle (°)	5
Time required for rotation (s)	668.9

Table 5.55.: The maximum torque of the thrusters around the x-axis and the time required to make a 5° roll maneuver.

Since there are currently no disturbance torques around the x-axis identified, there are no requirements imposed on the rolling agility. This means that no extra systems are needed to improve the motion around the x-axis. In case requirements are imposed on the x-axis control, the implementation of a Reaction Wheel or Control Moment Gyro is advised to increase the x-axis rolling agility.

Sizing case 4: SADM torque

To calculate the torque that is required to turn the solar arrays, first the mass moment of inertia of the solar array around its own rotational axis needs to be determined by using equation 5.84. The resulting mass moment of inertia is equal to $3.048 \cdot 10^4\,\mathrm{kgm}^2$. Together with the specified rotation rate, the torque that is required for the solar array can be determined by using equation 5.86, see table 5.56.

SADM Torque	
Mass moment of inertia (kgm^2)	$3.048 \cdot 10^4$
Required maximum rotation rate (rad/s)	$1.109 \cdot 10^{-3}$
Torque required (Nm)	$1.873 \cdot 10^{-2}$

Table 5.56.: The torque the stepper motor of the SADM has to generate in order to turn the solar array.

Resulting AOCS

From the presented sizing cases it can be concluded that the gimbaled thrusters can provide the required attitude control of the system. Due to the long arm to the center of mass, the thrusters can easily cancel out disturbances around the y- and z-axis. Around the x-axis this is more problematic, but no requirements are imposed on this agility. As a consequence, the thrusters only require extra propellant to execute the AOCS maneuvers. On the propellant required for AOCS, margins of 100% are applied according to the margin philosophy of ESA [75]. Also a set of sensors is identified to resolve the position of the spacecraft (see table 5.57).

	Total mass (kg)	Total power demand (W)
Sensors	50.4	89
Propellant for orbital movement	1.2	-
Propellant for solar pressure	29.6	-
Total AOCS	81.2	90

Table 5.57.: The sensors and extra propellant required for the AOCS, including margins.

The aerodynamic force exerted on the spacecraft was analyzed in the mission analysis and showed that the impact is negligible. The sizing cases do not account for the influence of thruster misalignment and gravity gradient torques. The impact of these torques is considered to be negligible at this stage. However, they should be evaluated in later design phases.

5.8. Telemetry, Tracking and Command and On-Board Data Handling

The Telemetry, Tracking and Command (TT&C) system provides the communication between the spacecraft and ground stations. The processing and execution of commands, coming from the TT&C, is performed by the On-Board Data Handling (OBDH) system. The TT&C and OBDH system are no driving systems for the spacecraft and therefore a simple conventional design can be selected. The systems have to comply with the following requirements:

	System Requirement	Created
8.	The transfer stage shall be able to communicate with an Earth based ground segment.	Sec. 2.2
9.	The transfer stage shall perform the mission automatically, meaning that the stage can perform some operations by itself (TBD) and for other commands can be given during the mission.	Sec. 2.2

For the OBDH system, the state of the art Leonardo computer from Thales Alenia is selected. The Leonardo computer provides AOCS support, on board data processing and telemetry and tele-command handling. Since the computer does not have to process data from highly sophisticated instruments, it is expected that the performance of the computer is sufficient for the SEP stage. Also, storage of some data is required, which is performed by a data recorder of Surrey Technology [97] that provides 16 GBytes of storage. The OBDH is a critical system and requires some redundancy, therefore, for both the computer and data, an extra unit is included. The amount of data harness that is required for the OBDH, is included in the total SEP stage's harness.

For the communications, the S-band is the chosen frequency band. Earlier, there were concerns that the plasma from the thrusters can result in a phase shift of the communication signal within the S-band. However, the effect is considered to be relatively small and thus an conventional S-band antenna can still be used [7] [19]. Due to the high heritage for S-band communication, existing equipment can be selected. To determine the required performance of the TT&C system, a link budget needs to be made. This is however a time-consuming task and therefore a conservative assumption on the total mass and power of the complete TT&C system has been made (see table 5.58). Compared to the deep-space S-band transponder of Thales Alenia (S/S DST), the budgeted mass and power are two times higher. The Satellite Management Unit (SMU) provides an interface between the transponder and the OBDH. Its main task is encoding and decoding of the communication signal. As baseline, the SMU-V1 of Thales Alenia is selected. For redundancy purposes, an extra transponder and SMU are included. The three helix antennas should be located such that omni-directional coverage is obtained, which is needed when the SEP stage is in a lunar orbit. All the equipment are off-the-

shelf or have a high heritage and thus margins of 5% are applied on the mass and power of table 5.58.

	Number (−)	Mass (kg)	Power demand (W)
Leonardo	2	46.2	47.3
Data recorder	2	2.1	15.7
Satellite Management Unit	2	19.3	26.3
S-Band transponder	2	14.7	78.7
S-Band helix antenna	3	2.1	-
Total	-	84.4	168

Table 5.58.: Results for the TT&C and OBDH systems for the SEP stage.

6. Final System Configuration and Performance Analysis

In the previous chapter, the complete SEP stage was designed. To verify if all mission objectives and requirements are met, the final system design is presented. In case one of the components of the stage fail, there will be an impact on the functionality and performance of the stage. The impact of these different failure modes and critical issues are discussed in section 6.1. Then, the final mass and power budget will be given and it will be verified if the proposed design meets the required performance (section 6.2). Finally, different mission scenarios are suggested and analyzed in section 6.3.

6.1. Critical Issues and Failure Modes

The SEP stage is a complex system, which requires a substantial engineering effort to make everything operate as desired. In the design, there are some critical issues and potential failure modes. The critical issues, should be studied more in subsequent design phases in order to come to a sensible and reliable design. In case a failure occurs in one of the identified failure modes, it will lead to complications in the mission, although the main mission objectives should still be met. There are two possible failure modes identified; engine failure and SADM failure, which will be discussed in section 6.1.1 and 6.1.2.

The operation of the solar array on high-voltages, could possibly lead to potential differences between the spacecraft's surfaces and ultimately to electrostatic discharges. To prevent this, the thruster cathodes are fired at all times, which lowers the spacecraft potential and thus functions as a plasma contactor. Also, in the lay-out of the solar array strings, the potential difference between adjacent cells is kept at a minimum. A substantial development effort is expected, to obtain a reliable design of the high-voltage solar array.

The operation of a DDU in combination with a Hall thruster, is a relatively new development and many questions remain. The research done on this topic (see section 5.4.6), indicates that DDU control is challenging and requires more development and testing on hardware level. Especially, the start-up of the whole power system and control of the operation point, by adjusting the Hall thruster mass flow, magnetic field strength and SSU, will remain a topic of future research. Also, a sudden Hall thruster failure, causing a short circuit, can possibly destroy the solar array. These practical problems have to be studied in more detail and solved. Recently, JPL tested a DDU set-up, which proved

that Hall thruster operation through a DDU is not much different than operation on conventional power supplies [61].

To validate the operation of a high-voltage solar array in combination with a DDU, flight tests in space are foreseen. Both the systems should be validated and tested in a precursor mission, to validate the high-voltage solar array design and secondly, to validate the interplay of solar array pointing and power generation with the Hall thruster mass flow and magnetic field strength.

The size of the fairing and the placement of the SADM and truss canister, make their design challenging. The high power demand of this mission, drives the size of the SADM and the deployable truss inside the canister to such an extent, that their length is almost longer than the launcher fairing diameter. As a consequence, the designs of the SADM and canister are critical and deserve a large engineering effort to keep them as small as possible. Also, the high voltage and power level across the SADM can be problematic and requires hardware development and testing for validation. In case higher power levels than the suggested mission are desired, a different configuration is required or a launcher with a larger fairing diameter should be selected.

As a results of the relatively large canister, the supporting structure of the electric propulsion is relatively small. This relatively narrow structure of $1.2 \times 2.0\,\mathrm{m}$ should provide space for the harness, Xenon feed lines, heat pipes and provide enough strength to support the thrusters during launch. Therefore, this section forms the 'neck' of the stage and is critical in supplying the engines with power and propellant and transporting heat from the EPS to the radiators. The relatively small area in which this has to take place, makes it critical in nature and requires special attention in future design phases.

Another critical issue is the deployment of the deployable trusses, which deploy the solar array and thruster plate to its final position. Especially, the deployment of the thruster plate, which is deployed by four deployable trusses inside a static enclosing structure, seems to be challenging. If one of the four deployable trusses jams, the plate will incline and can possible get stuck during the transition to the final position. This procedure, of moving the plate to the final position, only has to be performed once and can be tested on the ground extensively for space qualification, to ensure that it functions in orbit. Also, there is a substantial amount of heritage on these deployable structures, which have been used on the ISS, on the SRTM Space Shuttle mission and recently on the NuSTAR mission.

6.1.1. Engine Failure

The SEP stage has fifteen Hall thrusters to provide thrust. In case one engine fails, the symmetry will be lost and the total thrust vector will shift, which will result in thrust misalignment. This thrust misalignment can be compensated in two ways:

1. Shut down the mirrored engine.

2. Tilt the thruster axis of an engine on the opposite side towards the 'inside' of the stage, see figure 6.1. In the situation that engine five fails, the force vector of engine ten (F_{10}) should be pointed such that it coincides with the center of mass. This method does generate unwanted lateral forces in y- and z-direction, which cause the stage to shift into the y- and z-direction.

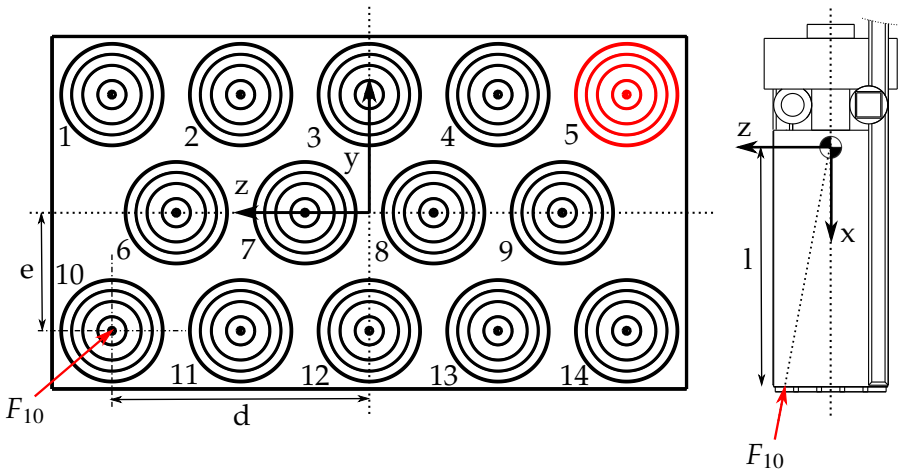

Figure 6.1.: A bottom view (left) and top view (right), with the failing engine indicated in red and the direction of the engine's force that needs to be adjusted to cancel out undesired torques.

Since the redundancy of the system is only one, it is preferred to gimbal one thruster to cancel out the undesired torques. In case the engine is not gimballed, the magnitude of the torque equals:

$$T = F_{10}\sqrt{d^2 + e^2}. \tag{6.1}$$

To cancel out this undesired torque, the thrust vector needs to be tilted with respect to the longitudinal axes:

$$\alpha = \arctan\frac{\sqrt{d^2 + e^2}}{l}. \tag{6.2}$$

The force that is contributing to the acceleration of the spacecraft is in the x-direction:

$$F_{10,x} = F_{10}\cos\alpha. \tag{6.3}$$

The force that is causing a lateral shift in the y-z plane is:

$$F_{10,yz} = F_{10}\sin\alpha. \tag{6.4}$$

This analysis shows, that if a single engine fails, the auxiliary engine is fired and the gimbaled thrusters are used to compensate for the undesired torque. The worst case

occurs when the center of mass is located most backwards and an outer engine fails, like indicated in figure 6.1. In this situation the thrust vector needs to be tilted with 11.6° degrees, which results in a thrust loss of 0.05 N in the x-direction and, as a consequence, reduces the thrust from 31.27 N to 31.22 N. This reduction will affect the transfer time, at most, with approximately one day and thus all the mission objectives will be met. The impact of a single engine failure upon the mission is therefore negligible.

Engine Failure			
F_{engine} (N)	2.4	T (Nm)	3.9
l (m)	7.8	α (°)	11.6
d (m)	1.46	$F_{10,x}$ (N)	2.36
e (m)	0.67	$F_{10,yz}$ (N)	0.49

Table 6.1.: In case one engine fails, in the worst case situation, the thrust vector needs to be tilted to compensate for the undesired torque.

If more than one engine fails, the mirrored engine has to be shut down as well to avoid any torque. This has an effect on the overall acceleration and will impact the total transfer time duration according to figure 4.18. The mission can still be performed, although the transfer duration will increase.

The resulting lateral force in the y-z plane (0.5 N) causes a lateral movement of the spacecraft. The impact of this force is not considered in the current design phase, since the force is relatively small. However, in future design phases more detailed analyses should be performed, which evaluates the impact of an engine failure on the mission analysis, especially concerning the trajectory.

6.1.2. SADM Failure

The SADM has two functions; applying rotation to the solar array and transferring power from the solar array to the spacecraft. The power is transferred through the roll ring assembly. This assembly requires no form of lubrication and the wear is extremely low, failure is therefore highly unlikely. In case the power transfer is interrupted, which is doubtfull, the discharge power to the electric engines is halved. As a consequence, the thrust and initial acceleration are halved and the transition time is approximately doubled, see figure 4.18. The figure also indicates, that the Δv required for this initial acceleration, is not much different. Thus, it is expected that the mission to the Moon can still be performed, only at the cost of extra transfer time. The transfer from LLO back to LEO might be more problematic, since an extra Δv of approximately 100 m/s is needed (see figure 4.19). However, this amount is relatively small (1.4% of the budget to go from LLO to LEO) and it is expected that the propellant reserves can be used to go to LEO or a slightly higher orbit. Thus, halving the power only affects the transfer time and all the other mission objectives can still be met.

In case the SADM is locked in position due to failure of the stepper motor, there is also an impact on the AOCS. This question is rather complex and requires elaborated analysis on AOCS to derive the impact on the propellant usage. However, stepper motors are applied in almost all space missions and therefore have a high heritage. This reduces the changes of a failure of this component and it is expected that a reliable design is feasible.

It can be concluded that the (partially) failure of a SADM, only affects the transfer time duration, while all the other mission objectives can be met. In case of a locked SADM, the effect on the AOCS has to be researched. Extensive ground testing is foreseen in order to qualify the SADM for this specific mission and obtain a reliable component, failure of the SADM is therefore unlikely.

6.2. System Configuration and Performance

An initial baseline for the system architecture was identified in section 5.2.5. During the design process, trade-offs were performed to come to a final baseline, which can be seen in figure 6.2.

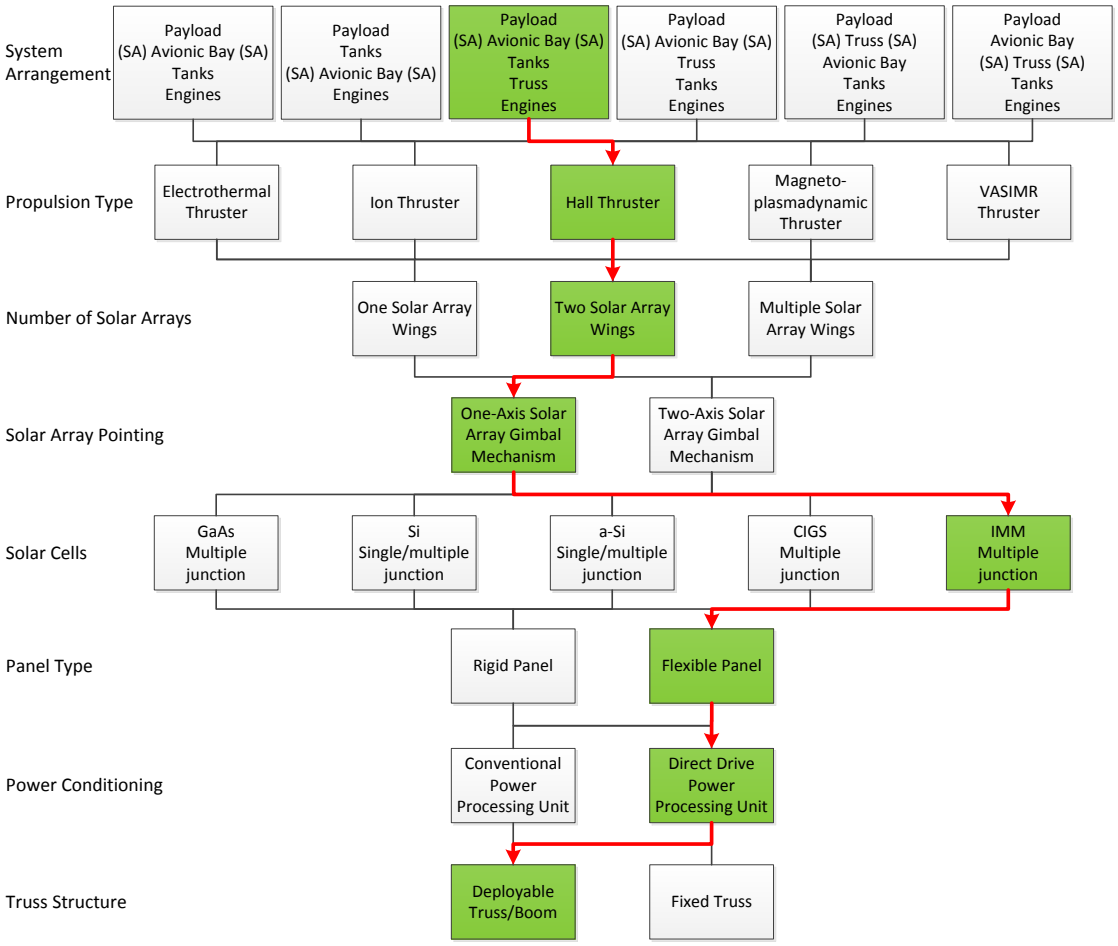

Figure 6.2.: Final Baseline for the System Architecture

The mission is executed in a sequence of events (see figure 6.3). The SEP stage and Payload Module are separately launched, by a Falcon Heavy launcher, to a LEO of $500 \times 500\,\text{km}$. In this orbit the docking occurs and the transfer to LLO is performed by using the propellant of the Payload Module. Once the spacecraft arrives in LLO, the SEP stage and Payload Module undock. The Payload Module lands on the Moon, while the SEP stage returns to LEO and can perform a second mission with another Payload Module. The SEP stage is designed to perform three missions in total.

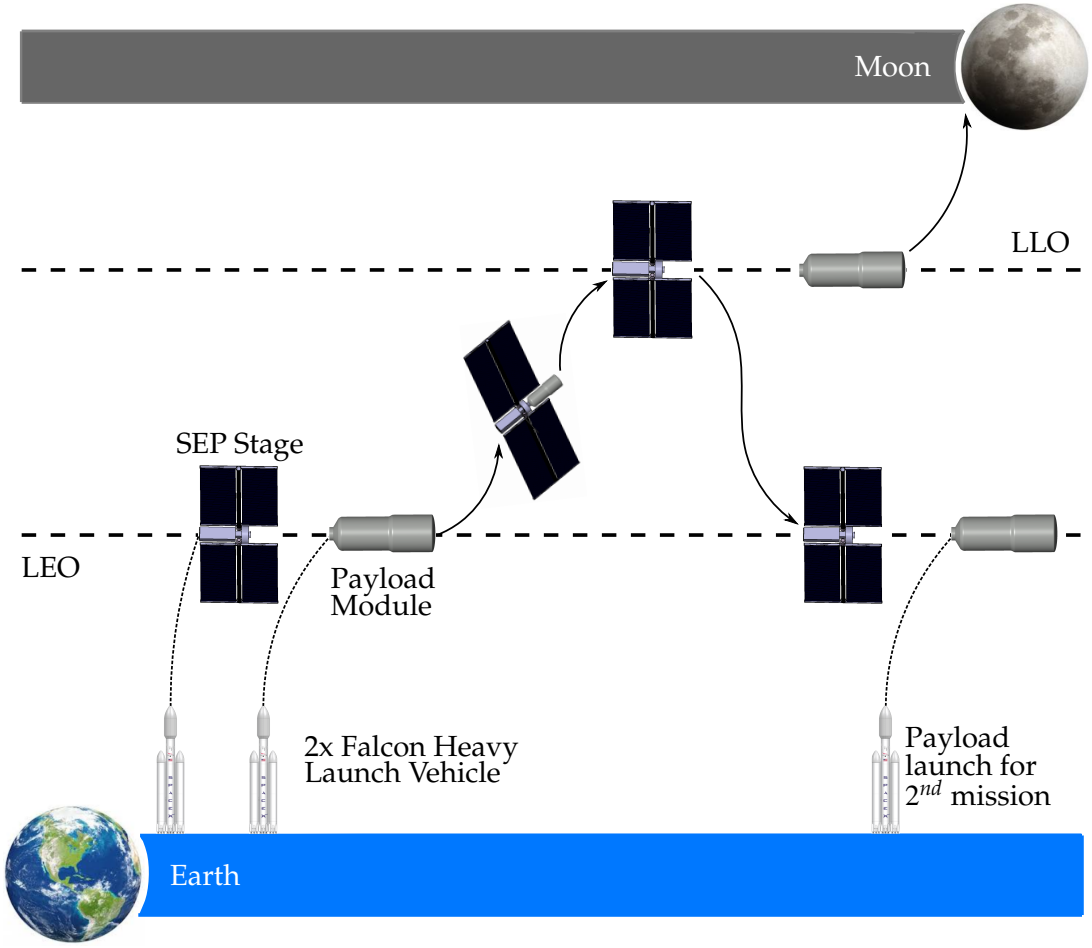

Figure 6.3.: The mission sequence of the SEP stage.

The folded and deployed system configuration can be seen in figure 6.4 and 6.5. The configuration is such that the heaviest components are located as close to the launcher adapter as possible. The cylindrical section contains the propellant tank, required for the return to Earth, and all the electronic equipment. On top of the cylinder, the Solar Array Wing (SAW) assemblies can be identified, which consists out of the Solar Array Drive Mechanism (SADM), a canister for storage of the deployable truss and the booms that contain the flexible solar array. The electric thrusters and DDU are located just above the canisters and enclosed by the rectangular structure. The radiators are attached to this rectangular structure. Once the SEP stage is in orbit and separated by the launcher, the thrusters, radiators and SAWs can deploy to its final position (see figure 6.5).

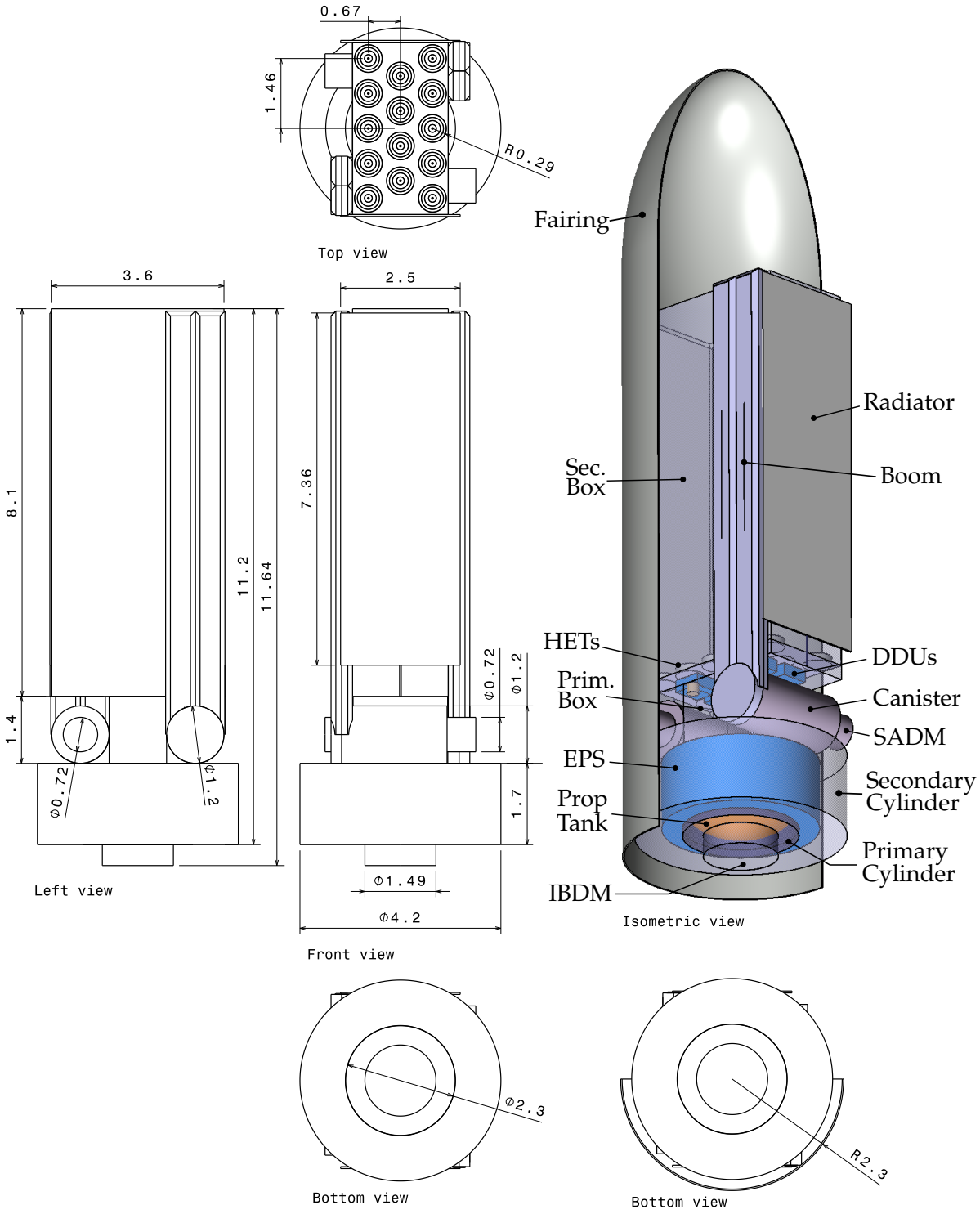

Figure 6.4.: The folded configuration and dimensions of the SEP stage, the isometric and second bottom view are inside the fairing.

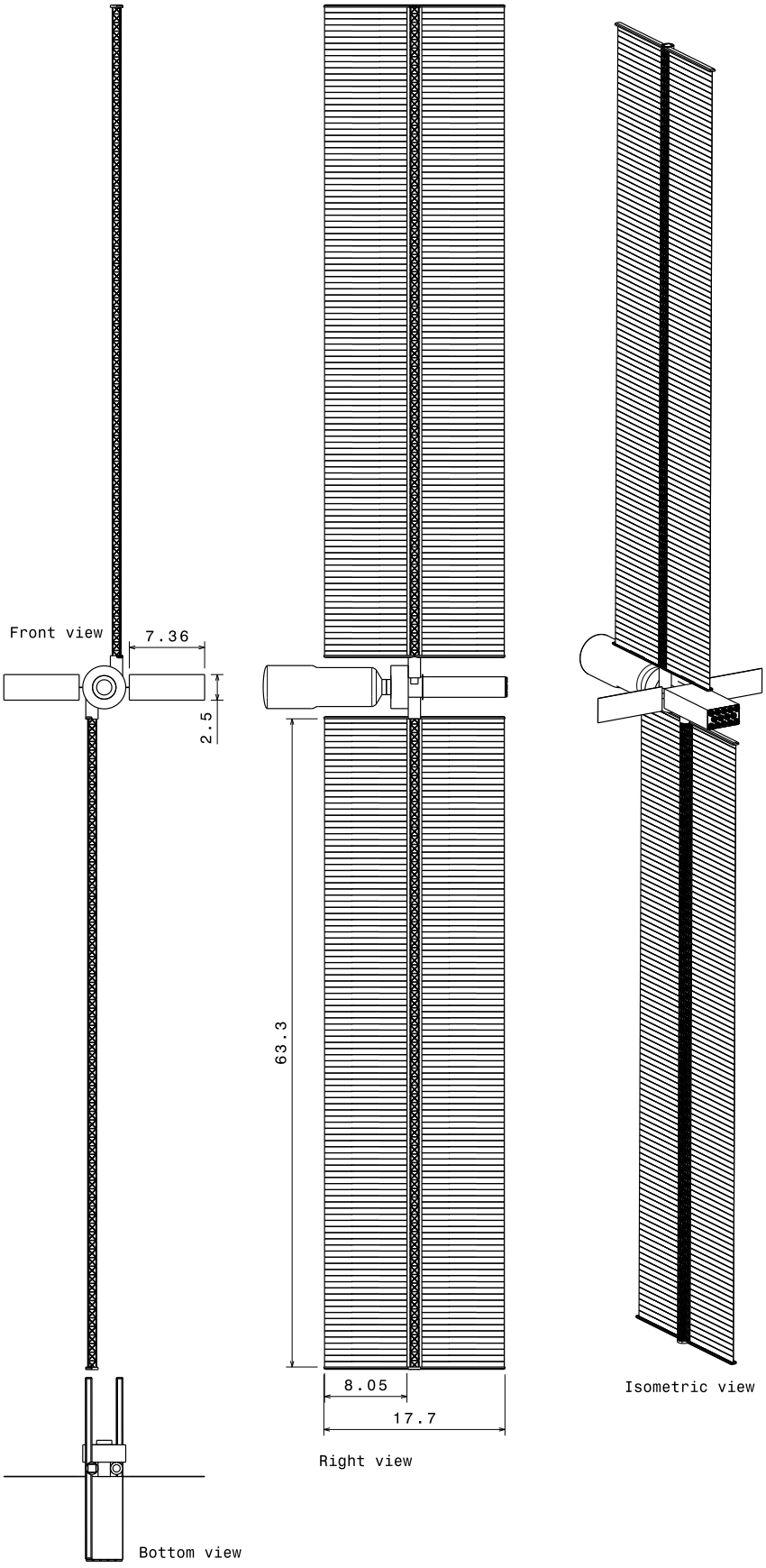

Figure 6.5.: The SEP stage in the deployed configuration, the front and bottom view are without payload, the right and isometric view are with the payload docked.

Mass and power budget

Experience learns that the mass budget of a phase 0 study has an accuracy of $\pm 10\%$. Due to this accuracy, it is chosen to apply iterations until the new initial mass budget is within 5% of the previous initial mass budget. The methodology, in which iterations are applied, can be seen in figure 6.6. A change in the initial mass has the highest impact on the propulsion and EPS mass, followed by the structure and TCS. The initial acceleration, specific impulse and required Δv are kept constant, aswell as the AOCS, TT&C and OBDH mass.

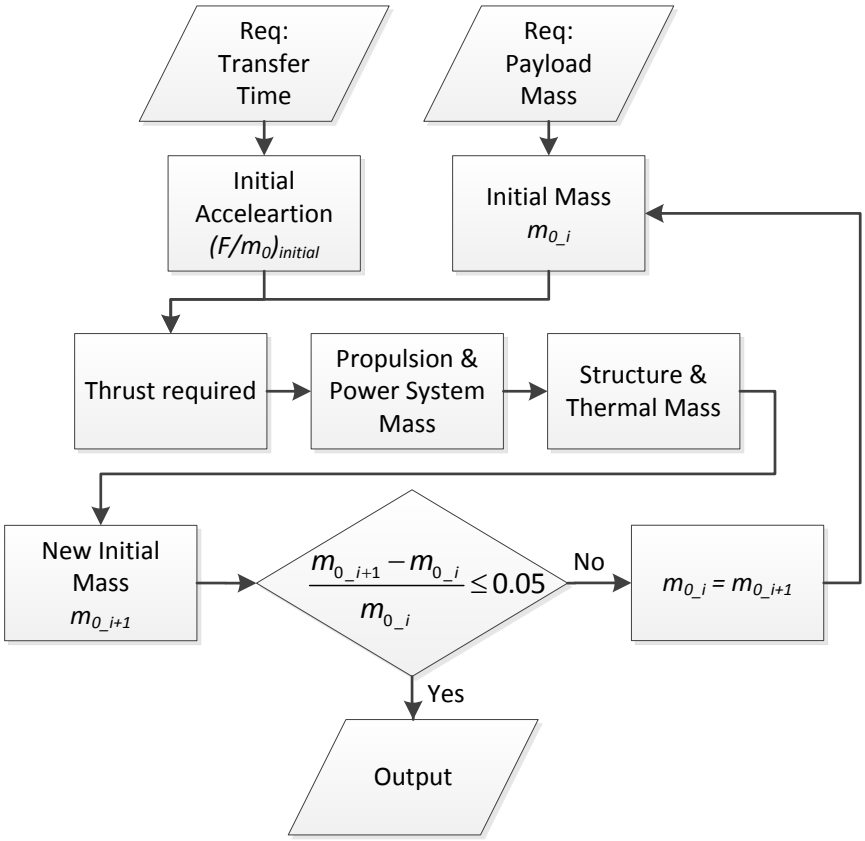

Figure 6.6.: Methodology for applying iterations to the design.

Three iterations had to be applied before the new initial mass was within 5% of the previous initial mass. The resulting mass and power budget can be seen in, respectively, table 6.2 and 6.3. In the preliminary mass estimate method (see section 4.3.1) it was estimated that an initial mass of $49,613\,\text{kg}$ is required to transport a payload of $14,705\,\text{kg}$. When the payload mass is scaled up to 17 ton in this method, an initial mass of $53,340\,\text{kg}$ is required, which is 22% less compared to the current method. It demonstrates that the current method, which is based upon physics, experience and applies ESA's margin philosophy, is more accurate and reliable than the preliminary method of section 4.3.1.

Mass budget	SEP stage	Payload Module	Total
$m_{structure}$ (kg)	2,308	-	2,308
$m_{propulsion}$ (kg)	2,815	1,818	4,632
m_{power} (kg)	6,834	-	6,834
$m_{thermal}$ (kg)	1,075	-	1,075
m_{AOCS} (kg)	81	-	81
m_{OBDH} (kg)	48	-	48
$m_{TT\&C}$ (kg)	36	-	36
$m_{harness}$ (kg)	1,320	-	1,320
$m_{subsystems}$ (kg) (20%)	17,420	2,181	19,601
$m_{payload}$ (kg)	-	17,000	17,000
m_{dry} (kg)	17,420	19,181	36,601
m_{prop} (kg)	8,248	23,222	31,470
m_0 (kg)	25,668	42,403	68,070

Table 6.2.: Resulting mass budget after the third iteration. Note that the payload module has to harbor the propellant to go from LEO to LLO.

Power budget	Mode 1 HVB	Mode 1 LVB	Mode 2 LVB
$P_{propulsion}$ (kW)	564.1	17.5	2.6
$P_{thermal}$ (kW)	-	-	0.32
P_{AOCS} (kW)	-	0.09	0.09
P_{OBDH} (kW)	-	0.063	0.063
$P_{TT\&C}$ (kW)	-	0.105	0.105
η_{total} (kW)	0.975	0.917	0.782
Margin	0%	20%	20%
P_{total} (kW)	578.5	24.5	6.4
$P_{SA,req}$ (kW)		606.8	

Table 6.3.: Resulting power budget and required solar array power after the third iteration. In Mode 1 the stage is in the Sun and the high- and low-voltage bus are operational, in Mode 2 the stage is in eclipse and only the low-voltage bus is operational.

The literature study (see chapter 3) provided two mass budgets of other SEP stage designs (see table 3.1 and 3.2). A NASA study from 2005 (see section 3.1) shows a vehicle with a comparable power level (600 kW) and configuration that transfers a payload from LEO to LLO and returns to LEO. The NASA SEP stage dry mass is 7,996 kg, delivers a

payload of 19,690 kg using a total propellant, for two-ways, of 23,000 kg. The HEFT study from 2010-2011 (see section 3.3) resulted in a vehicle with a power of 300 kW, capable of transferring a payload of 40,000 kg from LEO to HEO ($60,000 \times 400,000$ km), within 2 years. The total dry mass of this vehicle is 12,095 kg and total propellant mass is 40,150 kg. So, although the power is halved, the vehicle dry mass is 51% more compared to the 2005 study. Also, comparing the presented mass budget in table 6.2 to the work in 2005, indicates that the study of 2005 was too optimistic. When the mass budget is compared to the work of 2011 (see table 3.2), it shows comparable outcomes for most subsystems, except for the power, which is doubled due to the fact that the power is also doubled, from 300 kW to 600 kW. Another difference between the two budgets is in the harness mass, which is only 365 kg for the 300 kW version. Also, the HEFT study of 2011 does not apply an additional margin of 20% on the total subsystems mass. However, experience shows that these margins are required in order to control the mass budget in future design phases and is thus obviously a shortcoming of the HEFT study.

Compared to chemical rockets, a SEP stage is capable of transporting a larger payload while having the same initial mass. A study performed at OHB systems showed that a chemical propelled rocket, with LOX/LH2 as main propellant and an initial mass of 70 ton, is capable of transferring 13,325 kg of payload to the Moon [2], thus having a payload mass fraction of 0.19. Reducing the initial mass of this stage to 68 ton, reduces the payload mass to 12.9 ton. This indicates that an SEP stage can transfer 32% more payload than a chemical rocket while having the same initial mass, due to its higher specific impulse and despite the large power system.

Fulfillment of Requirements

The performance of the stage is reviewed by restating all the top-level requirements and validate if the requirements have been met. The complete requirements flow-down can be seen in appendix C. The flow-down is very extensive, although it should be noted that not all requirements are identified and only the top-level, of the most important subsystems, are given. It should also be noted that the current mission is very challenging and that in section 6.3 an alternative mission is suggested, which is less demanding. In case this alternative mission is accepted, a substantial amount of the identified requirements have to be changed to comply with the new mission.

For the current mission, all the top level requirements were created in section 2.2 and are again stated in table 6.4 to 6.6. The tables indicates if a requirement is driving the design and to what extent: high, medium or low. The top level mission requirements are shown in table 6.4, while the top level system requirements are indicated in table 6.5 and 6.6.

	Mission Requirement	Met	Driving
1.	The transfer stage shall transport a payload of minimal 17 ton (TBC) from Earth environment to a LLO of 100 × 100 km within 200 days (TBD).	Yes, Sec. 6.2	High
2.	The stage shall be reusable, meaning that the transfer stage shall return from LLO to the initial Earth orbit and perform at least two missions to LLO with the potential of extension to three missions.	Yes, Sec. 6.2	High
3.	The transfer stage shall primarily be propelled by electric propulsion.	Yes, Sec. 5.3	High
4.	The transfer stage shall be powered by solar panels as primary power source (nuclear power is excluded).	Yes, Sec. 5.4	High
5.	The transfer stage and cargo should be launched together (TBC) with one super heavy lift launch vehicle (TBD). The launcher has to be available in the next decade (i.e. SLS or Falcon Heavy).	No, Sec. 4.3.2	High
6.	The transfer stage shall dock and un-dock with the cargo, depending on the mission architecture.	Yes, Sec. 5.5.3	Low
7.	The transfer stage shall follow End-of-Life regulations.	Yes, Sec. 4.2.4	Low

Table 6.4.: Top level Mission Requirements that have been met and drive the design to a certain level.

	System Requirement	Met	Driving
1.	The transfer stage shall be able to operate in deep-space environment, specifically the environment surrounding the Earth and Moon. This includes the Van Allen belts, solar radiation, solar wind, cosmic radiation, debris and (micro-) meteoroids.	Yes, Sec. 6.2	Medium
2.	The transfer stage shall primarily be using electric propulsion.	Yes, Sec. 5.3	High
2.1	The electric propulsion shall be provided by Ion or Hall thrusters, since they have the most favorable characteristics for this mission type.	Yes, Sec. 5.2.2	Medium
2.2	The engine can provide thrust during eclipse.	No, Sec. 5.4.6	High
3.	The transfer stage shall be powered by solar panels.	Yes, Sec. 5.4.7	High
3.1	The solar array shall be deployed autonomously.	Yes, Sec. 5.4.7	Medium

Table 6.5.: Top level System Requirements that have been met and drive the design to a certain level.

	System Requirement	Met	Driving
3.2	The critical systems shall be powered by batteries during eclipse time.	Yes, Sec. 5.4.6	Medium
3.3	The EOL power generation of the solar panels shall be sufficient to maintain proper engine functionality.	Yes, Sec. 5.4.7	High
4.	The transfer stage shall have sufficient propellant capacity to perform the transfer.	Yes, Sec. 5.3.5	High
4.1	The most suitable propellant from performance point of view shall be identified.	Yes, Sec. 5.3.4	Medium
5.	The transfer stage shall provide thermal control and radiate all excess heat to space.	Yes, Sec. 5.6.4	Low
6.	The transfer stage shall provide a separation mechanism from its payload. Due to stage reusability, this shall be a docking mechanism to dock and un-dock with the payload.	Yes, Sec. 5.5.3	Low
7.	The transfer stage shall provide 3-axis attitude control during the entire mission.	Yes, Sec. 5.7	Low
8.	The transfer stage shall be able to communicate with an Earth based ground segment.	Yes, Sec. 5.8 (TBC)	Low
9.	The transfer stage shall perform the mission automatically, meaning that the stage can perform some operations by itself (TBD) and for other commands can be given during the mission.	Yes, Sec. 5.8 (TBC)	Low
10.	The transfer stage shall provide electrical power to the payload during the transfer.	Yes, Sec. 5.4.6	Low
11.	The transfer stage's configuration should be such that the direct impingement of the thrusters' exhaust on the solar arrays is limited (TBD).	Yes, Sec. 5.5	Low
12.	The configuration shall be such that the thermal radiators, solar panels and the docking mechanisms have a unobstructed field of view.	Yes, Sec. 6.2	Low
13.	The structure shall be rigid enough to withstand the launch loads and the frequencies that are imposed by the launcher.	Yes, Sec. 5.5.5 (TBC)	Low

Table 6.6.: Top level System Requirements that have been met and drive the design to a certain level.

In the tables it can be seen that two of the top level requirements have not been met. For mission requirement 5 it was decided, due to structural reasons and the fairing volume limitations, not to launch the transfer stage and cargo together. System requirement 2.2 is not met, since a battery mass of 8.6 ton would be required to power the thrusters during eclipse. The resulting performance benefit of firing the thrusters in eclipse is

limited, while the extra mass that is required is substantial (increase of approximately 50% of the SEP's subsystem mass). Therefore it is decided not to fire the engines in eclipse, which relieves the required battery capacity from 2140 kWh to 19.9 kWh.

The system requirements 8 and 9 are expected to be met by selecting off-the-shelf components, that fulfill similar tasks in other missions. Thus, it is expected that these components can meet the requirements, although further analysis in a subsequent design phase is required to confirm this statement. Also, for system requirement 13 a more sophisticated analysis is required to validate if the structure can withstand all the loads.

The design is directly driven by the mission requirements (see table 6.4 and figure 6.7), especially the transfer time and the derived initial acceleration have a significant impact on the thrust, power, propellant and finally on the initial mass. Also the payload mass drives the subsystems and initial mass. Therefore an analysis in the next section is done to study the impact on the design in case the payload mass and transfer time requirement are relieved.

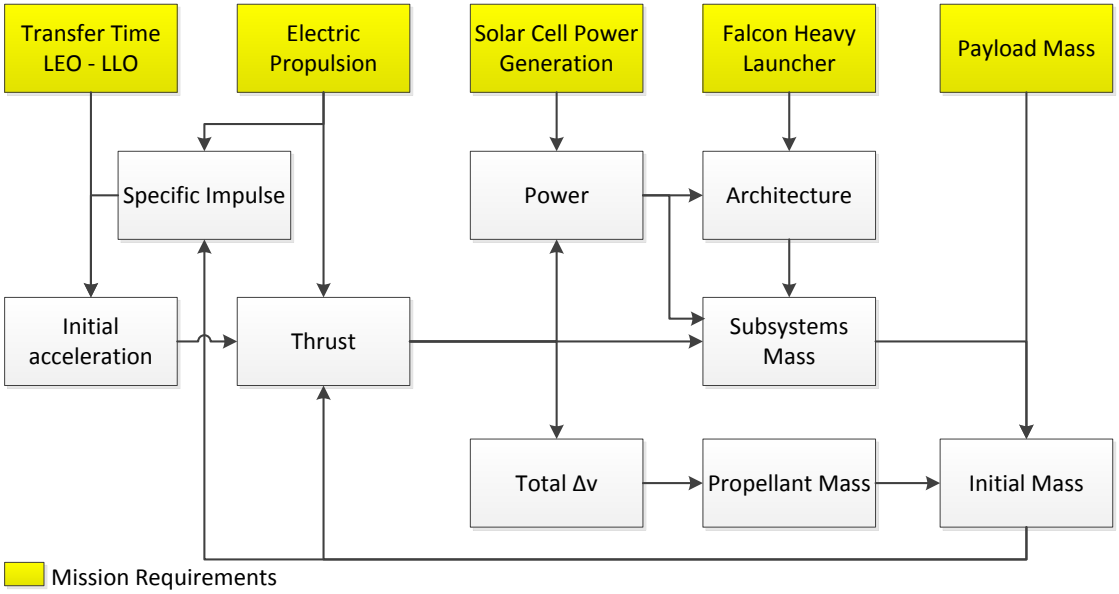

Figure 6.7.: Main system design drivers for the SEP stage.

6.3. Alternative Configurations

Relaxing certain requirements has an impact on the SEP design. The two most driving requirements, are the transfer time requirement and the payload mass requirement. The payload mass has an impact on the initial mass, while the transfer time requirement sets the required initial acceleration. Both have a significant impact on the total initial mass and therefore on the overall design. The influence of changing these requirements, leading to a different mission scenario, is analyzed in the current section. The different mission scenarios, besides the current scenario of a payload mass of 17 ton and transfer time of less than 200 days, are:

- Transfer a payload mass of 17 ton from LEO to LLO, with a time duration of approximately:
  - 400 days.
  - 800 days.
- Transfer a payload mass of 10 ton from LEO to LLO, with a time duration of approximately:
  - 200 days.
  - 400 days.
  - 800 days.

Relaxing the transfer time requirement, results in a new sub-optimum specific impulse. For a transfer time of 400 days and 800 days, the sub-optimum specific impulse changes to 2,500 s and 3,300 s, respectively (see table 6.7). For the 800 days, a sub-optimum of 3,800 s is a better choice and would lead to ion thrusters instead of hall thrusters. Since the tools are especially developed for Hall thrusters in combination with a DDU power system, the specific impulse that is selected equals the upper operation boundary of the 400M thruster, which is 3,300 s.

	Transfer time (days)		
Characteristic	200	400	800
I_{sp} (s)	2,000	2,500	3,300
$(F/M)_{initial}$ (m/s^2)	$4.8 \cdot 10^{-4}$	$2.4 \cdot 10^{-4}$	$1.5 \cdot 10^{-4}$
$\Delta v_{LEO-LLO}$ (m/s)	8,498	8,488	8,486
$\Delta v_{LLO-LEO}$ (m/s)	8,134	8,268	8,312

Table 6.7.: The specific impulse, initial acceleration and Δv for the analysis of the different mission scenarios.

As a consequence of the changing specific impulses, the required initial acceleration and Δv differs. Therefore, additional simulations were performed with the Spiral Tool (see figure A.17 to A.20 in appendix A.2). The resulting initial accelerations and Δv that comply with the transfer time, can be seen in table 6.7.

Iterations are applied on the different mission scenarios, according to the methodology given in figure 6.6. It has to be noted that during the iterations, the AOCS, OBDH and TT&C masses were left unchanged. Also the structure of the stage was kept the same, except for the deployable boom that supports the solar array. These assumptions result in conservative mass estimates for the new scenarios, since their systems are less demanding in terms of mass and volume and therefore expected to be lighter.

The impact of the different mission scenarios on the SEP dry mass can be seen in table 6.8. For the configuration with a payload of 17 ton, doubling of the transfer time from

200 to 400 days, results in a reduction of 42.0% in mass. When the time requirement is further increased to 800 days, only an extra reduction of 27.7% is obtained. For the 10 ton variant, the mass reductions are respectively 45.0% and 27.7% when increasing the time requirement to 400 or 800 days. It shows that an increase of the transfer time, has a significant impact on the SEP dry mass, especially when the time requirement is relaxed from 200 to 400 days. The reduction is much lower for a 800 days transfer, which indicates that there is a minimum system mass that is required to perform the mission.

If the SEP dry mass is compared for the different payload configurations (compare vertically in table 6.8), for 200 days, a decrease of 13.2% can be realized when transferring a payload of 10 ton instead of 17 ton. For 400 days this is 17.8% and for 800 days, also 17.8%. When it is considered that the payload mass is reduced by 41.2%, the reduction in SEP dry mass is relatively low.

$m_{SEP,dry}$ (ton)	Transfer time (days)		
	200	400	800
17 ton payload	17.4	10.1	7.3
10 ton payload	15.1	8.3	6.0

Table 6.8.: The SEP dry mass for the different mission scenarios.

The propellant that is appointed to the payload for the different mission scenarios, to transfer from LEO to LLO, can be seen in table 6.9. Increasing the mission time from 200 to 400 days, results in a propellant mass decrease, respectively for the 17 and 10 ton payload, of 38.8% and 43.2%. For a mission time of 800 days, the propellant decrease is respectively 38.7% and 44.8%. Decreasing the payload from 17 to 10 ton results in a reduction of 20.3%, 26.1% and 33.3% respectively for 200, 400 and 800 days.

For the transfer from LLO to LEO (see table 6.10), increasing the mission time from 200 to 400 days, results in a propellant mass decrease, respectively for the 17 and 10 ton payload, of 46.3% and 50.0%. For a mission time of 800 days, the propellant decrease is respectively 47.7% and 50.0%. Decreasing the payload from 17 to 10 ton results in a reduction of 7.3%, 13.6% and 17.4% respectively for 200, 400 and 800 days. The tables with the propellant masses indicate, that the most significant reductions are achieved when the transfer time requirement is relieved.

$m_{prop,LEO-LLO}$ (ton)	Transfer time (days)		
	200	400	800
17 ton payload	23.2	14.2	8.7
10 ton payload	18.5	10.5	5.8

Table 6.9.: The propellant mass required to transfer the payload from LEO to LLO, in different mission scenarios.

$m_{prop,LLO-LEO}$ (ton)	Transfer time (days)		
	200	400	800
17 ton payload	8.2	4.4	2.3
10 ton payload	7.6	3.8	1.9

Table 6.10.: The propellant mass required to return from LLO to LEO, in different mission scenarios.

For the total initial mass, doubling the transfer time from 200 to 400 days, results in a reduction of 31.1% and 36.7% for the 17 ton and 10 ton payload, respectively (see table 6.11). In case the transfer time requirement is further increased to 800 days, the initial mass only decreases 23.5% and 27.8%, respectively. This indicates that, for a specified payload mass, there exists a certain minimum initial mass which is required to transport the payload, irrespective of the transfer time. When comparing the different payload masses, the initial mass decrease, respectively, 22.5%, 28.8% and 32.9% for the 200 days, 400 days and 800 days transfer time.

m_0 (ton)	Transfer time (days)		
	200	400	800
17 ton payload	68.1	46.9	35.9
10 ton payload	52.8	33.4	24.1

Table 6.11.: Initial mass of the total spacecraft for the different mission scenarios.

Similar conclusions can be drawn about the payload mass fraction (see table 6.12). When the transfer time is increased from 200 to 400 days, the payload mass fraction increases significantly, by 44.8% and 58.2%, respectively for payload masses of 17 ton and 10 ton payload. In case the time is further increased to 800 days, the increase is, respectively, 30.7% and 38.5%. When transferring a smaller payload, the payload mass fraction drops by 24.4%, 17.4% and 12.5% compared to the large payload, for respectively a transfer duration of 200, 400 and 800 days. The results show that it comes at a relatively higher cost, in terms of initial mass, to transfer a smaller payload.

$m_{payload}/m_0$	Transfer time (days)		
	200	400	800
17 ton payload	0.250	0.362	0.473
10 ton payload	0.189	0.299	0.414

Table 6.12.: The payload mass fraction for the different mission scenarios.

Other important parameters that change due to the altered mission scenario, can be seen in table 6.13. From the discussion it can be concluded, that changing the mission scenario, can increase the payload mass fraction significantly. The preferred mission

scenario, depends upon the wishes of the customer, although it is advised not to select a 800 days mission, since the transfer time is long and the relative increase in payload mass fraction is limited. Also, the initial mission of transporting 17 ton within 200 days, is considered to be challenging, especially concerning the high power demand for the EPS. From the three scenarios that are left, there is a preference for the 17 ton, 400 days scenario, because of the high payload mass fraction, which is 90% higher compared to a LOX/LH2 chemical rocket, and a power level (285 kW) that is comparable to the maximum power of ISS, hence a power level familiar to EPS engineers. Though it has to be noted that the SEP stage requires an extremely compact design compared to the ISS.

	Transfer time (days)					
Characteristic	200		**400**		800	
$m_{payload}$ (kg)	17,000	10,000	**17,000**	10,000	17,000	10,000
F_{HET} (N)	31.3	24.9	**11.6**	8.6	5.7	3.9
P_{EOL} (kW)	608	486	**285**	212	189	129
A_{SA} (m^2)	2,040	1,630	**957**	712	627	434
m_{SEP} (kg)	25,668	22,647	**14,444**	12,084	9,574	7,833
m_{prop} (kg)	31,470	26,066	**18,596**	14,249	10,983	7,721
m_0 (kg)	68,070	52,800	**46,906**	33,420	35,937	24,145
$m_{payload}/m_0$	0.250	0.189	**0.362**	0.299	0.473	0.414

Table 6.13.: SEP stage characteristics when lowering the transfer time requirement and/or payload mass.

For the eventually advised mission scenario, no optimization of the launcher selection is performed. For a more thorough analysis, the launcher selection has to be re-assessed and therefore there is a probability that the overall design will change. However, the rational for this parameter study is to show the impact of different mission scenarios on the design and to advice the customer to reconsider its initial requirements.

7. Conclusion & Recommendations

The purpose of this study is to create a conceptual system design of a Solar Electric Propulsion (SEP) stage for Earth-Moon cargo transfer missions. The mission objective is to transport cargo, at minimum 17 ton, from Earth environment to a Low Lunar Orbit (LLO) by means of a Solar Electric Propulsion stage. It is required that the SEP stage is propelled by electric propulsion and powered by solar panels. Also, the SEP stage shall be reusable, meaning that the transfer stage shall return from LLO to the initial Earth orbit and perform at least two missions. The study is holistic in its nature, which means that all the aspects concerning an SEP stage will be covered and important systems will be studied into more detail than others.

The SEP stage performs a spiral transfer from the Earth to LLO. For the mission analysis, a SPIRAL PROGRAM is written that calculates the transfer as a two-body problem and is validated using GMAT. The Falcon Heavy is selected as launcher, and the SEP stage and payload are launched separately, due to launcher volume limitations. The launcher brings the SEP stage to a stable initial orbit, with limited atmospheric drag, of 500×500 km, from where the SEP stage docks with the payload and transfers to a LLO of 100×100 km. This transfer in total requires a Δv of $8,498$ m/s, while a Δv of $8,134$ m/s is required to return from LLO to LEO. A preliminary mass analysis is performed, which shows the initial mass as function of the specific impulse, to select the optimum specific impulse from the mass point of view. The mass optimum is at a specific impulse of 3200 s. However, since the required power for this optimum is very demanding, a sub-optimum of 2000 s is selected, which reduces the power demand with approximately 38% and increases the initial mass with only 7%. For this sub-optimum, the stage requires an initial acceleration of $4.8 \cdot 10^{-4}$ m/s^2 to transfer the payload in 200 days from LEO to LLO. The discussion demonstrates that there is a strong interdependency between the mission analysis and the design of the SEP stage, especially concerning the propulsion and Electric Power System (EPS).

The main focus of the design is on the propulsion and electric power system, since they are driving the SEP stage's mass and architecture. The other subsystems are also covered, although in less detail, to obtain a holistic design. Tools are developed to aid in the design by using physical relations, experience from OHB systems and methods from well-established literature. These aspects make the tools reliable in obtaining a holistic conceptual design for an initial phase 0 study and make it possible to evaluate different mission scenarios.

The baseline SEP stage employs Hall thrusters as type of propulsion, due to the large thrust-to-power ratio and compatible specific impulse. The engines are powered by two Solar Array Wing (SAW) assemblies, of which the flexible solar array blankets consist out of highly efficient Inverted Metamorphic Multi-junction (IMM) solar cells. The cells generate, at the highest operation temperature and at EOL, a power of 608 kW, while operating at a voltage of 400 V. The SAW is deployed and structurally supported by a deployable truss. The operation point of the power system is controlled by the Direct Drive power processing Unit (DDU) in combination with the Sequential Shunt Unit (SSU). The main advantage of the DDU, compared to a conventional Power Processing Unit, is that it is approximately 4% more efficient and therefore reduces the power demand and waste heat. In the launch configuration, the engine platform is located inside the structure just above the SAWs. Once the stage is in space, this engine platform is deployed to its final position by coilable booms.

The SEP stage is a complex system, which requires a substantial engineering effort to make everything operate as desired. The critical issues that are identified are; spacecraft charging, DDU operation, high-voltage solar array operation, high power transfer with the Solar Array Drive Mechanism (SADM), the truss canister dimensions and deployment of deployable trusses. The spacecraft charging is prevented by operating the thruster cathodes at all times, which lowers the spacecraft's potential and the probability of an electrostatic discharge. The operation of a DDU in combination with a Hall thruster is a new development in which still many questions remain. Especially, the start-up, control of the operation point and possible short circuits that can damage the solar array, are points of future research. Eventually, a flight test in space is foreseen to validate the operation of a high-voltage solar array in combination with a DDU. The high power demand drives the size of the SADM and the deployable truss inside the canister to such an extent, that their length is almost longer than the launcher fairing diameter. A large engineering effort is required to keep them as small as possible, while the SADM is still able to transfer the high voltage and power. In case higher power levels are desired, a different configuration or launcher with larger fairing is required to perform the mission. The relatively large canister also results in structural challenges, since connections from the tank and EPS to the propulsion system are situated in a small area. Moreover, deployment of the solar array and engine platform's deployable trusses are challenging and require extensive ground testing for space qualification.

The design of the propulsion system is incorporated with one redundant thruster, which means that the failure of a single engine does not affect the vehicle's performance. When a second engine fails, the mirrored engine should be shut down to eliminate torques acting on the spacecraft. The reduced thrust level has an impact on the mission duration, although the complete transfer from LEO to LLO and back can still be completed. In case a SADM fails, which is unlikely due to the roll ring assembly design and possibility of extensive ground testing, the generated power is halved and thus the resulting thrust is halved. As a consequence, the transfer time is doubled and it is expected that

the complete transfer can still be performed.

The complete SEP stage, with the payload docked, results in a total initial mass of 68.1 ton to fulfill all mission objectives and requirements. The budget shows a discrepancy of 22% with the method used for the preliminary analysis, which predicted an initial mass of 53.3 ton to transport a payload of 17 ton. Therefore, the current method, which is based upon physics, experience and applies ESA's margin philosophy, is more accurate and reliable than the preliminary mass method. Compared to chemical rockets, a SEP stage is capable of transporting a larger payload while having the same initial mass. A chemical propelled rocket, with LOX/LH2 as main propellant and an initial mass of 68 ton, is capable of transferring 12.9 ton of payload to the Moon. This indicates that a SEP stage can transfer 32% more payload than a chemical rocket while having the same initial mass. This can increase even further, to 90%, in case the 400 days mission scenario is selected.

The enabling technologies of the SEP stage are the key to mission success and are therefore the most critical systems. The enabling technologies that are identified are; the high power Hall thruster, high power SADM, deployable truss mechanisms, new generation IMM solar cells and the DDU. These systems are critical in fulfilling the mission objectives and therefore a substantial development effort should be allocated to these technologies.

As indicated, a large SEP stage brings forth technical challenges, which are mainly the large, high power, deployable solar arrays and power management. The high power demand results in complex and large solar arrays, therefore there is a strong desire to keep the power demand, and thus the solar array area, as small as possible. One requirement that drives the power demand is the transfer time requirement. By relaxing this requirement, the initial acceleration will be lower and the resulting power demand of the electric propulsion will be significantly lower. Alternative configurations were suggested, in which the transfer time is increased to 400 and 800 days and the payload mass reduced to 10 ton. When the transfer time is relaxed to 400 days, the required power is more than halved to 285 kW. As a consequence, the initial mass of the stage is lowered to 46.9 ton and the payload fraction of the stage increased to 0.36. The other configurations have proven to be less optimal and thus it is advised to the customer, to change the mission time duration to 400 days, such that a comparable power level to the one of ISS is obtained. Also, relaxing this requirement relieves some of the critical issues like the SADM, deployable truss mechanism and corresponding canister size. For the advised new mission scenario, no optimization of the launcher selection is performed. For a more thorough analysis, the launcher selection has to be re-assessed and therefore there is a probability that the overall design will change. However, the rational of the performed parameter study is to show the impact of a different mission scenario on the design and to advice the customer to reconsider its initial requirements. In case the mission scenario is changed to the one advised to the customer, the requirement

flow-down has to be re-assessed.

In conclusion, this thesis provides a conceptual design of a solar electric propulsion stage that can fulfill the mission objectives. Also, the effect of different mission scenarios on the design are researched, which results in the advice to change the transfer time requirement from 200 days to 400 days. For the future design phases it is advised to improve the mission analysis by improving the trajectory computation of the Spiral Program. Furthermore, the design of the subsystems can be performed in more detail, resulting in more accurate mass and power budgets. In these subsequent design phases, changes to the configuration and even architecture are anticipated.

Bibliography

[1] BOS C.R., *System Design of an Electric Transfer Stage*, AE4-005: Literature Research, Delft, January 2012

[2] ROHRBECK M., *Conceptual Study of Large Transfer Stages*, OHB System, Space Systems Studies, Bremen, Germany, 2012

[3] LARSON W. J., WERTZ J. R., *Space Mission Analysis and Design*, Third Edition, Microcosm Press and Kluwer Acadamic Publishers, ISBN: 1-881883-10-8, El Segundo, 2004

[4] VALLADO D.A., *Fundamentals of Astrodynamics and Applications*, Third Edition, Microcosm Press/Springer, ISBN: 978-0-387-71831-6, Hawthrone/New York, 2007

[5] SUTTON G.P., *Rocket Propulsion Elements*, Seventh Edition, A Wiley-Interscience Publication, ISBN:0-471-32642-9, New York, 2001

[6] PATEL M.R., *Spacecraft Power Systems*, CRC PRESS, ISBN: 0-8493-2786-5, Boca Raton, Florida, 2005

[7] GOEBEL D.M., KATZ I., *Fundamentals of Electric Propulsion: Ion and Hall Thrusters*, John Wiley & Sons, ISBN: 978-0-470-42927-3, Hoboken, New Jersey, 2008

[8] BATE R.R., MUELLER D.D., WHITE J.E., *Fundamentals of Astrodynamics*, Dover Publications Inc., ISBN: 978-0-486-60061-1 , New York, 1971

[9] TEWARI A., *Atmospheric and Space Flight Dynamics - Modeling and Simulation with MATLAB and Simulink*, Birkhäuser, ISBN: 978-0-8176-4437-6, Boston, 2007

[10] KOELLE D.E., *Handbook of Cost Engineering for Space Transportation System(Transcost 8.0)*, TCS - TransCostSystems, TCS-TR-190, Ottobrun, Germany, 2010

[11] FORTESCUE P., STARK J., SWINERD G., SPACECRAFT SYSTEMS ENGINEERING, Third Edition, John Wiley & Sons Ltd., ISBN: 0-471-61951-5, West Sussex, England, 2003

[12] GILMORE D.G., *Spacecraft Thermal Control Handbook - Volume 1: Fundamental Technologies*, Second Edition, The Aerospace Press, ISBN: 1-884989-11-X (v. 1), California, USA, 2002

[13] VASILIEV V.V., JONES R.M., *Composite Pressure Vessels - Analysis, Design and Manufacturing*, Bull Ridge Publishing, ISBN: 978-0-9787223-2-6, Blacksburg, Virginia, USA, 2009

[14] ESA - EUROPEAN COOPERATION FOR SPACE STANDARDIZATION, *Space Engineering - Technical requirements specification*, ESA Requirements and Standards Division, ECSS-E-ST-10-06C, Noordwijk, The Netherlands, March 2009

[15] ESA - EUROPEAN COOPERATION FOR SPACE STANDARDIZATION, *Space Engineering - Technical requirements specification*, ESA Requirements and Standards Division, ECSS-E-ST-10-06C, Noordwijk, The Netherlands, March 2009

[16] ESA - EUROPEAN COOPERATION FOR SPACE STANDARDIZATION, *Space Engineering - Space environment*, ESA Requirements and Standards Division, ECSS-E-ST-10-04C, Noordwijk, The Netherlands, November 2008

[17] DUCHEMIN O. B., CARATGE A., CORNU N., SANNINO J., LASSOUDIÈRE F., LORAND A., *Ariane 5-ME and Electric Propulsion: GEO Insertion Options*, American Institute of Aeronautics and Astronautics, AIAA-2011-6084, San Diego, California, USA, August 2011

[18] *The Global Exploration Roadmap*, International Space Exploration Coordination Group, National Aeronautics and Space Administration, Washington, September 2011

[19] SPORES R., MONHEISER J., DEMPSEY B.P., WADE D., CREEL K., JACOBSON D., DRUMMOND G., *A Solar Electric Propulsion Cargo Vehicle to Support NASA Lunar Exploration Program*, International Electric Propulsion Conference, IEPC-2005-320, 2005

[20] BROPHY J.R., GERSHMAN R., STRANGE N., LANDAU D., MERRILL R.G., KERSLAKE T., *300-kW Solar Electric Propulsion System Configuration for Human Exploration of Near-Earth Asteroids*, American Institute of Aeronautics and Astronautics, AIAA-2011-5514, San Diego, California, July 2011

[21] FERRANDO E., CROCI L., DAMONTE G., HAZAN D., RIVA S., ROMANI R., CASAREGOLA C., BRAMBILLA A., GRUOSSO G., GAJANI G.S., BLOTT R., BATTOCCHIO L., STEINER M., TUISSI A., CASATI R., CHIARELLI M., *Study Results on a Solar Electric Power System for High Power Electric Propulsion (HiPER) applications*, International Astronautical Congress, IAC-11-D2.4.7, Cape Town, South Africa, 2011

[22] CAPADONA L.A., WOYTACH J.M., KERSLAKE T.W., MANZELLA D.H., CHRISTIE R.J., HICKMAN T.A., SCHEIDEGGER R.J., HOFFMAN D.J., KLEM M.D., *Feasibility of Large High-Powered Solar Electric Propulsion Vehicles: Issues and Solutions*, National Aeronautics and Space Administration, NASA/TM-2012-217275, Glenn Research Center, Cleveland, Ohio, 2012

[23] JAHN R.G., CHOUEIRI E.Y., *Electric Propulsion*, Third Edition, Princeton University, Vol. 5, Princeton, 2002

[24] ESA, *Near-Earth Exploration Minimum System Assessment*, CDF Study Report: CDF-114(A), 2200 AG Noordwijk The Netherlands, May 2011

[25] BROWN D.L., BEAL B.E., HAAS J.M., *Air Force Research Laboratory High Power Electric Propulsion Technology Development*, Edwards AFB: Air Force Research Laboratory, AFRL-RZ-ED-TP-2009-375, October 2009

[26] PARISSENTI G., KOCH N., PAVARIN D., AHEDO E., KATSONIS K., SCORTECCI F., PESSANA M., *Non Conventional Propellants for Electric Propulsion Applications*, Space Propulsion 2010-1841086, 2010

[27] CASAREGOLA C., CESARETTI G., ANDRENUCCI M., *The European HiPER Programme: High Power Electric Propulsion Technology for Space Exploration*, International Electric Propulsion Conference, IEPC-2011-209, Wiesbaden, Germany, September 2011

[28] FLORENZ R., GALLIMORE A.D., PETERSON P.Y., *Developmental Status of a 100-kW Class Laboratory Nested channel Hall Thruster*, International Electric Propulsion Conference, IEPC-2011-246, Wiesbaden, Germany, September 2011

[29] ZURBACK S., LASGORCEIX P., CORNU N., *A 20kW High Power Hall Effect Thruster for Exploration*, International Astronautical Congress, IAC-10.C4.4.2, Prague, 2010

[30] SQUIRE J.P., OLSEN C.S., CHANG DIAZ F.R., CASSADY L.D., ET AL., *VASIMR VX-200 Operation at 200 kW and Plume Measurements: Future Plans and an ISS EP Test Platform*, International Electric Propulsion Conference, IEPC-2011-154, Wiesbaden, Germany, September 2011

[31] HOFFMAN D.J., KERSLAKE T.W., HOJNICKI J.S., MANZELLA D.H., ET AL., *Concept Design of High Power Solar Electric Propulsion Vehicles for Human Exploration*, International Astronautical Congress, IAC-11-D2.3.5, NASA, NASA/TM-2011-217281, Glenn Research Center, Cleveland, October 2011

[32] HOFER R.R., RANDOLPH T.M., *Mass and Cost Model for Selecting Thruster Size in Electric Propulsion Systems*, American Institute of Aeronautics and Astronautics, AIAA-2011-5518, San Diego, California, August 2011

[33] REED K., WILLENBERG H.J., *Early commercial demonstration of space solar power using ultra-lightweight arrays*, Science Direct Acta Astronautica, IAC-07-C3.2.04, 2007

[34] SUMMERER L., JACQUES L., *Prospects for Space Solar Power in Europe*, European Space Agency (ESA), International Astronautical Congress, IAC-11-C3.1.3, Cape Town, SA, 2011

[35] KAPUR V.K., BANSAL A., LE P., ASENSIO O., SHIGEOKA N., *Non-Vacuum Processing of CIGS Solar Cells on Flexible Polymeric Substrates*, 3rd Photovoltaic Energy Conversion Conference, International Solar Electric Technology Inc. (ISET), California, USA, May 2003

[36] BREEN M.L., STREETT A., COKIN D., STRIBLING R., MASON A., SUTTON S., *IBIS (Integrated Blanket/Interconnect System), Boeing's solution for implementing IMM (Inverted Metamorphic) Solar Cells on a Lightweight Flexible Solar Panel*, Boeing Com-

pany, California, USA, 2010

[37] PATEL P., AIKEN D., BOCA A., CHO B., CHUMNEY D., CLEVENGER M.B., ET AL., *Experimental Results From Performance Improvement and Radiation Hardening of Inverted Metamorphic Multijunction Solar Cells*, Journal Of Photovoltaics, Vol.2, No.3, July 2012

[38] STEINER M.A., GEISZ J.F., FRIEDMAN D.J., OLAVARRIA W.J., DUDA A., MORIARTY T.E., *Temperature-Dependent Measurements of an Inverted Metamorphic Multijunction (IMM) Solar Cell*, National Renewable Energy Laboratory, Golden, Colorado, USA, 2011

[39] PHILIPPS S.P., GUTER W., WELSER E., SCHÖNE J., STEINER M., DIMROTH F., BETT A.W., *Present Status in the Development of III-V Multi-Junction Solar Cells*, Next Generation of Photovoltaics, Springer, Fraunhofer Institute for Solar Energy Systems, Feiburg, Germany, 2012

[40] BRANDHORST H.W., *Evolution of Space Solar Cell and Array Technology for the next decade*, Space Research Institute, Auburn University, AL, USA, 2007

[41] OTTE K., MAKHOVA L., BRAUN A., KONOVALOV I., *Flexible Cu(In,Ga)Se2 Thin-Film Solar Cells for Space Application*, Solarion GmbH, Ostende, Leipzig, Germany, February 2006

[42] PUIG L., BARTON A., RANDO N., *A review on large deployable structures for astrophysics missions*, ESA ESTEC, Acta Astronautica 67, 2010

[43] TIBERT G., *Deployable Tensegrity Structures for Space Applications*, Doctoral Thesis, Royal Institute of Technology, Stockholm, Sweden, April 2002

[44] FERRANDO E., GROCI L., DAMONTE G., ET AL., *Study Results on a Solar Electric Power System for High Power Electric Propulsion (HiPER) Applications*, Selex Galileo, International Astronautical Congress, IAC-11-D2.4.7, Cape Town, SA, 2011

[45] FIONA V., *A major 'lunar standstill'*, Journal of the British Astronomical Association, Volume 115, No. 4, August 2005

[46] DE LUCA A., *Architectural Design Criteria for Spacecraft Solar Arrays*, VEGA Space GmbH, Germany, 2011

[47] *Space Launch System (SLS) Program Concept of Operations (CON OPS) Document*, NASA, SLS-PLAN-020, October 2011

[48] PEREZ E., *Ariane 5 - User's Manual*, ArianeSpace, Issue 5, Revision 1, July 2011

[49] *Delta IV Payload Planners Guide*, ULA - United Launch Alliance, Colorado, September 2007

[50] *Atlas V Launcher Services User's Guide*, ULA - United Launch Alliance, Littleton, March 2010

[51] *Falcon 9 Launch Vehicle Payload User's Guide - Rev 1*, SPACEX - Space Exploration

Technologies, SCM 2008-010 Rev. 1, 2009

[52] *IADC Space Debris Mitigation Guidelines*, IADC - Inter-Agency Space Debris Coordination Committee, IADC-02-01, July 2007

[53] RENZ D.D., *Multi-Hundred Kilowatt Roll Ring Assembly Evaluation Results*, NASA, NASA-TM-100865, Lewis Research Center, Cleveland, Ohio, August 1988

[54] BATISTA J., VISE J., YOUNG K., *Roll Ring Assemblies for the Space Station*, Honeywell Inc., N94-33294, Phoenix, Arizona, 1994

[55] *Diamond Roll-Rings, The Next Generation Slip Rings*, Diamond-Roltran Inc., Littleton, Massachusetts, USA

[56] HEINRICH B., ZEMANN J., ROTTMEIER F., *Development of the Bepi Colombo MPO Solar Array Drive Assembly (SADA)*, RUAG, 14th European Space Mechanisms & Tribology Symposium, September 2011

[57] FATEMI N.S., POLLARD H.E., HOU H.Q., SHARPS P.R., *Solar Array Trades Between Very High-Efficiency Multi-Junction And Si Space Solar Cells*, Emcore Photovoltaics, Albuquerque, September 2000

[58] CHO B., LUTZ R., PAPPAN J., DOWNARD E., CORNFELD A., FATEMI N., STAN M.A., SHARPS P., SU C., BILLETS S., GASNER S., HOWARD A., *IMM Experimentation in the Next Frontier: Emcore's Participation in the MISSE-8 Program*, Emcore Photovoltaics, Albuquerque, 2010

[59] KING L.B., GALLIMORE A.D., *Ion-Energy Diagnostics in the Plasma Exhaust Plume of a Hall Thruster*, Journal of Propulsion and Power, Vol. 16, No. 5, September-October 2000

[60] HOSKINS W.A., HOMIAK D., CASSADY R.J., KERSLAKE T., PETERSON T., ET AL. *Direct Drive Hall Thruster System Development*, American Institute of Aeronautics and Astronautics, AIAA-2003-4726, Huntsville, Alabama, USA, July 2003

[61] SNYDER J.S., BROPHY J.R., HOFER R.R., GOEBEL D.M., KATZ I., *Experimental Investigation of a Direct-Drive Hall Thruster and Solar Array System at Power Levels up to 10 kW*, American Institute of Aeronautics and Astronautics, AIAA-2012-4068, Jet Propulsion Laboratory, Pasadena, California, USA, August 2012

[62] BOEUF J.P., GARRIGUES L., *Low frequency oscillations in a stationary plasma thruster*, American Institute of Physics, Journal of Applied Physics, Volume 84, Number 7, October 1998

[63] BARRAL S., MAKOWSKI K., PERADZYNSKI Z., GASCON N., DUDECK M., *Numerical Study of the Current-Voltage Characteristic of Hall Thrusters*, Institute of Fundamental Technological Research - Polish Academy of Science, Electric Rocket Propulsion Society, IEPC-01-27, 2001

[64] PETERSON P.Y., JACOBSON D.T., MANZELLA D.H., JOHN J.W., *The Performance*

and Wear Characterization of a High-Power High-Isp NASA Hall Thruster, American Institute of Aeronautics and Astronautics, AIAA-2005-4243, Tucson, Arizona, USA, July 2005

[65] MANZELLA D.H., JANKOVSKY R.S., HOFER R.R., *Laboratory Model 50kW Hall Thruster*, American Institute of Aeronautics and Astronautics, AIAA-2002-3676, Indianapolis, Indiana, USA, July 2002

[66] KWON K. *A Novel Numerical Analysis of Hall Effect Thruster and its Application in Simultaneous Design of Thruster and Optimal Low-Thrust Trajectory*, Georgia Institute of Technology, August 2010

[67] SOULAS G.C., HAAG T.W., HERMAN D.A., HUANG W., KAMHAWI H., SHASTRY R., *Performance Test Results of the NASA-457M v2 Hall Thruster*, American Institute of Aeronautics and Astronautics, AIAA-2012-3940, Atlanta, Georgia, USA, August 2012

[68] POLK J., *High Power Electric Propulsion for Deep Space Missions*, Jet Propulsion Laboratory, California Institute of Technology, January 2011

[69] ROSSETTI P., CASAREGOLA C., ANDRENUCCI M., *30kW-Class Hall Thruster: a Key Building Block for Propulsion Needs of Future Space Transportation and Exploration*, International Electric Propulsion Conference, IEPC-2011-211, Alta SpA, Pisa, Italy, September 2011

[70] ZURBACH S., CORNU N., LASGORCEIX P., *Performance Evaluation of a 20 kW Hall Effect Thruster*, International Electric Propulsion Conference, Snecma Safran Group, Vernon, France, September 2011

[71] SNYDER J.S., RANDOLPH T.M., HOFER R.R., GOEBEL D.M., *Simplified Ion Thruster Xenon Feed System For NASA Science Missions*, International Electric Propulsion Conference, IEPC-2009-064, Jet Propulsion Laboratory, Pasadena, California, USA, September 2009

[72] BROPHY J.R., MARCUCCI M.G., GANAPATHI G.B., GARNER C.E., HENRY M.D., NAKAZONO B., NOON D., *The Ion Propulsion System for Dawn*, American Institute of Aeronautics and Astronautics, AIAA-2003-4542, Jet Propulsion Laboratory, Pasadena, California, USA, 2003

[73] KUGELBERG J., BODIN P., PERSSON S., RATHSMAN P., *Accommodating electric propulsion on SMART-1*, Acta Astronautica 55 (2004) 121-130, Swedish Space Corporation, Stockholm, Sweden, April 2004

[74] SZABO J., ROBIN M., PAINTAL S., POTE B., HRUBY V., *High Density Hall Thruster Propellant Investigations*, American Institute of Aeronautics and Astronautics, AIAA-2012-3853, Busek Co. Inc, Natick, Massachusetts, USA, August 2012

[75] ATZEI A., LYGVI A., WIELDERS A., *Margin Philosophy for Science Assessment Studies*, ESA - European Space Agency, SCI-PA/2007/022, November 2007

[76] ZANDBERGEN B.T.C., *Lecture notes: Thermal Rocket Propulsion*, University of Technology Delft, AE4-S01, Delft, January 2010

[77] WAKKER K.F., *Lecture notes: Astrodynamics II*, University of Technology Delft, Faculty of Aerospace Engineering, AE4-874, Part 2, August 2007

[78] ENCYCLOPEDIA ASTRONAUTICA, www.astronautix.com, Last-accessed: May 2012

[79] ZANDBERGEN B., ET AL., *Space Systems Engineering*, TU Delft, http://www.sse.lr.tudelft.nl/nl/organisatie/afdelingen-en-leerstoelen/space-engineering/space-systems-engineering/, Last-accessed: May 2012

[80] *Delta-v (velocity increment) budget*, TU Delft, http://www.sse.lr.tudelft.nl/organisatie/afdelingen-en-leerstoelen/space-engineering/space-systems-engineering/expertise-areas/spacecraft-engineering/blind-documents/delta-v-velocity-increment-budget/, Last-accessed: June 2012

[81] *Comparison of orbital launch systems*, Wikipedia, htttp://en.wikipedia.org/wiki/Comparison_of_orbital_launch_systems, Last-accessed: April 2012

[82] *Falcon Heavy Overview*, SpaceX, www.spacex.com/falcon_heavy.php, Last-accessed: April 2012

[83] *Automated Transfer Vehicle - ATV configuration*, ESA, www.esa.int/SPECIALS/ATV/SEM4RYOR4CF_0.html, March 2010, Last-accessed: October 2012

[84] *International Space Station*, Space Systems/Loral, Palo Alto, California, USA, http://www.ssloral.com/downloads/products/ispacest.pdf, Last-accessed: September 2012

[85] *Xenon Availability and Pricing*, U.S. Department of Energy, www1.eere.energy.gov/buildings/appliance_standards/residential/pdfs/app_3b_lamps_standards_final_tsd.pdf, July 2009, Last-accessed: September 2012

[86] NIST Chemistry WebBook, National Institute of Standards and Technology, www.webbook.nist.gov, Last-accessed: September 2012

[87] *Lithium-ion: Space VES cell range - Rechargeable battery*, SAFT, www.saftbatteries.com/Produit_Space_VES_cell_range_301_58/Default.aspx#DL2, Last-accessed: September 2012

[88] *Power Conditioning Unit Next Generation*, Thales Alenia Space, www.thalesgroup.com/Portofolio/Documents/Power_Conditioning_Unit_Next_Generation/, May 2012, Last-accessed: September 2012

[89] *Aluminum 7075-T73*, ASM Aerospace Specification Metals Inc., www.asm.

matweb.com/search/SpecifiMaterial.asp?bassnum=MA7075T73, Last-accessed: October 2012

[90] *International Berthing Docking Mechanism (IBDM) - European Docking System for the ISS*, ESA, Doc. Nr: ESA-HSF-COU-026, Rev. 2.0, www.esamultimedia.esa.int/docs/hsf_research/ISS_User_guide/FS052_10_IBDM.pdf, Last-accessed: October 2012

[91] LUPO C., *NDS Configuration and Requirements Changes since Nov 2010*, NASA, www.dockingstandard.nasa.gov/Documents/Configuration-Changes-post-CDR-public-revA.pdf, June 2011, Last-accessed: October 2012

[92] *Solar Array Drive Mechanisms*, RUAG, http://www.ruag.com/space/Products/Satellite_Structures2C_Mechanisms_Mechanical_Equipment/Satellite_Mechanisms/Solar_Array_Drive_Mechanisms2012, Last-accessed: October 2012

[93] *Solar Array Drive Mechanisms*, Astrium, http://www.astrium.eads.net/en/equipment/solar-array-drive-mechanisms-sadms.html, Last-accessed: October 2012

[94] *Solar Array and Drive Mechanisms*, Thales Alenia Space, http://www.thalesgroup.com/Portfolio/Space/space_product_solar-array_drive_deploy_mechanisms/?pid=1500, Last-accessed: October 2012

[95] *Mass-Optimized UltraFlex Solar Array with Integrated IMM Cell Flexible Blanket*, NASA SBIR/STTR - Deployable Space Systems Inc. http://www.sbir.gov/sbirsearch/detail/16067, 2010, Last-accessed: October 2012

[96] *SPENVIS - The Space Environment Information System*, ESA, http://www.spenvis.oma.be/, April 2012, Last-accessed: October 2012

[97] *High Speed Data Recorder*, Surrey Satellite Technology, http://www.sstl.co.uk/Downloads/Datasheets/HSDR_0118021_v116, July 2009, Last-accessed: November 2012

A. Validation and Results of the Spiral Program

A.1. Validation of Keplerian Parameters

To make an initial validation of the Spiral program a comparison of the shown behavior with the theory is needed. Therefore five simulation cases are defined to see if the program is behaving as expected.

The cases one to three are simulated with a predefined amount of fuel and therefore the simulation is stopped when 3,000 kg of fuel is burned. For case 2, it is assumed that the Earth' shadow is at the other side of the Earth at the moment the spacecraft starts firing. The shadow is rotating around the Earth with a period of one year. The cases four and five are stopped when the Moon's sphere of influence is reached. The specific impulse is for every case equal to 2800 s. In table A.1 the initial values for every simulation case can be found.

Variable	Case 1	Case 2	Case 3	Case 4	Case 5
Initial mass (kg)	50,000	50,000	50,000	50,000	50,000
Initial height (km)	1,000	1,000	10,000	200	35,786
Initial orbit (km)	7,371	7,371	16,371	6,571	42,157
Target orbit (km)	-	-	-	319,902	319,902
Time interval (s)	200	200	200	200	200
Initial burn time (s)	5,400	5,400	5,400	5,400	5,400
Propellant mass (kg)	3,000	3,000	3,000	-	-
Eclipse	No	Yes	No	No	No

Table A.1.: Different Test Cases

The simulations gave some interesting results (see table A.2) and show an unexpected behavior for the end value of the semi-major axis of case two, which is higher than that of case one. This can be explained by using the ideal Hohmann transfer, the eccentricity and orbital energy.

In the ideal case, an impulsive shot will result in an eccentricity increase and therefore an elliptical orbit. When another impulsive shot is applied in the apogee, the eccentricity is decreasing and the orbit is becoming circular again. With the behavior of the

eccentricity in the ideal case in mind, the spiral case can be discussed. The change of the eccentricity in time can be expressed by the variation of parameters equation in the Gaussian form [4], considering only tangential accelerations:

$$\frac{de}{dt} = \frac{\sqrt{1-e^2}}{\sqrt{\frac{\mu}{a}}} \left(\cos(\nu) + \frac{e+\cos\nu}{1+e\cos\nu} \right) \frac{F_t}{M} \tag{A.1}$$

The formula shows that when a tangential force, and therefore acceleration, is applied, the eccentricity changes. This change has a phase, frequency and amplitude (see A.1). In figure A.2 the oscillation of the eccentricity can be seen. It shows that the short periodic disturbance is equal to the orbital period of the satellite. The formula also illustrates that the eccentricity is depending on the acceleration and semi-major axis. So the exponential increase of the eccentricity is explained by the growing semi-major axis and acceleration.

Case	F (N)	M_p (kg)	ΔV (m/s)	R_{end} (km)	V_{end} (km/s)	e $(-)$	a (km)	t (days)
1	2	3000.2	1699	12465.7	5.655	0.0000	12465.6	476.8
1	4	3000.2	1699	12465.7	5.655	0.0001	12465.6	238.4
1	8	3000.2	1699	12465.4	5.656	0.0002	12465.6	119.2
1	16	3001.8	1700	12470.1	5.654	0.0002	12469.6	59.6
2	2	3000.0	1699	12662.7	5.567	0.0174	12468.3	632.0
2	4	3000.0	1699	12701.2	5.551	0.0200	12473.8	316.4
2	8	3000.0	1699	12577.6	5.621	0.0920	12536.5	159.5
2	16	3000.1	1699	12264.2	5.774	0.1231	12584.2	80.3
3	2	3000.2	1699	38078.7	3.236	0.0003	38078.4	476.8
3	4	3000.2	1699	38078.0	3.236	0.0007	38078.4	238.4
3	8	3000.2	1699	38072.9	3.236	0.0012	38078.4	119.2
3	16	3001.8	1700	38090.7	3.236	0.0023	38100.1	59.6
4	2	10638	6569	326344	1.106	0.0271	326823	1690.4
4	4	10641	6571	326511	1.108	0.0538	328370	845.4
4	8	10650	6577	326754	1.116	0.1054	333589	423.1
4	16	10673	6593	326794	1.141	0.2006	350028	212.0
5	2	3462.0	1970.3	326301	1.106	0.0228	326606	550.1
5	4	3464.4	1971.7	326342	1.108	0.0458	327726	275.3
5	8	3472.2	1976.3	326792	1.113	0.0897	331645	137.9
5	16	3492.7	1988.4	326369	1.132	0.1708	343398	69.4

Table A.2.: End results for the different simulation cases

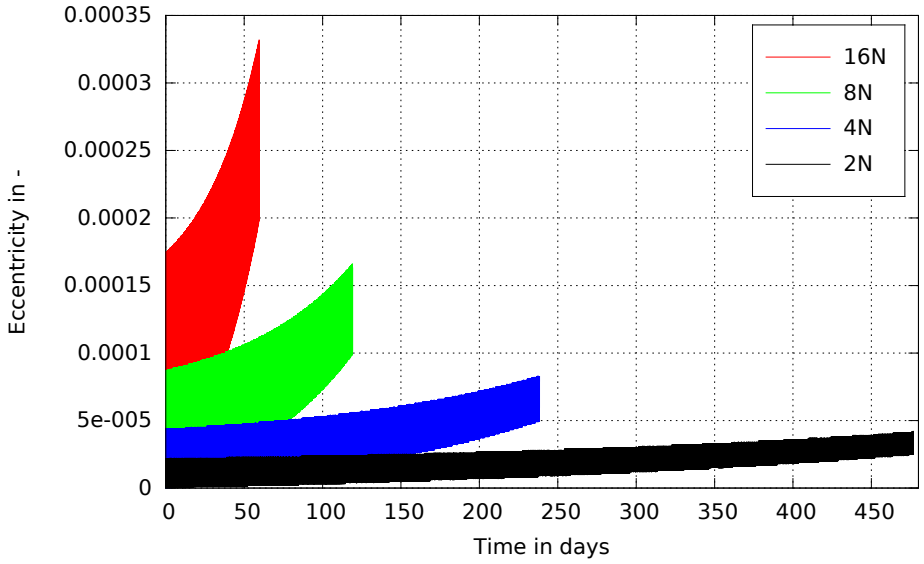

Figure A.1.: Case 1 - Change of eccentricity over time

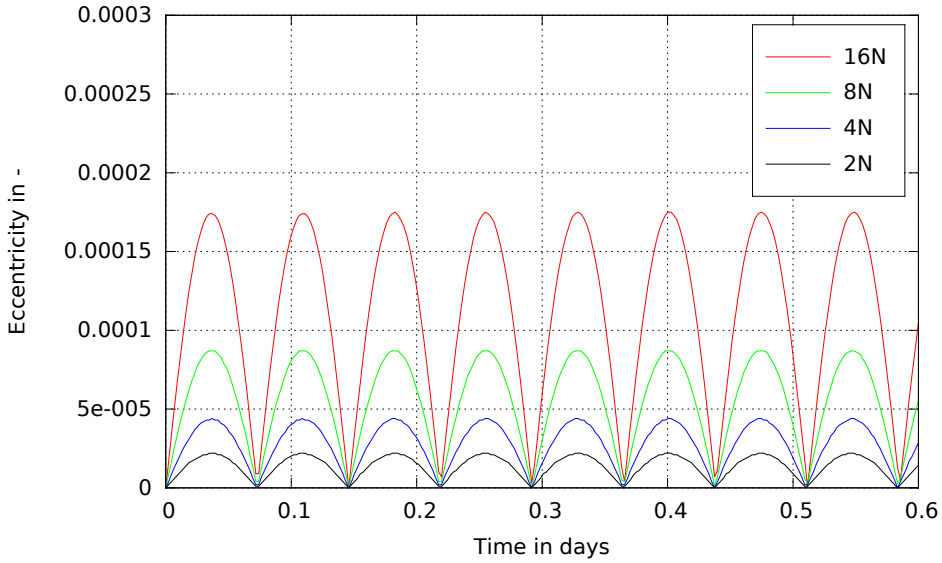

Figure A.2.: Case 1 - Change of eccentricity over for one day

If no thrust is applied in the Earth shadow, a new long periodic disturbance is added to the eccentricity with a period of one year, as seen in figure A.3. Figure A.4 indicates that when the satellite is in the shadow, there is no change in the eccentricity. In the beginning of the simulation this causes the eccentricity to increase rapidly, while after 180 days the effect is reversed and the eccentricity decreases (see figure A.5). This long periodic behavior explains why the eccentricity for this case is so much higher as for case one.

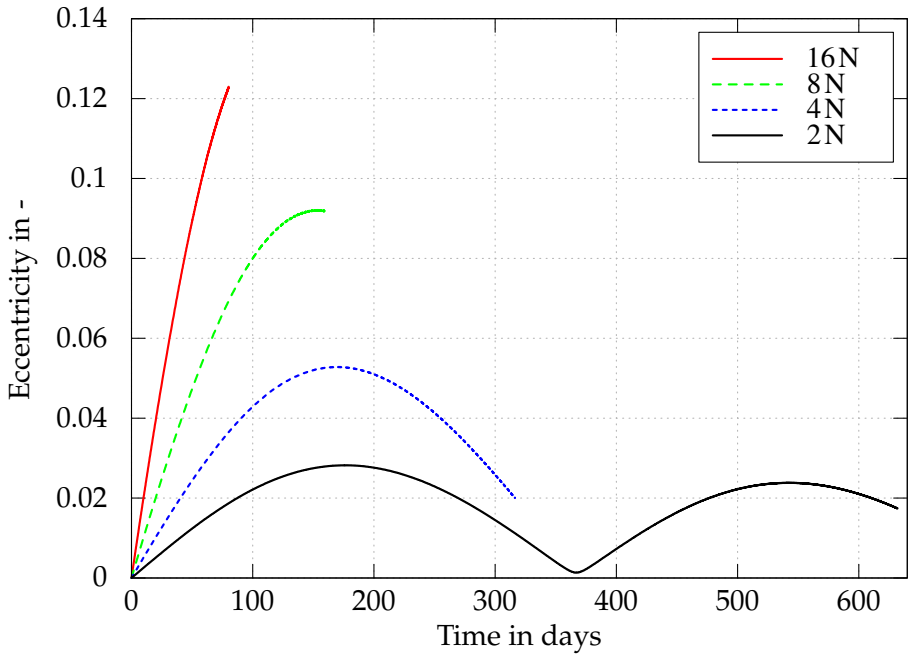

Figure A.3.: Case 2 - Change of eccentricity over time

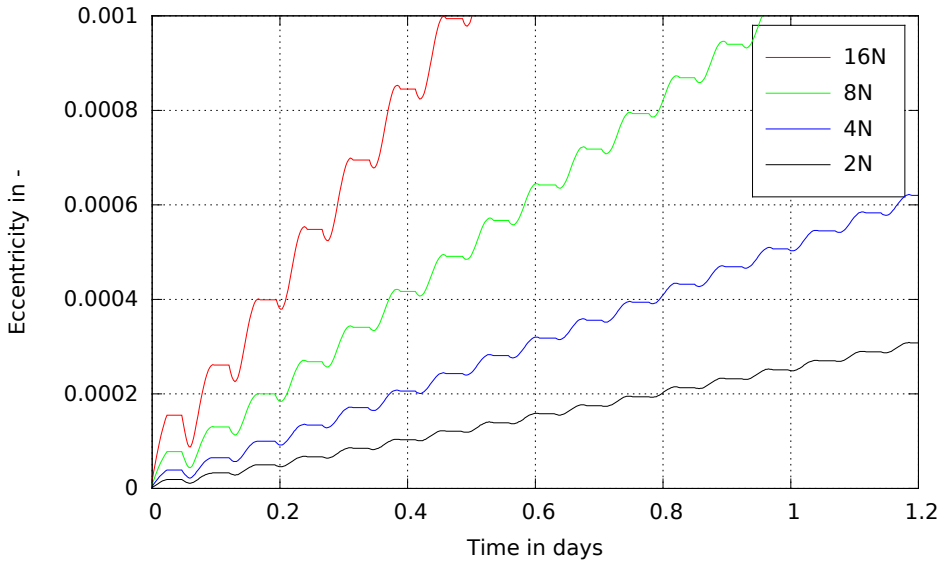

Figure A.4.: Case 2 - Change of eccentricity over time for one day

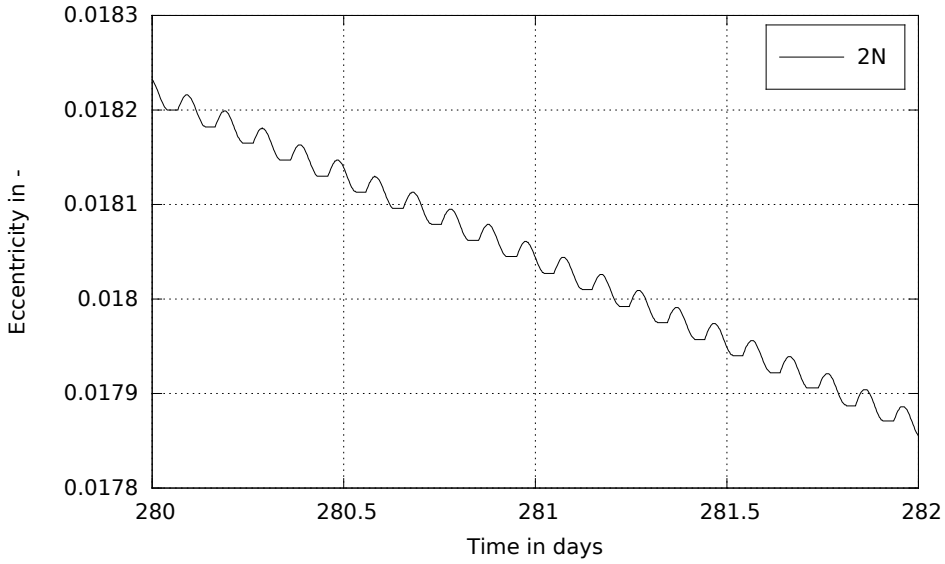

Figure A.5.: Case 2 - Change of eccentricity over time for two days

To explain why the semi-major axis is higher for case two a closer look is taken at the orbital energy:

$$C = \frac{v^2}{2} - \frac{\mu}{r} \tag{A.2}$$

In case an elliptical orbit is assumed with a perigee and apogee, the change in energy at the perigee side from one orbit to the next is:

$$\Delta C_p = C_{p1} - C_{p0} = \frac{\left(v_{p0} + \Delta v\right)^2}{2} - \frac{v_{p0}^2}{2} + \mu \left(\frac{1}{r_0} - \frac{1}{r_1}\right) \tag{A.3}$$

If we neglect the change in radius, which is especially at LEO orbits very small, and only focus on the velocity, the orbital energy change is equal to:

$$\Delta C_p = v_{p0}\Delta v + \frac{\Delta v^2}{2} \tag{A.4}$$

The same procedure can be applied for the orbital energy change in the apogee:

$$\Delta C_a = v_{a0}\Delta v + \frac{\Delta v^2}{2} \tag{A.5}$$

Now considering the fact that the velocity in perigee is larger than in apogee, a logical conclusion is:

$$\Delta C_p > \Delta C_a \tag{A.6}$$

In simulation case two the engines do not give thrust in the eclipse, which is positioned

in the apogee. This means that more propellant is burned in the perigee region and as a logical consequence the increase in orbital energy is for case two higher than for case one. This explains the higher semi-major axis. Together with the higher eccentricity for the eclipse case, it can be concluded that:

$$\left(\frac{dC}{dt}\right)_{eclipse} > \left(\frac{dC}{dt}\right)_{no-eclipse} \tag{A.7}$$

The comparison between case one and three shows that the initial orbit has a large impact on how much the orbit is raised by using a predefined amount of fuel. In case one the orbit is raised by 5,095 km, while for case three the orbit is raised by 21,708 km. It is expected that in case three the relative decrease in orbital energy is larger than in case one. The change in orbital energy for both cases, normalized to their initial orbit, is:

$$\frac{\Delta C_1}{C_{1-initial}} = \frac{1}{C_{1-initial}}\left[\frac{v_{end}^2}{2} - \frac{v_{initial}^2}{2} + \mu\left(\frac{1}{r_{initial}} - \frac{1}{r_{end}}\right)\right] = \frac{11,052,970}{-27,066,883} = -0.41 \tag{A.8}$$

$$\frac{\Delta C_3}{C_{3-initial}} = \frac{1}{C_{3-initial}}\left[\frac{v_{end}^2}{2} - \frac{v_{initial}^2}{2} + \mu\left(\frac{1}{r_{initial}} - \frac{1}{r_{end}}\right)\right] = \frac{6,941,671}{-12,176,861} = -0.57 \tag{A.9}$$

This shows that at an higher orbit less propellant is required to make a certain orbital energy change. This is logical since the effect of gravity decreases with increasing height.

The same can be seen when comparing case four and case five. In these simulations the radius propagates until the sphere of influence of the Moon is reached. It shows that roughly three times less propellant mass is required in case the initial orbit is GEO instead of LEO.

The eccentricity plots of case three to five, can be seen in figure A.6 to A.8. They all behave the similar to the first case. In case four and five it can be seen that the exponential increase of the eccentricity becomes more dominant when moving further away from the Earth, see equation A.1.

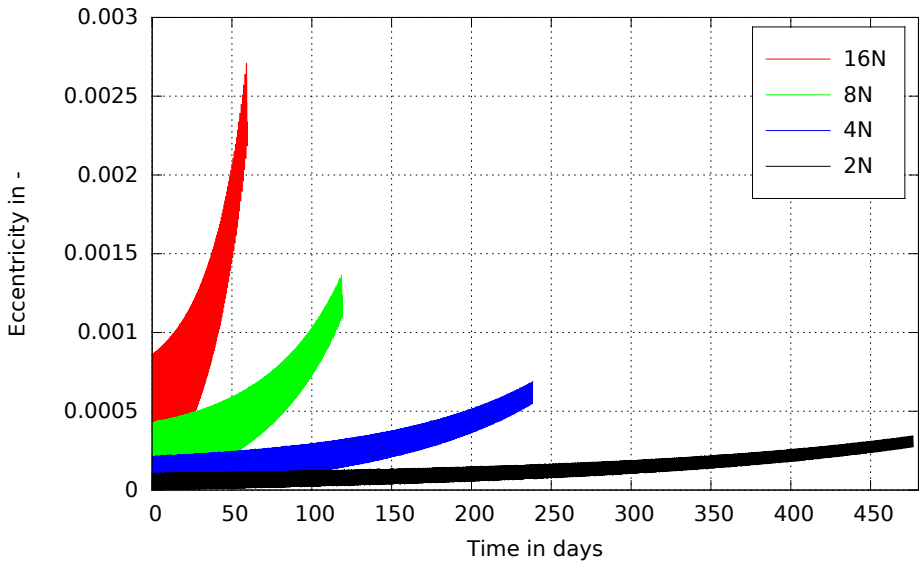

Figure A.6.: Case 3 - Change of eccentricity over time

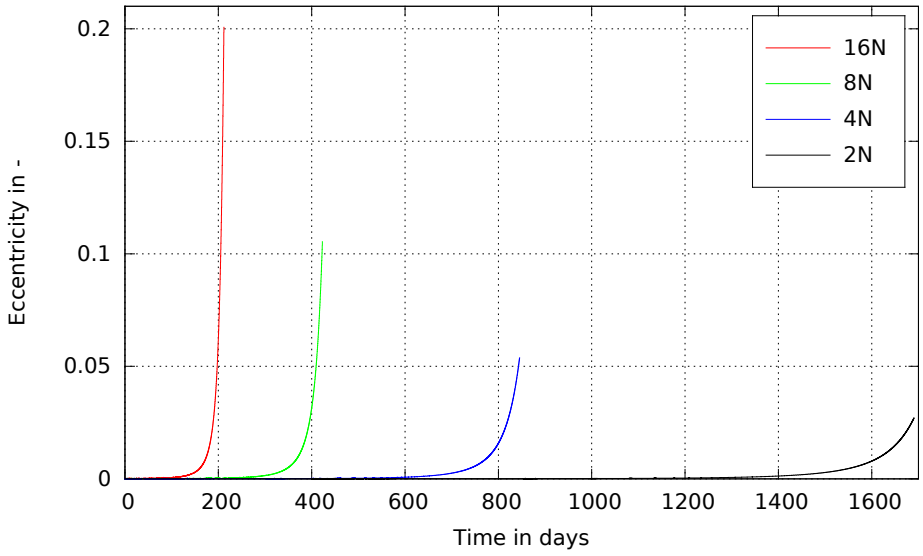

Figure A.7.: Case 4 - Change of eccentricity over time

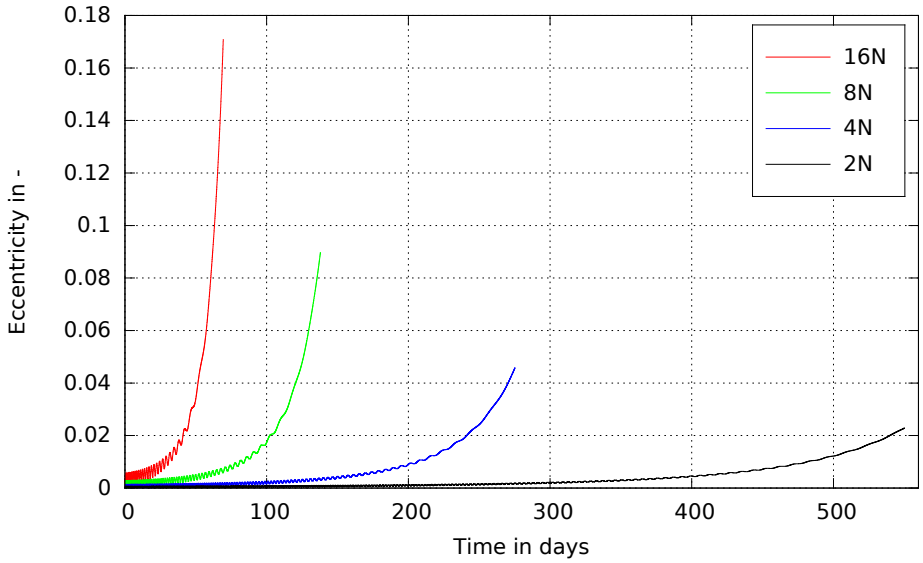

Figure A.8.: Case 5 - Change of eccentricity over time

All the plots of how the semi-major axis is behaving over time can be seen from figure A.9 to A.13. The change of the semi-major axis in time can also be expressed by the variation of parameters equation in the Gaussian form [4], considering only tangential accelerations:

$$\frac{da}{dt} = \frac{2}{\sqrt{\frac{\mu}{a^3}}\sqrt{1-e^2}}\left(1+e\cos(\nu)\right)\frac{F_t}{M} \tag{A.10}$$

Just as with the eccentricity, the semi-major axis changes when a tangential force is applied. The second term within brackets is very small, because of the small eccentricity in a spiral transfer. Therefore this periodic behavior is not seen in the results. The change of the semi-major axis is mainly dominated by the acceleration and by the semi-major axis itself. The higher the semi-major axis, the smaller the effect of gravity upon the spacecraft. This fact, together with the growing acceleration, explains the exponential growth of the semi-major axis, which can be seen in the figures.

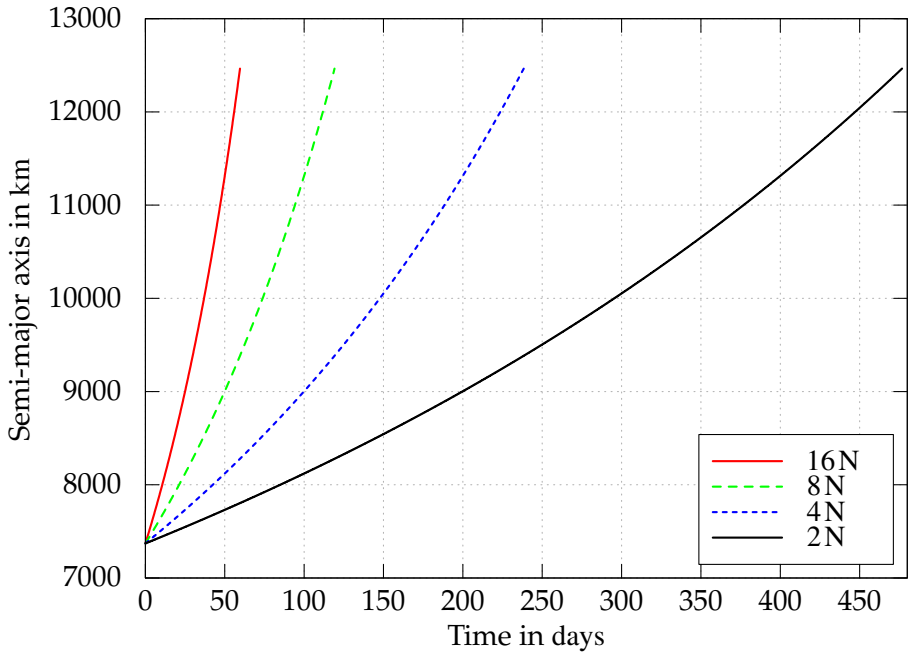

Figure A.9.: Case 1 - Change of semi-major axis over time

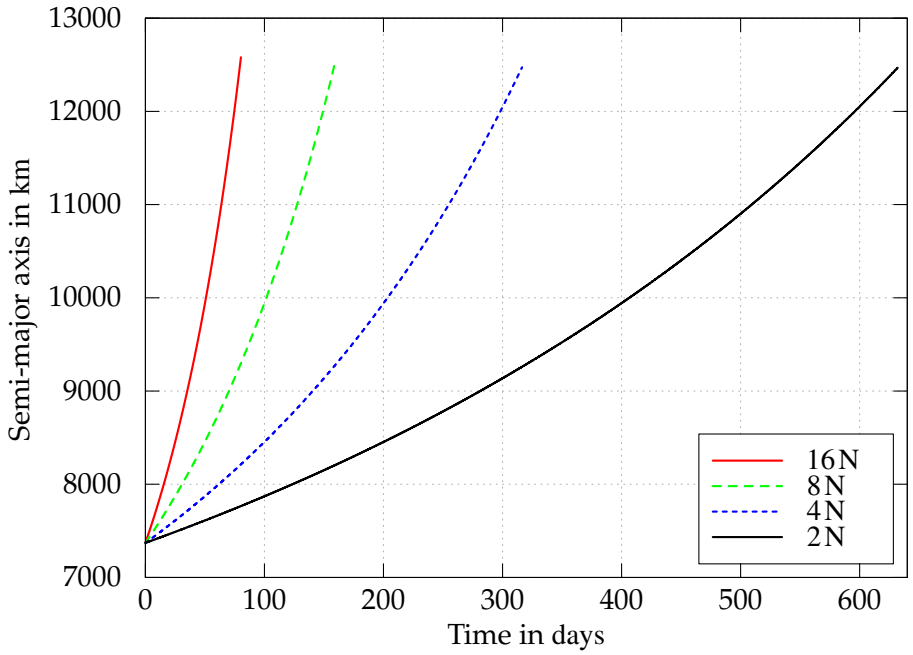

Figure A.10.: Case 2 - Change of semi-major axis over time

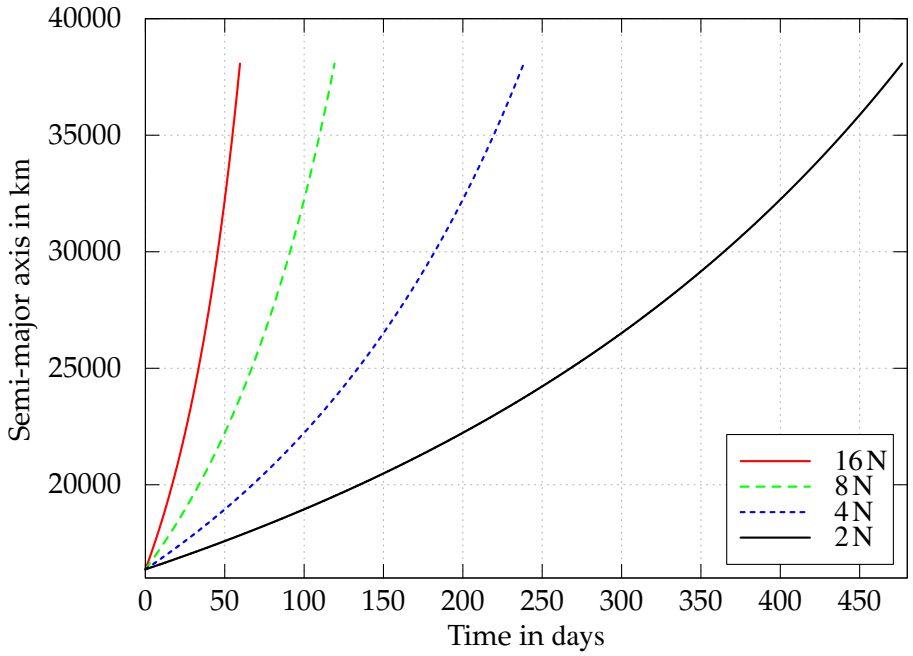

Figure A.11.: Case 3 - Change of semi-major axis over time

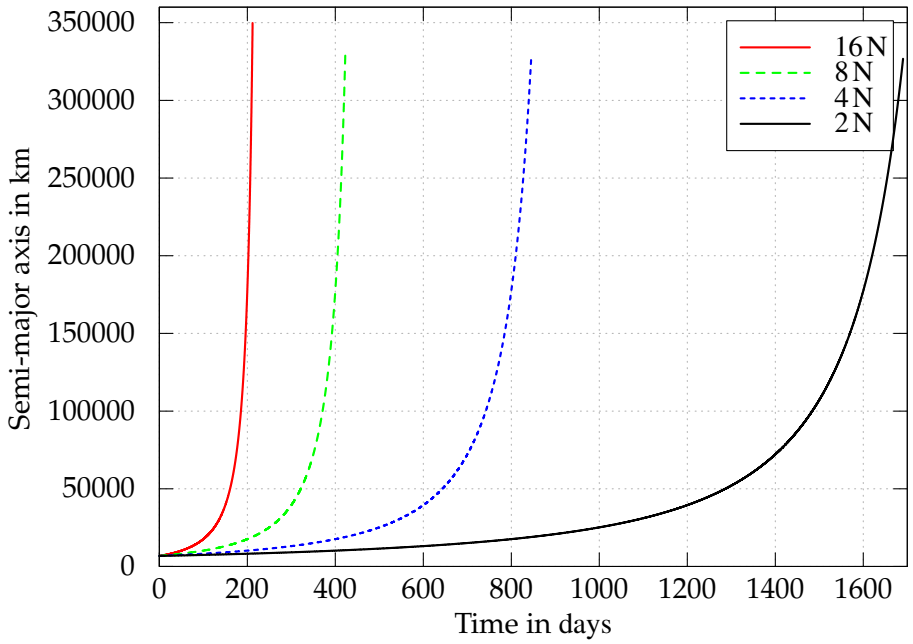

Figure A.12.: Case 4 - Change of semi-major axis over time

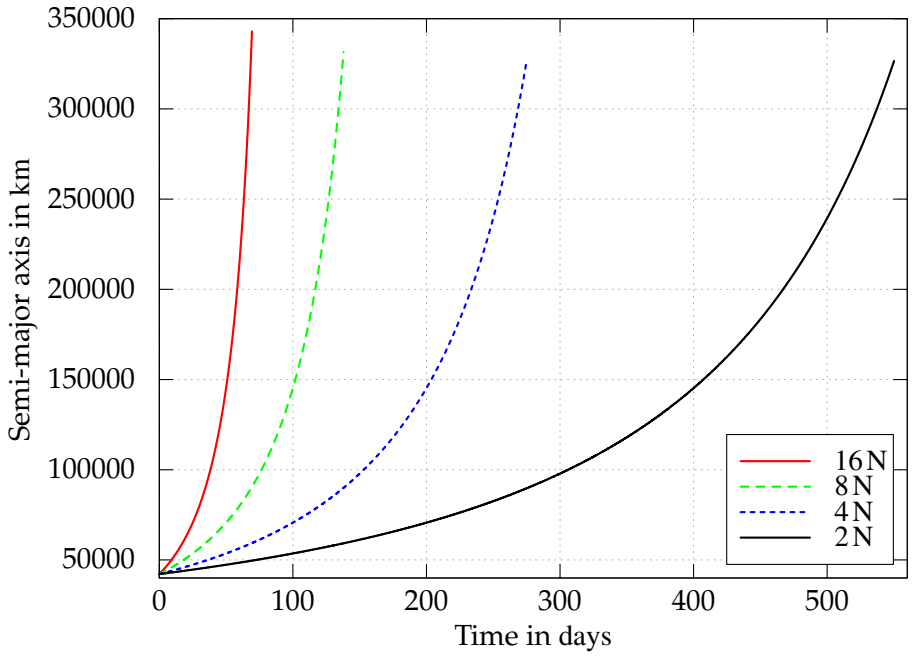

Figure A.13.: Case 5 - Change of semi-major axis over time

For case one and two also the polar plots of the trajectory are shown for illustration purposes (see figure A.14 and A.15). The black part in the second figure indicates the part of the eclipse. The plots show an expected behavior of a very slowly increasing radius of the orbit, resulting in a 'donut' shaped plot.

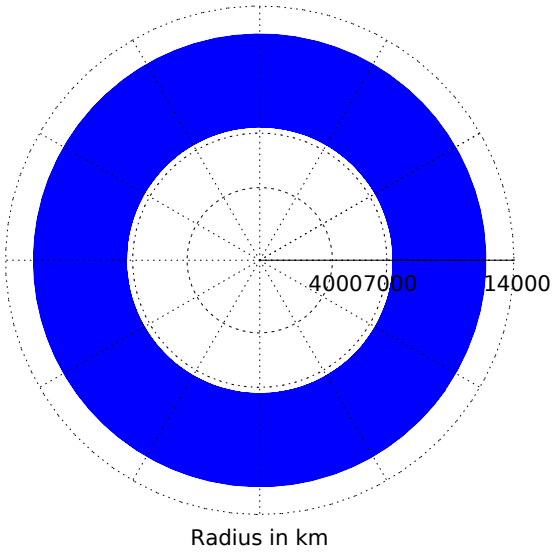

Figure A.14.: Case 1 - Polar plot of the trajectory

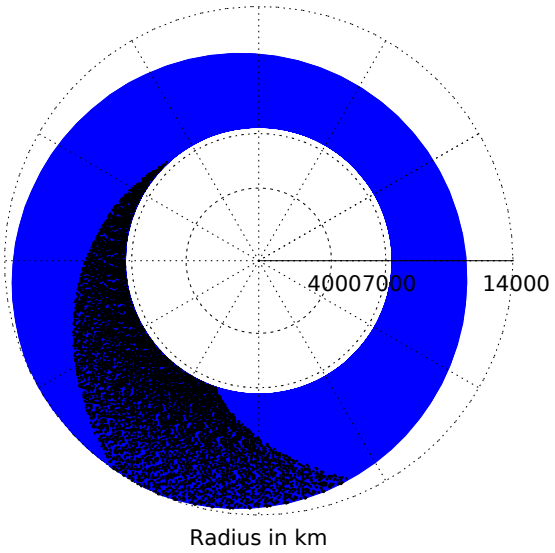

Figure A.15.: Case 2 - Polar plot of the trajectory with eclipse

A.2. Spiral Program Simulations

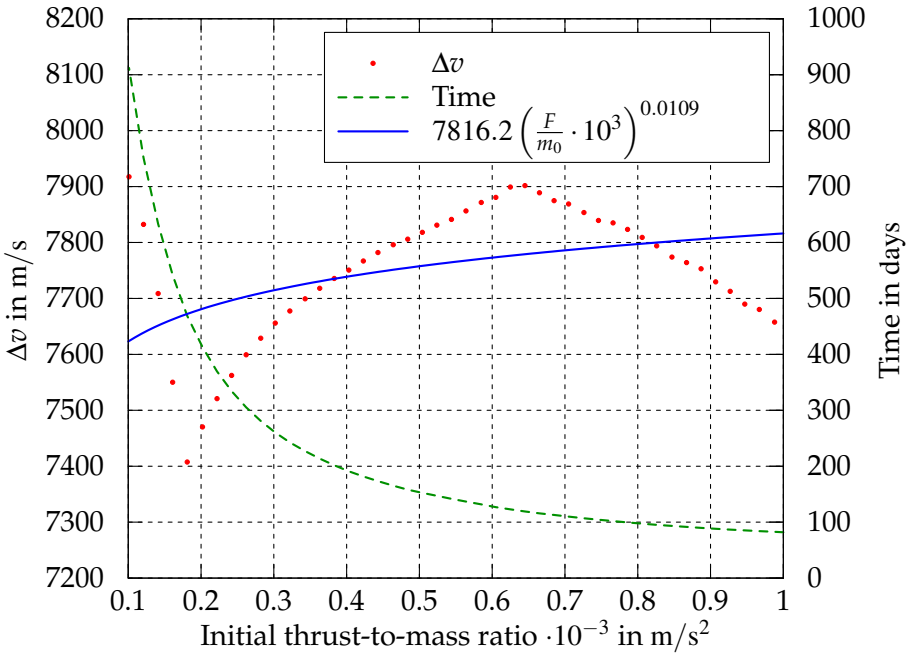

Figure A.16.: The time and Δv to go from LEO to LLO, as function of the initial acceleration for an I_{sp} of 2,000s, while the engines are fired continuously (also in eclipse).

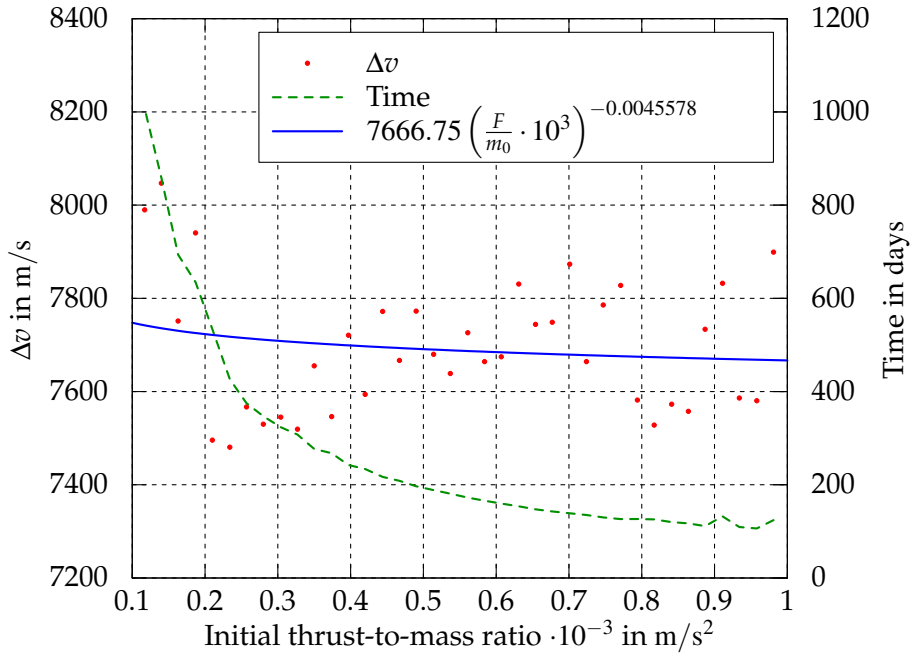

Figure A.17.: The time and Δv as function of the initial acceleration for an I_{sp} of 2,500s.

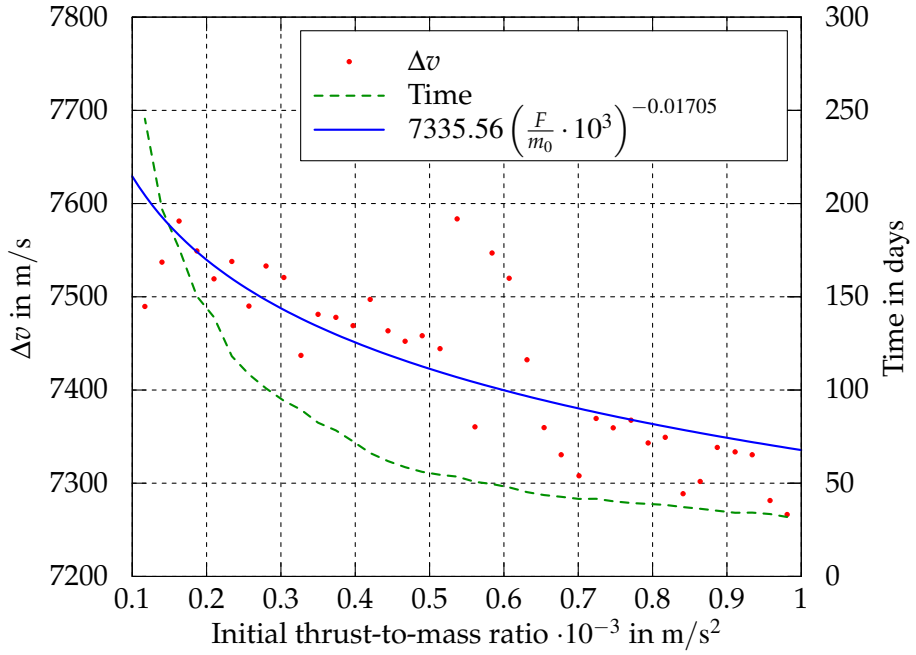

Figure A.18.: The time and Δv to return from LLO to LEO, as function of the initial acceleration for an I_{sp} of 2,500s.

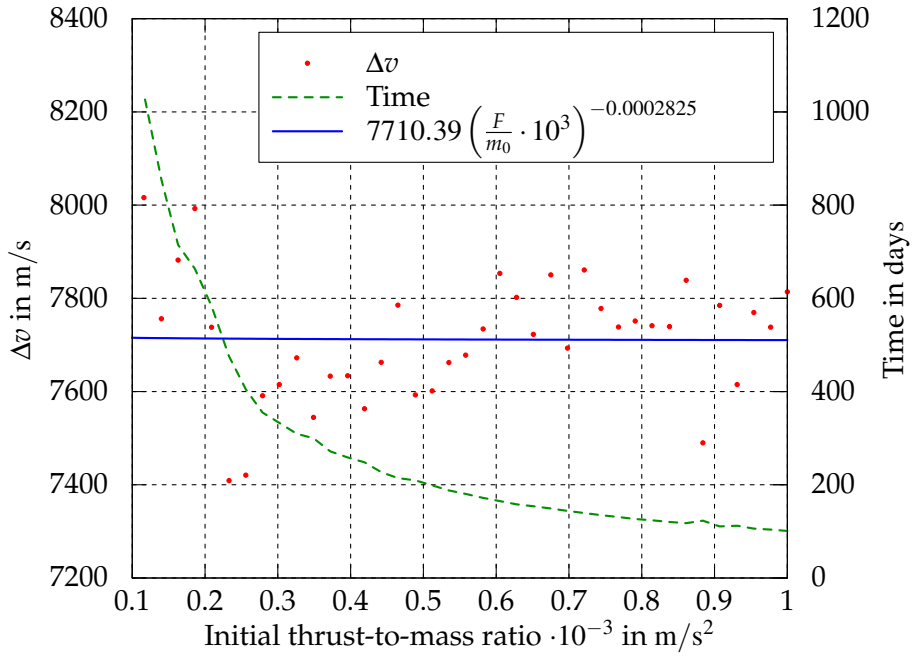

Figure A.19.: The time and Δv as function of the initial acceleration for an I_{sp} of 3,300s.

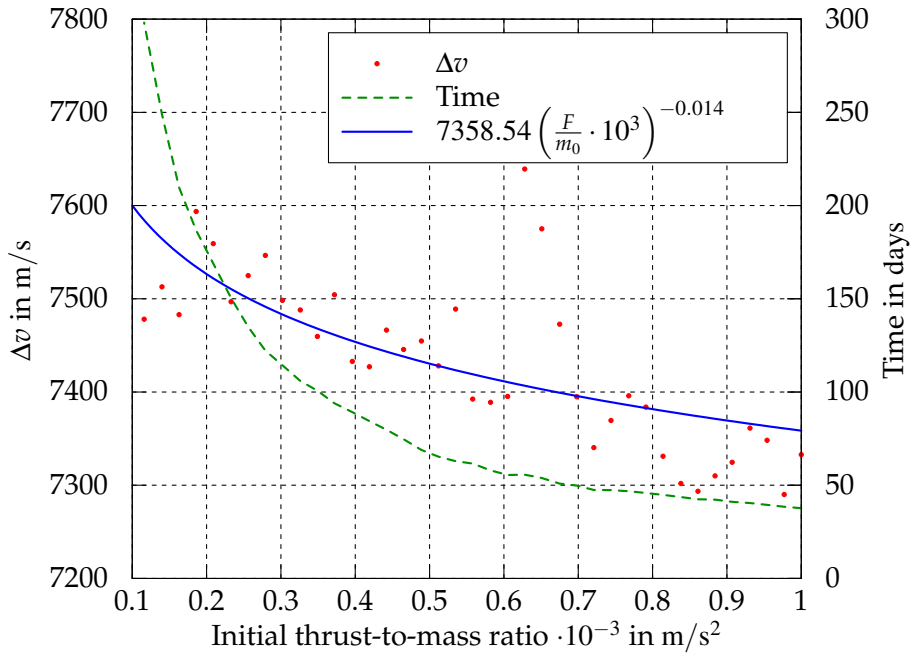

Figure A.20.: The time and Δv to return from LLO to LEO, as function of the initial acceleration for an I_{sp} of 3,300s.

B. Data

B.1. Solar Array Drive Mechanisms

SADM	Manufacturer	Type	Power (kW)	Mass (kg)	MRS (°/s)	NoR
BGA (ISS)	Honeywell	RR	45	24	5.73	
HP SADM	Astrium		26			5,475
High Power	Thales	SR	15	4.396		
Low Power	Thales	SR	4.5	4.31		
MP SADM	Astrium		9.9			5,475
RR C4	NASA LRC	RR	200		0.067	315,000
RR C8	NASA LRC	RR	400		0.067	599,000
SARJ (ISS)	Honeywell	RR	65.5	136	0.498	
SEPTA-14	RUAG		14	45		
SEPTA-23	RUAG	SR	4-9	6		
SEPTA-24	RUAG	SR	19.8	6	0.75	12,000
SEPTA-31	RUAG	SR	1-2	2.7	1	35,000
SEPTA-32	RUAG	SR	2-3	3.5	1	35,000
SEPTA-33CS		SR	2	4	0.4	
SEPTA-41		SR	0.8	1.5		
Type 2	NT Aerospace		7.5	22		

SR: Slip Ring RR: Roll Ring LRC: Lewis Research Center
MRS: Maximum Rotation Speed NoR: Number of Revolutions

Table B.1.: Database of Solar Array Drive Mechanisms [53] [54] [92] [93] [94].

B.2. Hall Thrusters

Engine	Type	F (N)	P (kW)	I_{sp} (s)	$\frac{F}{P}$ (mN/kW)	η (−)	m (kg)	OL (hrs)
BHT-10k	HT	0.556	10	2200	55.6			
BHT-20k	HT	1.08	20	2750	54.0	0.7		
BHT-8000	HT	0.512	8	1900	64.0		20	
BHT-RT-1500	RHT	0.15	4	2230	37.5	0.41		
BHT-RT-3000	RHT	0.2	3	1950	53.3	0.57		
BPT-2000	HT	0.12	2.2	1765	54.5	0.48	5.2	6000
BPT-4000	HT	0.27	4.5	1950	60.0	0.58	7.5	6000
D50	HT	0.048	0.8	1700	60.0			300
HET C3C	NHT	14	200	2500	70.0	0.64		
HET-300	HT	0.015	0.3	1300	50.0		1.5	1000
HIVHAC	HT	0.43	8	2800	53.8	0.62		6000
HT-30 ALTA	HT	1.55	30	2500	51.7	0.6		
NASA-1000M	HT	6.5	150	2900	43.3	0.65		30000
NASA-173GT	TSHT	0.194	5.5	1981	35.3			
NASA-300M	HT	1.1	20	2900	55.0	0.66		
NASA-400M	HT	1.02	43	4000	23.7	0.64		
NASA-457M	HT	3	50	3250	50.0	0.65	87	8000
P5 HT	HT	0.246	5	2326	49.2			
PPS-1350	HT	0.09	1.5	1660	60.0	0.55	5.3	
PPS-5000	HT	0.276	5	1763	55.2			
PPS-20k ML	HT	1	20	2500	50.0	0.6	25	
SPT-70	HT	0.04	0.7	1500	57.1	0.45	2	3000
SPT-100	HT	0.08	1.35	1600	59.3	0.5	3.5	9000
SPT-140	HT	0.3	5	1750	60.0	0.55		
SPT-290	HT	1.5	30	3300	50.0	0.65	23	27000
T-220	HT	1	20	2500	50.0			1000
VHITAL 160	TSHT	0.71	25	8000	19.7	0.79		
X2 NHT	NHT	0.46	6	2400	76.7			

OL: Operational Life HT: Hall Thruster NHT: Nested Hall Thruster
RHT: Racetrack Hall Thruster TSHT: Two Stage Hall Thruster

Table B.2.: Database of Hall Thrusters [1].

B.3. Solar Cells

Solar Cell	Company	η (%)	P_{spec} (W/kg)	A_{dens} (W/m^2)	P_{stow} (kW/m^3)	Ref.
a-Si:H SJ	SRS Tech.	9.5	1200	122	100	[34] [33]
a-Si:H SJ		12.4	5950	170		[33]
a-Si TJ		9	770			[6]
a-Si TJ		9	2750			[6]
a-Si TJ	GRC	12.0				[6]
a-Si TJ		9.5	2343			[34]
CIGS	DLR	12.7[a]				[34]
CIGS		20[a]				[34]
CIGS		18.7[a]				[34]
CIGS		8	1280			[41]
CIGS			466			[41]
CIGS			1863			[41]
GaAs DJ	Emcore	23.5	95	271		[57]
GaAs TJ	Emcore	26	108	306		[57]
GaAs TJ RP		30	45	300	15	[44]
GaAs TJ FP		30	180	300	40	[44]
GaAs TJ UF	ATK		118			[40]
GaAs TJ SLA		30	150	300	30	[44]
GaAs TJ SLA	Emcore	30	500	400	80	[34]
IMM TJ	Emcore	33	3650			[34]
IMM TJ	JAXA	24.9	4500			[34]
IMM TJ	Emcore	31.3		425		[58]
IMM TJ UF	ATK	27	175			[40]
IMM TJ UF	ATK	33	500		50	[95]
IMM 4J	Emcore	33.1		448		[58]
IMM 4J	Emcore	34.5				[37]
IMM 5J	Emcore	35.8				[37]
IMM 6J	Emcore	37.8				[37]
Si SJ	Emcore	17	75	169		[57]
Si (ISS)		14.5	30	100	1.20	[34]

a: Under AM1.5 conditions
SJ: Single Junction DJ: Double Junction TJ: Triple Junction
4J: Four Junction 5J: Five Junction 6J: Six Junction
RP: Rigid Panel FP: Flexible Panel UF: UltraFlex Panel
SLA: Stretched Lens Array GRC: NASA Glenn Research Center

Table B.3.: Database of the performance of Solar Cells under AM0 conditions.

B.4. Developed Tools

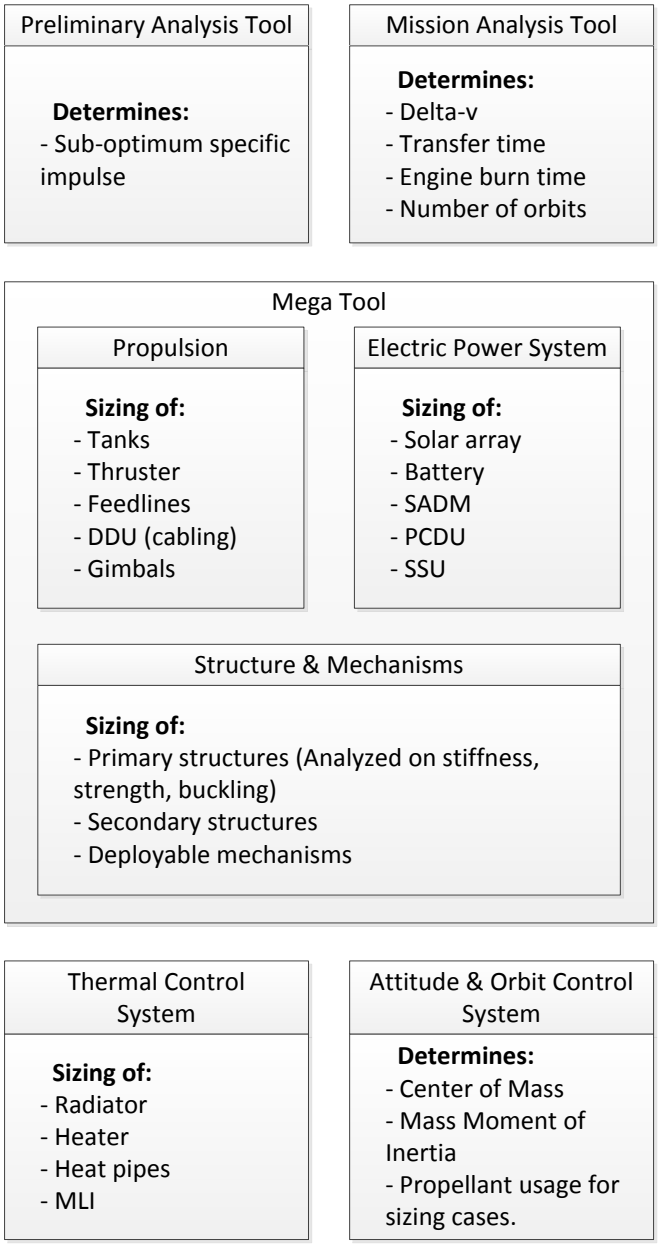

Figure B.1.: Overview of the developed tools.

C. Requirements Flow-Down

	Mission Requirement	Created	Met
1.	The transfer stage shall transport a payload of minimal 17 ton (TBC) from Earth environment to a LLO of 100×100 km within 200 days (TBD).	Sec. 2.2	Yes, Sec. 6.2
1.1	The initial orbit within the Earth environment shall be a LEO of 500×500 km.	Sec. 4.2.3	Yes, Sec. 6.2
1.2	To transfer from LEO to LLO, a Δv of 8498 m/s shall be provided by the engines.	Sec. 4.3.1	Yes, Sec. 6.2
1.3	The initial acceleration in LEO shall be $4.8 \cdot 10^{-4}$ m/s^2.	Sec. 4.3.1	Yes, Sec. 5.3.8
2.	The stage shall be reusable, meaning that the transfer stage shall return from LLO to the initial Earth orbit and perform at least two missions to LLO with the potential of extension to three missions.	Sec. 2.2	Yes, Sec. 6.2
2.1	To transfer from LLO to LEO, a Δv of 8134 m/s shall be provided by the engines.	Sec. 4.3.1	Yes, Sec. 6.2
2.2	The total transfer from LEO to LEO of a single mission shall be performed within 300 days.	Sec. 4.3.1	Yes, Sec. 6.2
3.	The transfer stage shall primarily be propelled by electric propulsion.	Sec. 2.2	Yes, Sec. 5.3
4.	The transfer stage shall be powered by solar panels as primary power source (nuclear power is excluded).	Sec. 2.2	Yes, Sec. 5.4
5.	The transfer stage and cargo should be launched together (TBC) with one super heavy lift launch vehicle (TBD). The launcher has to be available in the next decade (i.e. SLS or Falcon Heavy).	Sec. 2.2	No, Sec. 4.3.2
5.1	The transfer stage and cargo shall be launched by Falcon Heavy to a 500×500 km orbit.	Sec. 4.2.3	Yes, Sec. 6.2
5.2	The transfer stage and cargo shall be launched separately.	Sec. 4.3.2	Yes, Sec. 6.2

	Mission Requirement	Created	Met
6.	The transfer stage shall dock and un-dock with the cargo, depending on the mission architecture.	Sec. 2.2	Yes, Sec. 5.5.3
7.	The transfer stage shall follow End-of-Life regulations.	Sec. 2.2	Yes, Sec. 4.2.4
7.1	During the last mission the SEP stage shall be disposed by de-orbitting it from LLO to impact with the Moon's surface, which requires a Δv of 64.6 m/s.	Sec. 4.2.4	Yes, Sec. 5.3.5

	System Requirement	Created	Met
1.	The transfer stage shall be able to operate in deep-space environment, specifically the environment surrounding the Earth and Moon. This includes the Van Allen belts, solar radiation, solar wind, cosmic radiation, debris and (micro-) meteoroids.	Sec. 2.2	Yes, Sec. 6.2
1.1	The solar arrays shall be sized to endure, during its lifetime, a total current irradiation of $16.347 \cdot 10^{14}\,\mathrm{MeV/cm^2}$ and voltage irradiation of $21.132 \cdot 10^{14}\,\mathrm{MeV/cm^2}$.	Sec. 4.4	Yes, Sec. 5.4.7
2.	The transfer stage shall primarily be using electric propulsion.	Sec. 2.2	Yes, Sec. 5.3
2.1	The electric propulsion shall be provided by Ion or Hall thrusters, since they have the most favorable characteristics for this mission type.	Sec. 2.2	Yes, Sec. 5.2.2
2.1.1	The specific impulse of the engine shall be 2,000 s.	Sec. 4.3.1	Yes, Sec. 5.3.8
2.1.2	The initial acceleration in LEO shall be $4.8 \cdot 10^{-4}\,\mathrm{m/s^2}$.	Sec. 4.3.1	Yes, Sec. 5.3.8
2.1.3	A single engine shall operate 5,590 hrs per mission for at least two missions with the potential of extension to three missions.	Sec. 4.3.1	Yes, Sec. 5.3.8
2.1.4	The electric propulsion shall be provided by Hall thrusters.	Sec. 5.2.2	Yes, Sec. 5.3.8
2.1.5	The thrusters shall require a total power of 529 kW. The heater, keeper and magnet supply shall require 3% of this power.	Sec. 5.3.8	Yes, Sec. 5.4.6
2.2	The engine can provide thrust during eclipse.	Sec. 2.2	No, Sec. 5.4.6
2.2.1	The SEP stage requires a battery with a capacity of 2140 kWh.	Sec. 5.4.6	No, Sec. 5.4.6

	System Requirement	Created	Met
2.3	The engines should be placed such that the thruster exhaust plume is not in contact with the solar array surface, to mitigate solar array degradation.	Sec. 5.2.1	No[a], Sec. 5.3.3
2.3.1	To limit the plume impingement, the thrusters shall be placed in line with the solar array width.	Sec. 5.3.3	Yes, Sec. 5.5
2.3.2	The solar array shall be designed such that it accounts for the ion impingement losses.	Sec. 5.3.3	Yes, Sec. 5.4.7
2.4	The thruster's cathode shall operate continuously to prevent spacecraft charging, also in eclipse. A minimum power of 200 W per cathode is required.	Sec. 5.3.3	Yes, Sec. 5.4.6
2.5	The Xenon Feed System (XFS) shall transfer propellant from the tanks to the electric thrusters.	Sec. 5.3.6	Yes, Sec. 5.3.6 (TBC)
2.5.1	The XFS shall accept a inlet pressure of 12 MPa and provide a pressure of $0.245 - 0.265$ MPa (TBC) to the engines.	Sec. 5.3.6	Yes, Sec. 5.3.6
2.5.2	The XFS shall provide a maximum mass flow of 6.4 g/s and distribute it over all operating engines.	Sec. 5.3.6	TBD
3.	The transfer stage shall be powered by solar panels.	Sec. 2.2	Yes, Sec. 5.4.7
3.1	The solar array shall be deployed autonomously.	Sec. 2.2	Yes, Sec. 5.4.7
3.2	The critical systems shall be powered by batteries during eclipse time.	Sec. 2.2	Yes, Sec. 5.4.6
3.3	The EOL power generation of the solar panels shall be sufficient to maintain proper engine functionality.	Sec. 2.2	Yes, Sec. 5.4.7
3.3.1	The solar array should generate an EOL voltage of 400 V.	Sec. 5.4.7	Yes, Sec. 5.4.6
3.3.2	The solar array should generate an EOL power of 607 kW.	Sec. 5.4.6	Yes, Sec. 5.4.6
3.4	The solar array should consist out of two Solar Array Wings.	Sec. 5.2.1	Yes, Sec. 5.4.7
3.5	The solar array shall fit inside the launcher fairing.	Sec. 4.3.2	Yes, Sec. 6.2
3.6	The power system shall operate with a Direct Drive power processing Unit (DDU).	Sec. 5.2.3	Yes, Sec. 5.4.6
3.6.1	The DDU shall operate in combination with an Sequential Shunt Unit to obtain full control on the operation point.	Sec. 5.4.6	Yes, Sec. 5.4.6
3.6.2	The DDU shall contain a filter to compensate for thruster oscillations.	Sec. 5.3.8	Yes, Sec 5.4.6

a: Complete elimination of ion impingement to the solar arrays is impossible, although it is limited as much as possible.

	System Requirement	Created	Met
3.7	The power system should deliver a voltage of $300-600\,\mathrm{V}$ to the thrusters.	Sec. 5.3.8	No, Sec 5.4.6
3.7.1	A high voltage bus, operating between $400-815\,\mathrm{V}$ should deliver power to the thruster anode.	Sec. 5.4.6	Yes, Sec. 5.4.6
3.8	The Solar Array Drive Mechanism (SADM) shall provide an interface between the spacecraft and solar array.	Sec. 5.2.3	Yes, Sec. 5.4.2
3.8.1	The SADM should have one gimbal and thus be sized for off-pointing errors.	Sec. 5.4.1	Yes, Sec. 5.4.2
3.8.2	The SADM shall at least provide a total number of 4054 rotations.	Sec. 5.4.2	Yes, Sec. 5.4.2 (TBC)
3.8.3	The SADM shall have a minimum rotation speed of $0.064\,^\circ/\mathrm{s}$.	Sec. 5.4.2	Yes, Sec. 5.4.2 (TBC)
3.8.4	A single SADM shall transfer a maximum power of $569\,\mathrm{kW}$.	Sec. 5.4.2	Yes (Sec. 5.4.2)
3.9	The subsystems, payload and heater, keeper and magnet supply shall receive power from a low voltage bus operating at $50\,\mathrm{V}$ (TBC).	Sec. 5.4.6	Yes, Sec. 5.4.6
4.	The transfer stage shall have sufficient propellant capacity to perform the transfer.	Sec. 2.2	Yes, Sec. 5.3.5
4.1	The most suitable propellant from performance point of view shall be identified.	Sec. 2.2	Yes, Sec. 5.3.4
4.1.1	The transfer stage shall be propelled by Xenon.	Sec. 2.2	Yes, Sec. 5.3.4
4.2	The payload shall incorporate the propellant to transfer from LEO to LLO, for the first and final mission. For other missions, the payload shall incorporate propellant to perform the complete mission, from LEO to LEO.	Sec. 5.2.1	Yes, Sec. 5.3.5
4.3	The SEP stage's tanks shall have enough capacity to store the propellant required to transfer from LLO to LEO.	Sec. 5.2.1	Yes, Sec. 5.3.5
4.3.1	The propellant tanks should be kept at a temperature in between $20^\circ\mathrm{C}$ and $30^\circ\mathrm{C}$.	Sec. 5.3.5	Yes, Sec. 5.6 (TBC)

	System Requirement	Created	Met
4.4	The propellant tanks shall remain intact throughout the lifetime of the spacecraft	Sec. 5.3.5	TBD
4.4.1	The propellant tanks shall withstand a maximum pressure of 12 MPa.	Sec. 5.3.5	Yes, Sec. 5.3.5
4.4.2	The propellant tanks shall provide sufficient strength to carry it's own load, especially during launch.	Sec. 5.3.5	TBD
5.	The transfer stage shall provide thermal control and radiate all excess heat to space.	Sec. 2.2	Yes, Sec. 5.6.4
5.1	During eclipse, a heater shall operate at 320 W to keep the stage's temperature above 0°C	Sec. 5.6.4	Yes, Sec. 5.4.6
6.	The transfer stage shall provide a separation mechanism from its payload. Due to stage reusability, this shall be a docking mechanism to dock and un-dock with the payload.	Sec. 2.2	Yes, Sec. 5.5.3
6.1	The docking mechanism shall provide propellant transfer.	Sec. 5.2.1	Yes, Sec. 5.5.3
6.1.1	At a pressure of 12 MPa.	Sec. 5.3.6	TBD
7.	The transfer stage shall provide 3-axis attitude control during the mission.	Sec. 2.2	Yes, Sec. 5.7
7.1	Four gimbaled thrusters should provide enough agility for the stage.	Sec. 5.3.9	Yes, Sec 5.7 (TBC)
7.2	The attitude sensors shall operate at a total power of 90 W.	Sec. 5.7.1	Yes, Sec. 5.4.6
8.	The transfer stage shall be able to communicate with an Earth based ground segment.	Sec. 2.2	Yes, Sec. 5.8 (TBC)
8.1	The Telemetry, Tracking and Command system shall operate at a total power of 105 W.	Sec. 5.8	Yes, Sec. 5.4.6
9.	The transfer stage shall perform the mission automatically, meaning that the stage can perform some operations by itself (TBD) and for other commands can be given during the mission.	Sec. 2.2	Yes, Sec. 5.8 (TBC)
9.1	The On-Board Data Handling shall operate at a total power of 63 W.	Sec. 5.8	Yes, Sec. 5.4.6

	System Requirement	Created	Met
10.	The transfer stage shall provide electrical power to the payload during the transfer.	Sec. 2.2	Yes, Sec. 5.4.6
10.1	The payload shall operate at a maximum power of 1 kW.	Sec. 5.4.6	TBC
10.2	The docking mechanism shall provide power transfer between the payload and SEP stage.	Sec. 5.4.6	Yes, Sec. 5.5.3
11.	The transfer stage's configuration should be such that the direct impingement of the thrusters' exhaust on the solar arrays is limited (TBD).	Sec. 2.2	Yes, Sec. 5.5
12.	The configuration shall be such that the thermal radiators, solar panels and the docking mechanisms have a unobstructed field of view.	Sec. 2.2	Yes, Sec. 6.2
13.	The structure shall be rigid enough to withstand the launch loads and the frequencies that are imposed by the launcher.	Sec. 2.2	Yes, Sec. 5.5.5 (TBC)
13.1	The structural design shall aim for simple load paths and maximize the use of conventional materials.	Sec. 5.5	Yes, Sec. 5.5.5
13.2	The structure shall protect all systems, excluding solar array and radiators, to the radiation and debris of the space environment.	Sec. 5.5	Yes, Sec. 5.5.5
13.3	The structure shall fit into the adjusted Falcon Heavy fairing, with inner diameter of 4.6 m, cylindrical height of 12.4 m and total height of 16.6 m.	Sec. 5.5	Yes, Sec. 6.2
14.	The deployable mechanisms shall be designed to withstand a natural frequency of 0.1 Hz (TBC) in the deployed state.	Sec. 5.5	Yes, Sec. 5.5.5 (TBC)

D. Master Thesis Proposal

D.1. Introduction

Recently there is a renewed interest to go back to the Moon. The International Space Exploration Coordination Group (ISECG), consisting out of 14 space agencies, updated a Global Exploration Roadmap in September 2011 [18]. This roadmap examines possible pathways in the next 25 years and developed two mission scenarios. One of these scenarios is the 'Moon Next' scenario, where it is planned to go to the Moon around 2028 and establish a long lasting human campaign. This human campaign needs to be supplied by resources, which will be provided by cargo freighters. With the current means these cargo freighters are too expensive and therefore new developments in this area are required.

One of the options for such a cargo freighter is by using a Solar Electric Propulsion (SEP) transfer stage, which transports the cargo from an Earth Orbit to a Lunar Orbit. An SEP stage can transfer significantly more payload compared to a chemical propelled transfer stage while having the same initial mass [1]. Stage re-usability is an asset and has to be evaluated. It would make the SEP-stage cost effective and justifies further development [1]. The aim of this study is to realize a conceptual system design of such a SEP transfer stage for Earth-Moon cargo transfer missions.

Other lessons learned from the literature study [1], in short, are:

- For every mission there is an optimum specific impulse from the mass point of view.
- Ion and Hall thrusters have profound flight heritage and are reasonable candidates for the mission.
- For High Power Hall thrusters a Direct Drive Unit (DDU) should be considered as power conditioning system.
- Solar cells have a big impact on the design and therefore a trade-off between different solar cells is required to come to a good selection.
- The dimensions of the large solar array yield to complications regarding its rotation and shadowing. Solutions for the solar array configuration will be evaluated.

The further research within the Master Thesis will result in a conceptual design of the solar electric propulsion stage. This conceptual design shall serve as a reference for

understanding the interaction of the subsystems and the system layout. It will support the further development of the mission in such a way that enabling technologies and requirements are identified. So within the Master Thesis a holistic approach is preferred to tackle the main questions and get proper budgets. This work can then serve as a basis for further optimization.

The study will be done on behalf of OHB System AG located in Bremen, Germany. In this document first the mission and its initial requirements will be assessed in Section D.2. With this information the problem can be further elaborated and the tasks identified in Section D.3. Finally the work can be divided into different packages and a planning is made, see Section D.4 - Section D.6.

D.2. Mission Requirements

The mission is considered to be an international cooperation, since of the mission complexity and high amount of cost. The mission requirements defined by the customer are as follows:

- The transfer stage transports a payload from Earth environment to a Low Lunar Orbit (LLO).
- The transfer stage uses electric propulsion powered by solar panels, nuclear power is excluded.
- The system shall be launched with a heavy lift launch vehicle. It is preferred to have one launcher and a maximum of two.

During the master thesis LEO is not considered, because the literature study [1] showed that a pass through the Van Allen Belts result in a solar array degradation of around 8%. Passing the belts multiple times is therefore not considered to be an option. Above 6,000 km the influence of the inner Van Allen Belts becomes negligible, therefore an initial MEO can be considered [17].

A GTO (200 x 35786 km) can also be considered. In this case the vehicle will pass through the Van Allen Belts, but only for a short time interval such that in the end the fluence is comparable or even less than a MEO orbit [17]. The final trade-off between MEO and GTO therefore depends mostly on the different delta-V budgets and is performed in the thesis.

The freedom in the launcher selection leads to multiple possible configurations. In the thesis the multiple options will be assessed considering the amount of payload that can be transported. The stage and payload has to fit inside the launchers without violating the mass and volume limit. The Ariane V launcher, the Space Launch System (SLS) and Falcon Heavy are considered. The last two come available in the next ten years [1].

D.3. Task description

Transferring cargo from Earth to the Moon on a regularly basis is with the current means too expensive. A solution to this problem is to transport the cargo by using a reusable SEP stage. This study shows how to design a SEP stage that delivers cargo from Earth environment to LLO. Technological challenges concerning the design will be identified. A heavy lift launch vehicle is used to lift the cargo and stage into the initial orbit.

The goal of the master thesis is to investigate transferring a payload from Earth to Moon by using Solar Electric Propulsion. A technical feasibility study on a transfer stage which delivers the payload from Earth environment to LLO will be performed. The design of the transfer stage is limited to electric propulsion and uses solar panels for the total power production. The overall aim is to develop engineering software for designing major aspects of an SEP-stage.

The subgoals that are required to reach the goal are:

- Develop a simplified but robust orbital mechanics tool to assess the required ΔV budgets.
- Select a suitable launcher configuration for the spacecraft.
- Estimate the total radiation dose, the effect on the spacecraft and mitigation measures.
- Select a stage architecture and determine its configuration.
- Design the propulsion system, including tank and propellant feed system.
- Design the electrical power system, including solar array and power processing units.
- Design the other subsystems: thermal control system, attitude orbit control system, communication system and command & data handling system.
- Determine the stage performance, different failure modes and mission flexibility.

The focus will be on the design of the propulsion system and electrical power system. However, all other subsystems will be addressed ass well in order to achieve a holistic system design. The level of detail of these subsystems will be lower, since they do not drive the system architecture. The aim is the assessment of the system's mass feasibility and consistency, which is common for concept studies (phase 0).

The communications and command & data handling systems have no real emphasis, because the system requirements will be customary and do not drive the architecture. Therefore commercially off-the-shelf components will be selected to come to an initial mass budget.

The ΔV budget can be calculated by a commercial tool, a semi-analytical method or by a personal developed tool. A commercial orbital mechanics tool is expensive and licenses

are allocated to experts only. A semi-analytical method provides limitations on evaluating multiple scenarios. Therefore, to secure full flexibility, a personal tool is developed. The tool performs the orbit calculations by using a numerical approach based upon theory from Reference [77] and [4]. In this approach the initial orbit parameters are used to solve the equations of motion numerically in order to reach an end-orbit with a certain desired radius. This tool, though reasonable and elusive, will be validated in the course of the study by semi-analytical methods and commercial tools for mission analysis.

Lately, similar work has been performed on a SEP cargo stage, see reference [19], [20], [31] and [21]. The first three are performed by NASA and investigate the feasibility of a reusable cargo transfer stage to the Moon, Near-Earth Asteroid or Near-Earth Object, respectively. The last paper shows the development of new technologies within the European HiPER program, which serve the goal of making an SEP mission possible.

This study will implement the new technology developments and assess the performance of the overall system. Also a comparison will be made to existing technologies. This comparison will show if the development of the new technologies lead to improvement of the overall performance and are therefore justified.

To solve the problem statement and reach the goals a Work Breakdown Structure (WBS) is made, see Appendix D.4. For every block of the WBS there is a planning, which can be found in the Gantt Chart of Appendix D.5. A description of the workpackages is given in Appendix D.6 and a structure of the Master Thesis report is given in Appendix D.7. The literature which is considered to be of importance for the study can be found in the Bibliography.

The output of the work will be a computer tool to determine the delta-V budget for the spiral strategy, engineering software to design an SEP-stage, a thesis report describing the performed work including the obtained results, a summary paper and accompanying slides.

D.4. Work Breakdown Structure

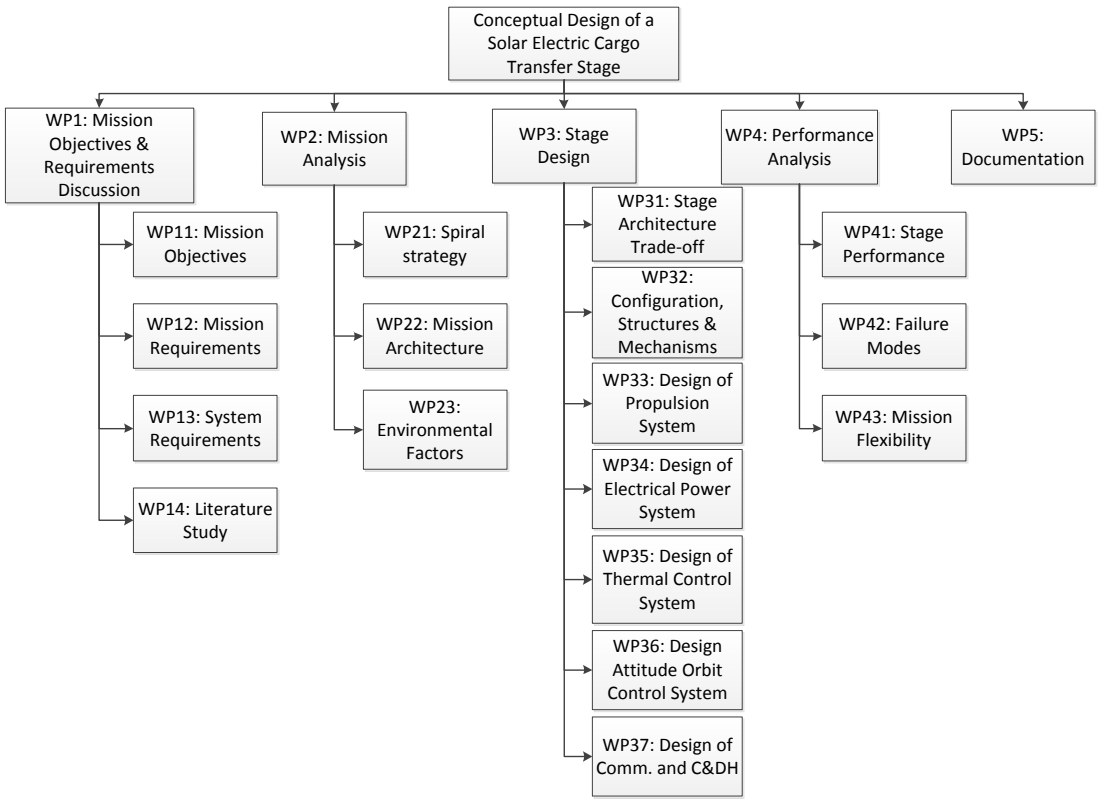

D.5. Gantt Chart

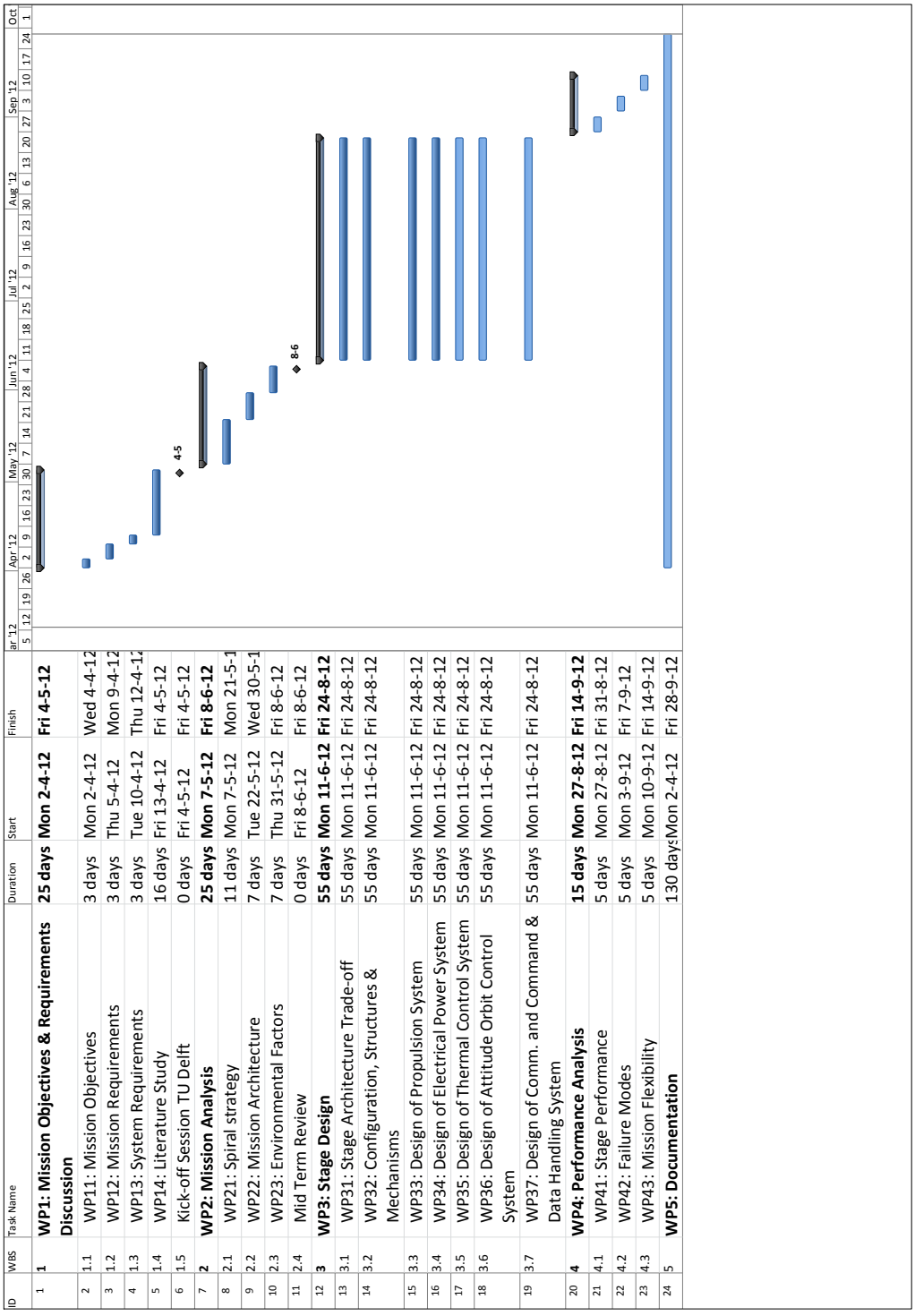

ID	WBS	Task Name	Duration	Start	Finish
1	1	**WP1: Mission Objectives & Requirements Discussion**	**25 days**	**Mon 2-4-12**	**Fri 4-5-12**
2	1.1	WP11: Mission Objectives	3 days	Mon 2-4-12	Wed 4-4-12
3	1.2	WP12: Mission Requirements	3 days	Thu 5-4-12	Mon 9-4-12
4	1.3	WP13: System Requirements	3 days	Tue 10-4-12	Thu 12-4-12
5	1.4	WP14: Literature Study	16 days	Fri 13-4-12	Fri 4-5-12
6	1.5	Kick-off Session TU Delft	0 days	Fri 4-5-12	Fri 4-5-12
7	2	**WP2: Mission Analysis**	**25 days**	**Mon 7-5-12**	**Fri 8-6-12**
8	2.1	WP21: Spiral strategy	11 days	Mon 7-5-12	Mon 21-5-12
9	2.2	WP22: Mission Architecture	7 days	Tue 22-5-12	Wed 30-5-12
10	2.3	WP23: Environmental Factors	7 days	Thu 31-5-12	Fri 8-6-12
11	2.4	Mid Term Review	0 days	Fri 8-6-12	Fri 8-6-12
12	3	**WP3: Stage Design**	**55 days**	**Mon 11-6-12**	**Fri 24-8-12**
13	3.1	WP31: Stage Architecture Trade-off	55 days	Mon 11-6-12	Fri 24-8-12
14	3.2	WP32: Configuration, Structures & Mechanisms	55 days	Mon 11-6-12	Fri 24-8-12
15	3.3	WP33: Design of Propulsion System	55 days	Mon 11-6-12	Fri 24-8-12
16	3.4	WP34: Design of Electrical Power System	55 days	Mon 11-6-12	Fri 24-8-12
17	3.5	WP35: Design of Thermal Control System	55 days	Mon 11-6-12	Fri 24-8-12
18	3.6	WP36: Design of Attitude Orbit Control System	55 days	Mon 11-6-12	Fri 24-8-12
19	3.7	WP37: Design of Comm. and Command & Data Handling System	55 days	Mon 11-6-12	Fri 24-8-12
20	4	**WP4: Performance Analysis**	**15 days**	**Mon 27-8-12**	**Fri 14-9-12**
21	4.1	WP41: Stage Performance	5 days	Mon 27-8-12	Fri 31-8-12
22	4.2	WP42: Failure Modes	5 days	Mon 3-9-12	Fri 7-9-12
23	4.3	WP43: Mission Flexibility	5 days	Mon 10-9-12	Fri 14-9-12
24	5	**WP5: Documentation**	130 days	Mon 2-4-12	Fri 28-9-12

D.6. Workpackage Description

Conceptual Design of a Solar Electric Transfer Stage		**WP 11**
Title	**Mission Objectives**	**Page:** 1 of 17
Responsible	Remco Bos	**Version:** 1.0
		Date: 15.03.2012
Start	T_0	
End	T_0 + 3 days	**Duration:** 3 days
Processor	Remco Bos	

Goals:

- Define Mission Objectives

Input:

- In negotiation with OHB System

Connection with other work packages:

- **WP12** Mission Requirements
- **WP13** System Requirements

Tasks:

- Define & Report Mission Objectives

Results:

- Overview of Mission Objectives

Conceptual Design of a Solar Electric Transfer Stage		**WP 12**
Title	**Mission Requirements**	**Page:** 2 of 17
Responsible	Remco Bos	**Version:** 1.0
		Date: 15.03.2012
Start	T_0 + 3 days	
End	T_0 + 6 days	**Duration:** 3 days
Processor	Remco Bos	

Goals:

- Define Mission Requirements

Input:

- Results of **WP11**

Connection with other work packages:

- **WP11** Mission Objectives
- **WP13** System Requirements

Tasks:

- Define & Report Mission Requirements

Results:

- Overview of Mission Requirements

Conceptual Design of a Solar Electric Transfer Stage		**WP 13**
Title	**System Requirements**	**Page:** 3 of 17
Responsible	Remco Bos	**Version:** 1.0
		Date: 15.03.2012
Start	T_0 + 6 days	
End	T_0 + 9 days	**Duration:** 3 days
Processor	Remco Bos	

Goals:

- Define System Requirements

Input:

- Results of **WP12** Mission Requirements

Connection with other work packages:

- **WP12** Mission Requirements

Tasks:

- Define & Report System Requirements

Results:

- Overview of System Requirements

Conceptual Design of a Solar Electric Transfer Stage		**WP 14**
Title	**Literature Study**	**Page:** 4 of 17
Responsible	Remco Bos	**Version:** 1.0
		Date: 02.04.2012
Start	T_0 + 9 days	
End	T_0 + 25 days	**Duration:** 16 days
Processor	Remco Bos	

Goals:

- Survey on Solar Electric Propulsion Stages and their technologies

Input:

- None

Connection with other work packages:

- **WP2** Mission Analysis
- **WP3** Stage Design

Tasks:

- Discuss prior SEP stage designs
- Identify suitable existing engines
- Identify suitable solar cells
- Identify enabling technologies

Results:

- Information of Solar Electric Propulsion Stages and their technologies

Conceptual Design of a Solar Electric Transfer Stage		**WP 21**
Title	**Spiral Strategy**	**Page:** 5 of 17
Responsible	Remco Bos	**Version:** 1.0
		Date: 02.04.2012
Start	T_0 + 25 days	
End	T_0 + 36 days	**Duration:** 11 days
Processor	Remco Bos	

Goals:

- Assess initial orbit: MEO/GTO
- Assessment of different spiral strategies
- Assessment of different orbit planes
- Assessment of eclipse time
- Assessment of gravity losses due to spiraling
- Determine the delta-V budget of the SEP-stage

Input:

- Results from **WP1**

Connection with other work packages:

- **WP1** Mission Objectives & Requirements Discussion
- **WP22** Mission Architecture
- **WP3** Stage Design

Tasks:

- Development of a basic orbit transfer tool for spiral orbits
- Development of gravity loss assessment tool
- Determine total ΔV requirement

Results:

- Initial orbit
- Performance demands
- Eclipse time
- Mission transfer time
- Dependency of losses on thrust, ΔV and I_{sp}

Conceptual Design of a Solar Electric Transfer Stage		**WP 22**
Title	**Mission Architecture**	**Page:** 6 of 17
Responsible	Remco Bos	**Version:** 1.0
		Date: 02.04.2012
Start	T_0 + 36 days	
End	T_0 + 43 days	**Duration:** 7 days
Processor	Remco Bos	

Goals:

- Assess availability of super heavy lift launch vehicles
- Asess performance of SEP-stage when using different launchers, not violating mass & volume limit
- Assess re-usability
- Select a mission architecture concept

Input:

- **WP1** Mission Objectives & Requirements Discussion
- **WP21** Spiral Strategy

Connection with other work packages:

- **WP1** Mission Objectives & Requirements Discussion
- **WP21** Spiral Strategy
- **WP23** Environmental Factors
- **WP3** Stage Design
- **WP4** Performance Analysis

Tasks:

- Identify Mission Architecture concepts
- Select a Mission Architecture concept

Results:

- A Mission Architecture

Conceptual Design of a Solar Electric Transfer Stage		**WP 23**
Title	**Environmental Factors**	**Page:** 7 of 17
Responsible	Remco Bos	**Version:** 1.0
		Date: 02.04.2012
Start	T_0 +43 days	
End	T_0 + 50 days	**Duration:** 11 days
Processor	Remco Bos	

Goals:

- Assessment of radiation due to space environment

Input:

- Results from **WP1** & **WP21**

Connection with other work packages:

- **WP1** Mission Objectives & Requirements Discussion
- **WP22** Mission Architecture
- **WP3** Stage Design

Tasks:

- Determine the effect of the space environment on the spacecraft
- Estimate the total radiation dose by using Spenvis (ESA-tool)

Results:

- Impact of the space environment on the design

Conceptual Design of a Solar Electric Transfer Stage		**WP 31**
Title	**Stage Architecture Trade-off**	**Page:** 8 of 17
Responsible	Remco Bos	**Version:** 1.0
		Date: 02.04.2012
Start	T_0 + 50 days	
End	T_0 + 105 days	**Duration:** 55 days
Processor	Remco Bos	

Goals:

- Assess different stage architectures with trade-tree
- Perform a trade-off between different architectures

Input:

- Results from **WP1** & **WP2**

Connection with other work packages:

- **WP1** Mission Objectives & Requirements Discussion
- **WP2** Mission Analysis

Tasks:

- Investigate different architecture concepts
- Perform a trade-off on the different concepts

Results:

- Baseline system architecture, this includes at the minimum:
  - Propulsion type
  - Solar cell type
  - Power processing type

Conceptual Design of a Solar Electric Transfer Stage		**WP 32**
Title	**Configuration, Structures & Mechanisms**	**Page:** 9 of 17
Responsible	Remco Bos	**Version:** 1.0
		Date: 02.04.2012
Start	T_0 + 50 days	
End	T_0 + 105 days	**Duration:** 55 days
Processor	Remco Bos	

Goals:

- Determine the configuration of the stage
- Assess, select & design structures and mechanisms for the stage

Input:

- Results from **WP1**, **WP2** & **WP3**

Connection with other work packages:

- **WP1** Mission Objectives & Requirements Discussion
- **WP2** Mission Analysis
- **WP3** Stage Design

Tasks:

- Identification of different configurations
- Design structures & mechanisms

Results:

- Configuration of the stage
- Structures & mechanisms design including mass & size estimation

Conceptual Design of a Solar Electric Transfer Stage		**WP 33**
Title	**Design of Propulsion System**	**Page:** 10 of 17
Responsible	Remco Bos	**Version:** 1.0
		Date: 02.04.2012
Start	T_0 + 50 days	
End	T_0 + 105 days	**Duration:** 55 days
Processor	Remco Bos	

Goals:

- Design the propulsion system

Input:

- Results from **WP1** & **WP2** & **WP3**

Connection with other work packages:

- **WP1** Mission Objectives & Requirements Discussion
- **WP2** Mission Analysis
- **WP3** Stage Design

Tasks:

- Assess the propellant storage and tank
- Assess the need for gimballing the engines
- Investigate performance demands and select engine
- Assess and design propellant feed system

Results:

- Configuration of propellant feed system and tank
- Suitable electric propulsion engine
- Estimation on the total mass and size

Conceptual Design of a Solar Electric Transfer Stage		**WP 34**
Title	**Design of Electrical Power System**	**Page:** 11 of 17
Responsible	Remco Bos	**Version:** 1.0
		Date: 02.04.2012
Start	T_0 + 50 days	
End	T_0 + 105 days	**Duration:** 55 days
Processor	Remco Bos	

Goals:

- Design the electric power system

Input:

- Results from **WP1** & **WP2** & **WP3**

Connection with other work packages:

- **WP1** Mission Objectives & Requirements Discussion
- **WP2** Mission Analysis
- **WP3** Stage Design

Tasks:

- Investigate power demands of the engine & other subsystems
- Investigate battery usage and power drop due to eclipse
- Investigate different solar cell options
- Perform trade-off and select solar cells
- Design solar arrays
- Investigate different power conditioning options
- Select & design a power conditioning system

Results:

- Configuration of solar arrays
- Design of electric power system by providing a block diagram
- Estimation on the total mass and size

Conceptual Design of a Solar Electric Transfer Stage		**WP 35**
Title	**Design of Thermal Control System**	**Page:** 12 of 17
Responsible	Remco Bos	**Version:** 1.0
		Date: 02.04.2012
Start	T_0 + 50 days	
End	T_0 + 105 days	**Duration:** 55 days
Processor	Remco Bos	

Goals:

- Design the thermal control system

Input:

- Results from **WP1** & **WP2** & **WP3**

Connection with other work packages:

- **WP1** Mission Objectives & Requirements Discussion
- **WP2** Mission Analysis
- **WP3** Stage Design

Tasks:

- Investigate heat leakage of power system
- Investigate different thermal control options
- Determine total radiator area
- Design a basic thermal control system

Results:

- Configuration of radiators
- Design of a basic thermal control system
- Estimation on the total mass and size

Conceptual Design of a Solar Electric Transfer Stage		**WP 36**
Title	**Design Attitude Orbit Control System**	**Page:** 13 of 17
Responsible	Remco Bos	**Version:** 1.0
		Date: 02.04.2012
Start	T_0 + 50 days	
End	T_0 + 105 days	**Duration:** 55 days
Processor	Remco Bos	

Goals:

- Assess attitude orbit control for the stage

Input:

- Results from **WP1** & **WP2** & **WP3**

Connection with other work packages:

- **WP1** Mission Objectives & Requirements Discussion
- **WP2** Mission Analysis
- **WP3** Stage Design

Tasks:

- Define required agility
- Investigate moment of inertia of the stage
- Assess different attitude orbit control systems

Results:

- Assessment of attitude orbit control system

Conceptual Design of a Solar Electric Transfer Stage		**WP 37**
Title	**Design Communications and Command & Data Handling System**	**Page:** 14 of 17
Responsible	Remco Bos	**Version:** 1.0
		Date: 02.04.2012
Start	T_0 + 50 days	
End	T_0 + 105 days	**Duration:** 55 days
Processor	Remco Bos	

Goals:

- Assess Communications for the stage
- Assess Command & Data Handling for the stage

Input:

- Results from **WP1** & **WP2** & **WP3**

Connection with other work packages:

- **WP1** Mission Objectives & Requirements Discussion
- **WP2** Mission Analysis
- **WP3** Stage Design

Tasks:

- Select commercially off-the-shelf products for Communications system
- Select commercially off-the-shelf products for Command & Data Handling system

Results:

- Assessment Communications and Command & Data Handling system

Conceptual Design of a Solar Electric Transfer Stage		**WP 41**
Title	**Stage Performance**	**Page:** 15 of 17
Responsible	Remco Bos	**Version:** 1.0
		Date: 02.04.2012
Start	T_0 + 105 days	
End	T_0 + 110 days	**Duration:** 5 days
Processor	Remco Bos	

Goals:

- Assess stage performance for current and future technology

Input:

- Results from **WP1** & **WP2** & **WP3**

Connection with other work packages:

- **WP3** Stage Design

Tasks:

- Investigate stage performance with respect to requirements

Results:

- Assessment of stage performance for current and future technology

Conceptual Design of a Solar Electric Transfer Stage		**WP 42**
Title	**Failure Modes**	**Page:** 16 of 17
Responsible	Remco Bos	**Version:** 1.0
		Date: 02.04.2012
Start	T_0 + 110 days	
End	T_0 + 115 days	**Duration:** 5 days
Processor	Remco Bos	

Goals:

- Assess failure modes of the stage

Input:

- Results from **WP1** & **WP2** & **WP3**

Connection with other work packages:

- None

Tasks:

- Investigate different failure modes

Results:

- Assessment of different failure modes and their consequences on performance

Conceptual Design of a Solar Electric Transfer Stage		**WP 43**
Title	**Mission Flexibility**	**Page:** 17 of 17
Responsible	Remco Bos	**Version:** 1.0
		Date: 02.04.2012
Start	T_0 + 115 days	
End	T_0 + 120 days	**Duration:** 5 days
Processor	Remco Bos	

Goals:

- Assess mission flexibility of the stage

Input:

- Results from **WP1** & **WP2** & **WP3**

Connection with other work packages:

- None

Tasks:

- Assess performance in case of different mission scenarios

Results:

- Assessment of mission flexibility

D.7. Report Structure Master Thesis

1. Introduction
2. Former SEP-stage concepts
3. Mission Objectives & Requirements
   - 3.1 Mission Objectives
   - 3.2 Mission & System Requirements
4. Mission Analysis
   - 4.1 Spiral Strategy
   - 4.2 Mission Architecture
   - 4.3 Environmental Factors
5. Stage Architecture Trade-off
6. Stage Design
   - 6.1 Configuration
   - 6.2 Structures & Mechanisms
   - 6.3 Propulsion
   - 6.4 Electrical Power System
   - 6.5 Thermal Control System
   - 6.6 Attitude Orbit Control System
7. Performance Analysis
   - 7.1 Stage Performance
   - 7.2 Failure Modes
   - 7.3 Mission Flexibility
8. Conclusion & Recommendations

Appendix A. Master Thesis Proposal